University of Strathclyde

Department of Electrical
and Electronic Engineering

Model Based Predictive Control with application to renewable energy systems

David MacKenzie Robb

Doctor of Philosophy, 2000

Acknowledgements

There are many people and organisations who helped in some way to bring this thesis together and the author would like to thank the following people in particular.

First and foremost the Engineering and Physical Sciences Research Council (EPSRC) for agreeing to fund the work and to Strathclyde University for allowing me to study there.

At Strathclyde University thanks must be given to Dr. Bill Leithead for supervising the project and giving much help and support. Also Mary Rodgers, Barry Connor and Helen Markou provided help with the wind turbine models.

The work at the solar power plant at Almería would not have been possible without funding from the the European Union Training and Mobility of Researchers (TMR) programme. Also the validation of the wind models in Chapter 7 was made possible through data from Garrad Hassan & Partners Ltd.

Finally many thanks are given to family and friends for providing much needed support and encouragement from start to finish. In particular special thanks must go to Lorna for her patience, love and support during the extended writing up period.

Abstract

In the promotion and development of renewable energy systems, control engineering is one area which can directly affect the overall system performance and economics and thus help to make renewable energies more attractive and popular. For cost effectiveness, ideally the renewable energy industry requires a control design technique which is very effective yet simple with methods that are transparent enough to allow implementation by non-control engineers. The objective of this thesis is to determine if Model Based Predictive Control (MBPC) is a suitable control technique for use by the renewable energy industry. MBPC is chosen as it uses simple and fairly transparent methods yet claims to be powerful and can deal with issues, such as non linearities and controller constraints, which are important in renewable energy systems.

MBPC is applied to a solar power parabolic trough system and a variable speed wind turbine to enable the general applicability of MBPC to renewable energy systems to be tested and the possible benefits to the industry to be assessed. Also by applying the MBPC technique to these two strongly contrasting systems much experience is gained about the MBPC technique itself, and its strengths and weaknesses and ease of application are assessed.

The investigation into the performance of Model Based Predictive Control and in particular its application in the renewable energy industry leads to two contrasting conclusions. For simple systems with non-demanding dynamics and having a good model of the system, MBPC provides a very good and effective solution. However for more demanding systems with complex dynamics and strong non-linearities, a basic MBPC controller, applied by a non-control engineer, cannot be recommended.

Contents

List of Figures

List of Tables

Chapter 1

Introduction

1.1 The need for renewable energy

Human beings need energy. Throughout history human civilization has depended upon it, from the primitive burning of wood for heat and cooking, through to the industrialization of the developed world, where today, modern homes and cities, transportation networks and industry could not operate without a reliable source of energy. On a world wide scale our need for energy is increasing. The vast majority of this energy still comes from fossil fuels, mainly in the form of coal, oil and gas. These resources have built up under the surface of the earth over hundreds of thousands of years and are now being brought to the surface and burnt in tens of years. There are however several important problems associated with this rapid use of fossil fuels—

It is not sustainable: Today fossil fuels are being used at about 100,000 times the rate at which they are formed. This means having to look harder for new reserves as the old are used up leading to higher and higher extraction costs. This will ultimately lead to a time when it becomes too expensive to justify extracting what is left.

They are not evenly distributed: Fossil fuels are not evenly distributed over the earth and, as stocks run out this will lead to an ever decreasing number of countries having control over these supplies. This can lead to an unreliable supply and an increased vulnerability to varying effects like workers strikes, wars, embargoes etc.

Today, 95% of proven oil reserves are in only 20 countries (mainly in the Middle East) and gas supplies are concentrated in the Middle East and the former

U.S.S.R. countries [92].

They are polluting: Fossil fuels are dirty and are damaging the earth's atmosphere at an ever increasing rate. This damage comes in several forms; local air pollution, which causes health risks for the population; acid rain, caused by the acidification of the atmosphere through emissions of sulphur dioxide, which affects neighbouring countries and can damage or destroy forests, lakes and rivers and the wildlife that depend on these; and global warming which could potentially have a serious negative impact on the planet. Global warming, also termed the greenhouse effect, is the warming of the earth's atmosphere due to increases in greenhouse gases (mainly carbon dioxide and methane and to a lesser extent nitrous oxides and CFCs) [18, 84].

With the growing realization of the damage which is being done to the environment by the use of fossil fuels, not to mention the dwindling reserves of these finite resources and the unpredictability of supply, has come a need to find alternative ways of supplying our energy needs.

Types of energy resources that are non-polluting (at least in terms of emissions to the atmosphere) and are non-depleting (or at least quickly replenishable), which would serve as good alternatives to the current use of fossil fuels, are generally known as Renewable Energy Sources. Of course none of our primary energy sources, the sun, the natural nuclear energy in the earth and the gravitational forces of the moon and sun, are truly renewable. The sun will eventually burn out, all fissile material in the earth will decay and the moon will lose its influence over the oceans as it moves further away from us. However, in normal time scales, gravitational forces and the sun can be considered constant. Table 1.1 shows a list of types of energy sources which are currently used or could be used. Also shown is their renewal period and whether they are normally considered to be a "Renewable Energy Source". Descriptions of the renewable energy systems shown in the table can be found in [92, 81, 11].

As can be seen from the table there is a large variety of sources and each has a large potential to provide clean energy. Also most of these sources are available in every country which will mean less dependency on certain countries for vital energy supply. However, in today's society, these arguments are not good enough on their own to promote change. In order for renewable energy systems to make a significant impact they must either be forced into use by governments or be economically viable. The latter option is preferable. However, current energy prices usually fail to include the external social costs caused by the production of the energy, i.e. the economic,

Energy Source		Renewable?	
Secondary	Primary	Renewal Period	Y/N?
Agricultural biomass	Solar	Months or years	YES
Diurnal storage of thermal energy	Solar	1 day	YES
Fossil fuels (coal, oil, gas)	Solar	Millions of years	NO
Fuelwood	Solar	Tens of years	YES
Geothermal	Nuclear	Infinite	YES
Hydropower	Solar	1 year	YES
Photovoltaic electricity	Solar	Immediate	YES
Refined fissile material	Nuclear	Infinite	NO
Refuse and other waste products	Solar	Months or years	YES
Seasonal storage of thermal energy	Solar	1 year	YES
Tidal energy	Gravitational	12 hours	YES
Wave energy	Solar	Immediate	YES
Wind energy	Solar	Immediate	YES

Table 1.1: Renewable and non-renewable forms of energy

ecological and human health costs associated with air pollution, acid rain and global warming. Also the full cost of the safe disposal of any waste produced and the final cost of decommissioning should be included during operation and not left for governments to pay for at the end of the operating life of the plant. A few renewable energy technologies are already nearly able to compete on the open market. However, they are all disadvantaged by the exclusion of these external costs. In order to redress this imbalance the pricing of electricity, or energy in general, must be altered to reflect the complete cost of production and environmental damage caused. Also all renewable energy technologies are still developing with increases in efficiency helping to bring down their cost and making them more competitive. An important factor which has the potential to improve the efficiency of renewable energy systems, and hence their competitiveness, is the controller.

1.2 Need for control

Control engineering is used to govern a process, increasing efficiency and cost effectiveness and also improving safety. Hence a good controller would help improve the efficiency and competitiveness of renewable energy technologies. However since most

renewable energy technologies are still developing there is usually very little money to be spent on developing a complex control system or employing specialised control engineers. The requirements of renewable energy developers are to have a controller which is powerful and effective, but which is also simple to understand and implement by non-control engineers.

One popular type of control technique is termed "Classical Control"[36] and its methods can support the design of very good control for many systems, however, the methods used lack the transparency necessary for non-control engineers to understand or implement them. Other types of control techniques which have been much developed in recent years are H_2, H_∞ and $\mu_{\text{synthesis}}$ [94]. These techniques increase the controller sophistication and are potentially more powerful. However these methods are even less transparent than the classical methods and also have the potential to create overly complex solutions.

However in recent years several new types of control methods have been developed which attempt to improve controller/system performance whilst allowing a certain amount of transparency into the method and therefore allow non-control engineers to understand and use the method. Two leading examples of this type of control technique are Fuzzy Control and Model Based Predictive Control.

Fuzzy control has three main parts. Firstly the inputs are fed into the "fuzzifier", "rules" are then applied to these fuzzified inputs, and lastly the outputs from the rules are "defuzzified". The fuzzifier converts numerical values of the input variables into linguistic variables. These normally take the form small, medium or large, all either positive or negative, or zero. The rules normally take the form of `IF, THEN` statements such as,

```
IF (error positive large AND change in error negative small) THEN
   Change control signal positive large
```

The defuzzifier then takes these linguistic commands to the control signal and converts them into a real control signal value. The tuning of such a controller is very application specific with very little guidelines as to how to set up the rules of the fuzzification values, although when some time has been spent on tuning the controller, good results can be obtained.

Model Based Predictive Control (MBPC) uses a model of the plant to predict into the future how the plant will change. The controller then uses this information to determine the best control move which will, theoretically, give rise to the desired response of the plant. The controller achieves this using information about past inputs

and outputs along with estimations of the disturbances now and into the future. MBPC has recently gone through a rapid development and is now gaining attention and being implemented in some industrial applications.

In the development of renewable energy systems computer models are very often created. The availability of such models give a good initial reason to consider applying MBPC to these systems. Secondly the fact that MBPC claims to be a straight-forward method which can be applied with little control knowledge makes it attractive to renewable energy systems. And thirdly, claims about its ease of dealing with issues like non-linearity of plant dynamics and the handling of actuator constraints, which are very important in renewable energy systems, make it appear to be a good choice. However these claims need further scrutiny to judge if it is an appropriate control method for the renewable energy industry. In Chapter 2 the principles of MBPC are discussed before going on to test its functionality through applying it to two contrasting renewable energy systems.

1.3 Applying MBPC to renewable energy systems

The Model Based Predictive Control technique's performance is investigated by choosing two applications to which an MBPC controller is applied and the results analysed. The applications chosen are a solar power plant and a wind turbine. The reasons for choosing these systems are that they are both renewable energy systems and also, importantly, because of their very contrasting characteristics. These contrasts, which represent the extremes of any type of renewable energy system (and most other systems in general), allow conclusions to be drawn on not only the general applicability of MBPC to renewable energy systems and the benefits that might be gained, but also, due to the different aspects involved in implementing the MBPC controller, much is learned about the MBPC technique itself, including the strengths and weaknesses of the technique and the general ease of application. Both systems, which are analysed in detail in later chapters, are described below and a summary of the the contrasting characteristics is shown in Table 1.2.

1.3.1 Solar parabolic trough system

Solar parabolic trough systems use a large array of parabolic, trough like, mirrors to concentrate the sun's rays onto a pipe carrying some fluid to be heated. The fluid is normally either water which is heated to become steam, or some type of oil which can be heated to high temperatures and stored until it is needed. Due to the size of the

Solar Parabolic Trough System	Variable Speed Wind Turbine
Very slow system	Fast system
Simple dynamics	Complex and demanding dynamics
Stable	Unstable
Minimum phase	Non-minimum phase with zeros and unstable poles close together
Slightly non-linear	Strongly non-linear with the poles-zeros moving rapidly with wind speed
Simulation and experimental investigation	Simulation investigation only

Table 1.2: Solar and wind energy systems

plant and the large thermal inertias involved, the system is very slow to react to changes in flow rate, solar radiation or input temperature. Rise times of several minutes are common. The system is also stable which makes control of the system relatively easy, although the plant's dynamics change with flow rate and are non-linear. A significant aspect of this system is that the controller can be implemented and tested on the actual plant.

1.3.2 Variable speed wind turbine

Wind turbines generate electricity from the wind. This is achieved by converting the kinetic energy of the wind into mechanical energy, through rotating blades, and then into electrical energy by means of a generator. Variable speed wind turbines differ from more conventional constant speed wind turbines by not fixing the speed of rotation of the blades in relation to the frequency of the electricity grid but allowing the speed of rotation of the blades to vary in sympathy with the wind. This has several potential advantages over the constant speed case although it is also slightly more complicated. In sharp contrast to the solar parabolic trough system, variable speed turbines are fast systems, with time constants measured in seconds, or fractions of seconds, rather than minutes. The dynamics are demanding, in that they are complex and unstable. The dynamics contain unstable poles and non-minimum phase zeros and these poles and zeros move rapidly with varying wind speeds and are close together, all of which results in a hard system to control. Added to this is the fact that the system is strongly non-linear. These aspects result in the system being very demanding and a challenging test

for any type of controller. The testing of the system is by simulation only. However, the design and testing of the controller through simulation is essential for many complex physical systems, and the process undertaken is therefore realistic. This is in contrast to the solar power plant where the controller can be implemented on the physical plant at a very early stage with very little testing or simulation.

As well as showing the applicability of MBPC to solar trough systems and variable speed wind turbines, the investigation of these two systems provides a basis for assessing the usefulness of MBPC to the renewable energy industry in general. In addition the varying properties of each system enables a clearer assessment of the MBPC technique to be made and any problems or shortcomings to be discovered.

1.4 Outline

The thesis is organised as follows. In chapter 2, the MBPC technique is fully described. In chapter 3 the solar parabolic trough system is described and a suitable MBPC controller developed. The application of the MBPC technique to the second system, a wind turbine, is considered in chapters 4– 8. A general discussion of wind energy is presented in chapter 4 and a review of wind turbine control objectives and strategies in chapter 5. Dynamic models of the wind turbine and of the wind are described in chapter 6 and chapter 7, respectively, and some new wind models derived. The MBPC technique is applied to a variable speed stall regulated wind turbine in chapter 8. In chapter 9 the conclusions are presented with some discussion of further work which might be carried out.

1.5 Original contributions

The principle original contributions presented in this thesis are the following,

1. The application of MBPC to a solar power plant, (Chapter 3). Although many controllers have been tested on the solar power plant in Almería the type of MBPC considered in this thesis had not been implemented. Also, as well as gaining an initial practical understanding of implementing an MBPC controller, detailed results are obtained which could be used as a basis of comparison with other future controllers tested at Almería. Such detailed results are missing from almost all published papers making comparisons between controllers difficult.

2. Development of some aspects of wind turbine dynamic models, in particular,

suitable models of the wind for wind turbines with blade tips, (Chapter 7). Models of the wind for wind turbines with blade tips have never been fully developed and the work in Chapter 7 brings together the current standard models for wind turbines before going on to develop and test these new models.

3. Application of MBPC to a stall regulated wind turbine (Chapter 8). MBPC has never been applied to a wind turbine system. Nearly all applications of MBPC described in its literature are for "slow" systems and the application of the technique to a "fast", non-linear wind turbine, provides new insight into the capability of MBPC.

4. Analysis of MBPC controller in the frequency domain (Appendix G). Finally, in order to understand the behaviour of the MBPC controller, a new method of taking the MBPC code and representing this in the frequency domain for analysis is developed for simple MBPC controllers.

5. The determination of the usefulness of MBPC to the renewable energy industry. Through examining the two contrasting systems conclusions are drawn about the general applicability of MBPC throughout the whole renewable energy industry (Chapter 9)

Through the work the following publications have been written:

"Application of Predictive Control Techniques to Wind Turbines", D.M. Robb and W.E. Leithead, European Wind Energy Conference, Dublin, October 1997, p564.

"Derivation and Validation of Simple Correlated Wind Speed Models", D.M. Robb and W.E. Leithead, submitted to Wind Energy.

Chapter 2

Model Based Predictive Control

2.1 Introduction

In the late 1970's separate developments in the U.S.A. and Europe resulted in a new type of control technique being developed based on model prediction. This started with the development of Dynamic Matrix Control (DMC) by Cutler and Ramaker in 1979 [31] and Identification and Command (IDCOM) by Richalet *et al.* in 1978 [85]. Thereafter there was a profusion of similar developments (some independent, some following on from previous work) along the same theme. e.g.

MAC	Model Algorithmic Control, 1982
EHAC	Extended Horizon Adaptive Control, 1984 [104]
EPSAC	Extended Prediction Self-Adaptive Control, 1985 [35]
LDMC	DMC with Linear programming techniques, 1985 [79]
QDMC	Quadratic programming techniques solution of DMC, 1986 [55]
GPC	Generalized Predictive Control, 1987 [19]
GPCC	Generalized Predictive Cascade Control, 1990
CRHPC	Constrained Receding Horizon Predictive Control, 1991 [21]
PFC	Predictive Functional Control, 1991
UPC	Unified Predictive Control, 1991 [95]

When all these different techniques are analysed they all have the same basic central theme. Model Based Predictive Control (MBPC) is one name used to describe the elements of all these control strategies. Essentially it is the explicit use of a model to predict the process output over a medium to long range period.

2.2 MBPC theory

Some of the stated advantages of MBPC are—

- It permits the solution of control problems with unusual dynamic behaviour;
- The concepts can be mastered in a short time, making it attractive to people with a limited control background;
- It can handle in a straight-forward way multivariable interactive control problems;
- It has inherent dead-time compensation;
- It can introduce, in a natural way, feed forward control action for compensation of measured disturbances;
- It is conceptually simple to extend the strategy to handle constraints;
- It is an open methodology based upon some key principles but allows future extensions to be added to the field.

These facts have made it a popular technique, not just in theory but in many industrial applications.

The main drawbacks with this technique are that it is computationally complex (although this is becoming less and less of a problem with advances in computer power), and there is the necessity of a suitable process model which is not always readily available.

MBPC is based on what is known as the receding horizon principle which can be summarized in 4 basic steps.

1. At each time interval the current output of the system is measured and a reference trajectory is calculated to guide the process output from its current value to the desired value or set-point.
2. Using the system model the predicted future output of the system is calculated, assuming no change in future control value. This is known as the free response of the system,
3. The best set of future control actions, which minimize the error between the reference trajectory and the free response, are then calculated, again using the system model. However only the first control action is actually implemented.

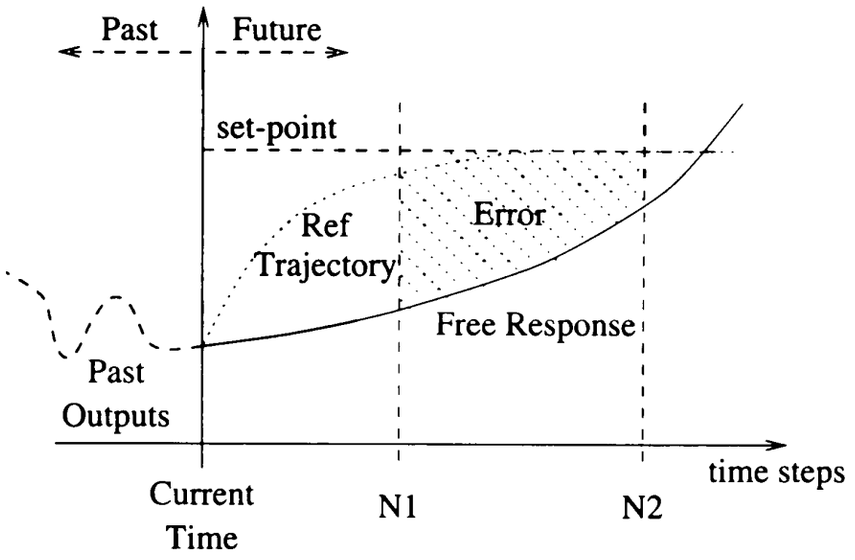

Figure 2.1: Time series of the MBPC method

4. The difference between the predicted and measured process output is used by the controller to either do some disturbance reconstruction or model realignment.

This 4-step procedure is repeated at every sampling instant, each time looking at a fixed length prediction horizon which recedes into the future. This is shown diagrammatically in Figure 2.1 and how each of these steps is realised is discussed below.

(In all the examples below the notation $f(t+k|t)$ means the value of f at time step $t+k$ but estimated at the current time t. $f(t+k|t+1)$ would be the same predicted value but estimated at the next time step $t+1$, etc. N_1 and N_2 are used to define the prediction horizon, or what range of time steps into the future MBPC utilizes at each time interval.)

2.2.1 Reference trajectory

The reference trajectory, $r(t+k|t)$, $k = 1 \ldots N_2$, is an idealistic way the system should move from its current output, $y(t)$, to the desired set point, $w(t+k|t)$, $k = 1 \ldots N_2$. In some cases it is not necessary to define a path and it can be assumed that the future reference trajectory is simply equal to the set point.

$$r(t+k|t) = w(t+k|t),\ k = 1 \ldots N_2 \tag{2.1}$$

However it is more common to initialize the reference trajectory on the current output

$$r(t|t) = y(t) \tag{2.2}$$

and then let this trajectory move to the set point according to a specified dynamic path. A simple first order trajectory is normally used —

$$r(t+k|t) = \epsilon r(t+k-1|t) + (1-\epsilon)w(t+k|t), \quad k = 1 \ldots N_2 \tag{2.3}$$

The value $\epsilon\,(0 \leq \epsilon < 1)$ is a tuning parameter which specifies how fast the response should move to the set point.

In the above method the future set point, $w(t+k|t)$, $k = 1 \ldots N_2$, is assumed to be known and this can be very useful in examples such as batch control or robotic systems, where this feature makes MBPC very attractive. However in most other cases the future set point is not predetermined and therefore it is assumed to be equal to the current set point, $w(t+k|t) = w(t)$, $\forall k > 0$.

2.2.2 Process models for prediction

The process model describes the relationship between plant outputs and inputs. There are many ways in which this can be done and below are described two methods which are used in later chapters.

Step response model

This method was first used in DMC, and uses a step response of the system that settles after n samples. That is, the input is suddenly changed from one level to another and the output observed. The output, y, is defined as—

$$y(t) = y_0 + \sum_{j=1}^{n} g_j \Delta u(t-j) = y_0 + G(q^{-1})(1-q^{-1})u(t) \tag{2.4}$$

g_j are output values of a step response of the system taken at time intervals $j = 1$ through $j = n$ (when the step input is applied to the system at time interval $j = 0$). $\Delta u(t) = u(t) - u(t-1)$, where u is the input to the system. $G(q^{-1}) = g_1 q^{-1} + g_2 q^{-2} + \ldots + g_n q^{-n}$ with q^{-1} being the backward shift operator ($q^{-1}u(t) = u(t-1)$). Also y_0 is the cumulative effect of control increments before n samples. This can be assumed to be zero as this is dealt with by the disturbance model.

The predicted output can then be calculated by —

$$y(t+k|t) = \sum_{j=1}^{n} g_j \Delta u(t+k-j|t) = G(q^{-1})(1-q^{-1})u(t+k|t) \tag{2.5}$$

This allows the modelling of many systems and the prediction is simple, however it cannot model unstable systems and could contain many parameters (n can be quite large, e.g. 30-50).

Transfer function model

The process can also be described by the difference equation, relating the current output, $y(t)$, to previous outputs, $y(t-n)$ and previous inputs, $u(t-n)$,

$$y(t) + a_1 y(t-1) + \ldots + a_{n_a} y(t-n_a) = b_1 u(t-1) + \ldots + b_{n_b} u(t-n_b) \tag{2.6}$$

This can be rewritten as

$$y(t) = \frac{B(q^{-1})}{A(q^{-1})} u(t) \tag{2.7}$$

where B and A are vectors of the b_n and a_n coefficients, respectively, and q^{-1} is the backwards shift operator. The predicted process output can then be calculated as

$$y(t+k|t) = \frac{B(q^{-1})}{A(q^{-1})} u(t+k|t) \tag{2.8}$$

This allows the modelling of unstable and lightly damped systems with the use of less parameters. However more knowledge of the system is necessary than when using the step response model.

2.2.3 Control laws

The future output of the process, $y(t+k|t)$, $k = 1 \ldots N_2$, depends partly on the future control input, $u(t+k|t)$, $k = 0 \ldots N_2 - 1$. However the output can be considered to be the sum of two parts —

$$y(t+k|t) = y_f(t+k|t) + y_c(t+k|t), \quad k = 1 \ldots N_2 \tag{2.9}$$

$y_f(t+k|t)$ is the "free response" of the system assuming no future change in control action and $y_c(t+k|t)$ is the controlled part of the response dependent on the control input. Therefore the free response can be calculated by setting all the future control moves to zero in the prediction model, $\Delta u(t+k|t) = 0$, $k = 0 \ldots N_2 - 1$. Assuming the step response model, equation 2.5, the controlled response becomes —

$$y_c(t+k|t) = g_k \Delta u(t|t) + g_{k-1} \Delta u(t+1|t) + \ldots + g_1 \Delta u(t+k-1|t) \tag{2.10}$$

Define the vector of future errors as

$$\vec{E} = \begin{bmatrix} e(t+1|t) \\ e(t+2|t) \\ \vdots \\ e(t+N_2|t) \end{bmatrix} \tag{2.11}$$

where $e(t+k|t) = r(t+k|t) - y(t+k|t)$. Applying equations (2.9) and (2.10),

$$\vec{E} = \vec{E}_0 - \vec{G}\vec{U} \tag{2.12}$$

where,

$$\vec{E}_0 = \begin{bmatrix} r(t+1|t) - y_f(t+1|t) \\ r(t+2|t) - y_f(t+2|t) \\ \vdots \\ r(t+N_2|t) - y_f(t+N_2|t) \end{bmatrix},$$

$$\vec{G} = \begin{bmatrix} g_1 & 0 & \dots & 0 \\ g_2 & g_1 & \ddots & \vdots \\ \vdots & \vdots & \ddots & 0 \\ g_{N_2} & g_{N_2-1} & \dots & g_1 \end{bmatrix} \text{ and, } \vec{U} = \begin{bmatrix} \Delta u(t|t) \\ \Delta u(t+1|t) \\ \vdots \\ \Delta u(t+N_2-1|t) \end{bmatrix}$$

However the size of $\vec{U}$ implies that whatever method is used to minimize the errors in $\vec{E}$ will be a function of N_2 independent variables. With N_2 being normally somewhere in the region of $10 \dots 30$, this can lead to a very computationally expensive solution. One way to reduce this complexity is to introduce some structuring into the control law.

The simplest way to do this is to introduce a control horizon N_u, where $N_u \leq N_2$, after which the predicted control value remains constant; that is $\Delta u(t+k|t) = 0$, $k \geq N_u$. This results in a control vector of dimension N_u which is normally much less than N_2. This would also mean using only the first N_u columns of $\vec{G}$ above. Typically N_u is chosen to be quite small (e.g. 2,3,4) with a limiting case of $N_u = 1$ where only one control move, $u(t|t)$, has to be calculated. This results in a simple scalar solution but can lead to very good control.

Another option is to look at a section of the future, from time step N_1 through to N_2, and not all the way from 1 to N_2. N_1 is used to ignore periods of dead time in the system response and can also be used to achieve other control objectives.

The Matrix $\vec{G}$ now becomes—

$$G = \begin{bmatrix} g_{N_1} & g_{N_1-1} & \dots & 0 \\ g_{N_1+1} & g_{N_1} & g_{N_1-1} & \vdots \\ \vdots & & \ddots & \\ g_{N_2} & g_{N_2-1} & \dots & g_{N_2-N_u+1} \end{bmatrix} \tag{2.13}$$

where $g_j = 0$, $j \leq 0$.

The solution to equation 2.12 is found from the minimisation of $\vec{E}$

$$\min_{\vec{U}} \sum_{k=N_1}^{N_2} \left[r(t+k|t) - y(t+k|t)\right]^2 \tag{2.14}$$

of which the least squares solution is

$$u_{opt} = (G^T G)^{-1} G^T E_o \tag{2.15}$$

where u_{opt} has size N_ux1 and E_o is the vector of errors from time N_1 to N_2 [34]. The basic least squares solution can result in very aggressive control action. Therefore the damping factor Λ is introduced,

$$u_{opt} = (G^T G + \Lambda I)^{-1} G^T E_o \tag{2.16}$$

2.2.4 Disturbance reconstruction

Disturbance reconstruction seeks to include the effects of disturbances acting on the plant into the prediction model. The way that the disturbance reconstruction is implemented depends on whether the disturbance is able to be measured.

If the disturbance, $d(t)$, can be measured and a model, showing the effect of the disturbance on the output, is available, then the disturbance is used in a similar way to the Process Model to predict future disturbance effects. The value of the future disturbance input can either be predicted using past values or, more commonly, it is assumed that all future disturbance values are equal to the current disturbance; that is, $d(t+k|t) = d(t)$, $k = 1 \ldots N_2$.

If the disturbance cannot be measured then the disturbance is assumed to be equal to the difference between the real and predicted output. Again the disturbance can be assumed to be constant in the future or may be predicted using past values. This unmeasured disturbance model also has the effect of correcting for any model mismatch and thus can be used along with the measured disturbance model.

2.3 Other MBPC issues

As was mentioned earlier, MBPC covers a wide range of techniques all containing a common theme. Only two types of process model have been discussed here but many types have been proposed including impulse response models, state space models and non-linear models including the use of neural networks. Other parts which may be added to the basic MBPC algorithm are constraints and self-tuning.

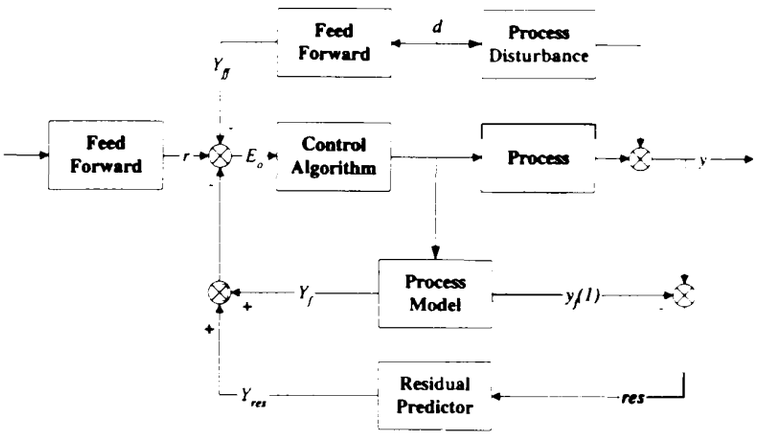

Figure 2.2: Block diagram of MBPC implementation

Constraints handling allows the system to operate effectively within certain limits. These limits can be on the inputs or outputs and can either be on the absolute values or the rate of change of these values. These restrictions are used in the MBPC controller when it is predicting ahead to ensure the best possible control moves are calculated that do not force the system to hit these limits.

Self-tuning involves allowing the model to adapt as the system operates. The actual results of control moves are analysed and new estimates made of the parameters of the system. This is either repeated every time sample or, more commonly, every few time samples.

2.4 Implementation

Shown in figure 2.2 is a block diagram of the basic implementation of MBPC bringing together all the previous sections.

Process Model The chosen type of process model (Section 2.2.2) is used to predict the expected current output value, $y_f(1)$, and also the future free response vector, Y_f.

Supervisory System Calculates future output trajectory, r, using the set point, w, (Section 2.2.1) and may also handle information on constraints.

Feed-Forward (FF) Can be used in some systems to calculate the future effect, $Y_f f$, of measured disturbances, d (Section 2.2.4).

Residual predictor The residual, res, which is the difference between the real and predicted current output, is due to the effect of the process disturbances and the modelling errors. The future trajectory of this residual, Y_{res}, may be predicted or assumed to remain constant.

Controller Calculates the future control action based on the total Error vector E_o (Section 2.2.3).

This is the basic model which is used in later chapters to implement MBPC controllers. In the next chapter the first of the two systems which are used to evaluate the MBPC technique is presented. From both the systems experience will be gained on many aspects of the MBPC technique, especially in its claims of ease of implementation and performance, and an evaluation of the potential of MBPC will be able to be made.

Chapter 3

Application to a Solar Power Plant

3.1 Solar energy

Solar energy used in electricity production can be split up into two main areas: Photovoltaics and Solar Thermal.

Photovoltaics is the direct conversion of the sun's light, or photons, to make electricity. This is achieved using a photovoltaic (PV) cell which is made of semiconductor material. When incoming photons hit atoms in the semiconductor material some of the electrons are knocked loose which in turn causes electricity to flow. The more photons striking the cell the more power is generated.

PV cells, which produce DC electricity, are usually grouped into modules inside protective casings. PV systems can either provide an independent, stand alone power system, usually using batteries for times when the sun is not shining, or they can be connected to the grid.

Solar thermal systems, on the other hand, use the the heat from the sun's rays rather than the light. Reflective surfaces concentrate the rays to heat a receiver filled with oil, or other heat exchange fluid. This heated fluid is then used in some form of heat engine to generate electricity. The reflective surfaces track the sun's movements throughout the day using, usually, mechanical drives. There are three main types of solar concentrators used in these types of systems — power towers, parabolic dish systems and parabolic trough systems, the latter of which is studied in detail below.

Power towers, which are also called central receivers, use a field of very large sun tracking mirrors, called heliostats, to reflect the sun's rays onto a single receiver that

sits on top of a tall tower. The fluid in the receiver is heated to around 560^oC before being passed to the heat exchanger to produce steam for electricity generation.

Parabolic dish systems, use a large dish shaped reflector to concentrate the sun's rays onto a receiver mounted at the focal point of the dish (something like a large TV satellite dish). The receiving fluid can be heated to around 800^oC, but instead of producing steam most dish systems today generate electricity by using the hot fluid to run a Stirling engine [61] mounted at the dish's focal point.

3.1.1 Parabolic trough systems

Commercial plants with parabolic-trough collectors originated with a sun power plant designed by Shuman and built at Philadelphia in 1911, which generated a maximum of 32 HP[1] at mid-day, with an average of about 14 HP over an eight-hour day. It was followed by a sun power plant constructed and put into operation at Meadi, a suburb of Cairo (Egypt). This plant produced 1000 lb/hr of steam for a ten-hour operating day. In spite of the encouraging results obtained during its operation it was shut down in 1915 due to World War I. Further development of this promising technology was delayed by several decades because of the intervention of two World Wars and cheap fossil fuels.

No further major activity in this field was reported until the 1970s and 80s when, during the oil crisis of 1973, oil prices increased enormously and unprecedented inflation gave rise to discussion of the need for development of alternative energy sources. As more and more interest was taken in electricity production from solar thermal energy, pilot plants were constructed to investigate and evaluate the competitiveness and technical feasibility of this application of solar energy.

In 1981, a solar thermal power plant with parabolic-trough-collectors was erected under the sponsorship of the International Energy Agency, in Tabernas, Almería, Spain, as part of the Small Solar Power Systems (SSPS) Project. This would later become part of the facilities of the Plataforma Solar de Almería, the largest European solar test centre [91]. Included in this facility is the Acurex Solar Field, to which the MBPC controller is applied.

Due to the intermittent nature of the primary energy source, solar radiation, the control scheme contributes to the overall efficiency of the system. The objective of the controller is to maintain the outlet oil temperature of the field as closely as possible to a desired value despite disturbances and uncertainties such as changes of the solar

[1]Horse Power, 1HP = 0.736kW

radiation, ambient temperature, inlet oil temperature, etc, by means of varying the oil flow pumped through the pipes.

3.2 Plant description

The Acurex Solar Field consists of twenty rows of east-west oriented, one-axis elevation-tracking, parabolic-trough Acurex Model 3001 collectors in ten parallel loops (see Figures 3.1 and 3.2). There are a total of 480 modules in the field. Twelve single collector 'modules' are connected in 'groups', each driven by one motor in the middle of the group to angle the modules towards the sun. There are two groups in a 'row' and two rows in a 'loop'. Each individual module is $3.05m$ long and has an aperture of $1.83m$. The north-south separation between two consecutive rows is 5 metres. The total reflective aperture area of the Acurex collector field is $2674m^2$ and the land use factor, showing ratio of land used for the collectors to the area of the collectors, is 0.27. The parabolic trough collector uses a parabolic surface to concentrate the direct normal beam on to the receiver tube, which is located at the focal point of the parabola. The glass covered mirrors give an effective concentration ratio of 35.5 to 1. The heat transfer fluid is pumped through the receiver tube, thus collecting the thermal energy gained through the receiver tube walls. A Pyrex glass tube over the metal absorber tube reduces convective heat losses at high temperatures and the outer surface of the absorber tube is coated with a selective black-chrome film. Both of these measures help to maximise energy capture.

Also included in the solar plant is an oil storage system and desalination plant. The 4 MWh oil storage system consists of a single $140m^3$ thermocline oil storage tank which holds $110m^3$ of Santotherm 55 oil and $30m^3$ of inertizing nitrogen gas (N_2). The desalination plant was coupled to the Acurex facility in 1988. It is a 14-cell multi-effect desalination plant capable of producing $72m^3/day$ of distilled water. The hot oil from the top of the storage tank is sent to the low pressure boiler, thus producing 70^oC, 35-bar steam which is sent to the first effect evaporator of the desalination plant.

3.3 Implementation of the controller

Figure 3.3 shows a block diagram representation of the Acurex plant showing how the MBPC controller is integrated into the system. T_{ref}, which is the desired output temperature of the oil from the field, is set manually and fed into the controller. T_{ref} is used along with the actual output temperature, T_{out}, by the controller to generate the

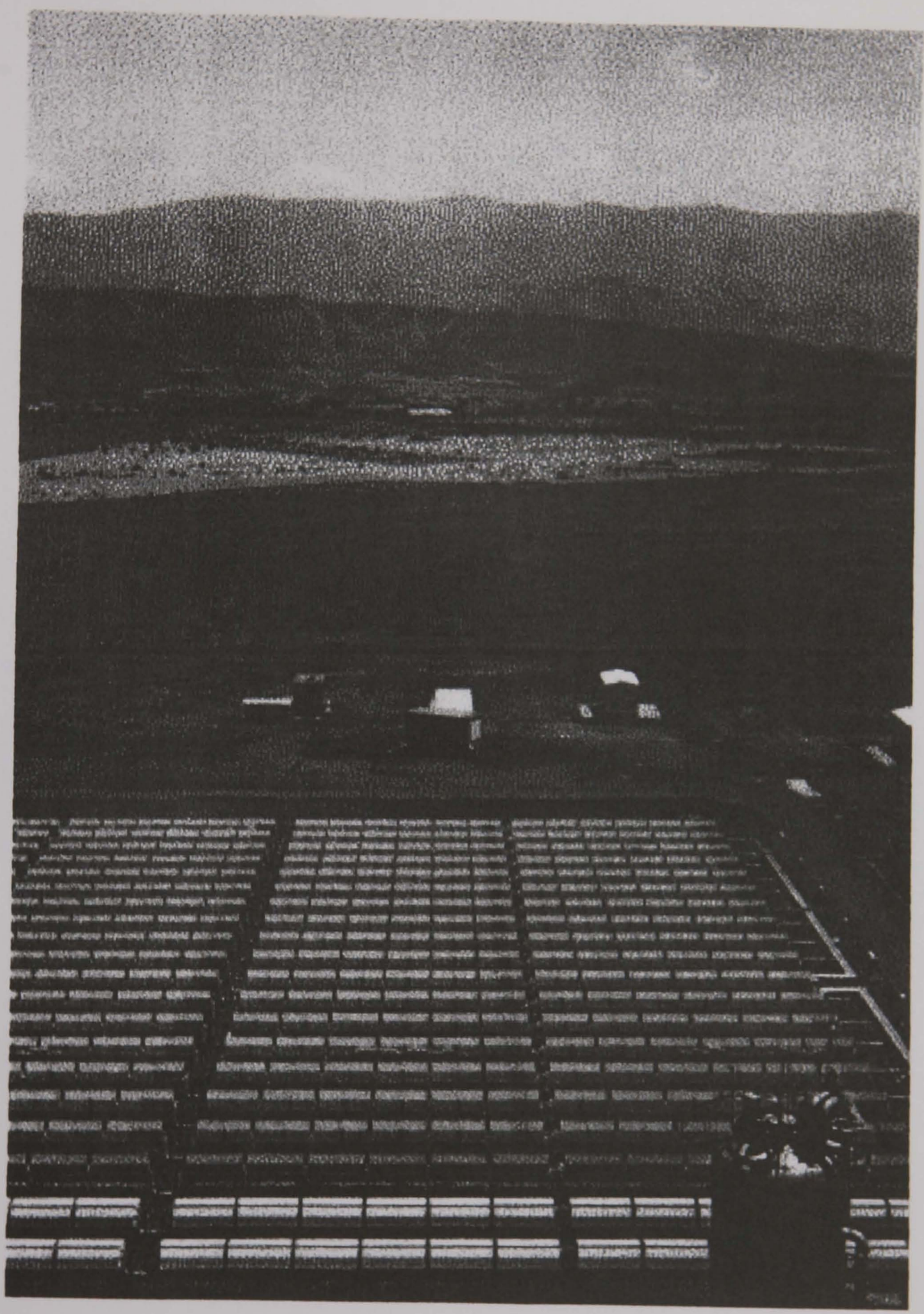

Figure 3.1: Photograph of the Acurex Solar Field, Almería

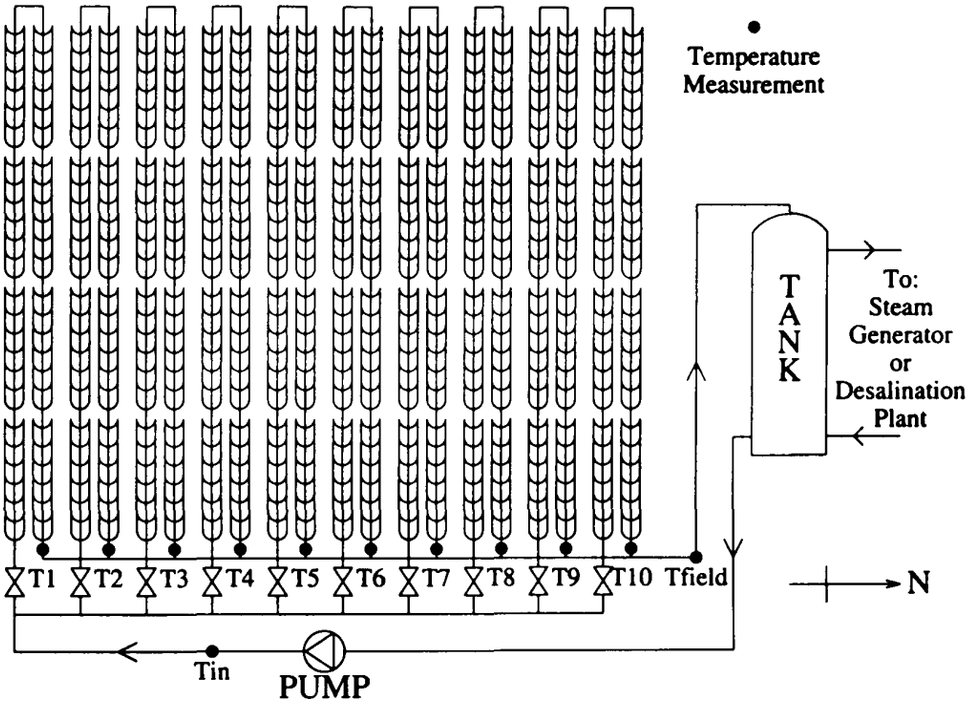

Figure 3.2: Diagram of the Acurex Solar Field, Almería

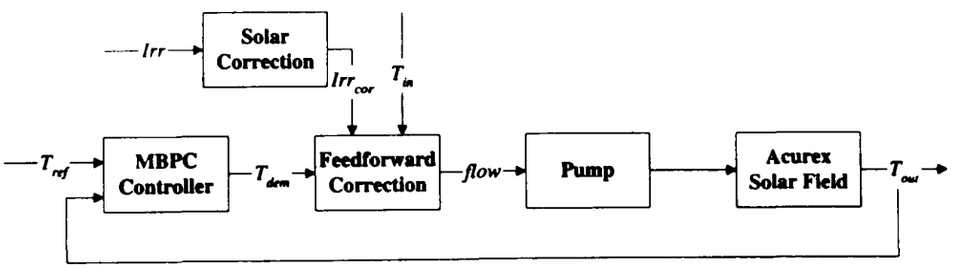

Figure 3.3: Block diagram of Acurex control

control signal, which is the demanded temperature, T_{dem}. The demanded temperature, T_{dem}, is converted into a desired flow of oil in the system and the flow signal is sent to the pump which drives the oil round the system. The blocks **Solar Correction** and **Feed-forward** are C language routines developed by Seville University [5] who have carried out extensive tests on the system. The **Solar Correction** block is used to correct the measured solar radiation to take into account that the parabolic mirrors can only rotate along one axis and therefore cannot keep the mirror at right angles to the sun's incident rays. This leads to a loss in the maximum possible energy capture although this is compensated for by reduced costs in building the plant and less moving parts in the system which could break down or need maintenance. The **Feed-forward** block calculates the flow of oil in the Acurex field which should, theoretically, result in the output temperature of the Acurex field (T_{out}) being equal to the demanded temperature (T_{dem}), taking into account the corrected solar radiation (Irr_{cor}) and inlet temperature of the oil (T_{in}). This was introduced to remove the complexity of modelling the non-linear effects of the solar radiation and input temperature on the output temperature of the field. The equation used is

$$flow = \frac{0.7869 Irr_{cor} - 0.485(T_{dem} - 151.5) - 80.7}{(T_{dem} - T_{in})} \tag{3.1}$$

As described in various papers on the Acurex field [13, 90] the plant's dynamics change at different operating points (flow rates). However, for the purposes of the MBPC controller, it was decided to use only one simple model as an average of the system and to rely on the robustness of the controller to take account of the varying system dynamics. The model chosen was one used in previous experiments with the system [89] and is

$$P(z) = \frac{0.027z + 0.052}{z^3 - 0.912z^2} \tag{3.2}$$

This model is an approximation for a flow of $8l/s$ and includes the dynamics of the feed-forward block. Thus the model relates the system output T_{out} to the system input T_{dem}.

A unit step input was applied to the model to generate the step response coefficients (g_a) of the MBPC step response model (see Section 2.2.2) to be calculated in order to construct the G matrix for the MBPC controller. A sampling time of 39 seconds is used to generate these coefficients as this corresponded to the standard simulation software sampling interval used on the plant. The open loop unit step response is shown in Figure 3.4.

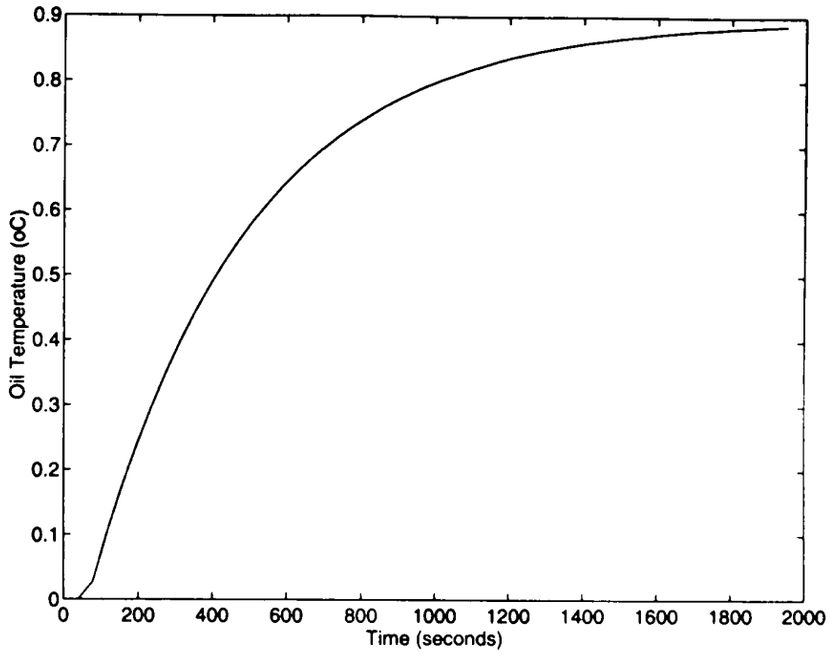

Figure 3.4: Unit Step response of the solar system model, $P(z)$

Using varying values of N_1, N_2, N_u and Λ, controllers were designed and first tested on a simulation package [5] and then taken to Almería to be tested on the real plant.

3.4 Simulations

Using a simulation package developed at Seville University [5] it was possible to test controllers before trying them on the real plant. This simulation, written in the 'C' programming language, takes in real recorded data from the solar power plant - inlet oil temperature, ambient temperature, solar radiation - and calculates the outlet oil temperature based on the demanded oil flow from the controller. Using this tool it was possible to test many controller parameters quickly and easily and find a subset which would be implemented on the real plant.

3.4.1 Simulation control parameters

In order to obtain an understanding of the effect of the four control parameters - N_1, N_2, N_u and Λ - many different combinations were chosen and tested on the simulation, the best of which are described below. First a single point in the future was chosen to be the controller horizons. Thus the controllers based on control parameters of the

form n,n,1,0 were tested, with n varying from 4 through to 20. After this different ranges of controller horizons (N_1 through N_2) were chosen along with varying values of Λ and N_u. One main example investigated was with $N_1 = 2$ and $N_2 = 50$, to look at minimizing all the errors between 2 and 50 steps ahead. N_1 was chosen to be 2 as there is one unit of delay in the process model (see Figure 3.4) and $N_2 = 50$ as the model takes approximately 50 time steps to settle. Some comparisons made with these horizons were 2,50,1,1 and 2,50,3,1 to look at the effect of N_u; and with 2,50,3,Λ, where $\Lambda = 0.2, 0.3, 0.4, 0.7, 1.0, 1.5$ to look at the effect of Λ. Another group of comparisons which gave good results were made with 15,30,3,Λ, with $\Lambda = .01, .03, .1$, thus taking in a mid range of horizons with varying damping factors. Within all of these ranges of controller parameters, the effects of varying N_u and Λ can be considered and, in comparing the different sets of ranges (15,30,3,x and 2,50,x,x), the effect of the control horizons is investigated.

In all the above cases it is not possible to have $N_u > 1$ and $\Lambda = 0$ as this does not allow the matrix inversion needed in equation 2.8. In general, when N_u is greater than 1, Λ must be greater than zero to allow the controller to be realised.

3.4.2 Simulation results

A selection of results taken from all the simulations carried out are shown in Figures 3.5, 3.6 and A.1 to A.4. Figure 3.5 shows the full simulation of a typical day's data at the solar power plant, attempting to control the outlet oil temperature (T_{out}) using the control parameters 6,6,1,0. The input data for oil inlet temperature (T_{in}), solar radiation (Irr), reference temperature (T_{ref}) and ambient temperature (T_{amb}, not shown in the graphs) are kept constant through all the simulations. Figures A.1 through A.4, on pages 163–166, show comparisons between different types of controllers, as discussed above, focusing on small illustrative parts of the simulation to highlight the effect of changing the various control parameters.

Through these simulations the effect of the various tuning parameters can be seen. Figure A.1 shows the effect of varying the prediction horizon, with a closer horizon (e.g. $N_1 = N_2 = 4$) making the controller work harder and quicker, although resulting in a more oscillatory response. Figures A.2 and A.3 shows the effect of Λ, with a higher value giving more damping and thus a slower response with less, or no, overshoot. In Figure A.4 calculating 3 control moves ($N_u = 3$) instead of 1, seems to result in a slightly faster settling time but more oscillatory, although this may be due to the higher value of damping relative to the number of control moves. From all the simulations three

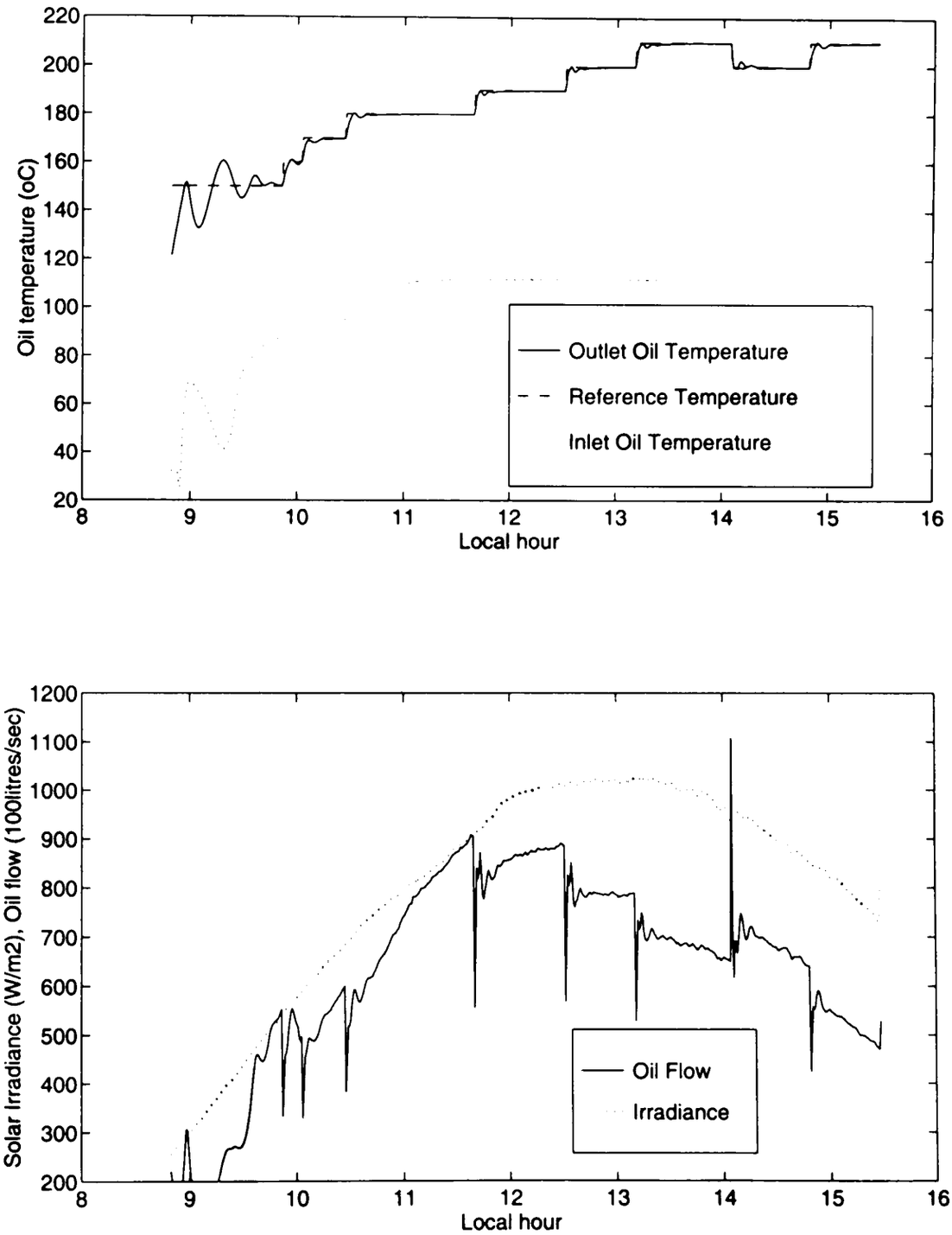

Figure 3.5: Acurex simulation results with control parameters 6,6,1,0

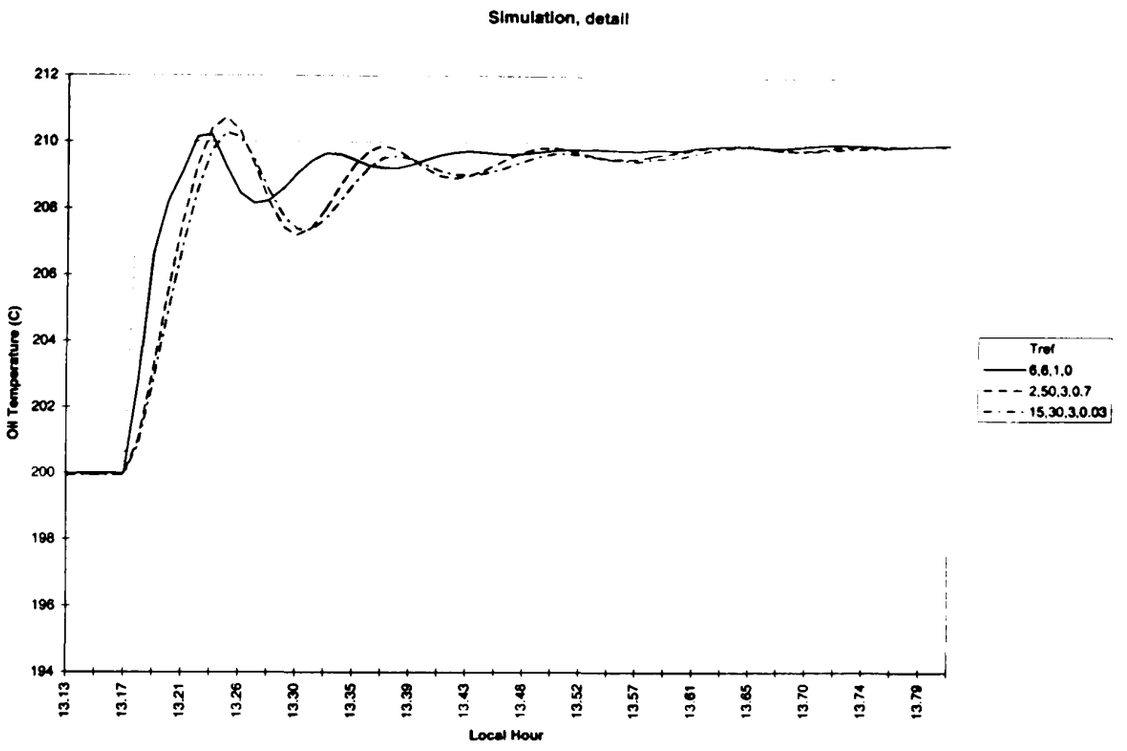

Figure 3.6: Various acurex simulation comparisons

controllers which gave a good response, but without too much overshoot or oscillations, and would therefore not drive the pump too hard, are shown in Figure 3.6. These controllers, with parameters 6,6,1,0; 2,50,3,0.7 and 15,30,3,0.03, were chosen to be the basis for the real implementation of the Acurex plant.

From these initial simulation results there appears to be a tendency for the system under the control of an MBPC controller to respond in a very oscillatory way. No combination of controller parameters appeared to eliminate the oscillation although it is unclear whether this is due to using the single linear model for the basis of the MBPC controller, which could provide inaccurate predictions to the controller, or whether this is a characteristic of MBPC.

3.5 Test campaign

After the initial tuning was carried out using the simulations, the controller was tested on the Acurex field. The performance of the various tuning combinations of the controller was measured by using three different tests -

Set point tracking This was the main basic test carried out to improve the perform-

ance of the controller. From the control room of the Acurex field it is possible to manually set and change the reference temperature (T_{ref}) at any time. The output temperature can then be watched and when the output temperature had settled another change made.

Inlet oil temperature disturbance The second type of test which can be carried out is to see how the controller performs with varying inlet oil temperature. This is achieved by starting the desalination plant mid way through a test. This resulted in a large initial inlet oil temperature disturbance and then usually a smaller continuing disturbance, for example a slow ramping of the oil temperature.

Solar radiation disturbance A final test is to see how the controller performed under fluctuating solar radiation. This was only possible when a cloud or clouds passed in front of the sun, causing a sharp reduction in the solar radiation on the field. During the test campaign there was only two days of clouds. However these occurred right at the end of the test campaign meaning that by this time the controller had been well tuned and a good test could be made.

The Set Point Tracking test is representative of the simulation test and the initial tuning parameters (6,6,1,0 and 2,50,3,1.0) are based on the experience gained from these simulations. Each day new control parameters were chosen based on results from previous days, or the same experiment was repeated in order to gain more information. Table 3.1 shows the full set of experiments carried out in Almería on the Acurex field. Figures showing the results from each day are located in Appendix B. The tests on the 29^{th} through 31^{st} May, involving a sampling time of 13 seconds, are described later.

3.5.1 Tuning parameters

Using the experience gained from the simulations the controller parameters (N_1, N_2, N_u, Λ) used on the plant were of the form $n, n, 1, 0$ where n =6, 7 & 8, and $2, 50, 3, \Lambda$ where Λ = 0.5, 0.7 & 1, and, at the end of the tests a final selection of $15, 30, 3, .03$.

3.5.2 Sampling interval

A different aspect which is briefly investigated is the effect of altering the sampling interval. The standard interval of 39 seconds was changed to 13 seconds on the 29th-31st May. The control parameters were adjusted to (24,24,1,0) to give a comparison with the controller tested on the 28th May (8,8,1,0). The step response coefficients for

Date	N_1	N_2	N_u	Λ	Type of test	Figure Number
23^{rd} May 1996	6	6	1	0	Set Point Following	B.1
24^{th} May 1996	2	50	3	1.0	Set Point Following	B.2
27^{th} May 1996	2	50	3	1.0	Set Point Following	B.3
28^{th} May 1996	8	8	1	0	Set Point Following	B.4
29^{th} May 1996	24	24	1	0	Set Point, Tsamp=13s	B.5
30^{th} May 1996	24	24	1	0	Set Point, Tsamp=13s	B.6
31^{st} May 1996	24	24	1	0	Set Point, Tsamp=13s	B.7
4^{th} June 1996	2	50	3	.7	Set Point Following	B.8
5^{th} June 1996	2	50	3	.5	Inlet Oil Temperature	B.9
6^{th} June 1996	7	7	1	0	Solar Radiation	B.10
10^{th} June 1996	15	30	3	.03	Set Point, Inlet, Solar	B.11

Table 3.1: Details of the Acurex test campaign

the new model were obtained by simply interpolating between the values obtained from the original model.

3.5.3 Implementation issues

Flow limits

For safety reasons the flow rate is strictly limited to between 2 and 9 litres per second. This upper flow limit meant, in practice, that on a clear sunny day the oil would gain at least 60^oC when passing through the field and thus the controller could not follow a set point which was less than 60^oC above the inlet temperature. This should have been ensured by the system operator, however in several cases the reference temperature was set too low which prevented the controller realising the desired response. This can be seen in Figure B.6, between 11.75 and 12.45 hours and again briefly at 13.2 hours and on Figure B.8 between 14.4 and 15.2 hours.

Output temperature

Figure 3.2 shows that temperature measurements are available at the output of each loop ($T_1 - T_{10}$) and at the output of the field (T_{field}). Due to the fact that in practice the individual loop temperatures can vary quite significantly, some loops can be operating at much higher temperatures than would be indicated by T_{field}. Therefore to ensure that none of the loops exceeded safety limits, rather than using T_{field} as the output

temperature for the controller, the maximum value of $T_1 - T_{10}$ is used as the input to the controller. However, since normally one loop is the highest throughout the day, this still gives a good indication of the control performance whilst remaining within operating safety limits.

Flow Saturation

One problem with the controller which was noticed fairly early on in testing was a poor performance during start-up, with the controller taking a long time to react to the output temperature rising above or below the set point. On further investigation this poor performance was identified to be due to the constraints on the flow rates resulting in the control output, the demanded temperature, not being realised. This effect is due to the fact that the demanded temperature, which is output from the controller, is converted by the feed-forward block into a flow rate. However the demanded temperature is used in the next time step by the controller to calculate the next control move. Thus the effect of the saturation meant that the controller 'thought' that the system should be reacting more than it was and thus tried to compensate, thus increasing the demanded temperature. The problem was solved however by ensuring that when the limits for flow were hit only the demanded temperature which would result in the flow being equal to the limit was actually used. The effect of this change can be clearly seen in the difference between startup on May 24th, Figure B.2 page 169, and that on June 6th, Figure B.10 page 177.

C-code

A complete listing of the file "regulaci.c" which was used on the 10th June is provided in Appendix C, page 179. This includes the G matrix and the matrix *gtgig*, where

$$gtgig = (G^T G + \Lambda I)^{-1} G^T \tag{3.3}$$

Since only one control move is to be implemented, only one row of this matrix is entered and used in the controller. For the controllers of the type (n,n,1,0) *gtgig* is a single value.

3.6 Results

Full results from each day of testing are presented in Appendix B Figures B.1 through B.11, on pages 168–178, and details of these plots presented below in Figures 3.7 to 3.11. As far as possible similar scales are used to allow easy comparison between days.

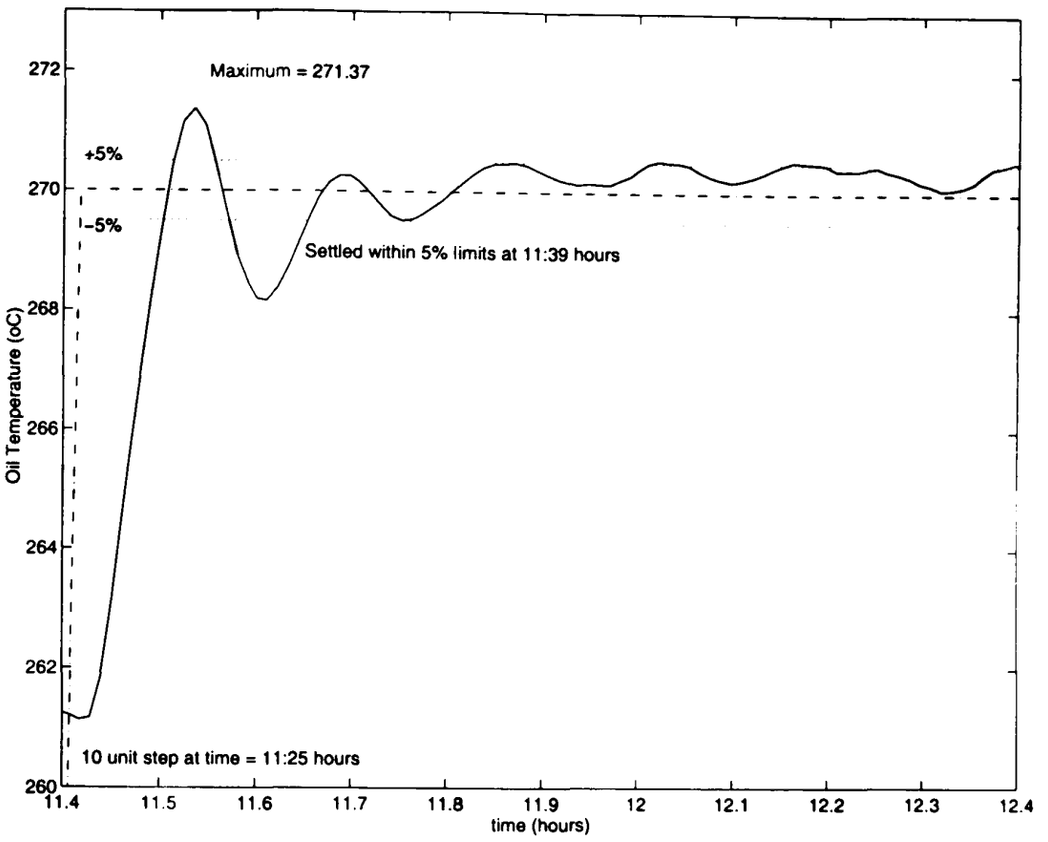

Figure 3.7: 4th June. Detail of set point following (2,50,3,.7)

Figure B.1 shows the first proper day of testing carried out at Almería. This first attempt at the tuning parameters uses a single point, 6 time steps ($6 \times 39secs$) into the future, to calculate its predictions and, apart from start up problems, where the output temperature rose far above the reference temperature, which were later eliminated, the system shows good responses to changes in set points.

3.6.1 Set point tracking

Figure B.8 shows another set of results, using the more complicated set of tuning parameters, and a detail from this is shown in figure 3.7. A full set of different performances for different tuning parameters is shown in Figure 3.8. These graphs show the expected effect of varying the parameters. Figure 3.8a. shows a much more aggressive response, with more overshoot and oscillatory behaviour than Figure 3.8b. This is due to N_1 and N_2 being smaller and making the system work harder to get to the reference temperature. Figures 3.8c., d. and e. show the effect of varying the damping factor Λ, with a lower value giving a less damped and more oscillatory response.

Note that in figure 3.8c. the experiment was completed before the step response

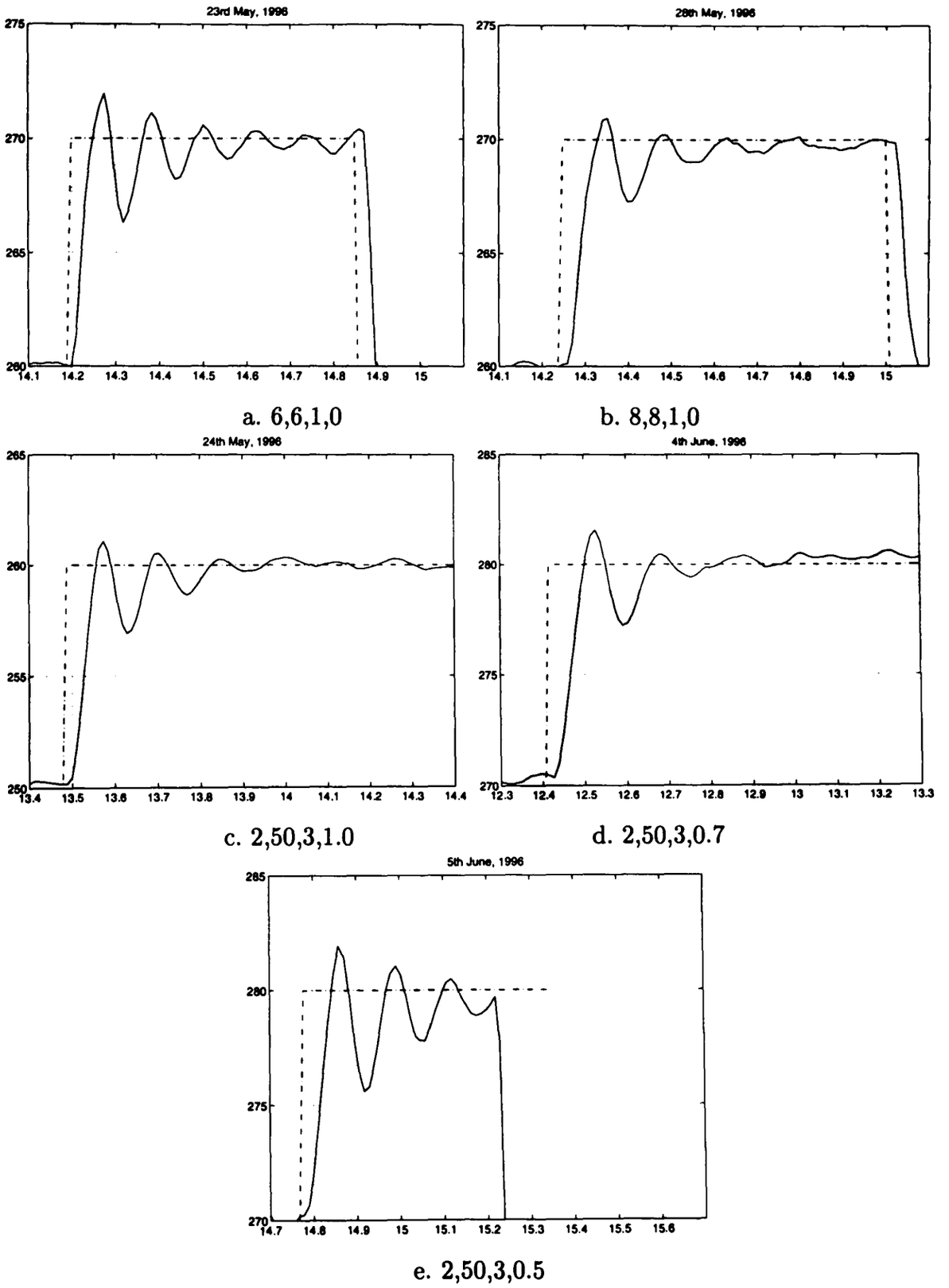

Figure 3.8: Response of T_{out} (—) to step changes in T_{ref} (- -) with varying MBPC parameters (N_1, N_2, N_u, Λ). All axes at the same scale. x-axes – time (hours); y-axes – Oil temperature (^oC).

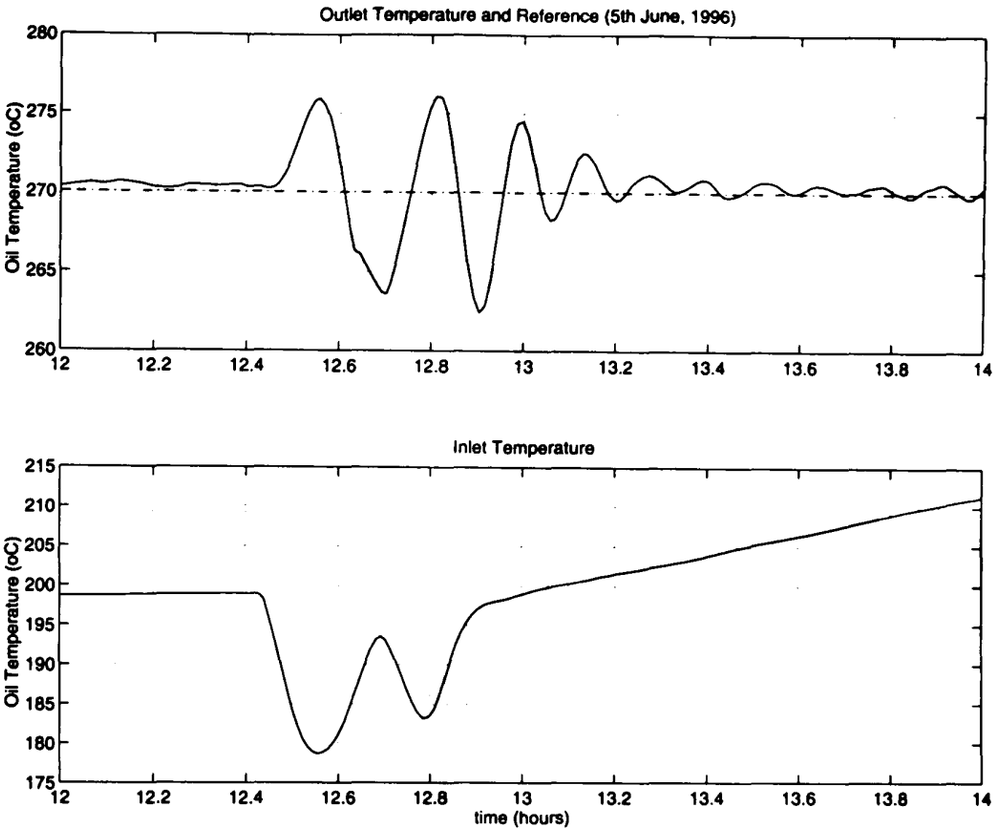

Figure 3.9: 5th June. Detail of inlet disturbance (2,50,3,.5)

had settled.

3.6.2 Inlet oil temperature

Figure B.9 shows the performance of the controller when the desalination plant, as described in section 3.2, is switched on. A detail from this is shown in Figure 3.9. After the desalination plant was connected at about 12.4 hours there were two large dips in inlet temperature followed by a slow ramping up of the inlet oil temperature. Unfortunately it was not possible to repeat this test with different parameters to see the change in performance, but this controller (2,50,3,.5) was able to minimise the effects of varying inlet oil temperature well.

3.6.3 Solar radiation disturbance

As noted above, due to the very good weather during the test campaign, there was only one good day of clouds to test the performance of the controller under varying solar radiation. Figure B.10 shows this day's results with Figure 3.10 showing a detail from this. It should be noted that due to the lower safety limit on the oil flow ($2l/s$) it is

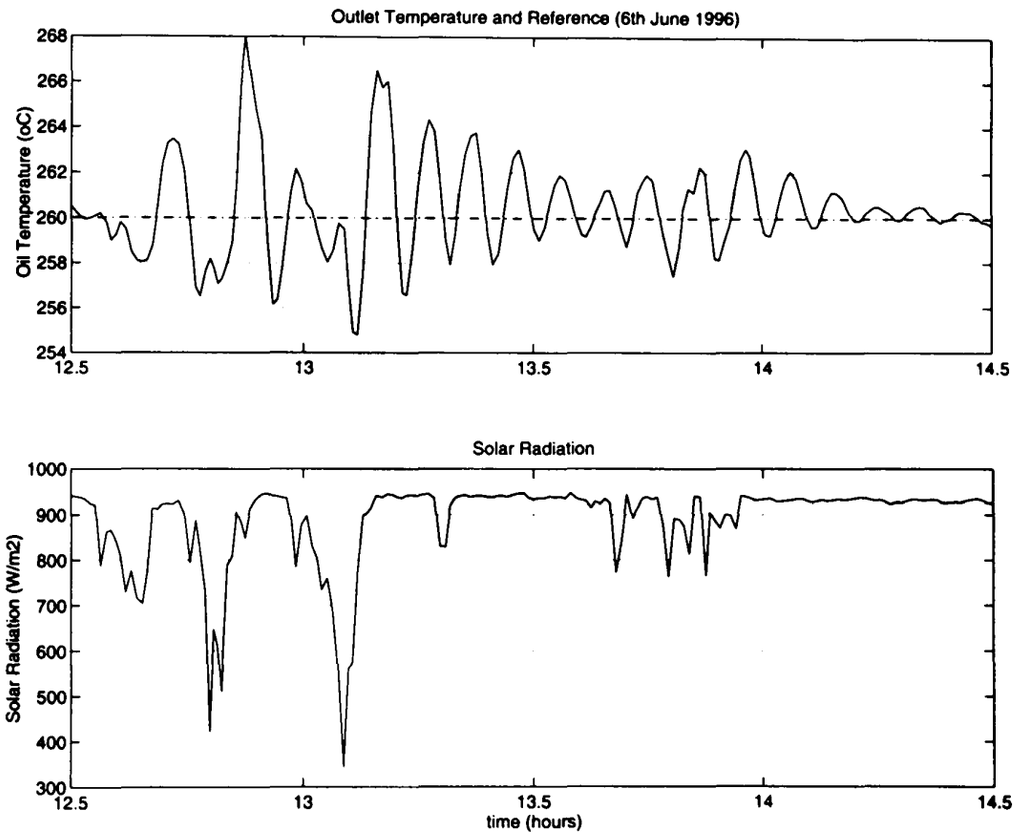

Figure 3.10: 6th June. Detail of solar disturbance (7,7,1,0)

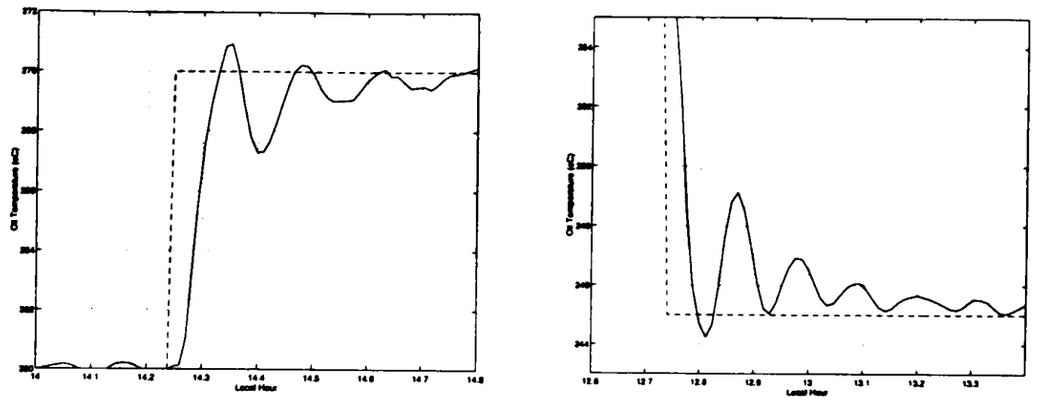

28th, Sampling time = 39seconds, (8,8,1,0)

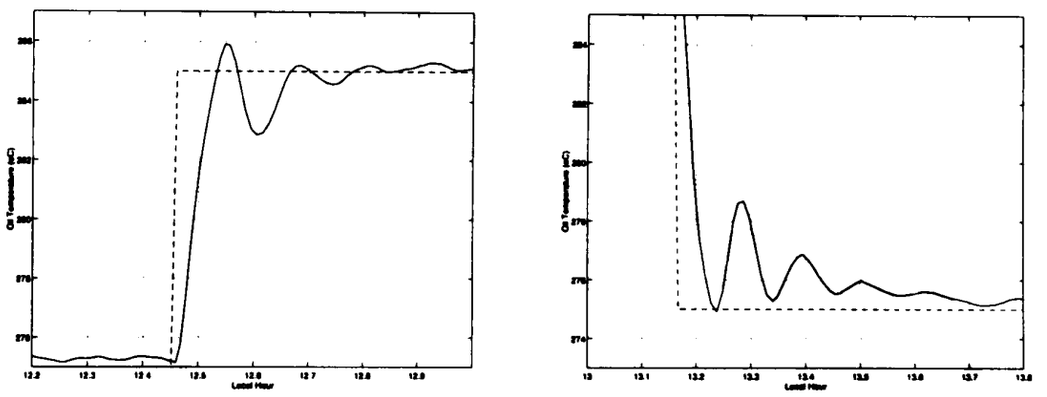

31st, Sampling time = 13seconds, (24,24,1,0)

Figure 3.11: Details of effect of varying sampling time

not always possible to successfully eliminate the effect of large drops in solar radiation, such as those seen at the beginning of the test. Also, below $300W/m^2$ of solar radiation the field is not able to heat up the oil. The one controller that was tested on the system gave a reasonable performance and kept the system stable through some very severe changes in solar radiation.

3.6.4 Sampling time

Figure 3.11 shows some details of the effect of changing the sampling time from 39 seconds down to 13 seconds, but in all cases looking the same time into the future. i.e. 8 time steps when the sampling time is 39 seconds and 24 time steps with a sampling time of 13 seconds. Although there is slight differences between the step responses the effect of changing the sampling time would appear to have little effect and no firm conclusions can be made, especially with such a small set of results.

3.7 Comparison with other controllers

Due to the fact that the solar plant at Almería is a popular test facility there are several papers published showing results obtained using different types of control methodologies. Therefore it is possible to compare the results obtained with the MBPC with these other type of controllers, although only by interpretation from the graphs in the published papers. Most of the published papers, regarding testing controllers on the plant, are written by one or more of Rubio, Berenguel and Camacho , e.g. [5, 13, 89, 90], who have spent many months analysing the plant and testing many types of controllers with large amounts of time for tuning. Comparisons with the controllers presented in these papers is not easy due to the different solar conditions and inlet oil temperature profiles and also due to the resolution of the graphs presented in the papers. From the published papers some suitable comparisons are with the Fuzzy Logic Controller from [90], which was tested and tuned over a period of 7 months, the Gain-scheduling generalized predictive controller from [13], and the LQG/LTR controller presented in [89]. All these controllers are claimed in the papers to have good responses. In comparing with each case the results presented above for the basic MBPC controller appear, in general, to be slightly more oscillatory than the other controllers but settle the system as quickly, if not quicker, than any of them.

3.8 Discussion

All the controllers tested were successfully implemented and in general gave good responses although all were slightly oscillatory. The use of the system gave a firm knowledge of the basic principles of MBPC and experience of the difficulties of implementing a controller in real life.

In particular, experience of the effect of varying the various tuning parameters was gained. The basic rules concerning the effect of looking further or closer into the future is confirmed through the use of the parameter combinations 6,6,1,0 and 8,8,1,0 (figures 3.8 a. and b.). These confirm that looking closer into the future results in harder control action and hence a faster although more oscillatory response. A similar effect is seen through varying the damping factor, Λ, in the tuning combinations 2,50,3,Λ. A lower value of Λ results in less damping and a faster more oscillatory response. Through the tests carried out on the plant it was not clear if there was any advantage in performance in using the more complicated 2,50,3,Λ form over the n,n,1,0 form, although there was insufficient time to properly test the controllers with solar radiation disturbances and

inlet temperature disturbances to see if there is any perceptible difference in these tests. For ease of implementation the form n,n,1,0 appears to give satisfactory results and the results obtained from all the MBPC tests compared well to other types of controllers tested on the same plant.

The use of the feed forward block is unsatisfactory as it does not allow direct control of the pump and also does not allow for prediction of the effect of solar radiation and inlet temperature disturbances into the future. Future work on this system would include a direct model for flow to T_{out} with disturbance models for Solar radiation and Inlet temperature available in order to predict their effect on T_{out} in the future. Also the benefits of reducing the standard sampling time from 39 seconds should also be further investigated.

The results from he work carried out in Almería give an initial indication of the usefulness of MBPC to the renewable energy industry in general. Due to the ease of implementing the controller on the plant and the performance of the controller in practice the prospect of MBPC being suitable for, at least, some other renewable energy applications is strong. However before any firm conclusions are made the application to wind turbines is considered.

Chapter 4

Wind Turbines

4.1 Introduction

The second application for the MBPC technique is a variable speed wind turbine. In this chapter a general introduction to wind turbines is presented, discussing their development and current status, before going on in later chapters to examine the modelling of wind turbines in detail and then finally applying the MBPC technique.

4.2 Wind energy

Wind arises from uneven heating of the earth's surface. The earth's equatorial regions receive more solar energy than the polar regions and this causes large scale convection currents in the atmosphere. The amount of energy contained in these winds is huge. It is estimated that about 1% of the incoming solar energy to the earth is converted into wind energy and of that only 1% is equivalent to the world's daily energy consumption. [76]

The power in the wind is very apparent (as when trying to walk against a strong wind) but converting this energy into useful work is not so simple. Historically windmills have been used for the last thousand years, providing mechanical power all over Europe, the Middle East and the Far East. Windmills gained maximum usage in the 17th and 18th Centuries before starting to decline in the face of alternative forms of mechanical power based on thermal energy from the combustion of fossil fuels. These steam engines, steam turbines, and oil and gas engines provided more power from smaller machines which were continuously available and could be taken to where the power was needed. By comparison windmills had to be situated where the wind blew and even then the wind would not always be strong enough. However they did survive

through the industrial revolution mainly in remote areas of the USA, USSR, Australia and Argentina. Their latest revival came with the increase in electricity usage and also the development of aerodynamic knowledge with the advent of the aeroplane. This resurgence continued slowly through the 20th Century until the international oil crisis of 1973 gave a very large boost to the field. Before this point wind energy had been seen as being an uneconomical form of electricity production but after the oil crisis it became more and more apparent that it is actually a very economical source of electricity production with many beneficial side effects (e.g. environmentally benign, reduced dependency on oil producing countries, creation of jobs). The conversion of wind power into electricity overcomes the problems of variability (and sometimes unreliability) of the wind resource and also the problems of location (i.e. it is not always windy where you want work done). The electricity produced by the turbine can be either used, in remote locations, to charge batteries to enable the power to be used whether the wind is blowing or not, or be fed directly into the electrical grid which accommodates the fluctuation in supply in the same way as fluctuations in demand. Studies done in the U.K. have estimated that 20% of our current electricity demand could be met by a variable source like wind without any restructuring of the current grid system. [73]

4.3 The wind resource

Although this resource is not evenly distributed around the globe studies in Europe [105] have shown that 10% of the European Community's electricity could be generated by 100,000MW of wind turbine installed capacity. This is equivalent to less than 20% of Europe's readily usable wind resource and spread throughout Europe this plant would require a total land area no greater than the the size of the Island of Crete. Also all but 1% of this land would be available for agriculture [52]. This also ignores the very large off-shore resource which is just beginning to be exploited off Denmark and which could be harnessed in many areas of shallow water.

The United Kingdom itself has 40% of Europe's total realizable wind energy potential. Extensive studies by ETSU [44] in 1994 have shown that if all suitable sites were used about 143,000 300kW turbines (quite small sized turbines by today's standards) could be deployed capable of an annual production of about 122TWh. However planning permission restrictions, remoteness of sites and economic considerations are likely to reduce this to about 50 TWh per year (20% of the present U.K. electricity demand). The current trend for using larger sized wind turbines is likely to increase this possible target.

4.4 Power in the wind

For air, with a density ρ ($= 1.23kg/m^3$) travelling at speed $V\,m/s$, the kinetic energy ($\frac{1}{2}mv^2$) per unit volume E is

$$E = \frac{1}{2}\rho V^2 \tag{4.1}$$

Taking an area A $units^2$ at right angles to V, then a volume of AV $units^3$ per second flows through A. Hence

$$\text{Power} = \text{energy per unit volume} \times \text{volume per second}$$

$$\therefore P = \frac{1}{2}\rho V^2 \times AV = \frac{1}{2}\rho AV^3 \tag{4.2}$$

This is the power that the wind contains. As can be seen the power is directly proportional to the area and proportional to the cube of the wind speed. This shows the importance of selecting a site with a good mean wind speed, as doubling the wind speed results in eight times the power. It is however impossible to extract all the power from the wind as this would result in the air stopping dead after the wind turbine blades and building up. The theoretical maximum that can be extracted from the wind is known as the Betz Limit and is 59.3% of the total power. In practice the actual factor of extraction (or power coefficient C_p) is usually about $0.4 \ldots 0.45$ for a well designed turbine. For example, a wind turbine with a swept area of diameter 30m and a $C_p = 0.4$, could theoretically produce, at a wind speed $V = 12m/s$,

$$P = C_p \times \frac{1}{2}\rho AV^3 = 0.4 \times 0.5 \times 1.23 \times \pi \times 15^2 \times 12^3 = 300.4kW$$

4.5 Wind turbines

Modern day wind turbines for the production of electricity come in two forms — horizontal axis and vertical axis turbines. Practically all the commercial turbines today are horizontal axis with vertical axis turbines being mainly restricted to research purposes.

Figure 4.1 shows a photograph of a typical wind farm containing several three bladed horizontal axis wind turbines. At the top of the tower the nacelle, see the cut away diagram in Figure 4.2 [32], contains the key components of the wind turbine, including the gearbox, and the electrical generator. Service personnel may enter the nacelle from the tower of the turbine. The rotor blades capture the wind and transfer its power to the rotor hub. On a modern 600 kW wind turbine each rotor blade measures about 20

Figure 4.1: A wind farm

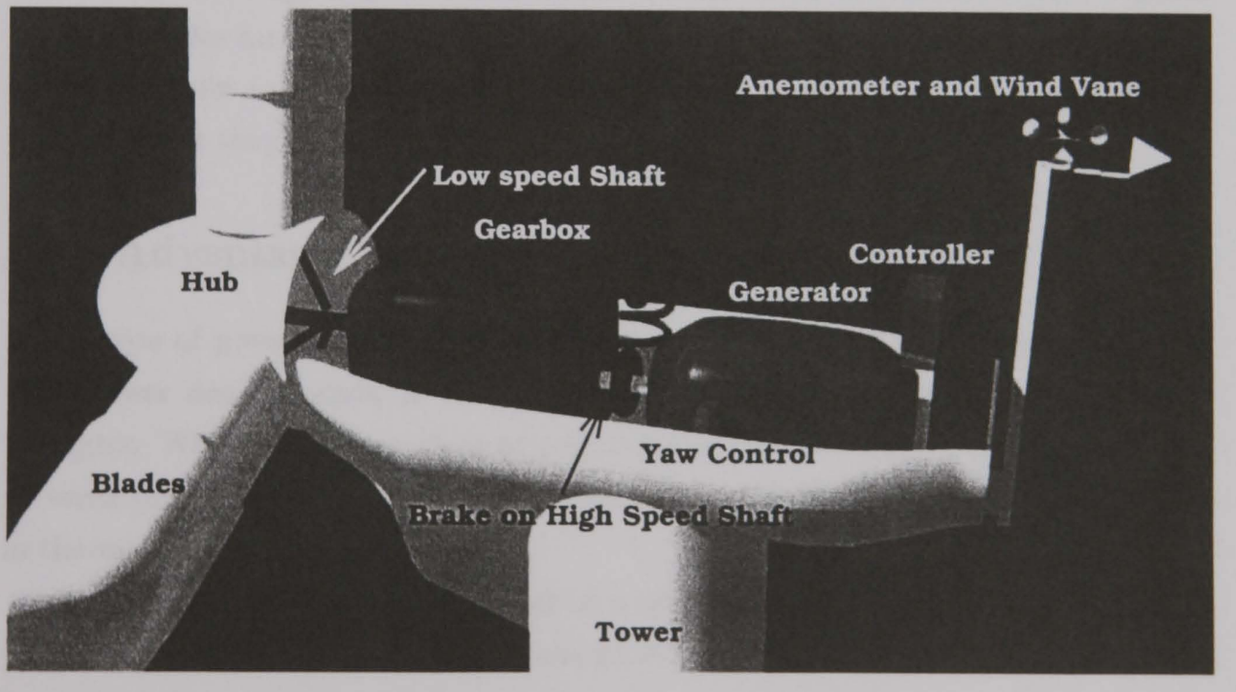

Figure 4.2: Wind turbine nacelle

metres (66 ft.) in length and looks like a wing of an aeroplane. The hub of the rotor is attached to the low speed shaft of the wind turbine which in turn is connected to the gearbox. Most rotors rotate relatively slowly, about 19 to 30 revolutions per minute (RPM) and the gearbox makes the high speed shaft turn approximately 50 times faster than the low speed shaft, making it rotate at approximately 1500 RPM, driving the electrical generator. An emergency mechanical disc brake is located on either the high or low speed shaft and is used in case of failure of the aerodynamic brake or when the turbine is being serviced. The electrical generator is usually an induction generator or asynchronous generator rated, for a modern large wind turbine, at between 500 and 1,500kW. The nacelle also contains the controller (unless there is a separate area for this at the base of the turbine) which controls the wind turbine operation and also monitors the condition of the wind turbine and controls the yaw mechanism. In case of any malfunction, (e.g. over-heating of the gearbox or the generator), the controller automatically stops the wind turbine and alerts the turbine's operator. The tower of the wind turbine carries the nacelle and the rotor. Generally, it is an advantage to have a high tower, since wind speeds increase farther away from the ground. A 600 kW turbine has typically a tower height of 40 to 60 metres (132 to 198 ft., the height of a 13-20 story building), may be either a solid tubular tower or a lattice tower. Tubular towers are safer for the personnel who have to maintain the turbines, as they may use an inside ladder to get to the top of the turbine. The advantage of lattice towers is primarily that they are cheaper.

4.6 Advantages and disadvantages of wind turbines

Every type of power generation has an impact on the environment, but the effect of wind power developments, in sharp contrast to conventional energy technologies, is negligible. Wind turbines produce no pollutants, no harmful gas emissions, no effluent, no waste products and no radioactivity. There are no ill effects to populations elsewhere in the world or to future generations.

Although the environmental impact of wind turbines is far lower than other power producing technologies, there are some local impacts on the environment which should be mentioned.

Visual intrusion

The most significant impact that a wind development will have is on the landscape. Although wind turbines are unavoidably conspicuous their effect can be minimised

by careful site selection and placing of individual turbines. Such sensitively designed schemes can fit into and be a welcome part of the existing landscape and this has been shown, through many surveys [10], to be the general opinion of people living near wind farms.

Noise

Unfortunately some wind turbines used in early wind farms were very noisy and this has led to a general perception that they are still so. However this is not the case and much work has been carried out in minimising noise from the blades, by careful attention to their design and manufacture, and also from the gearbox and generator, by efficient engineering and sound insulation in the nacelle. This has led to a great reduction in noise to a point where at the nearest dwelling to a wind farm any noise from the wind turbines will generally be masked by the noise of the wind in the trees, bushes, etc. or other background noise.

Birds

Concerns were raised early on in the development of wind farms about the possibility of birds flying into the rotors. However extensive studies carried out in Germany, the Netherlands, Denmark and the U.K. have shown that wind turbines, despite their size and moving blades, do not pose any special problem. In general birds either seem at ease with them or do not approach closer than about 100m to a turbine. Overhead powerlines, cars, and most of all household cats, pose a far greater threat to birds than wind turbines.

Radio and TV signals

There is the potential for wind turbines to cause interference on telecommunication systems, but this can be easily overcome with careful siting and minor technical adjustments [10].

4.6.1 Environmental benefits

Every unit of electricity (kWh) produced by wind power displaces a unit of electricity which would have been produced by a power station burning fossil fuels [83]. In the U.K. this would be from a coal fired power station. It does not displace nuclear or gas as these are normally run continuously as "base-load". In practice this means that a single 600kW wind turbine will displace 1350-2250 tonnes of carbon dioxide (CO_2)

per year, 15.7-34.3 tonnes of sulphur dioxide (SO_2) per year and 4.7-11.1 tonnes of nitrous oxides (NO_x) per year. Also this single wind turbine would produce enough electricity for between 370 and 500 homes [10]. (Based on the U.K. average household consumption of electricity and a factor of 0.3-0.4 representing the amount of time the turbine will be producing its rated power due to the variability of the wind.)

So as can be seen, power from the wind can have a significant positive environmental effect with very little adverse environmental impact of its own.

4.6.2 Other benefits

Other benefits offered by wind are

- Free fuel. The wind costs nothing.
- Negligible decommissioning costs. Turbines do not pollute the soil and dismantling a wind farm is cheap, quick and easy and the land can be returned to its previous condition [48].
- Very low land use factor. Wind farms take up only 1-2% of the land and the rest can continue to be used as before [48].
- Local jobs are created when the turbines are erected and also for their maintenance [47].
- The fact that electricity use is normally higher when it is windier (usually in the winter) means that wind power matches the energy demand profile of many countries [49].
- If the costs of pollution were to be taken into account, wind energy is one of the cheapest sources of power available [46].

4.7 Current world status

Most of the wind energy programmes which were carried out throughout the early parts of this century had been ended by the late 1960s due to the price of energy from fossil fuels and nuclear power being inexpensive. At the end of the 1960s there was little useful documentation and almost no experimental data from these several decades of activities around the world. Despite some large advances made since the end of the 19th century, wind turbine designers in the early 1970's had little firm information upon which to build.

New growth in the wind industry was prompted by a response to market and regulatory forces resulting from a rapid rise in oil prices first with the 1973 Arab oil embargo and then again in 1980 following the Iranian revolution. Coinciding with this in 1980, California's governor held a conference to attract financial interest in wind power development and this, coupled with excellent wind resources, abundant low cost land with few land use conflicts, very favourable purchase rates and strong state regulatory support for alternative sources of energy, partly in the form of tax credits, prompted the "California Wind Rush". Between 1981 and 1987, 15000 wind turbines were erected in California with a capacity of almost 1500MW. Most of these were small scale turbines, and many of them failed due to bad design. However, the setting up and running of so many turbines proved invaluable experience for many manufacturers and developers as well as proving the reliability in the field of various types of wind turbines [97].

With the removal in 1987 of the attractive tax credits American installation of new wind turbines has continued only slowly. However in Europe, where there was not any initial "rush", wind installations developed slowly in the early 1980's and later much more rapidly, partly prompted by the Chernobyl nuclear accident in 1986. Table 4.1 [32, 1, 10, 45] shows this rapid growth, mainly in Europe, in the last 5 years ('95-'99). This growth has been helped by some subsidies and government aid but has allowed the industry to develop and prices for electricity production have fallen quickly to levels where it is, in certain areas, competitive with other *new* electricity generating installations, ignoring subsides to wind turbines and also ignoring external costs which should be added to many other form of electricity generation. Table 4.2 [32] shows the largest manufacturers of wind turbines in 1997, dominated by Denmark, a country with no indigenous forms of fossil fuels which has built up its wind turbine technology slowly and steadily over many years. The popularity of the industry in Denmark has much to do with the system of community ownership rather than ownership by large electricity companies. Table 4.3 [10] shows the situation in the United Kingdom since the government started its Non-fossil fuels obligation (NFFO) programme in 1991.

4.8 Constant speed and variable speed machines

Horizontal axis wind turbines operate in the field in one of two ways: constant speed operation or variable speed operation. In constant speed wind turbines the turbine's blades rotate at a fixed speed, regardless of the speed of the wind. This is due to the generator being directly linked to the grid and thus the frequency of the grid dictates the speed of rotation of the high speed shaft. There are however several potential

Country or Region	End of year installed Capacity (MW) 1995	1996	1997	1998	1999
Denmark	637	835	1135	1433	1733
Germany	1132	1552	2002	2872	4444
Greece	28	29	69	69	121
Ireland	7	11	51	63	68
Italy	32	70	110	199	249
Netherlands	249	299	349	375	428
Spain	133	249	449	822	1722
Sweden	69	103	123	176	216
U.K.	200	273	333	334	343
Total Europe	2548	3514	4789	6384	8915
U.S.A.	1591	1596	1646	1770	2502
India	576	820	870	1015	1077
Total World	4821	6105	7679	9751	13400
Increase each year	-	26.6%	25.8%	27.0%	37.4%

Table 4.1: Wind turbine markets

	Manufacturer	Country	MW Sold 97	%
1	NEG Micon	Denmark	309	19.7
2	Vestas Wind Systems	Denmark	290	18.5
3	Enercon	Germany	223	14.2
4	Bonus Energy	Denmark	222	14.1
5	Gamesa	Spain	93	5.9
6	Made	Spain	75	4.8
7	Nordex	Denmark	67	4.3
8	Desarrollos	Spain	54	3.4
9	Zond	USA	38	2.4
10	Wind World	Denmark	29	1.9
11	Tackle	Germany	29	1.8
	Other companies		113	7.2
	Total all companies		1542	98.4

Table 4.2: World's largest wind turbine manufacturers in 1997

Year	No. of new Windfarms	Year total	Total
91	1	4.00	4.00
92	6	24.98	28.98
93	10	89.95	118.93
94	4	23.35	142.28
95	7	45.10	187.38
96	5	70.33	257.71
97	6	50.30	308.01
98	2	12.40	320.41
99	4	18.60	339.01
Average size of windfarms			9.4MW
Avg. size of turbines in 1992			300kW
Avg. size of turbines in 1999			660kW

Table 4.3: Installed capacity of windfarms in the U.K. (MW)

advantages in using variable speed wind turbines and allowing the rotor to change speed in sympathy with the wind speed. The main potential advantages of variable speed wind turbines (VSWTs) are,

1. Increased energy capture in low wind speeds.
2. Reduced aerodynamic noise in low wind speeds. Noise from wind turbines in low wind speeds is more significant than in high wind speeds where the noise from the turbine is normally masked by noise caused by the wind on the surrounding landscape, e.g. bushes, trees, etc.
3. Reduced drive train loads in high wind speeds, which helps extend the working life of the turbine.
4. A wide choice of operating strategies which can be employed for different operating conditions and requirements.

The main disadvantage is the increased cost and complication of the introduction of power electronics. Power electronics ensure that the wind turbine can be connected to the grid safely by matching the frequency of the output to the frequency of the grid. The cost of installing power electronics is sometimes seen as prohibitive, but with

advances in their technology (mainly through their increased use in other fields) the costs are reducing and the added potential benefits of variable speed are being seen as more attractive.

Table 4.4 summarises some of the relative advantages of both types of systems [51].

Constant Speed	Variable Speed
Simple and cheap electrical system	Higher Energy Capture
Higher reliability	Low transient torques
Lower probability of excitation of structural Resonances	Cheaper gearbox
No frequency conversion interface meaning current free of harmonics	Electrical interface could provide damping if required
Lower capital cost	No problems with synchronization
	Better quality electrical power

Table 4.4: Advantages of constant speed and variable speed systems

4.9 The need for control

As windspeed increases the energy available for capture increases as roughly the cube of the windspeed. High windspeeds are not encountered frequently enough to make it economic to extract the total energy available. To do this would require a very high rating for the power-train (rotor, low-speed shaft, gearbox, high-speed shaft and generator), which during normal windspeeds would operate at a fraction of its capability and in a very inefficient manner. Also the cost of over engineering involved makes this prohibitive. To avoid this a form of aerodynamic power limiting is required. At some predetermined windspeed (rated windspeed) the power input to the turbine will have reached the limit for normal operation (rated power). When the windspeed exceeds the rated value the excess power in the wind must be discarded by the rotor to prevent the turbine overloading. The power is maintained at its rated value until a maximum windspeed is reached when the turbine is shut down for safety reasons (cut out windspeed). A typical power curve is shown in Figure 4.3. Wind turbines follow this power curve

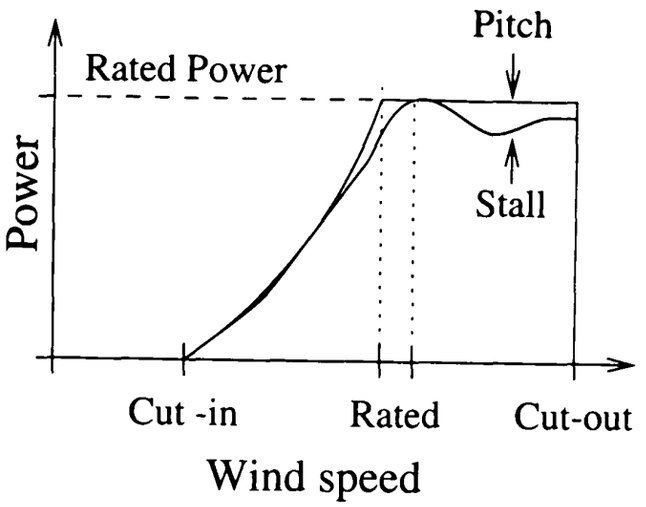

Figure 4.3: Power curves for stall and pitch regulation

in different ways. Variable speed operation is discussed in detail in a later chapter. Constant speed machines achieve this power limiting either by pitch control or stall control as described below.

Pitch control, which can be thought of as the active rather than passive approach, uses blades which can be rotated in high wind speeds in order to reduce the lift on the blade and thus reduce power production. During start-up and shutdown the blade pitch is set to, what is termed, full feather (90^o). During operation at below rated windspeeds the pitch is set to fully-fine ($\approx 0^o$) and as wind speed rises above that which would give rated power, pitch is increased to part feather, thus reducing the lift-coefficient and limiting torque. The advantages of this are good power control, flapwise aerodynamic damping, load reduction with wind speed, low loads when stationary, assisted start-up and in built braking. The disadvantages are the extra cost of the pitch mechanism and control system along with the associated extra complexity and reduced reliability.

Stall controlled wind turbines have the rotor blades bolted onto the hub at a fixed angle. The geometry of the rotor blade profile, however, is aerodynamically designed to ensure that when the wind speed becomes too high, it creates turbulence on the side of the rotor blade which is not facing the wind. This turbulence, or stall, prevents the lifting force of the rotor blade from acting on the rotor. The basic advantage of stall control is that it does not require a system for pitching the blades which can significantly reduce the complexity of the control system. On the other hand, stall control represents a very complex aerodynamic design problem, and has related design problems in the structural dynamics of the whole wind turbine, e.g. stall-induced vibrations. Stall control also loses some energy compared to pitch control (see Figure 4.3), has higher

stationary loads, does not provide an assisted start-up and a separate brake is needed to prevent over speed.

Both types of machine are being used in developments all over the world. The control system implemented in the turbine can influence the effectiveness of operation and also the working life of the machine. In the case of constant speed machines an active controller is only necessary for pitch regulated systems as the stall case only requires supervisory control for startup and shut down. However in variable speed case both stall and pitch regulated require active control while operating.

The effect of implementing an MBPC controller on a variable speed wind turbine stall regulated machine is investigated in Chapter 8 to see what benefits, if any, may be gained. However before this, in chapter 5 a review of control techniques used in variable speed wind turbines is presented. After this a full description of the models used to simulate a wind turbine is detailed in chapter 6 and in chapter 7 the wind models used in the design, simulation and testing of wind turbines.

Chapter 5

Variable Speed Wind Turbines — Control Objectives and Strategies

5.1 Introduction

Before MBPC is implemented and assessed for a variable speed wind turbine (VSWT) a discussion of general wind turbine control objectives and strategies is presented. Control objectives define the aims of the VSWT controller. These objectives are very important as a control system can only be as good as the criterion to which it is designed.

Control strategies define the way the controller will try to achieve these aims. By looking at the multitude of strategies available a set is chosen which should best achieve the control objectives. The chosen strategy is fully described before going on to review some techniques that have been used previously in practice and studied in academic research.

5.2 Control objectives

The blades of a wind turbine sweep through a complex time-varying three-dimensional wind field. The structure of the wind field is a combination of wind speed turbulence (local variations in wind speed), wind shear (increase in wind speed with height) and tower shadow (reduction in wind speed at the tower). The turbine is subject to induced torques and loads which depend on not only the local variations on wind field but also in variations which occur upstream and downstream from the turbine by as much as ten rotor diameters. Hence the wind speed experienced by a wind turbine is very different from that experienced by an anemometer. Therefore it is unrealistic to base a control

strategy on wind speed measurement.

The interaction of the wind turbine with this wind field induces transient loads which vary both in time and space over the machine. For high wind speeds, these transient loads need to be smoothed to avoid excessive ratings of components. The fluctuating loads can manifest themselves as very rapid and large fluctuations in generated power. One control objective could be to smooth the generated power when operating in high winds. However, this in itself is not sufficient. The cost effectiveness of a wind turbine depends heavily on being able to have a long working life whilst minimising over-engineering. It follows that the real purpose of the control system is not to smooth power but to reduce these transient loads and thus reduce fatigue throughout the turbine. In smoothing these loads the generated power is smoothed, but the converse is not necessarily true.

A second objective of the control system is to ensure that the power-train (the drive train and power generation unit) has the appropriate dynamics. Due to the fact that the generator in a variable speed wind turbine is not coupled directly to the grid the drive train has very little natural damping, and the control system should aim to provide this extra damping.

A third objective, which is important for all wind turbines, is the maximising of energy capture which is very dependent on the choice of control strategy and effectiveness of the controller.

The emphasis in the discussions below concentrates on the first and third objectives as these are directly related to the potential advantages of variable speed wind turbines. In achieving these objectives both the control strategy and the synthesis of the controller must be addressed as both have an effect.

In general the control strategy determines the drive-train loads corresponding to very low turbulent wind conditions. The amount of extra drive-train loads resulting from normal turbulent wind conditions are determined by the effectiveness of the controller in realising the control strategy. Similarly when considering power capture the control strategy determines the maximum amount of power the wind turbine can capture. Whether this power capture is achieved depends on the controller performance. However when considering structural loads, which contribute to dynamically induced fatigue, these are highly dependent on the control strategy being employed but less dependent on the performance of the controller. Thus it can be seen that the choice of control strategy is crucial to attaining the control objectives. If the control strategy is inappropriate then the controller implementation can never attain the control objectives.

5.3 Control strategies

Variable speed turbines allow the rotor speed to be varied with windspeed. However there are a multitude of possible strategies that can define that relationship. The most obvious manner in which to define a control strategy would be to specify the rotor-speed simply as a function of windspeed; that is, defined in the rotor speed/windspeed plane. However, both the operating point (nominal rotor speed, torque, etc) and the local dynamics vary with the wind speed experienced by the turbine, which, as mentioned above, cannot be directly measured. Hence the wind speed must be estimated from, for example, electrical power and rotor speed, and then the operating point calculated from this estimate. This approach has several problems as the aerodynamics are non-linear and non-uniquely related to the windspeed; that is, there may be more that one wind speed for a given operating point and more than one operating point for a given windspeed. Therefore, this method should be avoided.

A better way for defining control strategies is using the torque/rotor speed plane. Any control strategy can be uniquely defined by a curve in this plane and relies on the rotor speed and an estimate of aerodynamic torque with no knowledge of the windspeed being required. This strategy, or curve, in the torque/rotor speed plane defines the minimum loads and maximum energy capture of the turbine and the associated control is simply required to track the line as closely as possible to minimise any extra loads or losses in energy capture.

The operation of the variable speed wind turbine is split into four main areas relating to wind speeds that can be described as very low, low, high and very high. The machine is shut down in very low and very high wind speeds, normally below 5m/s and above 25 m/s, and the operations of startup and shut down associated with these wind speeds is covered by the supervisory controller and is not discussed here. The active control of the wind turbine concerns itself with below and above rated wind speeds. Both these ranges of wind speeds require different control strategies and this in turn results in a need to switch between one to the other as the wind speed fluctuates. Both above and below rated control strategies and the method of switching are discussed below after the description of the power coefficient to tip speed ratio ($C_P - \lambda$) relationship which is used as the basis of below rated operation.

5.3.1 The $C_P - \lambda$ relationship

One of the main relationships that is used to define the operation of a variable speed wind turbine, at least in low wind speeds, is the $C_P - \lambda$ curves of the blades. C_P is the

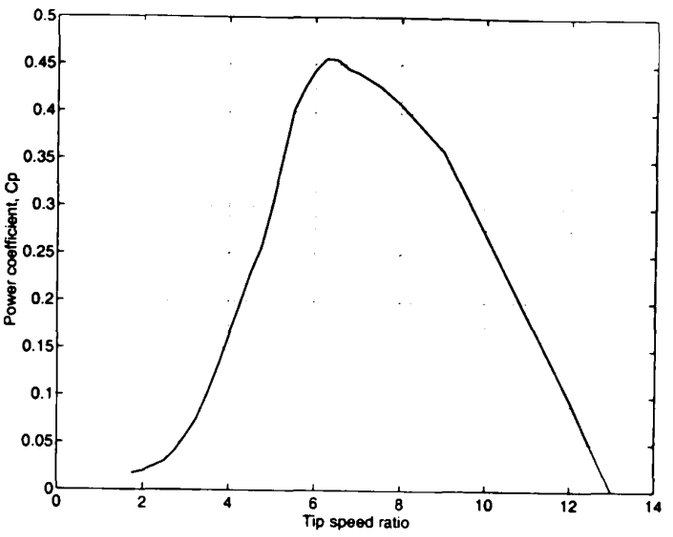

Figure 5.1: $C_P - \lambda$ relationship

power coefficient, which, as described previously, is the factor of extraction of power from the wind and λ is the tip speed ratio, defined as the ratio of tip speed to wind speed, V, by

$$\lambda = \frac{\Omega R}{V} \tag{5.1}$$

with R the radius of the rotor and Ω the angular velocity of the blades. A plot of this relationship for the blades of the turbine being investigated is shown in Figure 5.1. As can be seen there is a value of λ, λ_{opt}, which results in a maximum value of C_P, C_{Pmax}. Therefore, for every wind speed V there is a corresponding angular velocity, Ω, which results in λ_{opt}. As can be seen from (5.1), with a constant λ and R then V is directly proportional to Ω and thus the rotor speed must be varied in sympathy with the wind speed to optimise the power extraction. It should be noted that constant speed machines cannot vary their rotor speed and therefore can only realise C_{Pmax} at one particular wind speed. The $C_P - \lambda$ curve in Figure 5.1 is quite sharp and thus would result in a large loss in power when the turbine is not operating at λ_{opt}. However, other blades can be designed to flatten the $C_P - \lambda$ curve and thus reduce this effect of not operating at λ_{opt}.

5.3.2 Below rated wind speeds

The main aim when operating in below rated wind speeds is to maximise energy capture. This is achieved by varying the firing angle of the generator, α, to induce a variation

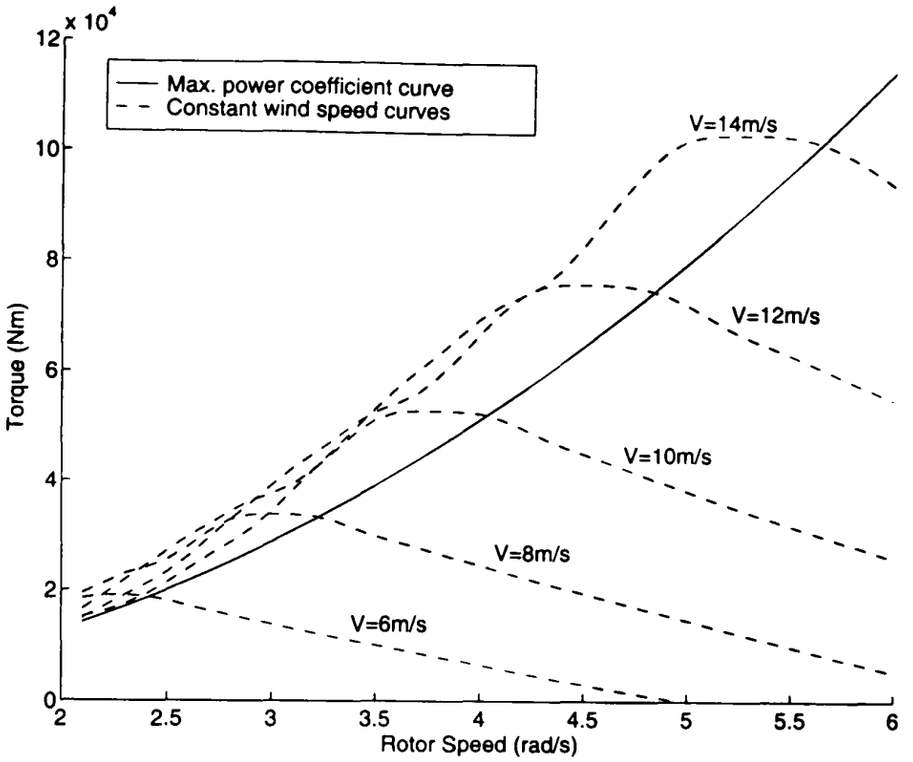

Figure 5.2: Below rated wind speed strategy

in the generator reaction torque such that the correct relationship between rotor speed and wind speed is achieved.

The relationship between aerodynamic torque, T_f, and rotor speed, Ω, is defined as

$$T_f = \frac{1}{2}\rho\pi R^3 V^2 \frac{C_P(\lambda)}{\lambda}, \quad \lambda = \frac{\Omega R}{V} \tag{5.2}$$

with ρ the density of air, viz. $1.225kg/m^2$. From equation 5.2 it is possible to obtain a set of curves for each wind speed V and also one curve describing the path of C_{Pmax}, see Figure 5.2. On the C_{Pmax} line, $C_P(\lambda) = C_{Pmax}$ and $\lambda = \lambda_{opt} = R\Omega/V$. Rearranging equation 5.2 in terms of Ω gives

$$T_f = \frac{1}{2}\rho\pi R^5 \frac{C_{Pmax}}{\lambda_{opt}^3}\Omega^2 \tag{5.3}$$

hence,

$$T_f = k_1\Omega^2, \qquad k_1 = \frac{1}{2}\rho\pi R^5 \frac{C_{Pmax}}{\lambda_{opt}^3} \tag{5.4}$$

Equation 5.4 defines, in the torque/rotor speed plane, the control strategy for below rated operation.

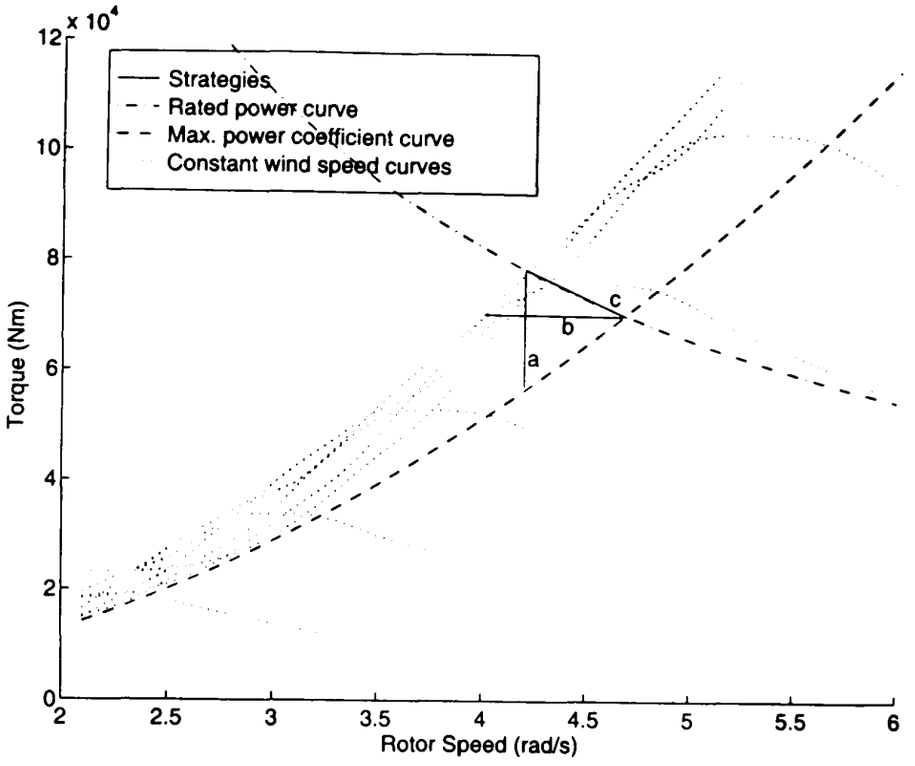

Figure 5.3: Above rated wind speed strategies

5.3.3 Above rated wind speeds

In high wind speeds there is too much power in the wind for the generator of the turbine to cope with and thus some of the extra aerodynamic power must be dissipated by the turbine. In a pitch regulated wind turbine the blades can be turned out of the wind to reduce the lift from the blades, reducing torque and hence power. However in a fixed pitch system, as is being considered here, the variable speed capability of the turbine is used to stall the wind turbine in high winds.

In Figure 5.2, the wind turbine cannot operate on the top left hand area where there are no lines of constant wind speeds and the boundary between this and the operating area is termed the stall front. In high winds the controller will normally attempt to move the operating point of the wind turbine into the stall front to cause the blades to stall and lose power. Also the fact that the windspeed lines are tightly packed here means that when the turbine is operating in this area it is insensitive to sharp changes in windspeed which could otherwise damage the wind turbine.

There are three main strategies that can be used to operate variable speed wind turbines in this high wind speed region and are described below.

Constant speed

In the constant speed strategy, once the rotor speed reaches a certain value it is held constant in all above rated wind speeds. This strategy is shown as line 'a' in Figure 5.3, and moves from the C_{Pmax} line up to the point on the stall front which generates rated power. Intersecting the stall front here ensures that the power generated by the turbine is always equal to or below the rated power of the turbine.

Constant torque

A second possible control strategy is to track a line of constant torque, shown as line 'b' in Figure 5.3. Here the aim is to minimise loading on the turbine and a horizontal line, intersecting the point on the C_{Pmax} curve which would generate rated power, is tracked. However, although loads on the turbine are reduced this method results in an even lower energy capture than the constant speed method.

Constant power

The main problem with both the constant speed and constant torque methods is that they only generate rated power at one particular wind speed (at the point where they touch the rated power curve). To generate rated power at all above rated wind speeds the line of constant power must be tracked, shown as line 'c' in Figure 5.3. This line, like the C_{Pmax} line, is a parabola but takes the form, $T = k_2/\Omega$, where k_2 is a constant specific to a turbine.

5.3.4 Switching

In order to work over the whole range of wind speeds encountered by a wind turbine, the below and above wind speed strategies, must be in some way combined. This is achieved by the introduction of switching.

At any point in time the operating point of the wind turbine can be estimated using signal measurements from the wind turbine. On the torque/rotor speed plane the operating point can be plotted and the distance from both the above and below rated strategy lines calculated. If, as shown in Figure 5.4, e_1 is the error in tracking the C_{Pmax} curve and e_2 is the error in tracking the constant power curve, then the appropriate line to track is found from the minimum of e_1 and e_2. The dividing line between the two strategies, shown in Figure 5.4, need not be equidistant from the two lines and a scaling constant can be introduced to change the relative distance from each

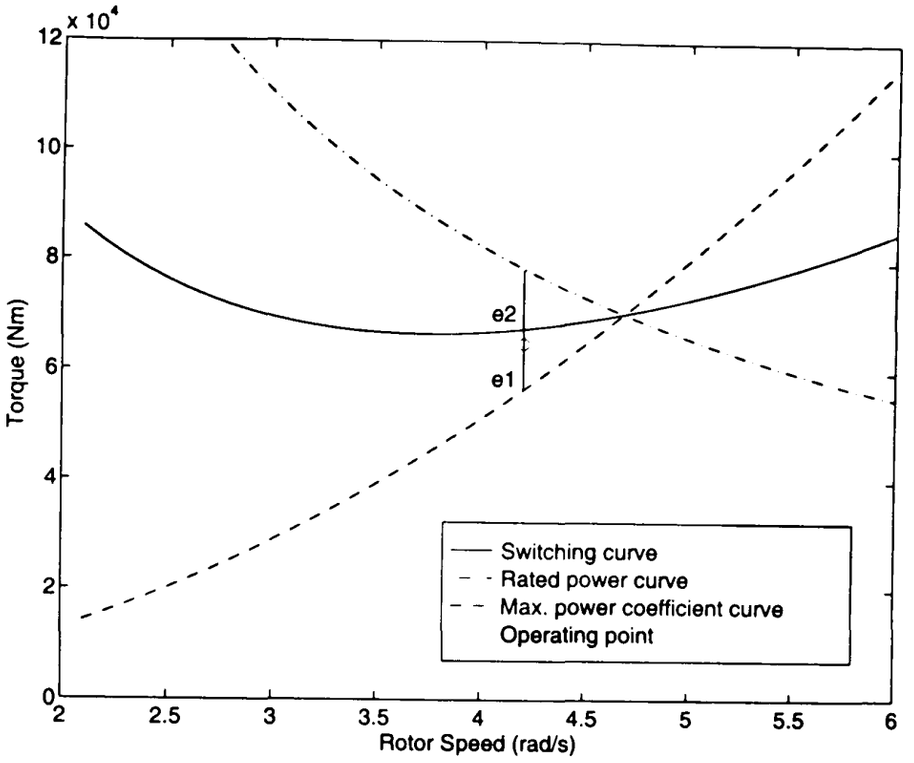

Figure 5.4: Switching strategy

curve. By introducing this scaling the time spent tracking the above or below rated strategies can be affected and thus the overall performance is altered.

5.4 A review of control studies

Below is presented a brief overview of some investigations into the control of variable speed wind turbines which have been reported in the literature. Three types of studies are identified: "feasibility studies", where the aim is basically to prove a particular mode of operation rather than develop the design of the controller; "synthesis studies", where a particular type of control technique is investigated with respect to a single control strategy; and "design studies" where the complete control design task is investigated. For each type of study the most common strategy in the literature, termed "conventional strategy" below, is that of tracking the C_{Pmax} curve in below rated windspeeds with pitch regulation to maintain constant speed and constant power above rated. However for each type of study stall regulation strategies, similar to those used in Chapter 8 are also discussed. Also unless otherwise stated studies are carried out by analysis and simulation studies only (rather than laboratory or field tests).

5.4.1 Feasibility studies

Several feasibility studies of the conventional strategy, as defined above, have been carried out. Ernst and Leonhard [42], Nayar and Bundel [82] and Wilmshurst [103] consider below rated operation only. Ernst and Leonhard compare three approaches to tracking the C_{Pmax} curve; namely setting the tip-speed ratio to its optimal value from a measurement of windspeed, setting the generator torque directly to $k_1\Omega^2$ and maximising energy capture by hill-climbing optimization. From laboratory tests it is concluded that the second method is the most appropriate of these three choices. Nayer and Bundel investigate tracking the C_{Pmax} curve by load control using a measurement of windspeed and Wilmshurst details some field tests on a 5m diameter turbine with freely hinged blades in low to intermediate wind speeds. However the nature of the controller used by Wilmshurst is not described. Ernst [43] and Law et al [64] consider both below and above rated operation, with Ernst describing the control system for a test rig and Law et al, describing the control system for the MS-1 turbine which employs a measurement of mean wind speed to adjust the controller gain.

Feasibility studies of stall regulated strategies have been undertaken by Thiringer and Linders [99], Tsiolis et al [100] and Mercer [77]. The study by Thiringer and Linders is of particular interest as they consider a stall regulated variable speed machine using a form of predictive control, and this paper is looked at in detail below in section 5.5. Tsiolis et al describe the control scheme for the Hönö variable speed fixed pitch test machine in Sweden. The strategy combines C_{Pmax} tracking in below rated windspeeds, by setting the generator reaction torque directly to $k_1\Omega^2$, with constant speed tracking in above rated wind speeds. During above rated operation, aerodynamic torque is treated as a disturbance and directly cancelled by a windspeed dependent feedforward term. This feed forward term is calculated from rotor speed and windspeed which is subject to the same lack of accuracy as that employed by Thiringer and Linders (see Section 5.5). Mercer considers strategies which combine C_{Pmax} tracking in below rated windspeeds, by setting the generator reaction torque directly to $k_1\Omega^2$, with constant speed control and constant power control for above rated windspeeds. However the analysis is based on basic models which do not represent important aspects of the above rated strategy. Also for constant power tracking, generated power rather than the more appropriate aerodynamic power is used. Regulating the wind turbine to maintain constant generated power using drive-train torque causes the system to be unstable and thus aerodynamic power and aerodynamic torque should be used instead.

5.4.2 Synthesis studies

Synthesis studies of the conventional strategy have been undertaken by several authors. Steinbuch [98] and Bongers et al [6, 7] consider above rated only. Both Steinbuch and Bongers et al apply the linear quadratic optimal control synthesis methodology, including state and output feedback, with constant and, by the former author, frequency dependent cost weightings. Cardenas-Dobson et al [14, 15] investigate below rated and above rated operation with supporting experimental tests in the laboratory. The controller, which acts on the generator reaction torque to cause the drive train torque to track the C_{Pmax} curve, not only operates in below rated conditions but continues to operate in above rated conditions. In above rated conditions, to maintain constant power and constant rotor speed, the pitch control system need only regulate the power or torque. Three different approaches to the synthesis of the pitch controller are discussed. The first controller acts in response to the error in generated power and the second controller acts in response to the error in an estimate of aerodynamic torque, $\hat{T}_f$. The synthesis procedure adopted is to tune PI controllers using the root locus technique. The third controller is a fuzzy logic controller acting in response to pitch angle and aerodynamic power which is estimated using the aerodynamic torque observer. The second and third controllers are judged to perform better but that is essentially due to the restricted form of the controllers.

Synthesis studies of pitch regulated strategies, other than the conventional strategy, have been undertaken for above rated operation by Bongers et al [7] and Caselitz et al [16]. Bongers et al investigate the application of linear quadratic control, with constant cost weightings and output feedback, to a passive pitch regulated wind turbine with the objective maintaining constant power, speed being regulated by the passive pitching. Caselitz et al describe the synthesis, by a method undefined, of a controller with the objective of regulating the flapwise blade bending moment and the generated power. This work is supported by field tests on a 33 kW wind turbine.

Synthesis studies of stall regulated strategies have been undertaken by Ekelund [39]. (This work is also reported in Ekelund and Scmidtbauer [40] and Ekelund [41]). The chosen strategy is to combine tracking of the C_{Pmax} curve and a line of constant speed in low wind speed with tracking of the constant power curve in high wind speed. To determine the limits to performance and to investigate the design trade-off, state feedback Linear Quadratic Gaussian control is applied to a very simple model, while assuming a measurement of wind speed is available. When tracking constant power, the error term in the cost function is inappropriately defined in terms of generated

power rather than aerodynamic power. Although global stability is not necessarily a consequence of local stability the Linear Quadratic Gaussian controller fortunately does globally stabilise the system on this occasion. In addition, the output feedback Linear Quadratic Gaussian control is applied to more realistic models using a Kalman filter to estimate wind speed. Since this estimate of wind speed is not used directly but is always used in effect to obtain an estimate of aerodynamic torque, the Kalman filter may be interpreted to be an aerodynamic torque estimator. An alternative constant power controller discussed consists of an inner speed regulation loop together with an outer power regulation loop. The inner loop, as in Ganander et al [53], stabilises the wind turbine, both locally and globally, whilst the outer one causes the system to track the constant power curve. The performance is similar to that attained by the Linear Quadratic Gaussian controller.

5.4.3 Design studies

In Connor and Leithead [25, 26, 27], Leithead and Connor [71] and Munz et al [80], the following restricted ranges of strategies are discussed: in below rated operation, tracking the C_{Pmax} curve by drive train torque, T_D, and estimated aerodynamic torque $\hat{T}_f$ [25]; tracking constant speed curve in intermediate wind speed combined with pitch regulation in high wind speeds [71]; in below rated operation with the aerodynamics having a flat or a peaked $C_P - \lambda$ curve, tracking both the C_{Pmax} curve and a 99% efficiency curve by T_D and by a combination of T_D and $\hat{T}_f$ [26]; the same strategies as in the previous case in below rated operation combined with constant speed, constant torque, constant power and a modified power stall regulation in above rated operation [27]; the same strategies as in the previous case but for a variety of rotor inertias [80]. In addition, in Connor and Leithead [28] the performances attained by two variable speed wind turbines, one with a flat the other with a peaked $C_P - \lambda$ curves, and a constant speed wind turbine is assessed and compared. The strategies for the two variable speed wind turbines are chosen to be the most appropriate for their aerodynamic characteristics.

In Iqbal et al [59], four different approaches to the conventional strategy are discussed: causing the rotor speed to maintain optimal tip-speed ratio in below rated wind speed combined with maintaining constant power in above rated wind speed, maximising the energy capture by hill-climbing optimisation in below rated wind speed combined with maintaining constant power in above rated wind speed; causing the power to follow the wind speed cubed in below rated wind speed combined with main-

taining constant power in above rated wind speed; causing the rotor speed to maintain the optimal tip-speed ratio in below rated wind speed combined with maintaining constant shaft torque (measured by a strain gauge) in above rated wind speed. The first and third below rated operation strategies require a measurement of wind speed. One non-conventional strategy is discussed: causing the rotor speed to maintain the optimal tip-speed ratio in below rated wind speed combined with maintaining constant shaft power (with the shaft power measured by a strain gauge) by stall regulation in above rated wind speed. In addition, constant speed operation both pitch regulated and stall regulated, is investigated with support of field tests on a 5kW wind turbine, Iqbal et al [60].

5.5 Analysis of the paper by Thiringer and Linders

As mentioned above, one paper which had particular relevance to the work being discussed here was the paper by Thiringer and Linders [99]. The main point of interest is that the controller is a form, although quite basic, of predictive control. Therefore before designing a controller based on the MBPC method presented in Chapter 2, the predictive control method used by Thiringer and Linders on a small scale stall regulated variable speed wind turbine is investigated to determine its effectiveness and to see if any lessons can be learned.

Thiringer and Linders consider variable speed control of a fixed pitch wind turbine operating in a speed range of 0 to 38rpm and having a rated power of 20kW. The basic control strategy employed is to maintain peak efficiency at low wind speeds for rotor speeds less than maximum rotor speed. The rotor speed is held at this point until rated power is reached, at which point the rotor speed is reduced to induce stall in high winds. The operating region is defined by inferring wind speed from the ratio C_P/λ^3 , which is calculated from rotor speed and electrical power. It is unclear whether the wind speed estimate is effective in the stall region as here the accuracy of the steady state aerodynamic model used is dubious and the aerodynamics include unstable dynamic effects such as stall hysteresis.

Although the type of control described in the paper is dead-beat control, the controller uses present and past values of rotor speed to predict the inertia effect on the electrical power error, that is the difference between the reference power and the generated power. This is a very crude form of predictive control and the results presented in the paper are disappointing with the graphs, even using 1 minute averages, showing a wide dispersion of results. It would be expected that 1 minute average results would

show very tight control.

In order to understand the results better a computer simulation was set up to try and reproduce the results. However this proved to be impossible mainly due to the lack of detail of the exact workings of the controller. The controller operates using a non-linear parameter K which is used to inversely scale the power error to give the change in supply frequency fed into the generator. For below rated wind speeds K is stated to be zero resulting in infinite gain and therefore relies on the system constraints to limit the change in frequency. Also when the power error is positive the controller should act to reduce the rotor speed for below rated operation but increase it for above rated operation. For the controller to achieve this effect the sign of K must be opposite for above and below rated operation, however in the paper the value of K is given as positive for all wind speeds.

Although the form of predictive control used by Thiringer and Linders showed several flaws, at least in the way it is described in the paper, and the results appear poor, the paper illustrates the potential problems associated with controlling a wind turbine using predictive control and provides a baseline for applying the MBPC technique to a variable speed wind turbine.

5.6 Discussion

Control objectives and strategies have been examined and a literature review presented. The paper by Thiringer and Linders was examined in detail and found to be a poor implementation of a form of predictive control, although a good practical introduction to the control of wind turbines. However, before a proper test of the MBPC controller can be undertaken, models of the variable speed wind turbine need to be investigated and developed to ensure that any simulations are realistic and provide useful results. In the next chapter modelling of the wind turbine is examined and in Chapter 7 the equally important aspect of modelling of the wind is investigated.

Chapter 6

Modelling the Wind Turbine

6.1 Introduction

The basic structure of variable speed wind turbines is shown in Figure 6.1. In order to design a control system the wind turbine must be modelled simply whilst retaining all significant dynamic components. These components should be modelled to comparable degrees of complexity so that no part is over elaborate nor poorly modelled. The model consists of a rotor, low speed shaft, gearbox, high speed shaft and generator. Pitch control is available if the blades are pitchable, however the firing angle, α, is the main parameter for control of the variable speed wind turbine. In most cases, where the controller will be tested by simulation, two types of models are required. First, simulation models are required which represent the full range of dynamics including system non-linearities. These will be used to thoroughly test the controller and give as accurate a representation of real-life as possible. Secondly control models are required. These models are used in the design of the controller and have simplified and linearised dynamics, although still represent the key dynamic aspects of the system.

The descriptions below cover both the non-linear and simpler linearised dynamics of

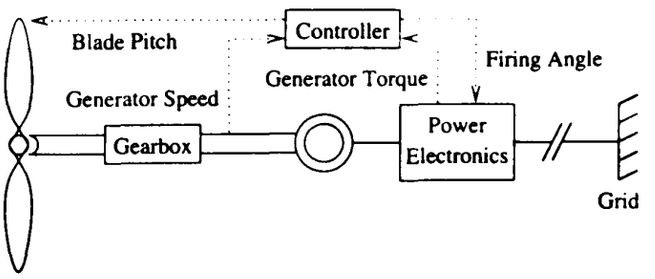

Figure 6.1: Basic variable speed turbine structure

a stall regulated variable speed wind turbine, starting with very basic models and then developing the models for the aerodynamics, drive-train and generator individually.

6.2 Basic models

Variable speed wind turbines are often represented [9, 77, 14] by a simple model consisting of an inertial mass with viscous damping. That is, the rotor speed, Ω is related to the aerodynamic torque, T_f, and the drive-train torque, T_D, by the equation,

$$I\frac{d\Omega}{dt} + B\Omega = T_f - T_D \tag{6.1}$$

where I is the total inertia, $B\Omega$ is the total viscous damping in the drive-train and the aerodynamic torque is a function of rotor speed and wind speed, V. The power generated by the turbine, P_g, is

$$P_g = E_{ff}\Omega T_D \tag{6.2}$$

where E_{ff}, which may depend on Ω, is the efficiency of the electrical aspects of the power generation unit. It follows that the overall efficiency, E, of the wind turbine is

$$E = \frac{E_{ff}(\Omega)P_g}{P_g + E_{ff}(\Omega)B\Omega^2}$$

Many control strategies can be defined as attempting to make the drive-train torque attain some value defined by a function, $f(\Omega)$, of the rotor speed. This is sometimes realised [42, 100, 77] by assuming that the electrical aspects of the power generation unit dynamics are sufficiently fast and assigning the generator reaction torque directly to the required value, i.e.

$$T_D = f(\Omega) \tag{6.3}$$

This is shown in Figure 6.2a. In the steady state, $\dot{\Omega} = 0$ and, combining equation (6.1) with equation (6.3), gives

$$T_f = f(\Omega) + B\Omega \tag{6.4}$$

Using the Laplace transform of equation (6.1) the system can be reorganised into the the standard feedback form as shown in Figure 6.2b., with the controller, C, set to 1 (i.e. $T_D = 1.f(\Omega)$).

In attempting to cause T_D to track $f(\Omega)$, the controller in Figure 6.2b. is actually attempting to keep the error, $T_D - f(\Omega)$, small. Hence, Figure 6.2b. can be redrawn

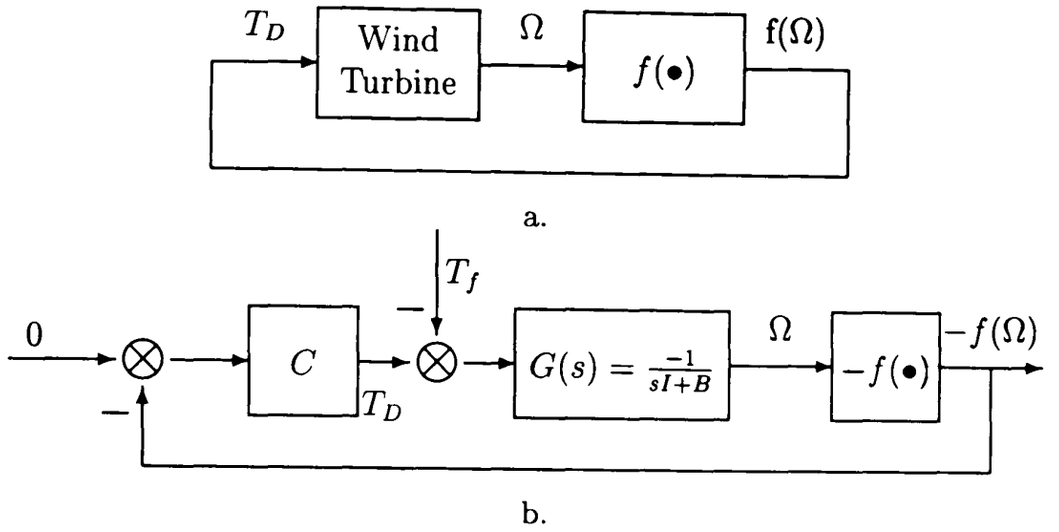

Figure 6.2: Basic control models

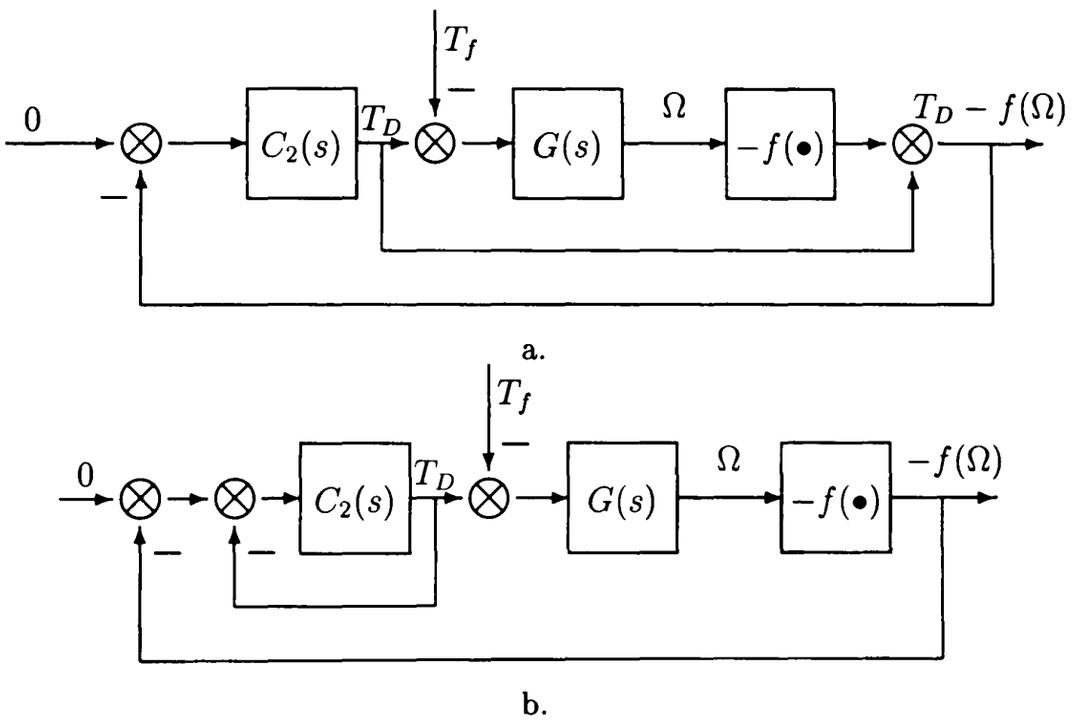

Figure 6.3: Alternative basic models

as Figure 6.3a. Further, Figure 6.3a. can be redrawn as Figure 6.3b. which shows the equivalency to Figure 6.2b. with

$$C = \frac{C_2}{1 + C_2} \tag{6.5}$$

Two frequently considered strategies used for variable speed wind turbines are

1. Tracking the C_{Pmax} curve in below rated wind speeds by setting the drive train torque directly to $k\Omega^2$, i.e. choosing

$$f(\Omega) = k\Omega^2$$

2. In above rated wind speeds to track the constant power curve

For strategy 1, local to some equilibrium point denoted by Ω_0, the linear dynamics [102] relating the perturbations in rotor speed, $\Delta\Omega$, to perturbations in wind speed, ΔV, are

$$\Delta\Omega = \frac{\left(\frac{\partial T_f}{\partial V}\right)_0 \Delta V}{\left(Is + B + 2k\Omega_0 - \left(\frac{\partial T_f}{\partial \Omega}\right)_0\right)} \tag{6.6}$$

The time constant for this system is $I/(B + 2k\Omega_0 - \frac{\partial T_f}{\partial \Omega})$ and is large for large scale wind turbines. For the wind turbine considered in this thesis the time constant varies between 2.6 seconds and 6.4 seconds and this results in the response of the turbine to changes in wind speed being rather sluggish.

In the second strategy the controller acts on T_D in response to an error from the maximum power curve. In this case, as mentioned in Section 5.4.1, the controller must react to the error in aerodynamic power, P_a, not generated power, P_g. P_a cannot be measured directly and must be estimated from measurements of T_D and Ω. From equation (6.1), the controller must respond to the error in

$$P_a = \Omega(I\dot{\Omega} + T_D + B\Omega) \tag{6.7}$$

Thus the relevant dynamics [102] are those relating the perturbations in aerodynamic power, ΔP_a, to perturbation in both wind speed, ΔV, and drive train torque, ΔT_D,

$$\Delta P_a = -\frac{\left(\frac{\delta T_f}{\delta \Omega}\right)_0 \Omega_0 + \frac{P_{a0}}{\Omega_0}}{sI + B - \left(\frac{\delta T_f}{\delta \Omega}\right)_0} \Delta T_D + \frac{\Omega_0 \left(sI + B + \frac{P_{a0}}{\Omega_0^2}\right)}{sI + B - \left(\frac{\delta T_f}{\delta \Omega}\right)_0} \left(\frac{\delta T_f}{\delta V}\right)_0 \Delta V \tag{6.8}$$

From equation (6.8) it can be seen that this model for above rated wind speeds is unstable when $\left(\frac{\delta T_f}{\delta \Omega}\right)_0 > B$.

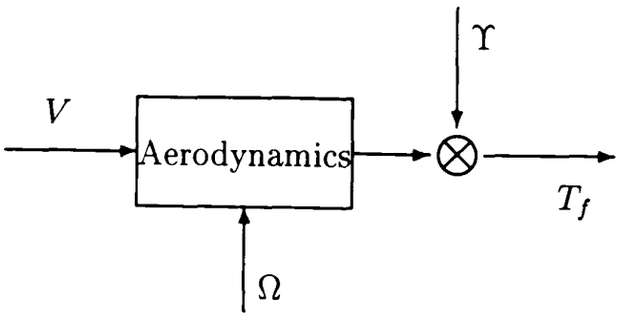

Figure 6.4: Nonlinear aerodynamic model

λ	2	3	4	5	6	6.25	6.5	7	8	9	12	15
C_p	.02	.057	.164	.3	.444	.45625	.455	.441	.408	.36	.096	-.195

Table 6.1: Aerodynamic power coefficients

6.3 Aerodynamic models

Slightly more advanced models used to describe the interaction of the wind turbine with the wind are described below. However, since the rotor is subject to a spatially and temporally distributed wind field, there is no such thing as the "wind speed". A wind turbine may be considered to experience an effective wind speed. Effective wind speed models are described in detail in Chapter 7. A representation of the aerodynamics is shown in Figure 6.4. The aerodynamic torque, T_f, depends nonlinearly on the effective wind speed, V and the rotor speed, Ω, such that

$$T_f = \frac{1}{2}\rho\pi V^2 R^3 \frac{C_p(\lambda)}{\lambda} \tag{6.9}$$

with R the rotor radius, ρ air density, C_p the aerodynamic power coefficient and λ the tip speed ratio ($= \frac{R\Omega}{V}$). As mentioned in Chapter 5 there is a value of tip speed ratio for each wind speed which will produce the maximum aerodynamic power coefficient and, hence, the optimum power for the particular wind speed.

To account for the averaging of the wind speed over the rotor, which induces a spectral difference between the effective wind speed and point wind speed, the latter is modified by a filter (see Chapter 7). The aerodynamic power coefficients for the rotor used in this thesis, which is designed for variable speed stall regulation, are shown in Table 6.1. Equation (6.9) can be linearised, local to some equilibrium point, to give

$$\Delta T_f = K_\Omega \Delta\Omega + K_V \Delta V \tag{6.10}$$

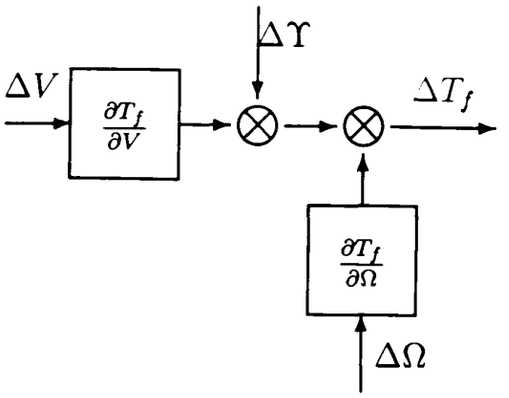

Figure 6.5: Linearised aerodynamic model

where $K_\Omega = \frac{\partial T_f}{\partial \Omega}$, $K_V = \frac{\partial T_f}{\partial V}$ and Δ denotes small perturbations in variables about their nominal values. This linearised aerodynamic model is shown in Figure 6.5.

The rotation of the rotor induces spectral peaks at integer multiples of the rotor speed, Ω, the most significant of which for a three bladed machine is the 3Ω peak. Rather than adjusting the wind speed itself the 3Ω peak can be more conveniently modelled by adjusting the aerodynamic torque, as shown in Figures 6.4 and 6.5 where Υ represents the 3Ω disturbance. The models for spectral peaks are described in more detail in Chapter 7. The only other significant aerodynamic effect, which is termed the dynamic inflow, or induction lag, is omitted from the dynamic models as it has little impact on the control design task [66].

6.4 Drive train dynamics

The dynamics of the drive train of a variable speed wind turbine are represented in Figure 6.6 [68, 72], with the parameters associated with the wind turbine under consideration here shown in Table 6.2.

The equations relating rotor speed, Ω, and generator speed, ω_g, to aerodynamic torque, T_f, and generator reaction torque, T_e, are

$$\Omega = \left(\frac{A}{K_1} + C + AD\right) T_f + \left(\frac{B}{K_1} + BD\right) T_e \tag{6.11}$$

$$\omega_g = (AE)T_f + (BE + F)T_e \tag{6.12}$$

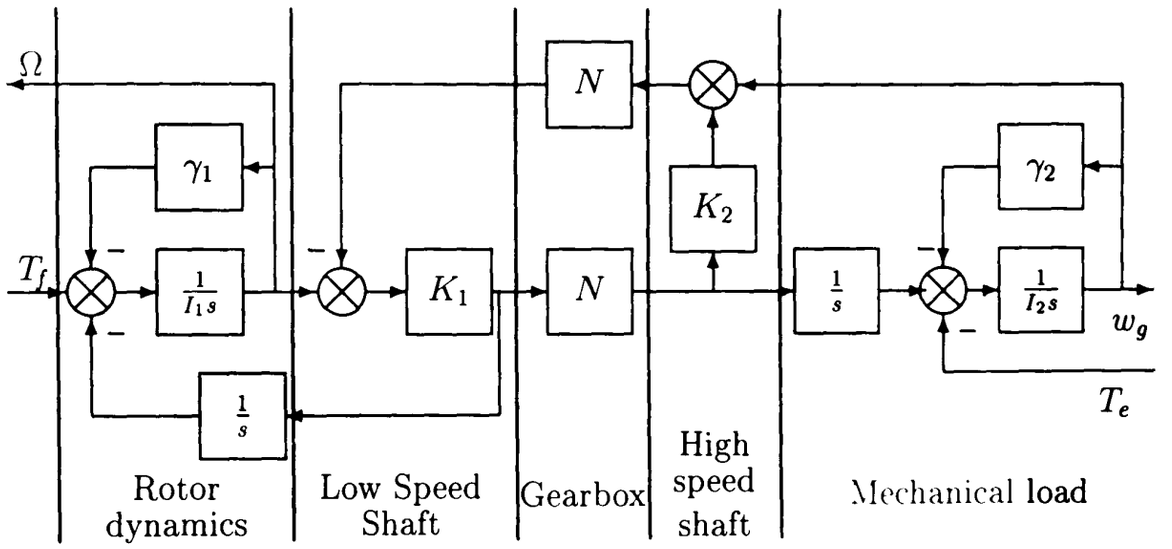

Figure 6.6: Drive train model

Symbol	Description	Value
N	Gearbox ratio	38.06
I_1	Rotor Inertia	$1e5\,kgm^2$
I_2	Generator Inertia	$3.8\,kgm^2$
K_1	Low speed shaft stiffness	$1e6\,Nm/rad$
K_2	High speed shaft stiffness	$5e4\,Nm/rad$
γ_1	Low speed shaft damping	$980\,Nm/rad/sec$
γ_2	High speed shaft damping	$0.2\,Nm/rad/sec$

Table 6.2: Drive train parameters

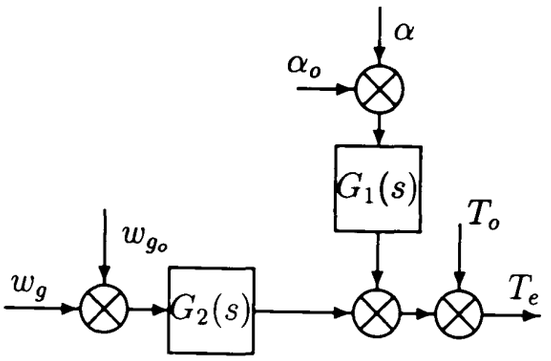

Figure 6.7: Power generation unit dynamics

where

$$A = \frac{N^2 x s(I_2 s + \gamma_2)}{c_0 + c_1 s + c_2 s^2 + c_3 s^3}, \quad B = \frac{N x s(I_1 s + \gamma_1)}{c_0 + c_1 s + c_2 s^2 + c_3 s^3}, \quad C = \frac{1}{I_1 s + \gamma_1},$$

$$D = -\frac{K_1 + I_1 s^2 + \gamma_1 s}{K_1 s(I_1 s + \gamma_1)}, \quad E = \frac{1}{sN(I_2 s + \gamma_2)}, \quad F = -\frac{1}{I_2 s + \gamma_2},$$

$$x = \frac{K_1 K_2}{K_1 + K_2 N^2}, \; c_0 = x(N^2 \gamma_2 + \gamma_1), \; c_2 = I_2 \gamma_1 + I_1 \gamma_2, \; c_3 = I_1 I_2$$

These equations are linear and are of suitable complexity to be used for both the simulation and control models.

6.5 Power generation unit dynamics

In the variable speed turbine under consideration here a synchronous generator is indirectly connected to the grid via a rectifier and an inverter. The operating state of the power generation unit can be set by varying some suitable variable, such as the rectifier current when using vector control or, as used here, by setting the rectifier firing angle, α. A representation of the power generation unit dynamics is shown in Figure 6.7. It is assumed here that the unit's dynamics are sufficiently fast that no distinction between the demanded and actual firing angle need be made. Suitable values that are used for the constants in Figure 6.7 are $\alpha_o = 0.4697 rads$, $\omega_o = 194.502 rad/sec$ and $T_o = 2154.572 Nm$. Leithead *et al* [67] describe how the generator dynamics are identified using experimental data from a test rig. Initially the dynamics are determined for α to rectifier current (I_g) and from ω_g to I_g and then scaled to make appropriate

electrical dynamics from α to T_e ($G_1(s)$) and from ω_g to T_e ($G_2(s)$), as shown below

$$G_1(s) = \frac{-295.429(s+7.6383)(s-200)(s-644.552)}{[(s+13.0128)^2+56.0852^2](s+186.6475)} \tag{6.13}$$

$$G_2(s) = \frac{-37.8805(s+10.3674)(s+23.1307)(s-200)[(s+62.806)^2+345.5235^2]}{[(s+6.04054)^2+46.4054^2](s+200)[(s+98.835)^2+315.6169^2]} \tag{6.14}$$

Frequently the generator reaction torque is regulated by a torque demand signal, rather than using the firing angle directly. This former configuration employs a feedback loop from T_e and extra controller which sets the firing angle and has the general advantages of closed loop feedback systems. However, the performance of the wind turbine control system with a torque demand signal and associated feedback control loop is very similar to using the firing angle directly [88], and therefore the inclusion of this extra control loop is not considered here.

6.6 Combined models

6.6.1 Simulation models

The non-linear aerodynamics are combined with the drive train and generator models to provide the full simulation models. These dynamics are implemented using the *MatrixX* simulation program and the block diagrams which are used to implement the dynamics of the variable speed wind turbine are shown in Appendix D. Figure D.1 shows the top level of the whole system and the interconnections between the different parts. The block "The Wind" is described more fully in Chapter 7 and the controller block ("var controller") is described in Chapter 8. The conversion of the spatially filtered wind into the aerodynamic torque (block "Tqrtr") is shown in Figure D.2 with the generation of the torque coefficient and then the aerodynamic torque using equation (6.9). This block also outputs the aerodynamic power coefficient, C_p which is useful in analysing the performance of the controller. The drive train dynamics are shown in Figure D.3. This appears slightly different from the structure shown in Figure 6.6 above, however they are equivalent, with a new gain K,

$$K = \frac{K_1 N^2 K_2}{K_1 + K_2 N^2} \tag{6.15}$$

The gain (which equals 998621 in the figure), removes the need for the extra $\frac{1}{K_2}$ loop and simplifies the simulation. Finally the dynamics of the generator are shown in Figure

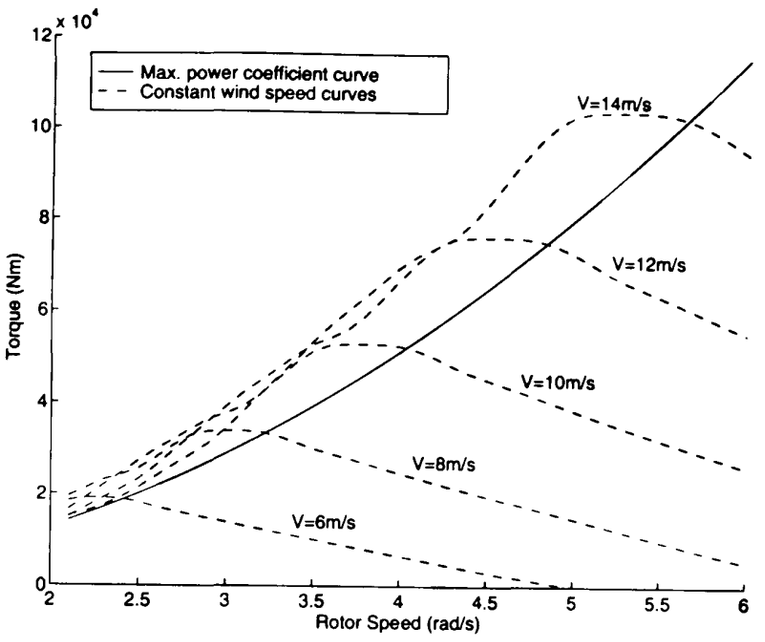

Figure 6.8: C_{Pmax} curve and below rated constant wind speed lines

D.4 and includes the representation of the power generation, where

$$Power = 0.95(T_e\omega_g + 1269.7\Omega^2 - 15000) \tag{6.16}$$

15000 (15kW) is the fixed loss of the generator which has an overall efficiency of 95% [67].

6.6.2 Controller models

The same drive train dynamics and generator dynamics as used in the simulation models are used along with the linearised aerodynamics as the controller models. How these models are used in designing the controller is described in Chapter 8. The linearised aerodynamics used in the control design make use of the aerodynamic gain factor, K_Ω, equation (6.10). K_Ω is equivalent to the slope of the constant wind speed lines in the Torque-rotor speed plane. As can be seen in Figure 6.8 for below rated wind speeds the slopes of these lines along the C_{Pmax} curve does not change very much and hence the dynamics do not vary dramatically. However, for above rated control K_Ω varies dramatically along the Constant Power line, as shown in Table 6.3 and Figure 6.9. The table and figure show clearly the nonlinearity of the above rated system and also how widely the control dynamics will vary when operating in high winds. In practice the higher value of K_Ω results in a harder system to control and thus K_Ω = 53311,

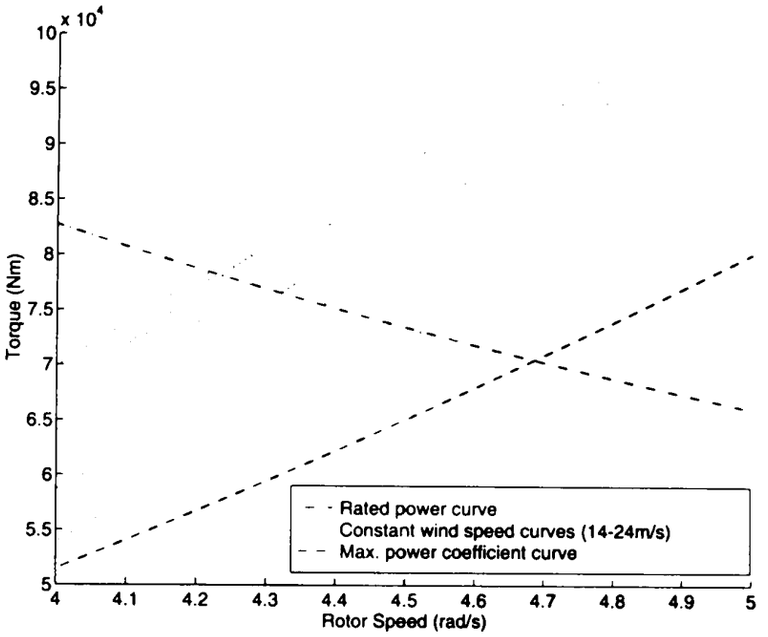

Figure 6.9: Intersections of the rated power curve with the constant wind speed curves

Wind (m/s)	11.6	12	13	14	16	18	20	22	24
Ω (rad/s)	4.64	4.36	4.30	4.31	4.22	4.27	4.38	4.47	4.52
K_Ω	-10316	5105	37539	30121	35898	47980	53311	39095	42648

Table 6.3: Aerodynamic gain values along the rated power curve

corresponding to a wind speed of 20m/s, is chosen to design the above rated controller. For below rated wind speeds, a mean value of $K_\Omega = -13757$, corresponding to a mean wind speed of 8m/s, is used to design the below rated controller.

6.7 Discussion

Models suitable for both simulation and controller design for variable speed wind turbines have been developed and discussed. The wind/aerodynamic models are worthy of further discussion and these are investigated in depth and developed in the next Chapter, before going on in Chapter 8 to use all these models in the design of the MBPC variable speed controllers.

Chapter 7

Modelling the Wind

7.1 Introduction

Arising from the discussion, in Chapter 6, on modelling wind turbines is the requirement for models which describe, accurately, the wind and its interaction with the wind turbine. A detailed discussion on modelling the wind, summarising and bringing together many different sources of information about wind models is presented below, before going on to develop new models for wind turbines that have blade tips and are not adequately covered by existing models.

7.2 Introduction to wind models

The dynamics of horizontal-axis wind turbines are driven by transient torques and moments that are induced by the interaction of the rotor with the wind. Consequently, the utility of any dynamic analysis of a wind turbine or assessment of its performance is strongly dependent on the appropriateness of the wind speed model employed. In early investigations, e.g. Krause & Man [62] or Anderson & Bose [2], the model consisted of a simple wind speed, acting uniformly over the rotor disc, obtained by the addition of components representing various aspects of the wind. The components might be deterministic, representing the mean wind speed or a wind gust [62, 2], or stochastic, representing wind turbulence [2]. The statistical properties of a point wind speed were typically adopted in the latter case [2]. However, it was realised that these models are inadequate.

The blades of the wind turbine sweep through a complex time varying three dimensional wind-field. The structure of the wind-field is a combination of stochastic contributions, due to wind speed turbulence, and deterministic contributions, due to wind

shear and tower shadow. As far as any wind induced torque or moment is concerned, much of the variation in the wind speed over the swept disc is reduced by averaging over the blades but the rotation of the rotor induces significant periodic components with frequencies equal to integer multiples of the rotational angular velocity, Ω_o. The net result is that, in comparison to the spectrum of point wind speed, the power in the spectrum of the wind speed at integer multiples of Ω_o is greatly enhanced but depleted elsewhere, Connell [22] and Connell & George [23]. Similarly to the structure of the wind-field, the spectral peaks have both a deterministic and stochastic component. However, the stochastic component is by far the most significant [22]. For the torques and moments acting on a single blade, such as the root bending moment, the most significant spectral peak is at Ω_o. For the forces and torques acting on the complete rotor, such as the axial hub torque, the most significant is at $n\Omega_o$, where n is the number of blades.

Clearly, the simple early models need to be modified to account for the full wind-field/rotor interaction. A statistically correct description of the three-dimensional wind-field is required. The forces acting on a rotating blade-element can then be determined by subjecting the rotating blade-element to the wind speed it would encounter as the wind-field moves through the rotor disc. By integrating over a complete blade or rotor, the total forces acting on them are determined. This procedure or its equivalent is followed amongst others by Holley *et al.* [58] and Connell [22].

Although wind-field models of the type described in the preceding paragraph are very successful, they are not appropriate for all applications; in particular, their complexity may be unwarranted for the context within which models of the wind-field/rotor interaction are to be applied. For example, in control system analysis and design, it is necessary to model the wind-field/rotor interaction by simple ordinary differential equations. Furthermore, since the performance of control systems and the dynamic behaviour of the wind turbine are frequently assessed from relatively short data sequences of a few minutes duration, high resolution statistical measures of performance/behaviour are not possible. In these circumstances a simple ordinary differential equation model, being computationally efficient, is a representation convenient for wind turbine simulation.

A class of simple ordinary differential equation models of the wind-field/rotor interaction is described below. Models with appropriate statistical properties are derived for single torques and moments, and pairs of torques and moments. In the latter case, the torques have both the correct auto-correlation and cross-correlation properties. The models are validated against site data. In section 7.3, the derivation and validation of

the wind speed model to represent a single torque or moment is discussed. In section 7.4 and section 7.5, the derivation and validation of the wind speed model to represent a pair of correlated torques or moments is presented. In section 7.6, the modification of the models to include the spectral peaks due to the rotational sampling of the wind-field is considered.

7.3 Single wind speed model

When it is necessary to model only one torque or moment, the torque or moment could be derived from a suitable average of the wind speed rather than point wind speed; that is, the wind-field can be represented by one effective wind speed. For example, the total axial hub torque could be obtained from a simple effective wind speed which essentially is an average of the wind speed over the whole rotor disc. It is sufficient that the effective wind speed, whilst uniform over the swept area, continues to induce the same torques and moments as the full wind-field. In particular, their spectra must remain unchanged whether the torques and moments are derived from the full wind-field or the effective wind speed. Since it is uniform over the swept area, the time variation of this effective wind speed can be modelled by simple ordinary differential equations as required. The effective wind speed model may be interpreted as a filtered point wind speed in which context the ordinary differential equations are replaced by transfer functions.

The derivation of the effective wind speed models [102], using a method originally proposed by Madsen and Frandsen [75], is described below. It is applied to the example previously mentioned whereby the total axial hub torque is derived from a single effective wind speed representing the averaging of the wind-field over the rotor disc. This model for the transient component of the hub torque has been used successfully in many control studies [68, 8, 69].

The effective wind speed model is only intended to represent the low frequency turbulent component of the wind-field. It is not intended to represent deterministic components of the wind-field such as tower shadow and wind shear, nor to represent high frequency spectral peaks due to the rotational sampling of the wind-field. However, the very low frequency components of the turbulent fluctuations in the wind-field may be considered uniform over the rotor disc. Hence they constitute a quasi-static mean wind speed which varies slowly and the derivation of the effective wind speed model need only cater for the perturbations in the wind-field about this quasi-static mean wind speed.

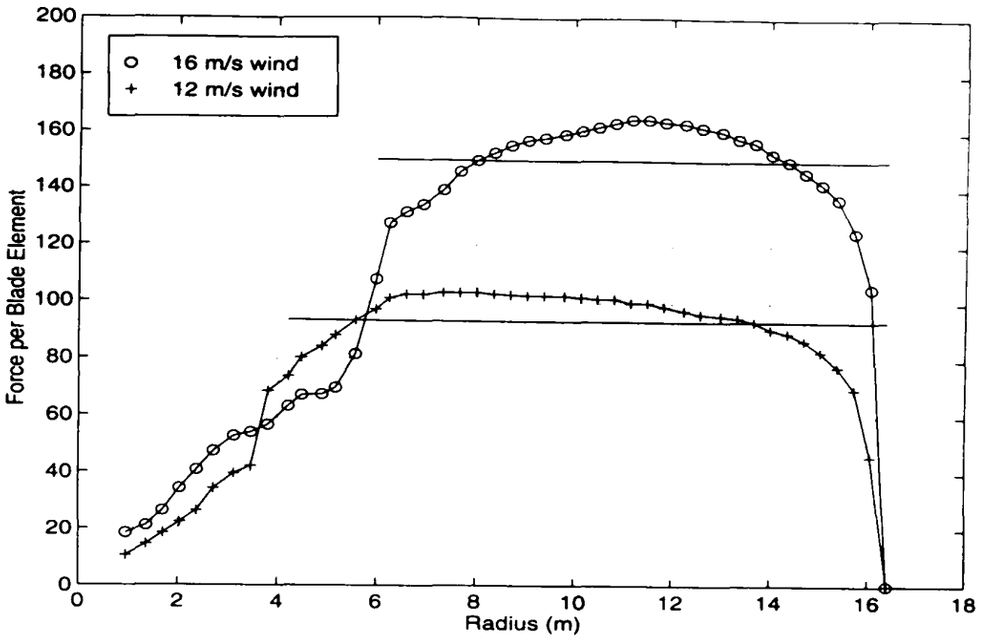

Figure 7.1: Force per unit blade element

The axial hub torque, $T_A(t)$, induced by the wind on a blade is given by

$$T_A(t) = \int_A \Xi(\mathbf{r}, \mathbf{V}(\mathbf{r}, t))dA \tag{7.1}$$

where $\mathbf{V}(\mathbf{r}, t)$ is the field of wind speed over the rotor disc, Ξ is a weight function dependent on both position, $\mathbf{r}$, and wind speed (it may be interpreted as the contribution to the total torque of an element of a blade) and A is the area of a blade. The expression, (7.1), can be simplified by exploiting the two following observations

1. Driving forces on the blades are roughly independent of the radius and thus the aerodynamic torque appears linear in the hub distance [3].

2. At low frequencies the time scale of change in the wind-field is comparable to or longer than the period of revolution of the rotor and the contribution, at any instant, of the low frequency components to the torque is related to wind-field over the complete rotor disc.

Observation 1 is supported by Figure 7.1 [3] which depicts the variation with distance from the hub of the force due to a blade element. Above 6m the driving force remains roughly constant. Below 6m, it varies with position but this section of the blade contributes relatively little to the total torque, T_A. It follows that

$$T_A(t) \simeq \int_{A_r} \xi(\mathbf{V}(\mathbf{r}, t))dA \tag{7.2}$$

where ξ is some weight function dependent only on the wind speed and A_r is the area swept by the rotor.

Further simplification is possible since only the perturbations in the wind-field about the quasi-static mean and the corresponding turbulence induced fluctuations in torque need be considered. On linearising (7.2) about the quasi-static mean wind speed, the torque transients, $T(t)$, induced by the perturbations in the wind-field is given by

$$T(t) \simeq k \int_{A_r} v(\mathbf{r}, t) dA \tag{7.3}$$

where $v(\mathbf{r}, t)$ is the field of turbulent perturbations in the wind speed about the quasi-static mean perpendicular to the rotor disc and k is some normalising constant.

The auto-correlation function for the torque transients is

$$\begin{aligned} R_T(t) &= \int_{-\infty}^{\infty} T(s)T(t+s)ds \\ &\approx k^2 \int_{A_r}\int_{A_r}\int_{-\infty}^{\infty} v(\mathbf{r}_1, s)v(\mathbf{r}_2, t+s)dsdA_1dA_2 \\ &= k^2 \int_{A_r}\int_{A_r} R_{v(\mathbf{r}_1)v(\mathbf{r}_2)}(t)dA_1dA_2 \end{aligned} \tag{7.4}$$

with $R_{v(\mathbf{r}_1)v(\mathbf{r}_2)}$ the cross correlation function between the wind at $\mathbf{r}_1$ and the wind at $\mathbf{r}_2$. It follows that the spectrum of T, $S_T(\omega)$, is related to the cross-spectrum for turbulent wind fluctuations, $S_{v(\mathbf{r}_1)v(\mathbf{r}_2)}$, by

$$S_T(\omega) \simeq k^2 \int_{A_r}\int_{A_r} S_{v(\mathbf{r}_1)v(\mathbf{r}_2)}(\omega)dA_1dA_2 \tag{7.5}$$

Assuming that the power of wind speed fluctuations at a fixed point is independent of the position of the rotor disc

$$S_T(\omega) \simeq k^2 S_v(\omega) \int_{A_r}\int_{A_r} \mathcal{X}(\mathbf{r}_1, \mathbf{r}_2, \omega)dA_1dA_2 \tag{7.6}$$

where $S_v(\omega)$ is the spectrum of wind speed fluctuations at a fixed point and

$$\mathcal{X}(\mathbf{r}_1, \mathbf{r}_2, \omega) = \frac{S_{v(\mathbf{r}_1)v(\mathbf{r}_2)}(\omega)}{\sqrt{S_{v(\mathbf{r}_1)v(\mathbf{r}_1)}(\omega)S_{v(\mathbf{r}_2)v(\mathbf{r}_2)}(\omega)}} \tag{7.7}$$

The coherence of the wind speeds at the two points, $\mathbf{r}_1$ and $\mathbf{r}_2$, depends primarily on their separation, l, such that

$$l = \sqrt{\mathbf{r}_1^2 + \mathbf{r}_2^2 - 2\mathbf{r}_1.\mathbf{r}_2} \tag{7.8}$$

Hence, assuming the form of the coherence function for the wind from Davenport [33]

$$\mathcal{X}(\mathbf{r}_1, \mathbf{r}_2, \omega) \simeq exp\left(\frac{-\gamma l\omega}{\bar{V}}\right) \tag{7.9}$$

where γ is the turbulent wind speed decay factor and $\bar{V}$ is the mean wind speed. A priori, the quasi-static mean wind speed employed when linearising (7.2) is not necessarily the same as the mean wind speed, $\bar{V}$, since the wind intervals over which they are averaged may be of different duration. However, $\bar{V}$ is assumed here to be identical to the quasi-static mean wind speed with γ adjusted to account for any difference between the two mean wind speeds.

An explicit form for the spectrum of the aerodynamic torque transients for a blade is thus,

$$\begin{aligned} S_T(\omega) &\simeq k^2 S_v(\omega) \int_{A_r} \int_{A_r} exp\left(\frac{-\gamma l \omega}{\bar{V}}\right) dA_1 dA_2 \\ &= k^2 S_v(\omega) \Phi(x) \end{aligned} \tag{7.10}$$

where

$$x = \left(\frac{\gamma R}{\bar{V}}\right) \omega = \sigma \omega \tag{7.11}$$

and

$$\Phi(x) = R^4 \int_D \int_D exp(-x\bar{l}) d\bar{A}_1 d\bar{A}_2 \tag{7.12}$$

R is the rotor diameter, D is a disc of radius one and $\bar{l}$ is the normalised separation between the two points on D. From Madsen and Frandsen [75]

$$\begin{aligned} \Phi(x) &= \frac{2\pi^2 R^4}{x^2} \left\{ 1 + \frac{4}{\pi} \int_0^{\frac{\pi}{2}} (1 - 3sin^2\theta) e^{-2xcos\theta} d\theta \right\} \\ &\simeq \pi^2 R^4 \frac{(2 + x^2)}{(2 + ax^2)(1 + x^2/a)} \quad ; a = 0.55 \end{aligned} \tag{7.13}$$

that is

$$S_T(\omega) \simeq k^2 R^4 \pi^2 S_v(\omega) \frac{(2 + x^2)}{(2 + ax^2)(1 + x^2/a)} \tag{7.14}$$

The perturbations in the torque are interpreted as being due to the perturbations in an effective wind speed uniform over the rotor disc. It follows that the spectrum of the effective wind speed, $S(\omega)$, is

$$S(\omega) = \frac{(2 + x^2)}{(2 + ax^2)(1 + x^2/a)} S_v(\omega) \tag{7.15}$$

The spectrum, $S(\omega)$, is normalised such that,

$$S(0) = S_v(0) \tag{7.16}$$

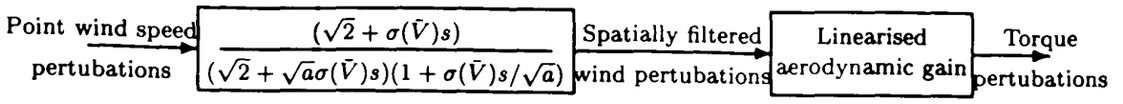

a. Linear model of torque perturbations

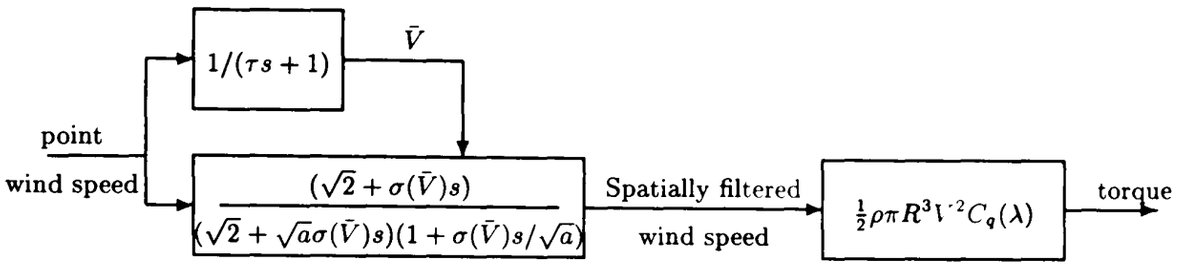

b. Non-linear model of torque

Figure 7.2: Models of axial hub torque

since the very low frequency component of the turbulent fluctuations in the wind speed are uniform over the rotor disc. The spectrum, $S(\omega)$, being a function of x^2, it can be spectrally factorised to obtain the linear model relating perturbations in torque to perturbations in point wind speed depicted in Figure 7.2a. The rotational averaging of the wind speed is modelled by the filter with transfer function, $f(s)$, where

$$f(s) = \frac{(\sqrt{2}+\sigma s)}{(\sqrt{2}+\sqrt{a}\sigma s)(1+\sigma s/\sqrt{a})} \tag{7.17}$$

The output from the filter may be used in conjunction with the non-linear torque coefficients to estimate the axial hub torque generated by the blade, see Figure 7.2b. In this case, the input to the spatial filter is the total point wind speed including the quasi-static mean. The relationship between torque and wind speed is

$$T = \frac{1}{2}\rho\pi R^3 V^2 C_q(\lambda) \tag{7.18}$$

where λ, the tip speed ratio,

$$\lambda = \Omega R/V$$

with ρ the density of air, viz. $1.225kg/m^2$, R is the radius of the rotor, V is the wind speed and Ω the angular velocity of the rotor. Of course the torque coefficient, $C_q(\lambda)$, is particular to the wind turbine of concern. The coefficients of the filter depend on the quasi-static mean wind speed, $\bar{V}$. From the derivation of the filter, it is clear that this mean wind speed must not deviate by much from the mean wind speed over the rotor

disc at a given time but must be averaged over a time scale significantly longer than the period of rotation of the rotor. Accordingly, the quasi-static mean wind speed, $\bar{V}$, is estimated by subjecting the point wind speed to the filter $1/(\tau s+1)$, see Figure 7.2b, which is equivalent to averaging the wind speed over τ seconds. An appropriate choice for τ is equivalent to a small number of rotations by the rotor. It should also be noted that, by observation 2, the same procedure may be used to estimate the axial hub torque due to the complete rotor. The point wind speed input to the simple torque model depicted in Figure 7.2 can either be measured site data or simulated data. In the latter case, an appropriate procedure for generating the point wind speed data is described in Appendix F.

The model, Figure 7.2b, of the wind speed/rotor interaction is validated with respect to monitored data for a commercial wind turbine sited at Altamont Pass, California. The radius of the rotor is 16.5m and its rotational velocity is 4.189 rad/sec. Representative time series of filtered wind speed are derived by simulation using measured point wind speed data as input to the model, Figure 7.2b. The spectrum for the filtered wind speed, Figure 7.3a, is estimated using data from 6 simulation runs of 204.8 seconds duration with a sampling rate of 10Hz. From Figure 7.3a which also depicts the spectrum for the measured point wind speed, the action of the filter is clear. Representative time series of low speed shaft torque are also derived by simulation using the measured point wind speed data as input to a model of the wind turbine which incorporates the model, Figure 7.2b, of the wind speed/rotor interaction. The wind speed is always below rated, thereby avoiding any distortion of the torque spectra by pitch regulation. The spectrum for the simulated low speed shaft torque, Figure 7.3b, is estimated using data from 6 simulation runs of 102.4 seconds with a sampling rate of 10Hz. The spectrum for the low speed shaft torque, Figure 7.3b, is also estimated from direct measurement. The strong $1\Omega_0$ peak exhibited by the latter is caused by slight inevitable misalignment on the low speed shaft of the strain gauges used to measure the torque. However the model can only be expected to be valid at frequencies below $1\Omega_0$ and prior to this peak the agreement between the spectra of simulated and measured low speed shaft torque is good. It should be noted that the nominal value for σ is used in the simulation, from which Figure 7.3 was obtained, with the value of γ set to 1.3 as suggested by Madsen and Frandsen [75] and the value used for τ is 10 seconds.

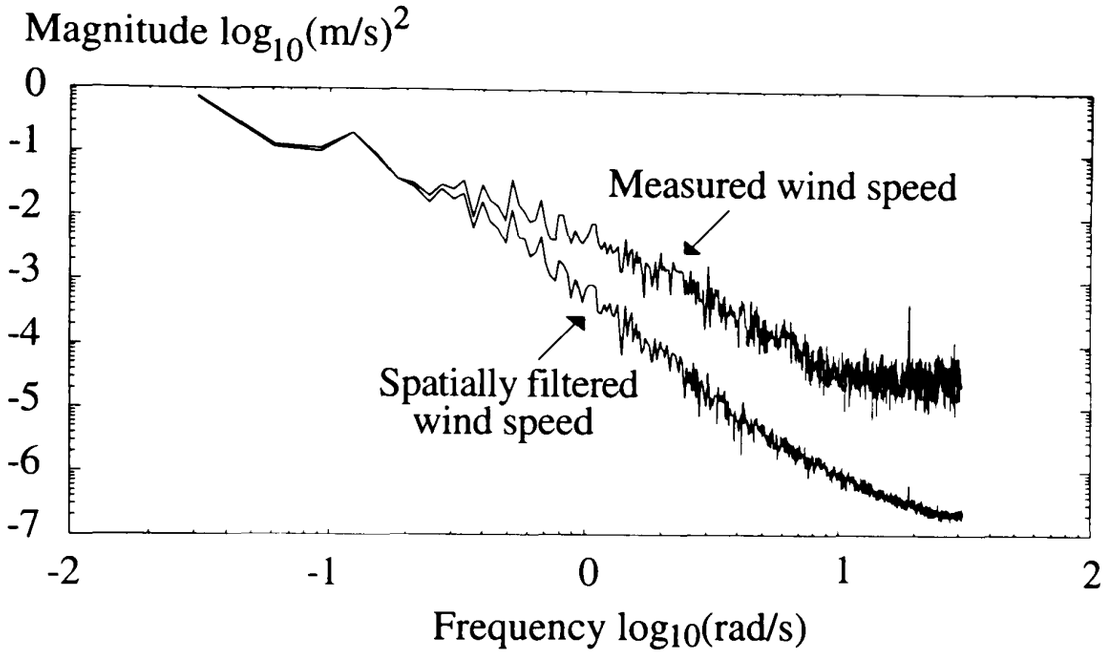

a. Measured and filtered wind speeds

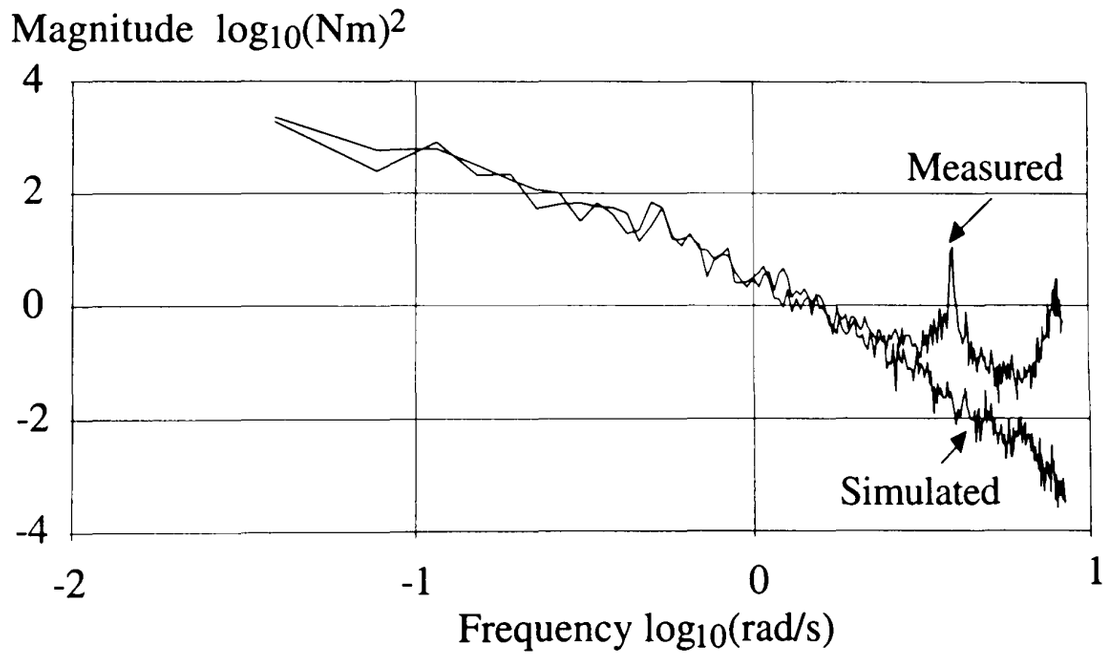

b. Measured and simulated low speed shaft torque

Figure 7.3: Spectra for wind speed and low speed shaft torque

7.4 Correlated wind speeds model

When it is necessary to model two correlated torques or moments, the torques or moments could be derived from suitable correlated averages of wind speed. For example, the axial hub torque due to the inner section of the blade, i.e. the main blade, and the axial hub torque due to the outer section of the blade, i.e. tip, could be derived from two simple correlated effective wind speeds. It is sufficient that the effective wind speeds, whilst, respectively, uniform over the swept area of the main blade and over the swept area of the tip, continue to induce the torques with the same auto-correlation and cross-correlation functions; that is, their spectra and cross-spectra remains unchanged whether the torques are derived from the full wind-field or the effective wind speeds. The derivation of correlated effective wind speed models, previously partially reported in [70], are described below. They are applied to the previously mentioned example whereby correlated axial hub torque due to the main blade and axial hub torque due to a tip are derived from correlated effective wind speeds.

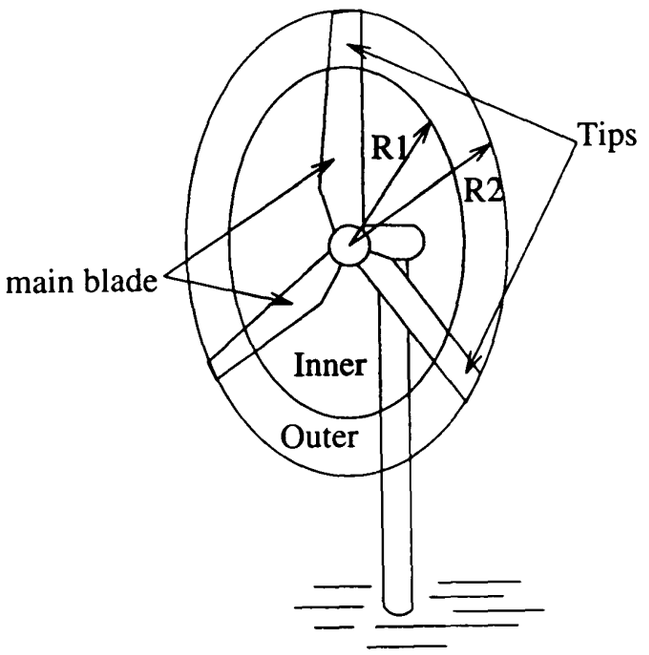

Figure 7.4: Inner and outer sections of rotor swept disc

Consider a single inner blade and its associated tip with A_I and A_O the areas swept by the main blade and tip, respectively, as shown in Figure 7.4. From the previous section, the spectrum for the effective wind speed over the inner swept disc is

$$S_{II}(\omega) = S_v(\omega)\Phi_{II}(x) \quad ;\Phi_{II}(x) = \bar{\Phi}_{II}(x)/\bar{\Phi}_{II}(0) \tag{7.19}$$

where

$$\bar{\Phi}_{II}(x) = \pi^2 R_1^4 \frac{2}{x^2}\left\{1 + \frac{4}{\pi}\int_0^{\frac{\pi}{2}}(1 - 3sin^2\theta)e^{-2xcos\theta}d\theta\right\} \tag{7.20}$$

The cross-correlation, $R_{T_O T_I}(t)$ between T_O and T_I, the torques due to tip and main blade respectively, is

$$R_{T_O T_I}(t) = k^2 \int_{A_O}\int_{A_I} R_{v(\mathbf{r}_1)v(\mathbf{r}_2)}(t)dA_1 dA_2 \tag{7.21}$$

where $R_{v(\mathbf{r}_1)v(\mathbf{r}_2)}(t)$ is the cross-correlation between the wind at $\mathbf{r}_1$ and wind at $\mathbf{r}_2$. Following section 7.3, the cross-spectrum $S_{T_O T_I}(\omega)$ is determined to be

$$\begin{aligned} S_{T_O T_I}(\omega) &= k^2 S_v(\omega)\int_{A_O}\int_{A_I} \mathcal{X}(\mathbf{r}_1, \mathbf{r}_2, \omega)dA_1 dA_2 \\ &= k^2 S_v(\omega)\bar{\Phi}_{IO}(x) \end{aligned} \tag{7.22}$$

where,

$$\bar{\Phi}_{IO}(x) = 4\pi R_1^4 \int_0^{\delta} dz(1+z)\int_0^{sin^{-1}(\frac{1}{1+z})} d\theta \int_{(z+1)cos\theta - \sqrt{1-(z+1)^2 sin^2\theta}}^{(z+1)cos\theta + \sqrt{1-(z+1)^2 sin^2\theta}} d\bar{l}\,\bar{l}e^{-x\bar{l}} \tag{7.23}$$

$$\delta = \frac{R_2 - R_1}{R_1} \quad \text{and} \quad x = \left(\frac{\gamma R_1}{\bar{V}}\right)\omega = \sigma_1 \omega \tag{7.24}$$

Hence the cross-spectrum between the effective wind speed over the inner disc and the effective wind speed over the outer annulus is

$$S_{IO}(\omega) = S_v(\omega)\Phi_{IO}(x) \quad ; \Phi_{IO}(x) = \bar{\Phi}_{IO}(x)/\bar{\Phi}_{IO}(0) \tag{7.25}$$

It follows that the spectrum for the effective wind speed over the outer annulus is

$$S_{OO}(\omega) = S_v(\omega)\Phi_{OO}(x) \quad ; \Phi_{OO}(x) = \bar{\Phi}_{OO}(x)/\bar{\Phi}_{OO}(0) \tag{7.26}$$

where

$$\bar{\Phi}_{OO}(x) = \bar{\Phi}_{(I+O)(I+O)}(x) - \bar{\Phi}_{II}(x) - 2\bar{\Phi}_{IO}(x) \tag{7.27}$$

and

$$\bar{\Phi}_{(I+O)(I+O)}(x) = \pi^2 R_2^4 \frac{2}{x^2}\left\{1 + \frac{4}{\pi}\int_0^{\frac{\pi}{2}}(1 - 3sin^2\theta)e^{-2xcos\theta}d\theta\right\} \tag{7.28}$$

Spectrally factorising the spectral matrix

$$\begin{bmatrix} S_{II}(\omega) & S_{IO}(\omega) \\ S_{IO}(\omega) & S_{OO}(\omega) \end{bmatrix} = \begin{bmatrix} \Phi_{II}(x)S_v(\omega) & \Phi_{IO}(x)S_v(\omega) \\ \Phi_{IO}(x)S_v(\omega) & \Phi_{OO}(x)S_v(\omega) \end{bmatrix} \tag{7.29}$$

models are derived for the inner and outer effective wind speeds, V_I and V_O, such that

$$\begin{aligned} V_I &= f_1(s).w_1 + f_3(s)/f_4(s).w_3 \\ V_O &= f_2(s).w_2 + f_3(s)f_4(s).w_3 \end{aligned} \tag{7.30}$$

where w_1, w_2 and w_3 are independent point wind speeds and $f_1(s)$, $f_2(s)$, $f_3(s)$ and f_4 are suitable filters. It should be noted that the phase of $S_{IO}(\omega)$ is implicitly assumed in the derivation of (7.29) and (7.30) to be zero; that is,

$$S_{IO}(\omega) = S^*_{IO}(\omega) = S_{OI}(\omega) \tag{7.31}$$

The derivation of the filters $f_1(s)$, $f_2(s)$, $f_3(s)$ and $f_4(s)$ is described below.

The functions Φ_{II}, Φ_{OO} and Φ_{IO} are reformulated as functions of x^2, rather than x, and suitable fits, Φ_{xx}, Φ_{yy} and Φ_{xy} respectively, determined. The fits must have the following properties:

a) Φ_{xx}, Φ_{yy} and Φ_{xy} must be proper rational polynomial expressions in x^2

b) none of the roots of the numerators and denominators of Φ_{xx}, Φ_{yy} and Φ_{xy} must lie in the right-half of the complex x^2 plane.

Requirements a) and b) can be met in a relatively simple manner provided the fitted functions roll off in x^2 as an integer multiple of -20db/decade. Since the correlation factor, μ, defined by

$$\mu = \Phi_{IO}/\sqrt{\Phi_{II}\Phi_{OO}} \tag{7.32}$$

is the most important measure of cross-correlation it must be fitted with greatest accuracy. Unfortunately, both $\sqrt{\Phi_{II}}$ and $\sqrt{\Phi_{OO}}$ roll off at -10db/decade. However, $\mathcal{A}$ and $\mathcal{B}$, where

$$\mathcal{A} = \sqrt{\Phi_{II}\Phi_{OO}}; \quad \mathcal{B} = \sqrt{\Phi_{II}/\Phi_{OO}} \tag{7.33}$$

roll off at -20db/decade and 0db/decade, respectively. Consequently, the most appropriate way to represent the numerically calculated data is by the fits, μ_{fit}, $\mathcal{A}_{fit}$ and $\mathcal{B}_{fit}$, to μ, $\mathcal{A}$ and $\mathcal{B}$, respectively. Subsequently, Φ_{xx}, Φ_{yy} and Φ_{xy} are determined from

$$\Phi_{xx} = \mathcal{A}_{fit}\mathcal{B}_{fit}; \; \Phi_{yy} = \mathcal{A}_{fit}/\mathcal{B}_{fit}; \; \Phi_{xy} = \mu_{fit}\mathcal{A}_{fit}; \tag{7.34}$$

Clearly from (7.30),

$$|f_3(j\omega)|^2 = \Phi_{xy}(x) \tag{7.35}$$

and

$$|f_1(j\omega)|^2 = (\Phi_{xx}(x) - \Phi_{xy}/\Psi(x)) \tag{7.36}$$

$$|f_2(j\omega)|^2 = (\Phi_{yy}(x) - \Phi_{xy}\Psi(x)) \tag{7.37}$$

where, $\Psi(x)$ has the properties a) and b), such that the magnitude of $\Psi(0)$ is one and the degree of the numerator and denominator are the same, and

$$|f_4(j\omega)|^2 = \Psi(x) \tag{7.38}$$

The spectrum, $\Psi(x)$, is chosen to ensure that both $(\Phi_{xx}(x) - \Phi_{xy}(x)/\Psi(x))$ and $(\Phi_{yy}(x) - \Phi_{xy}(x)\Psi(x))$ have no roots in the right-half complex x^2 plane. By the Nyquist stability criterion (see any control text), this requirement is met provided the magnitude of both $(\Phi_{xx}(x)/\Phi_{xy}(x))/\Psi(x))$ and $(\Phi_{yy}(x)/\Phi_{xy}(x).\Psi(x))$ are less than one for all x. Since

$$|\Phi_{xy}^2(x)/(\Phi_{xx}(x)\Phi_{yy}(x))| \simeq |\bar{\Phi}_{IO}^2(x)/(\bar{\Phi}_{II}(x)\bar{\Phi}_{OO}(x))| \leq 1 \tag{7.39}$$

it is straightforward to find a suitable $\Psi(x)$ using standard control methods.

The transfer functions for $f_1(s)$ to $f_4(s)$ are determined by factorising the right-hand side of the expressions (7.35) to (7.38), respectively; that is, the overall gain, K^2, corresponds to a gain, K, in the transfer function, each factor of (x^2+a^2) corresponds to a factor $(\sigma s+a)$ in the transfer function and each factor $((x^2)^2+ux^2+v^2)$ corresponds to a factor $(\sigma^2 s^2+\sqrt{u+2v}\sigma s+v)$ in the transfer function. Because of the number of steps involved, the filters $f_1(s)$ to $f_4(s)$ can be high order but low order approximations for each can be readily determined using standard control methods. However, rather than $f_3(s)$ and $f_4(s)$, themselves, low order approximations $f_{31}(s)$ and $f_{32}(s)$ are directly determined for $(f_3(s)/f_4(s))$ and $(f_3(s).f_4(s))$, respectively. Of course the filters $f_{31}(s)$ and $f_{32}(s)$ tend to one and $f_1(s)$ and $f_2(s)$ tend to zero on the limit as s tends to zero.

7.5 Illustrative example and model validation

The procedure described in section 7.4 is illustrated for the suggested example; that is, the axial hub torque due to the main blade and the axial hub torque due to a tip. Consider the case when

$$R_1 = 13m \quad ; R_2 = 16.5m \tag{7.40}$$

The approximations μ_{fit}, $\mathcal{A}_{fit}$ and $\mathcal{B}_{fit}$ to μ, $\mathcal{A}$ and $\mathcal{B}$, respectively, see Figure 7.5, are

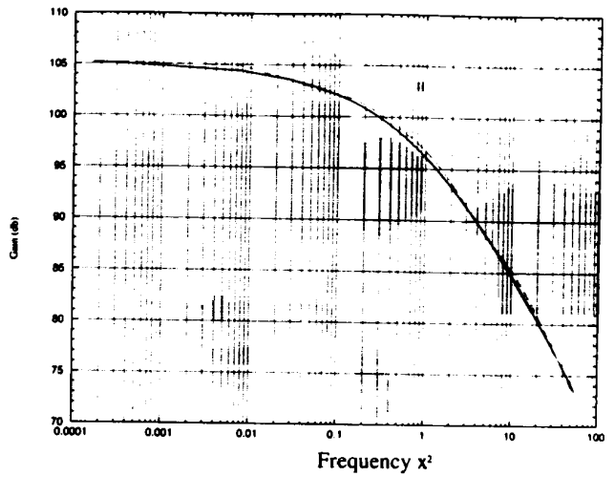

a. A and A_{fit}

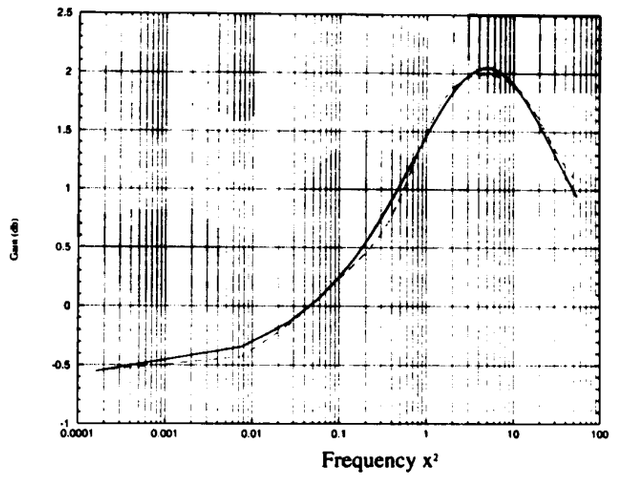

b. B and B_{fit}

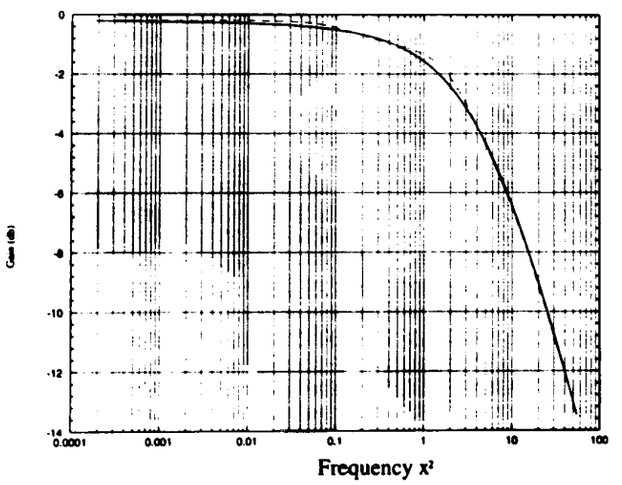

c. μ and μ_{fit}

Figure 7.5: Comparison of data (—) and fits (- - -) to μ, A and B

$$\rho_{fit} = \frac{23.94(x^2+0.175)(x^2+4)(x^2+27.417)}{(x^2+0.159)(x^2+2.864)(x^2+13.034)(x^2+79.548)} \tag{7.41}$$

$$\mathcal{A}_{fit} = \frac{255087(x^2+0.027)(x^2+0.41)(x^2+4.78)}{(x^2+0.0197)(x^2+0.251)(x^2+1.315)(x^2+12)} \tag{7.42}$$

$$\mathcal{B}_{fit} = \frac{1.635(x^2+0.011)(x^2+0.132)(x^2+0.715)(x^2+26.883)}{(x^2+0.0115)(x^2+0.141)(x^2+0.814)(x^2+21.326)} \tag{7.43}$$

and a suitable choice for $\Psi(x)$ is

$$\Psi(x) = \frac{0.891(x^2+0.411)(x^2+0.115)}{(x^2+0.132)(s^2+0.011)} \tag{7.44}$$

The corresponding simplified filters are

$$f_1(s) = \frac{1.204\sigma s}{(\sigma s+0.35)(\sigma s+3.7)} \tag{7.45}$$

$$f_2(s) = \frac{1.203\sigma s(\sigma s+0.32)}{(\sigma s+0.184)(\sigma s+5.4)(\sigma s+0.52)} \tag{7.46}$$

$$f_{31}(s) = f_3(s)/f_4(s) = \frac{6.386\sigma s(\sigma^2 s^2+20.108\sigma s+7.344)}{(\sigma s+0.263)(\sigma s+20.5)(\sigma^2 s^2+8.85\sigma s+8.7)} \tag{7.47}$$

$$f_{32}(s) = f_3(s).f_4(s) = \frac{5.69\sigma s(\sigma^2 s^2+20.09\sigma s+10.11)}{(\sigma s+0.263)(\sigma s+20.5)(\sigma^2 s^2+9.54\sigma s+10.11)} \tag{7.48}$$

The procedure is repeated with R_1 varying from 11.5m to 14m in steps of 0.5m. The complete set of results are detailed in Appendix E. That the filters, $f_1(s)$, $f_2(s)$, $f_{31}(s)$ and $f_{32}(s)$, adequately represent the original data can be confirmed from Figure 7.6 which depicts the correlation factor, μ, together with μ_{fit}, where

$$\mu_{fit} = \frac{|f_3(j\omega)|^2}{[|f_1(j\omega)|^2+|f_{31}(j\omega)|^2]^{\frac{1}{2}}[|f_2(j\omega)|^2+|f_{32}(j\omega)|^2]^{\frac{1}{2}}} \tag{7.49}$$

The model, (7.30), of correlated effective wind speeds for the main blade, V_I, and the tip, V_O, and the related total, main blade and tip torques, is depicted in Figure 7.7. The effective wind speeds, V_I and V_O, can be used in a similar manner to estimate the blade bending moments, both chord and flap, since the moments like the torques vary with radial position. The representative time series for V_I and V_O, depicted in Figure 7.8, and the estimated correlation factor, μ_{sim}, depicted in Figure 7.9, are derived by simulation using below rated point wind speeds, v_1, v_2 and v_3, generated as described in Appendix F, with means of $8.5m/s$ and turbulence intensities 20%. From 20 simulation runs of 112.5 second duration with a sampling rate of 40Hz, μ_{sim} is estimated by

$$\mu_{sim} = |\beta| \tag{7.50}$$

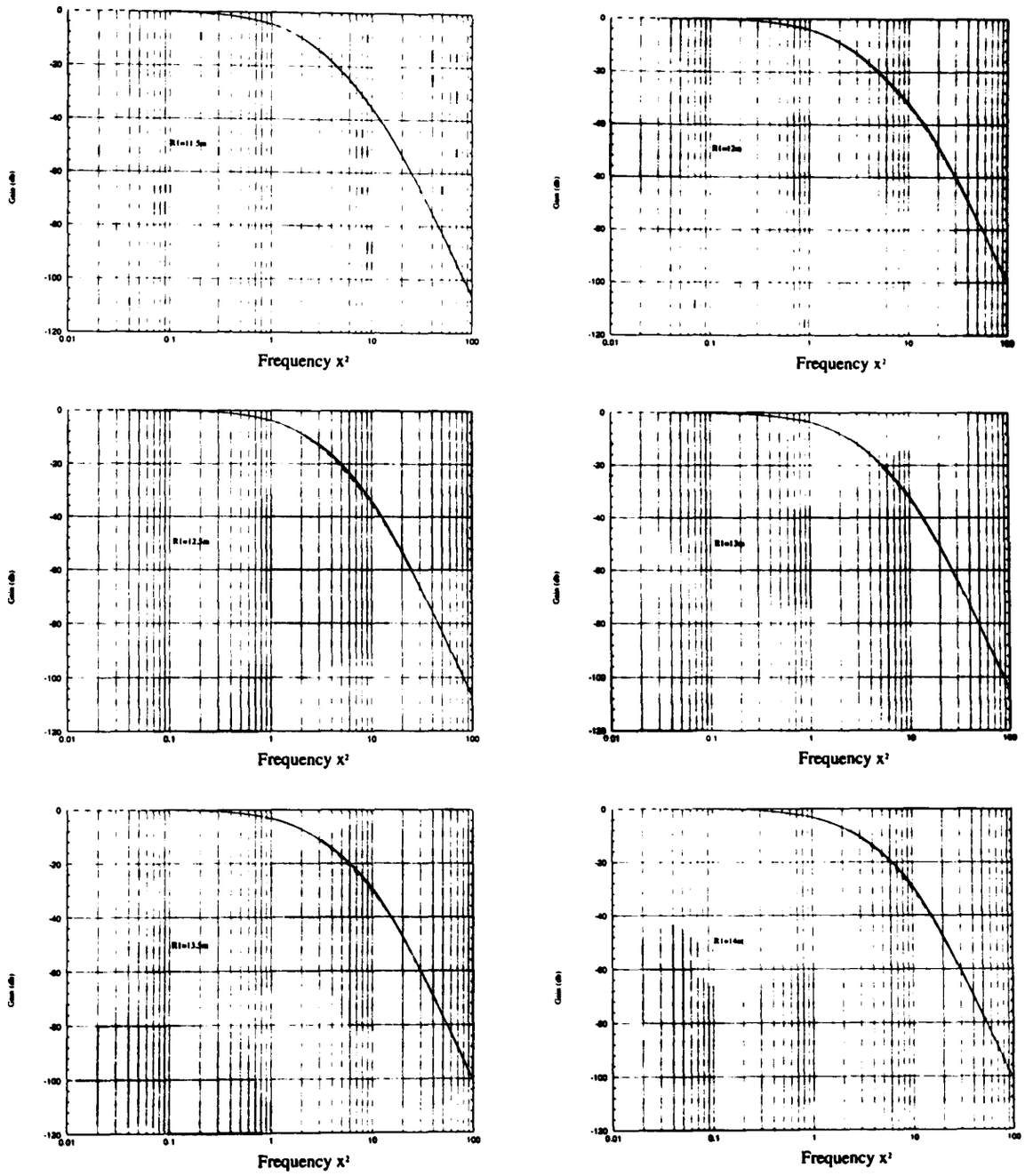

Figure 7.6: Comparison of original (—) and simplified (- - -) fits of μ

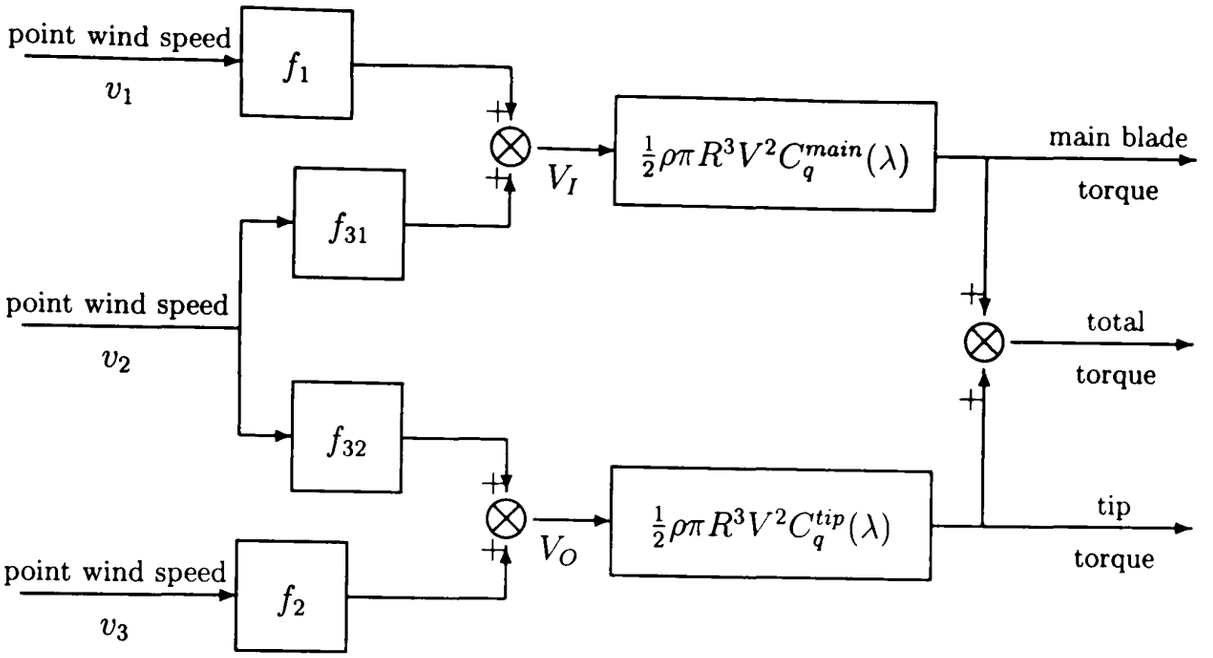

Figure 7.7: Model for correlated main blade and hub torque

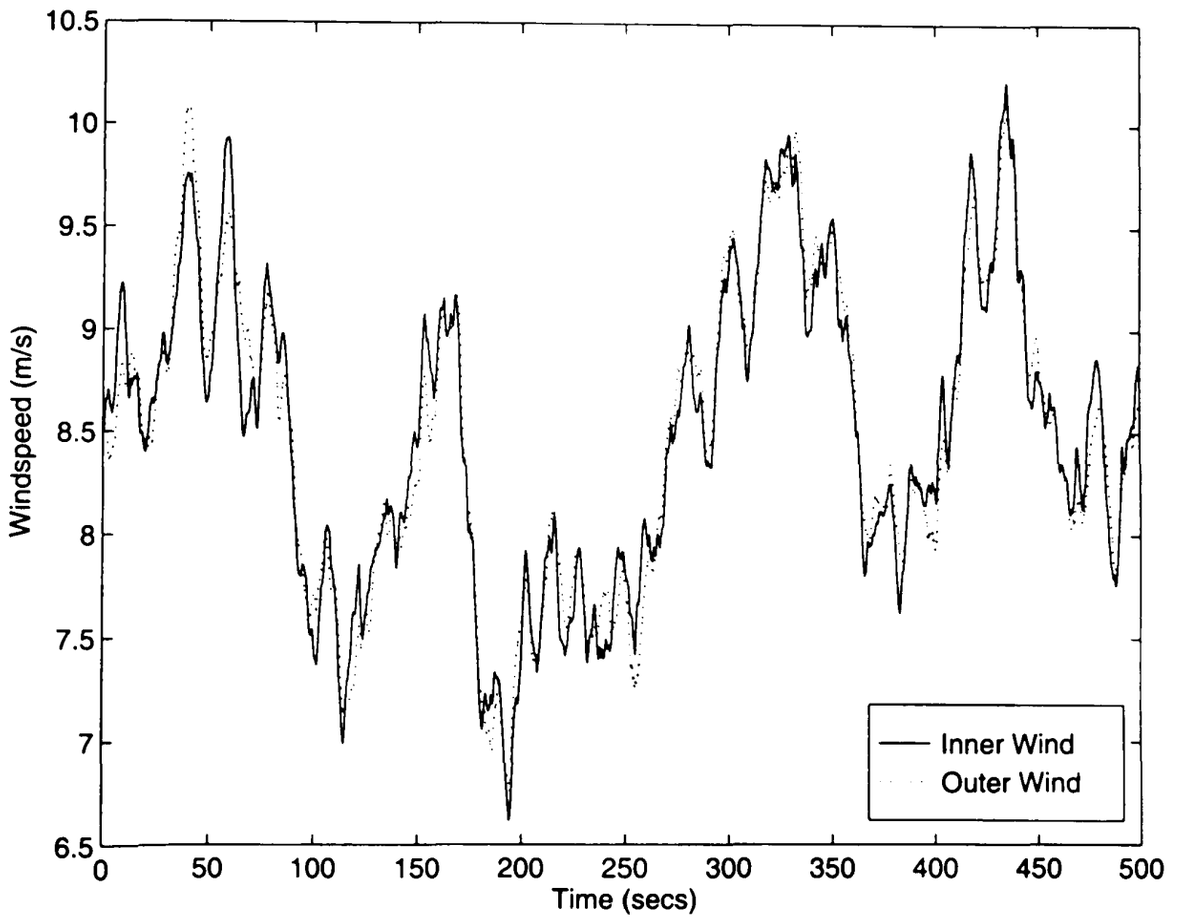

Figure 7.8: Inner and outer effective wind speeds

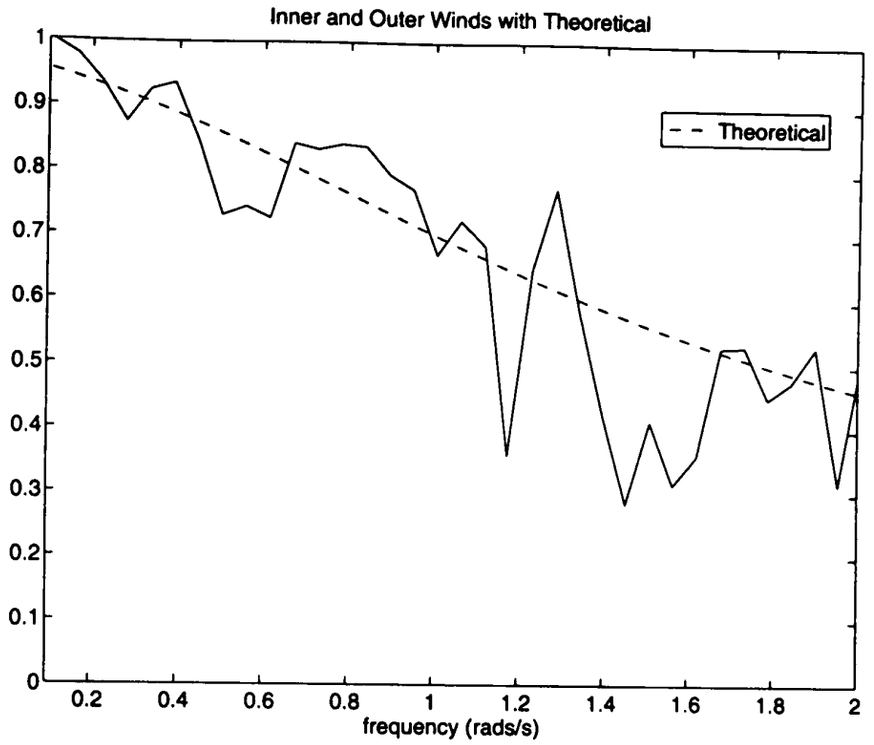

a. Correlation factors μ_{fit} and μ_{sim}

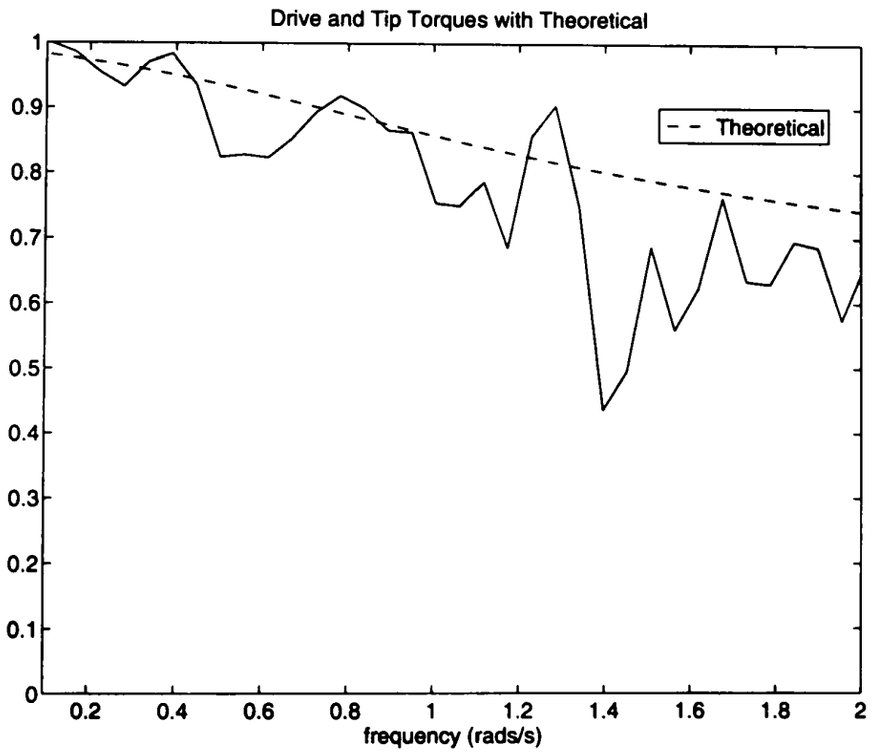

b. Correlation factors ν_{fit} and ν_{sim}

Figure 7.9: Comparison of simulated to theoretical correlation factors, μ and ν

with

$$\beta(\omega) = \frac{\sum_{i=1}^{20} x_i(\omega).y_i(\omega)^*}{\sqrt{\sum_{i=1}^{20} |x_i(\omega)|^2 . \sum_{i=1}^{20} |y_i(\omega)|^2}} \tag{7.51}$$

where $x_i(\omega)$ and $y_i(\omega)$ are the FFT of the simulated time series for V_I and V_O, respectively. It should be noted that the relative phase between V_I and V_O is estimated by the argument of β. Due to its asymmetric nature the estimated correlation factor, μ_{sim}, is biased with a tendency to be less than the exact correlation factor, μ_{fit}. Even though μ_{sim} is estimated from 2250 seconds and 90,000 points of data, its bias can be clearly observed in Figure 7.9. In addition, the spread of μ_{sim} relative to μ_{fit} is quite marked in Figure 7.9 since the estimate is very slow to converge. The correlation factor, ν, between the torques is also estimated, see Figure 7.9 where ν_{fit} is the correlation factor between the wind speed over the total blade and the tip, i.e

$$\nu_{fit} = \frac{\Phi_{(I+O)O}}{\sqrt{\Phi_{(I+O)(I+O)}\Phi_{OO}}} = \frac{\Phi_{IO} + \Phi_{OO}}{\sqrt{(\Phi_{II} + 2\Phi_{IO} + \Phi_{OO})\Phi_{OO}}} \tag{7.52}$$

and ν_{sim} is the correlation factor between the axial hub torque due to the complete blade and the axial hub torque due to the tip.

The model, (7.30), of the wind speed/rotor interaction is validated with respect to monitored data for the commercial wind turbine. The parameters of the wind turbine, the number of events in the data sample and sampling rate conform to those assumed in the above discussion. The wind speed is always below rated. The correlation factors, ν_{ch} and ν_{fl} respectively, are estimated from measured blade root and tip chord bending moments and flap bending moments, Figure 7.10. The agreement between ν_{sim} and ν_{fl} is well within the resolution of the data but the agreement between ν_{sim} and ν_{ch} is not so good for frequencies less than 1 rad/sec. (The estimates of ν are essentially independent of the torques and moments used). The reason for the latter is the dominance of the chord bending moment by the gravity loads which greatly reduces the resolution of the data. In addition, the relative phase between the moments are estimated, Figure 7.11, to confirm the assumption of zero relative phase.

7.6 Spectral peaks model

No attempt is made to represent the spectral peaks in the models described in sections 3 are 4. In Figure 7.12, the peaks at $1\Omega_0$, $2\Omega_0$, $3\Omega_0$ and higher multiples of Ω_0 can be clearly seen on the measured spectrum of blade root flap bending moment. Except for the deterministic spike at $1\Omega_0$ the peaks are essentially stochastic. Other than a

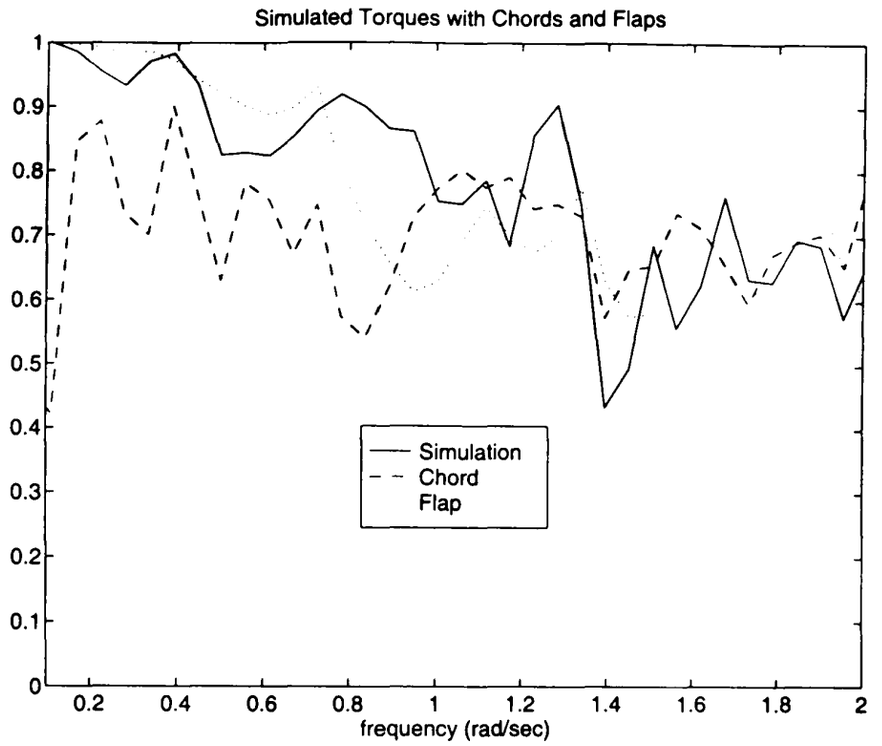

Figure 7.10: Comparison of correlation factors, ν_{sim}, ν_{ch} and ν_{fl}

greatly enhanced deterministic spike at $1\Omega_0$, the peaks on the blade root chord bending moments are very similar. Rather than modifying the effective wind speeds, the torques and moments are directly modified by the addition of components to represent the spectral peaks. This approach is justified for the model of two correlated effective wind speed since the correlation factors, μ and ν, are unity in the vicinity of the spectral peaks, see Figure 7.13. Furthermore, ignoring the deterministic spike at $1\Omega_0$ and taking into account the distortion caused by the log frequency scale in Figure 7.12, there is little difference in the shape of the different spectral peaks; that is, their shapes can be assumed to be the same. Consequently, the same model can be used for all the spectral peaks provided a simple rescaling in frequency is applied.

A model for the spectral peak at $1\Omega_0$ is derived in Holley et al. [58]. When $n = 1$ it is equivalent to the representation of the spectral peak in the torque or moment, $L_{n\Omega_0}$, by

$$L_{n\Omega_0} = \epsilon_1 cos(n\Omega_0 t) + \epsilon_2 sin(n\Omega_0 t) \tag{7.53}$$

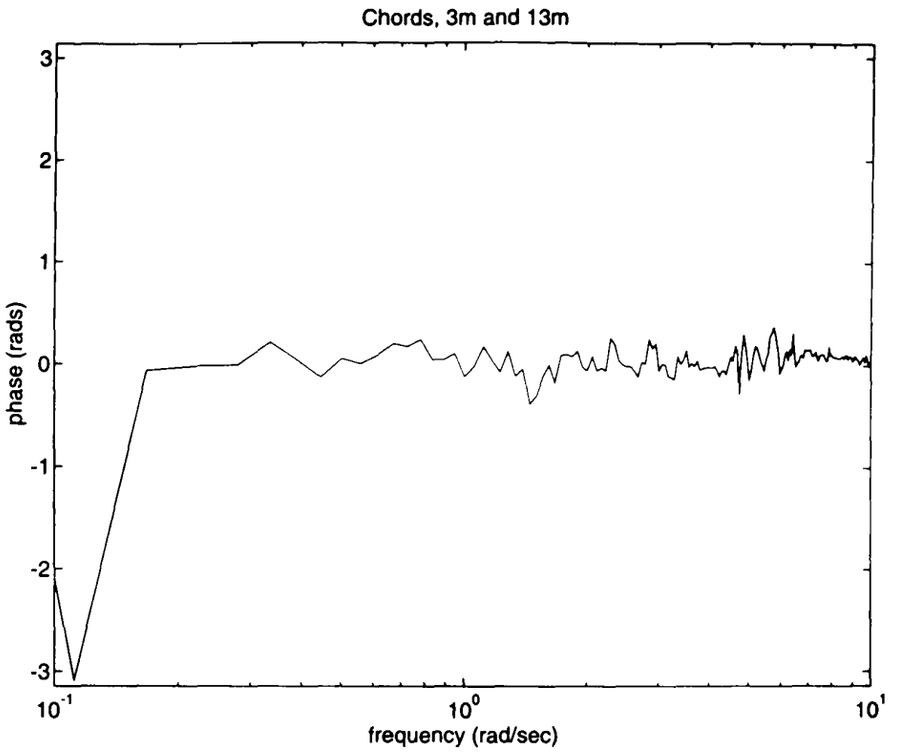

a. Phase between chord moments

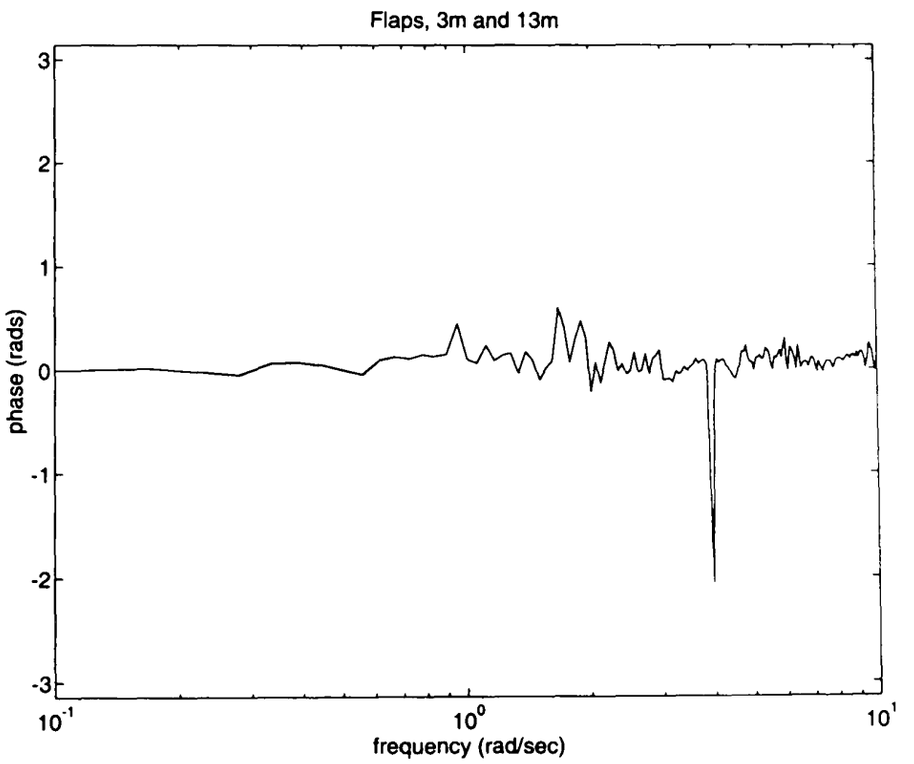

b. Phase between flap moments

Figure 7.11: Estimates of phase from measured data

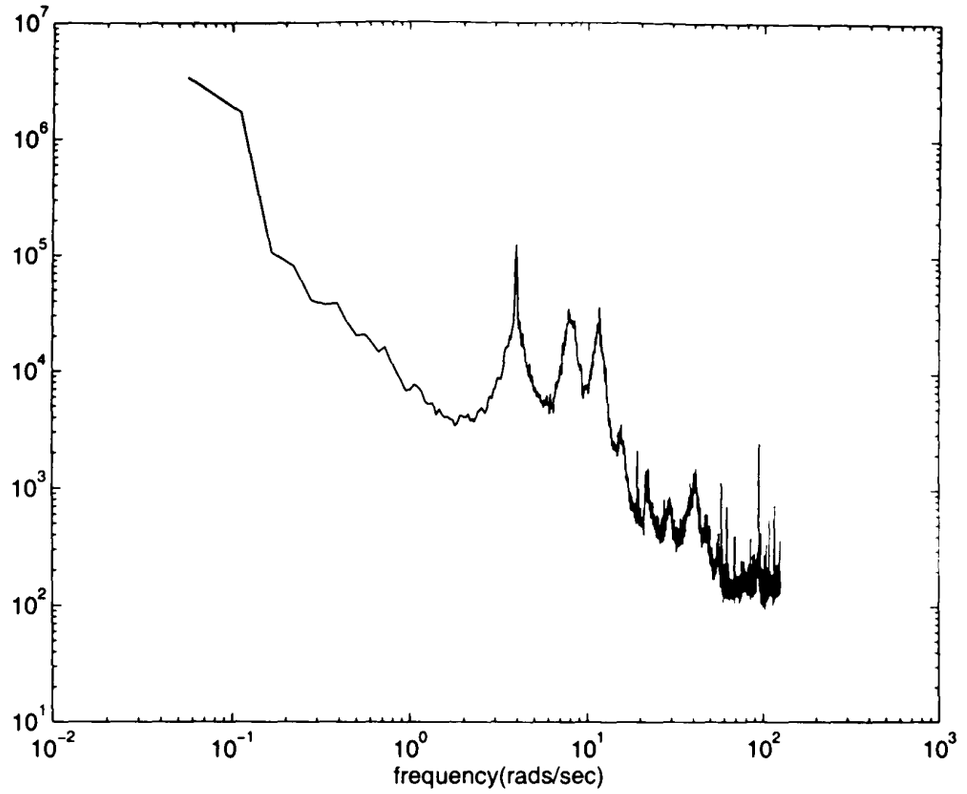

Figure 7.12: Estimate of spectra of blade root flap moment from measured data

with ε_1 and ε_2 independent coloured noise outputs of

$$\dot{\varepsilon}_1 = -a_{n\Omega_0}\varepsilon_1 + b_{n\Omega_0}g_1 \tag{7.54}$$

$$\dot{\varepsilon}_2 = -a_{n\Omega_0}\varepsilon_2 + b_{n\Omega_0}g_2 \tag{7.55}$$

where both g_1 and g_2 are white Gaussian noise. The spectrum, $S_{n\Omega_0}(\omega)$, for $L_{n\Omega_0}$ is

$$S_{n\Omega_0}(\omega) = \frac{b^2_{n\Omega_0}}{2\pi(a^2_{n\Omega_0} + (\omega - n\Omega_0)^2)} \tag{7.56}$$

which has the required peak centred at $n\Omega_0$. The height and width of the peak can be adjusted by varying $b_{n\Omega_0}$ and $a_{n\Omega_0}$, respectively.

The model is depicted in Figure 7.14 with the filter $p(s)$ defined by

$$p(s) = \frac{b_{n\Omega_0}}{(s + a_{n\Omega_0})} \tag{7.57}$$

When required, e.g. to represent tower shadow or wind sheer, a deterministic component can be included in the model of the spectral peak by setting $A_{n\Omega_0}$ to a non-zero value. The filter, $h(s)$, is included in Figure 7.14 to cause the spectral peak to roll off in an appropriate manner. When the model represents an isolated spectral peak at $n\Omega_0$, the

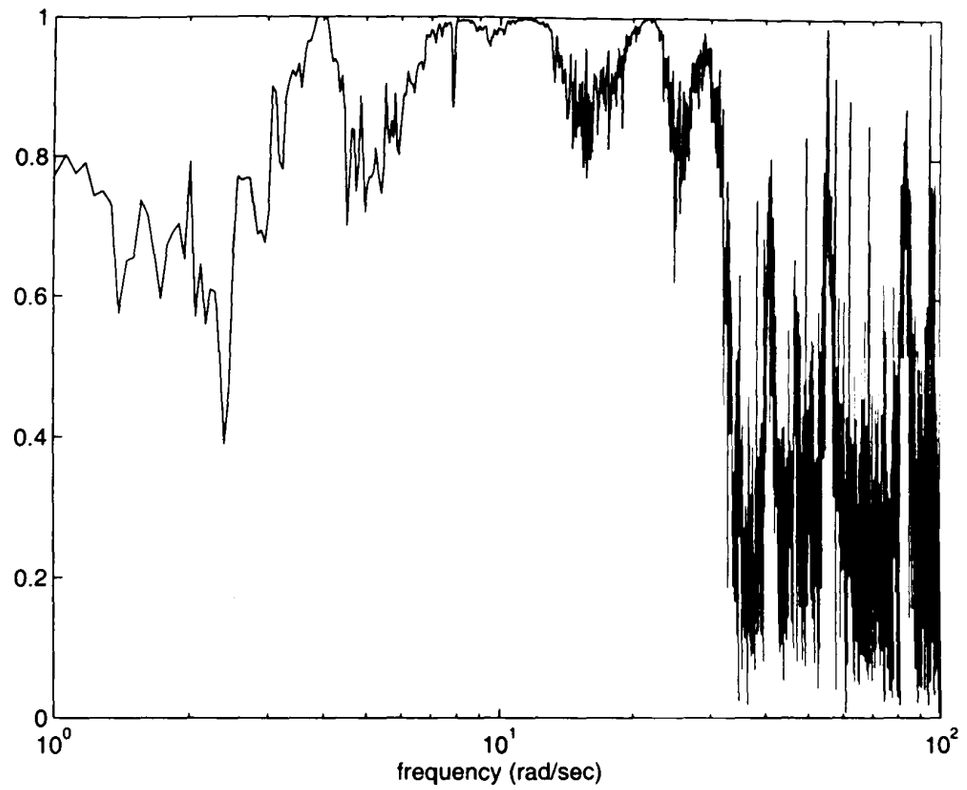

Figure 7.13: Estimate of correlation factor, ν_{ch}, from measured data

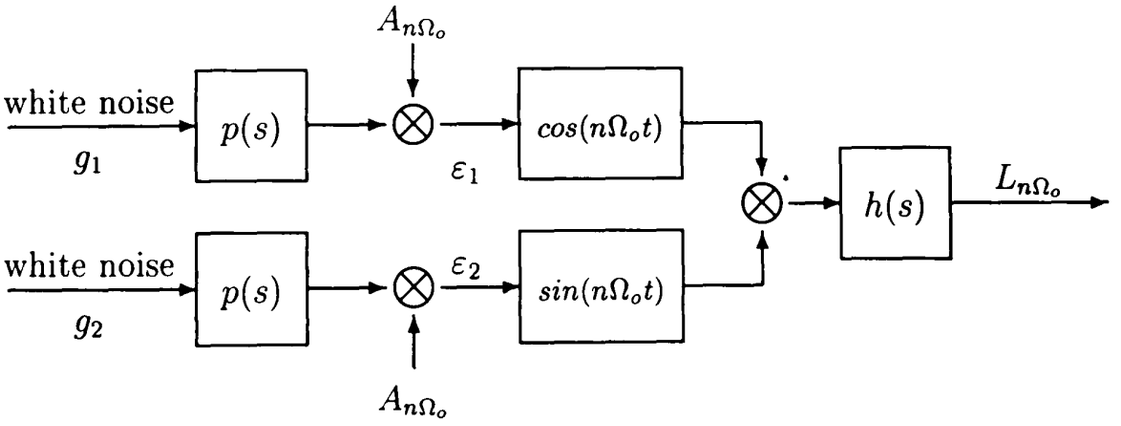

Figure 7.14: Model of spectral peaks

spectrum, (7.56), does not roll off sufficiently fast and it is necessary to increase the roll-off by choosing $h(s)$ to be the first order filter

$$h(s) = \frac{1.25}{((s/n\Omega_0) + 1.25)} \tag{7.58}$$

When the model represents not only the spectral peak at $n\Omega_0$ but also the spectral peaks at higher frequency albeit smeared to form a continuous tail, $h(s)$ is chosen to be the fourth order filter

$$h(s) = \frac{3.692(s/n\Omega_0)^2((s/n\Omega_0)^2 + 0.242(s/n\Omega_0) + 0.919)}{((s/n\Omega_0)^4 + 2.382(s/n\Omega_0)^3 + 2.720(s/n\Omega_0)^2 + 2.157(s/n\Omega_0) + 0.822)} \tag{7.59}$$

For a particular torque or moment, one or more spectral peaks, as appropriate, can be represented by the above model. Typically for the axial hub torque on a 3-bladed wind turbine only the $3\Omega_0$ peak need be modelled but on a 2-bladed teetered-hub machine both the $2\Omega_0$ and $4\Omega_0$ peaks are required. For the torque or moment on a single blade $1\Omega_0$ is usually sufficient although it may need to be augmented by the filter, (7.59), to represent higher frequency peaks.

The model, Figure 7.14, for spectral peaks is validated with respect to monitored data for the commercial wind turbine. Measured generated power is used rather than measured low speed shaft torque to avoid the problem associated with the misalignment of strain gauges. The simulation of the wind turbine considered in Section 2 is modified by inclusion of the model for an isolated spectral peak at $3\Omega_0$ with

$$a_{3\Omega_0} = 0.4 \quad ; b_{3\Omega_0} = 3000$$

Representative time series of generated power are derived by simulation using measured point wind speed data in Figure 7.2b. Again, the wind speed is always below rated. The spectrum for simulated generated power, Figure 7.15, is estimated from 24 sets simulation runs of 51.2 seconds duration with a sampling rate of 10Hz. The spectrum for measured generated power, Figure 7.15, is also estimated from measurements of generated power made simultaneously as the measurements of point wind speed. The spectra are in very good agreement except for the very sharp peaks at $1\Omega_0$ and $2\Omega_0$ in the measured power spectrum. The peaks at $1\Omega_0$ and $2\Omega_0$ are caused by blade imbalance which is not modelled in the simulation. Since the simulated generated power is dependent on the wind turbine drive-train dynamics, the results, depicted in Figure 7.15, validate not only the effective wind speed model and the $3\Omega_0$ spectral peak model but also the drive-train model used in the simulation.

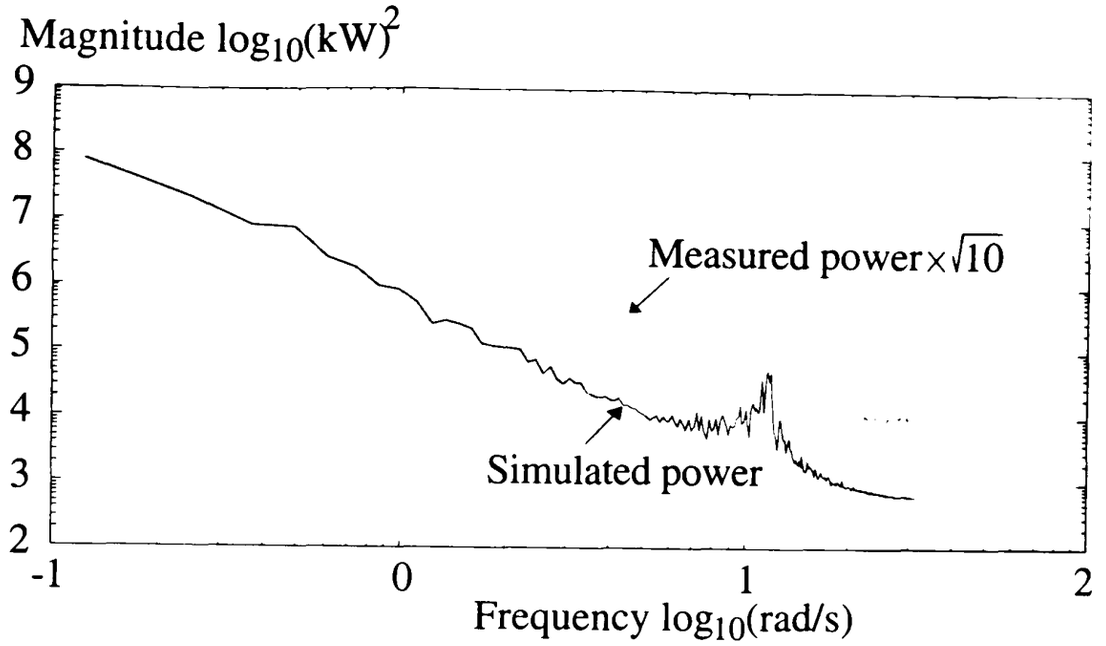

Figure 7.15: Power spectrum of measured and simulated power

7.7 Summary

Simple ordinary differential equation models of the wind-field/rotor interaction are derived above for both for single torques and moments and for correlated pairs of torques and moments. The models ensure that the torques and moments have appropriate statistical properties; that is, appropriate auto-spectral and cross-spectral properties. Explicit models are derived for the axial hub torque due to a complete blade and for the correlated axial hub torques due to separate inner and outer section of the blade for several geometries. However, the methods are quite general and might also be applied to other torques and moments such as blade flap or chord bending moments.

The models represent both the averaging of the wind-field and the rotational sampling of the wind-field by the blade. For a particular choice of parameters, the explicit models are validated against monitored data for a commercial wind turbine sited at Altamont Pass, California. The agreement between simulated and measured data is good.

Now that suitable models have been derived for both the wind turbine and the wind, MBPC can be applied to a variable speed wind turbine.

Chapter 8

Applying MBPC to a Variable Speed Wind Turbine

8.1 Introduction

The realization of the potential advantages of variable speed wind turbines (VSWTs) described in Chapter 4 are largely dependent on the rotor aerodynamics and the control system used. The latter aspect is investigated below. In particular the application of MBPC is investigated and its performance assessed. In doing this all the work presented in the previous chapters is brought together and gives a good indication of the potential for MBPC to be used on wind turbines and renewable energy systems in general. Also, through applying MBPC to what is a demanding control problem, much is learned about the claims made in support of MBPC in Chapter 2, and a realistic judgment about its potential benefits made. The main claims in support of MBPC which are examined are its ease of implementation and its performance.

The analysis described below is based on the 300kW, 3 bladed, up wind, horizontal axis variable speed wind turbine described in Chapter 6 and uses some of the aerodynamic models from Chapter 7.

8.2 Designing a MBPC controller for VSWTs

How the MBPC controller is implemented on the variable speed wind turbine is described below, detailing the steps necessary to achieve this.

The MBPC controller takes, as inputs, the outputs from the VSWT and uses the rotor speed and generator reaction torque to determine the current operating point

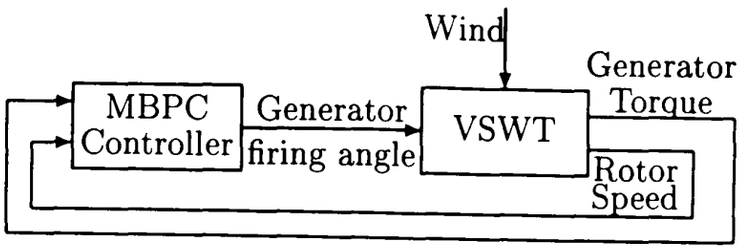

Figure 8.1: MBPC applied to a VSWT

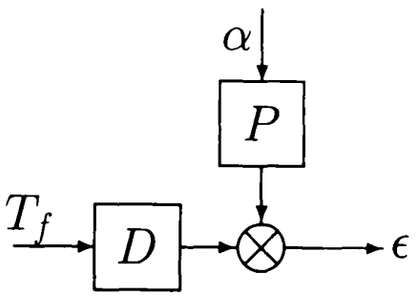

Figure 8.2: Plant, P, and disturbance, D, models for generator firing angle and aerodynamic torque

on the torque-rotor speed plane. This information gives the distance, or error, from the desired control strategy curve. Then, following the MBPC techniques described in chapter 2, the controller calculates a trajectory from the current error to the ideal error (i.e. zero). Models of the system are used to determine the future response of the system and the optimal change to the system input (in this case the generator firing angle, α) is calculated. This configuration of the MBPC controller is shown in Figure 8.1. The technique used below differs from that implemented on the Solar Power plant in Chapter 3 as, due to the unstable nature of the VSWT in above rated wind conditions, step response models are not suitable. Instead of these, transfer function models are used as described in Section 2.2.2.

The steps necessary to implement the MBPC controller are:

Generation of models Using the chosen control strategies for below and above rated wind speeds, along with the appropriate models of the system, a relationship describing the error, ϵ, from the control strategy is derived in terms of the two system inputs, i.e. the firing angle of the generator, α, (the wind turbine input) and the aerodynamic torque, T_f, (the wind disturbance) as shown in Figure 8.2. (The models of disturbance, D, and plant, P, are defined later in the chapter.)

Simplification of models The models generated above are quite complex and before they are used in the MBPC controller they are to be simplified and then converted from a continuous to a discrete model.

Simulation Using the discrete models of the system the controller is coded and then simulated. Firstly simulations will be run separately for below and above rated wind speeds to allow refinement of the controllers before combining them into one system and testing for a range of windspeeds.

Analysis Results obtained from the simulation are used for refining the system and then used to compare the system to a classically designed controller. This comparison enables a true evaluation of the performance and potential of MBPC.

8.3 Implementation issues

8.3.1 Below and above rated wind speeds

As mentioned above, a distinction is made between above and below rated wind speeds. Due to the nature of wind turbines their operation is very different for below and above rated wind speeds. This fact leads to two very different control strategies, two different models of the system and two different controllers. Thus in the discussion below both these controllers require to be developed and tested separately before trying to combine these controllers together.

8.3.2 Sample time

In order to implement the MBPC controller a sample time must be chosen to determine how often the controller will act. (This sample time will also be used in the conversion of continuous models into discrete models). That is, a rate must be chosen at which the controller will sample the signal from the wind turbine and calculate the new firing angle of the generator. When determining the sample time a balance is made between operating the controller too fast or too slow. The controller should accept that, due to the high inertia of the system, high frequency disturbances cannot be eliminated and it must concentrate on minimizing the effect of the lower frequency trends within the disturbances. However the controller needs to be fast enough to ensure the wind turbine does not drift too far from the ideal control strategy and thus require large changes in the generator firing angle to correct this as these large changes cause unwanted sudden

large jumps in the system which can be destabilising. A good balance of these two conflicting requirements is to initially set the sample time to 0.5 seconds.

However, due to the MBPC controller only operating every sample, several factors need to be addressed. First, the error signal, ϵ, which is fed into the controller should be smoothed by a filter, f_ϵ, to provide for the controller an accurate value representing an average value of the error rather some spurious spike appearing at the sampling instant. Secondly the output from the controller is a series of step changes. Thus, in order to protect the system from these sudden changes in α which may cause unwanted sudden transients in the system, a filter, f_α, is placed on the output of α. After investigation into the effects of these filters, the most effective models are simple first-order filters,

$$f_\epsilon = 1.2/(s+1.2) \quad \text{and} \quad f_\alpha = 10/(s+10) \tag{8.1}$$

8.4 Generation and simplification of the models

Below is described the methods used to determine suitable models for use in designing the controller, and how they are simplified to be used by the MBPC technique. Initially below rated wind speeds are considered, before going on to above rated.

8.4.1 Below rated models

As described in Chapter 5 the below rated controller strategy is to track the C_{Pmax} curve, defined as $T_f = k_1\Omega^2$. The actual transfer function of the system used in the control of α for below rated wind speeds depends on the choice of torque, T, in the relationship. Since the actual aerodynamic torque cannot be measured directly, either the drive train torque, T_D, can be used as an approximation to the aerodynamic torque or, alternatively, a proper estimate of the aerodynamic torque can be calculated, $\hat{T}_f$. In order to be used in the design of the controller the equation $T = k_1\Omega^2$ is linearised for a constant rotor speed, Ω_B, to give the linear approximation to the tracking error, ϵ, defined as,

$$\epsilon = \Delta T - 2k_1\Omega_B\Delta\Omega \tag{8.2}$$

where ϵ is the distance from the C_{Pmax} curve to be minimised by the controller. The use of Δ indicates the the linear dynamics are only valid for small changes in the variables. For the controllers, designed below, Ω_B is set to 3.23rad/s, corresponding to a mean wind speed of 8m/s. Substituting values for the turbine being examined into equation 5.4 for k_1 gives $k_1 = 3217$.

Tracking C_{Pmax} curve using drive train torque, T_D

The first estimate of aerodynamic torque uses simply drive train torque, which can be determined from the equation,

$$T_D = NT_e \tag{8.3}$$

where N is the gearbox ratio and T_e the generator reaction torque. Equations of the system, as defined in Chapter 6, are used to evaluate the tracking error, ϵ equation 8.2, in terms of the generator firing angle, α, and aerodynamic torque, T_f. The resulting system for tracking C_{Pmax} using T_D is,

$$\epsilon_1 = P_1\alpha + D_1T_f \tag{8.4}$$

where P_1 and D_1 are the plant and disturbance transfer functions respectively which are defined, using the notation from Chapter 6, as,

$$P_1(s) = \frac{G_1}{1 - G_2(EB + F)}\left[N - 2k_1\Omega_B B\left(D + \frac{1}{K_1}\right)\right] \tag{8.5}$$

$$D_1(s) = \frac{G_1EA}{1 - G_2(EB + F)}\left[N - 2k_1\Omega_B B\left(D + \frac{1}{K_1}\right)\right] - 2k_1\Omega_B\left[A\left(D + \frac{1}{K_1}\right) + C\right] \tag{8.6}$$

Tracking C_{Pmax} curve using estimated aerodynamic torque, $\hat{T}_f$

The second estimate of aerodynamic torque is defined by the relationship,

$$\hat{T}_f = NT_e + H(s)\Omega, \qquad \text{where} \qquad H(s) = \frac{10Js + 10\gamma}{s + 10} \tag{8.7}$$

where T_e is the generator reaction torque, J the rotor inertia (105504.5) and γ the viscous damping coefficient (0.012035). Similar to tracking by T_D the tracking error is calculated in terms of α and T_f, resulting in the equation

$$\epsilon_3 = P_3\alpha + D_3T_f \tag{8.8}$$

Again using the notation from Chapter 6,

$$P_3(s) = \frac{G_1}{1 - G_2(EB + F)}\left[N + B\left(H - 2k_1\Omega_B\right)\left(D + \frac{1}{K_1}\right)\right] \tag{8.9}$$

$$D_3(s) = \frac{G_1EA}{1 - G_2(EB + F)}\left[N + B\left(H - 2k_1\Omega_B\right)\left(D + \frac{1}{K_1}\right)\right] + \left(H - 2k_1\Omega_B\right)\left[A\left(D + \frac{1}{K_1}\right) + C\right] \tag{8.10}$$

8.4.2 Below rated MBPC models

The models P_1 (equation 8.5) and P_3 (equation 8.9), combined with the added filters f_ϵ and f_α (equation 8.1), result in the damped systems P_{1d} and P_{3d} respectively, and are the basis on which the controller is designed. In order to be used by the MBPC technique, these models are first simplified, ensuring that the time and frequency responses still accurately reflect those obtained from the original models, before converting them to discrete systems.

To simplify the models, partial fraction expansion is used to first reduce the models from 13th order (14th order for P_{3d}) to a second-order system. In each case the second-order approximation obtained is checked against the original in both the frequency domain, using Bode plots, and in the time domain, using an open-loop step response, to ensure that a good approximation has been made and any small adjustments made to improve the approximation. For tracking with T_D the original plant with filters, P_{1d}, is

$$P_{1d}(s) = \frac{\begin{array}{c}-134928(s+.339)(s+7.638)(s^2-0.139s+189.1)\\ (s^2+12.08s+2190)(s-200)(s+200)(s^2+197.7s+109382)(s-644.6)\end{array}}{\begin{array}{c}(s+0.205)(s+1.2)(s+10)(s^2+0.771s+162.7)(s^2+18.97s+2858)\\ (s^2+26.03s+3314)(s+178.4)(s+186.6)(s^2+201.6s+109995)\end{array}} \tag{8.11}$$

and the simplified plant, P_{1dp}, is

$$P_{1dp}(s) = \frac{-21092(s+.3406)}{(s+.2051)(s+1.2)} \tag{8.12}$$

P_{1dp} is then converted into a discrete model. The specific method chosen to do this is the Tustin method with a sampling frequency of 0.5 seconds (corresponding to the chosen step size of the MBPC controller) and a Tustin prewarped frequency of .1 rad/s. The resulting system is adjusted slightly by introducing a delay and also the factors slightly adjusted to give a better time and frequency response. The one-step delay is introduced by dividing the system by z and is used as the system created by the Tustin method demands instantaneous changes in output on changes on input which is not possible. The effect of this can be seen in Figure 8.5. The final discrete system, P_{1dpz}, is

$$P_{1dpz}(z) = \frac{-6996.2z^{-1}+5978z^{-2}}{1-1.532z^{-1}+0.567z^{-2}} \tag{8.13}$$

A Bode plot showing the original system, P_{1d} and the simplified version, P_{1dp}, is shown in Figure 8.3 and a second Bode plot showing the original system and P_{1dpz} is shown in

Figure 8.4[1]. The open-loop unit step response of all three systems is shown in Figure 8.5

In a similar way, for below rated tracking using $\hat{T}_f$, P_{3d} is simplified to obtain P_{3dp}, and then converted to the discrete system, P_{3dpz}, where,

$$P_{3d}(s) = \frac{\begin{array}{c}-134928(s^2+0.166s+3.326)(s+7.638)(s^2+10.03s+186.1)\\(s^2+12.08s+2190)(s-200)(s+200)(s^2+197.7s+109382)(s-645)\end{array}}{\begin{array}{c}(s+.205)(s+1.2)(s+10)^2(s^2+0.771s+162.7)(s^2+18.97s+2858)\\(s^2+26.03s+3315)(s+178.4)(s+186.6)(s^2+201.6s+109995)\end{array}} \tag{8.14}$$

$$P_{3dp}(s) = \frac{-2097.5s^2 - 348.0s - 6977}{s^2 + 1.405s - 1.246} \tag{8.15}$$

and

$$P_{3dpz}(z) = \frac{-1921.2z^{-1} + 2389.6z^{-2} - 1791.9z^{-3}}{1 - 1.431z^{-1} + 0.478z^{-2}} \tag{8.16}$$

The Bode plot showing the simplification of P_{3d} to P_{3dp} is shown in Figure 8.6, and the comparison of the P_{3d} and P_{3dpz} in Figure 8.7. Open-loo unit step responses of all three systems are shown in Figure 8.8

8.4.3 Above rated models

The above rated wind speeds strategy is to track the rated power curve. This curve has an equation $T = k_2/\Omega$ where k_2 is the aerodynamic power corresponding to the rated power, P (300kW). Using the equation for power generation with losses in the drive train, $P = 0.95(k_2 - 15000) + 1269.7\Omega^2$, yields $k_2 = 331kW$. The equation $T = k_2/\Omega$ is linearised around the rotor speed, Ω_A, to give the above rated error from the C_{Pmax} curve, ϵ_2,

$$\epsilon_2 = \delta T - k_p \delta\Omega, \text{ where} \qquad k_p = -k_2/\Omega_A^2 \tag{8.17}$$

For the controllers described below $\Omega_A = 4.375$ corresponding to a wind speed of 20m/s. The plant and disturbance dynamics, P_2 and D_2 respectively, are the same as those for P_3 (equation 8.9) and D_3 (equation 8.10), with $2k_1\Omega_B$ replaced with k_p.

[1]The Bode plot of a discrete system is only valid up to the frequency π/T where T is the sample time, and thus this Bode plots is only shown up to this frequency (6.28 rad/sec)

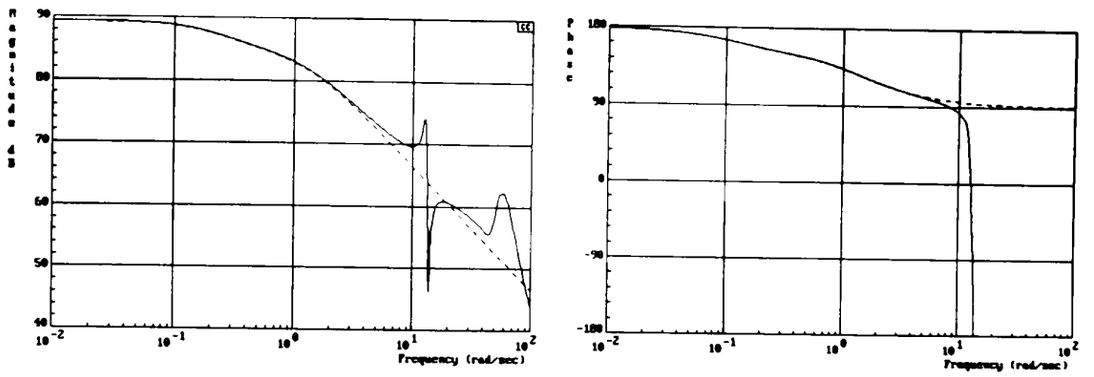

Figure 8.3: Simplifying the system, P_{1d} (—) and P_{1dp} (- -)

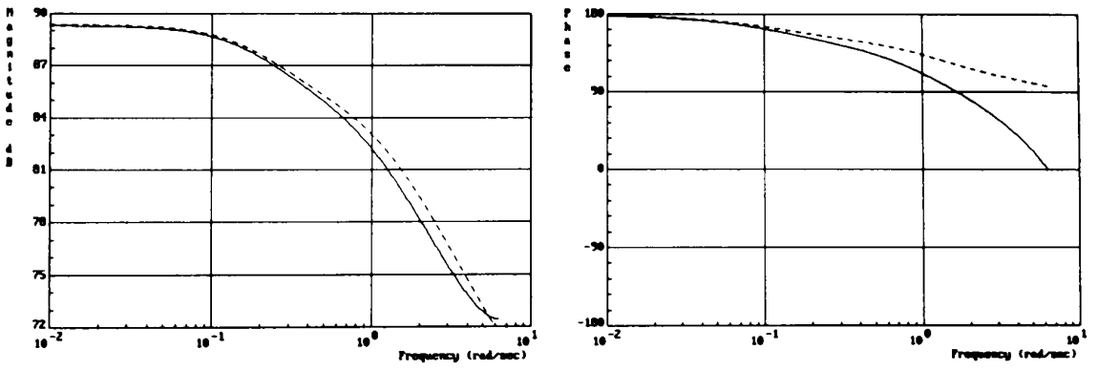

Figure 8.4: Discretizing the system, P_{1d} (- -) and P_{1dpz}(—)

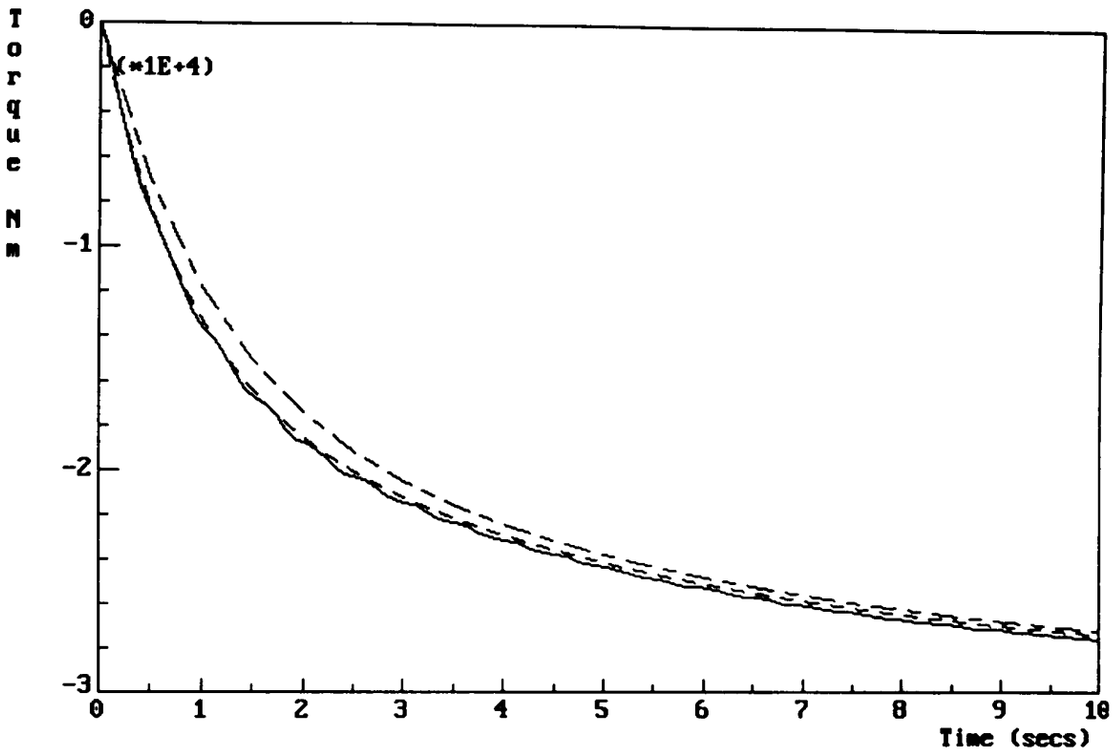

Figure 8.5: Time responses of P_{1d} (—), P_{1dp} (- -) and P_{1dpz} (— -)

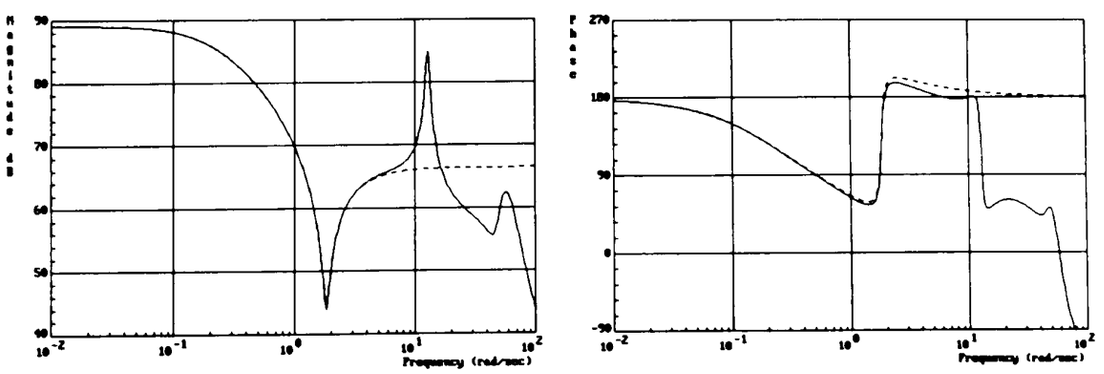

Figure 8.6: Comparison of P_{3d} (—) and P_{3dp} (- -)

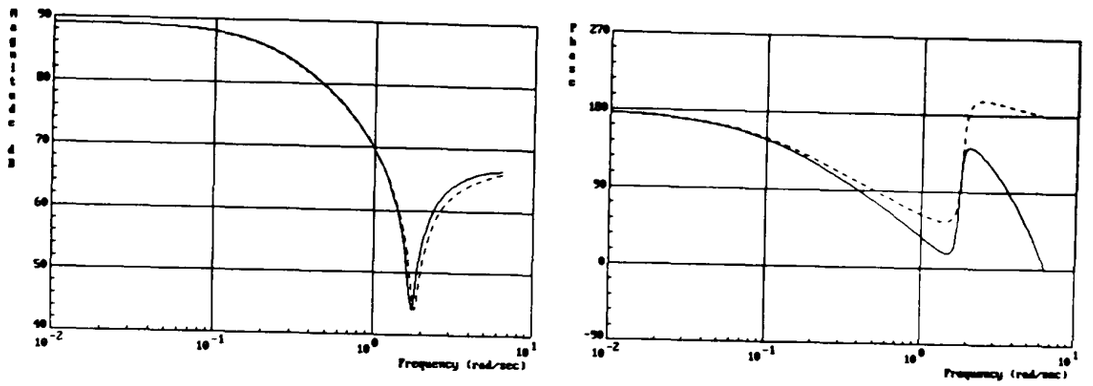

Figure 8.7: Comparison of P_{3d} (- -) and P_{3dpz} (—)

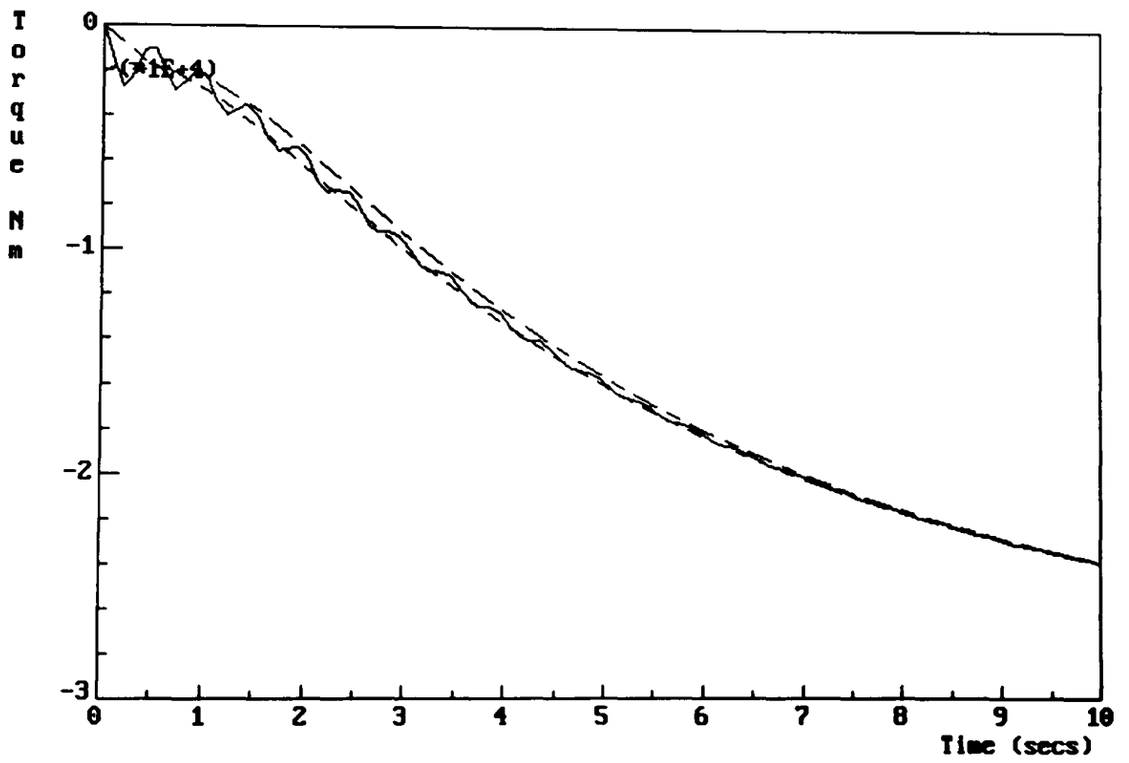

Figure 8.8: Time responses of P_{3d} (—), P_{3dp} (- -) and P_{3dpz} (— -)

8.4.4 Above rated MBPC model

In the same way as for below rated wind speed models, the plant, P_2, combined with the filters (equation 8.1) gives the new system P_{2d}, which is then simplified to give $P_{2dp}(s)$, and then converted to the discrete system, $P_{2dpz}(z)$. These systems are shown below,

$$P_{2d} = \frac{\begin{array}{c}-134928(s+2.332)(s-2.621)(s+7.638)(s^2+9.872s+193.8)\\(s^2+12.98s+2190)(s-200)(s+200)(s^2+197.7s+109382)(s-644.6)\end{array}}{\begin{array}{c}(s-0.376)(s+1.2)(s+10)^2(s^2+0.735s+162.6)(s^2+18.97s+2858)\\(s^2+26.03s+3315)(s+178.4)(s+186.6)(s^2+201.6s+109995)\end{array}} \tag{8.18}$$

$$P_{2dp}(s) = \frac{-2186(s+2.33)(s-2.621)}{(s-.376)(s+1.2)} = \frac{-2186s^2+632.6s+13358}{s^2+0.824s-0.451} \tag{8.19}$$

and

$$P_{2dpz}(z) = \frac{-976.7z^{-1}+5177z^{-2}-1250z^{-3}}{1-1.743z^{-1}+0.644z^{-2}} \tag{8.20}$$

It should be noted that the in the conversion from equation 8.18 to 8.19 both the unstable pole term, $(s-0.376)$, and the significant right half plane zero term, $(s-2.61)$, are preserved to ensure these important characteristics are contained in the simplified model, equation 8.20. The Bode plot showing the simplification of P_{2d} to P_{2dp} is shown in Figure 8.9, and the comparison of the P_{2d} and P_{2dpz} in Figure 8.10. Time responses of all three systems are shown in Figure 8.11

8.5 MBPC controllers

The three discrete models of the system developed above, P_{1dpz} (equation 8.13), P_{2dpz} (equation 8.20) and P_{3dpz} (equation 8.16) are used as the process model in three separate MBPC controllers, in a similar way as the step response models are used in the solar power plant. For each of the controllers, optimal control parameters are determined and tested through computer simulations. As mentioned above, each controller is developed and tested separately before attempting to join above and below rated wind speed controllers into one complete controller. Initially the simple type of control parameters (n,n,1,0) is analysed fully before moving on to more complex combinations of parameters.

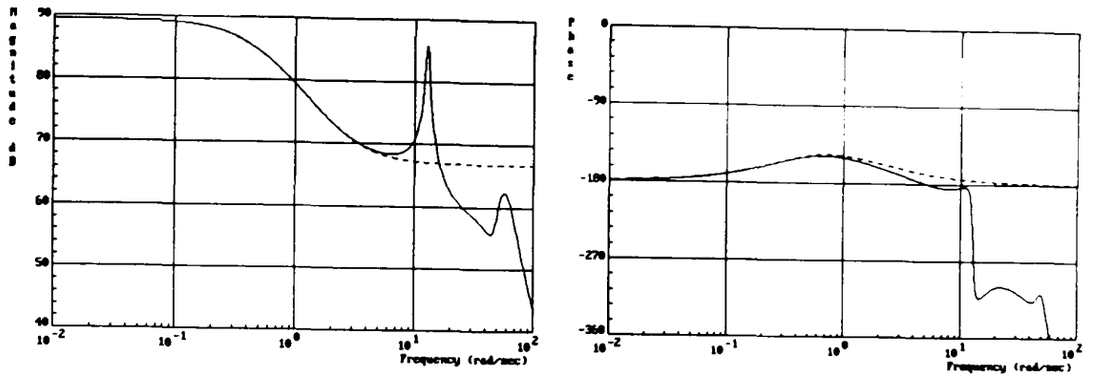

Figure 8.9: Comparison of P_{2d} (—) and P_{2dp} (- -)

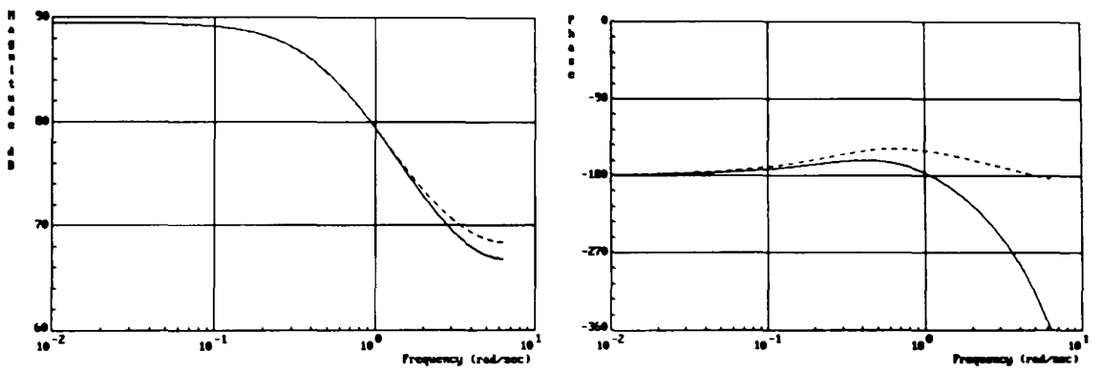

Figure 8.10: Comparison of P_{2d} (- -) and P_{2dpz} (—)

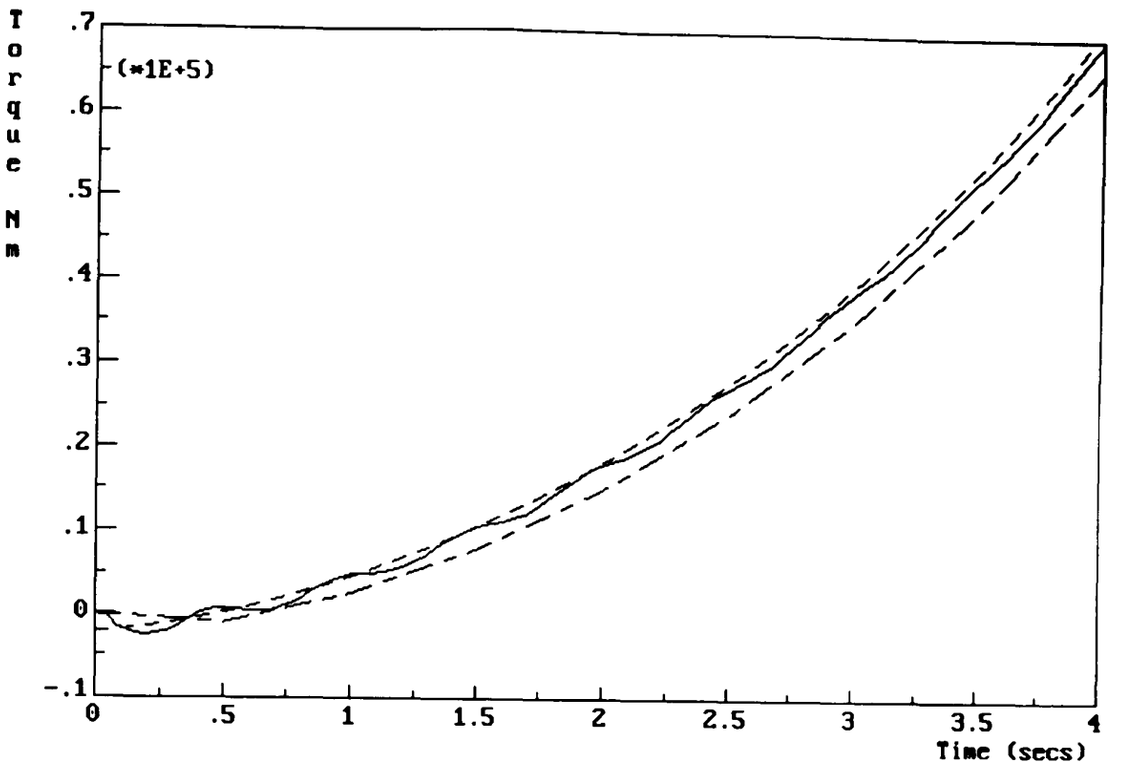

Figure 8.11: Time responses of P_{2d} (—), P_{2dp} (- -) and P_{2dpz} (— -)

8.5.1 Analysis of simple parameter MBPC controllers

In Chapter 3 when a MBPC controller was applied to a solar power plant good results are obtained when using the simple form of the MBPC control parameters (n,n,1,0) and thus this is the first type of MBPC controller to be tested on the VSWT. In Chapter 3 a purely trial and error method is used to try and determine the optimal value of n for the controller. A much better way to determine the optimal value of n for a simple MBPC controller would be to analyse the system and look at the effect n has on the frequency response of the combined controller and plant system. The frequency response would allow the theoretical optimal value of n to be determined and would also allow the stability and robustness of the system to be examined.

However obtaining such a frequency response has two major problems. First, the MBPC controller takes the form of lines of code and to examine this in the frequency domain, a single equation describing the controller is necessary. Secondly, when this equation is derived it will be a discrete system and combining this with the continuous system, which describes the wind turbines dynamics, to obtain a frequency response is not straight forward.

Appendix G describes the method derived to obtain a single equation which de-

scribes the operation of the VSWT MBPC controllers. This process is quite complex and is only derived for MBPC controllers of the simple form (n,n,1,0), although it is possible to extend it to take any form of controller.

It should also be noted that this analysis is only possible as the system has been linearised and therefore any controllers based on it will only be designed for the one operating point chosen for the linearisation. The performance of the controlled system at other operating points determine the robustness of the controller.

Frequency Response

Now that the simple form of the MBPC controller has been converted into a single equation it can be analysed using standard system analysis tools. Below is shown the method used to obtain the open loop frequency response $M(\omega)$ for a system containing a discrete system, in this case the controller $G(z)$, with the continuous system, in this case the wind turbine $P(s)$, where the discrete system has a time step of T seconds [63],

$$M(\omega) = \frac{1}{T} \sum_{m=-\infty}^{\infty} H_0(\omega - m\Delta\omega) P(j(\omega - m\Delta\omega)) G(e^{j(\omega - m\Delta\omega)T}) H_1(\omega - m\Delta\omega) \quad (8.21)$$

where,

$$H_0(\omega) = (1 - e^{-j\omega T}), \quad H_1 = \frac{1}{j\omega}, \; and \quad \Delta\omega = \frac{2\pi}{T}$$

The summation in equation 8.21 is from $-\infty$ to $+\infty$, however the contribution to $M(\omega)$ in the range $-\Delta\Omega$ to $+\Delta\Omega$ becomes much less when m is far from zero. A good approximation can be found by setting the range to be, for example, from -50 to 50. This allows the frequency response to be calculated reasonably quickly and accurately. Figure 8.12 shows the Bode plots of the open loop frequency response of the below rated system P_{3dpz} with MBPC controller parameters n,n,1,0 with n = 5, 10, 15 and 20. Similarly Figure 8.13 shows Bode plots for the above rated system P_{2dpz} with the same MBPC control parameter combinations. Figures 8.14 and 8.15 show Nyquist diagrams for the same systems and controllers. When analysing simple systems measures such as Gain Margin and Phase Margin [36] would give an straightforward measure of the systems stability and robustness. However the plots 8.12 through 8.15 do not allow the easy application of such simple measures. One way of analysing the stability and robustness is through applying the rule of stability for Nyquist diagrams, i.e.

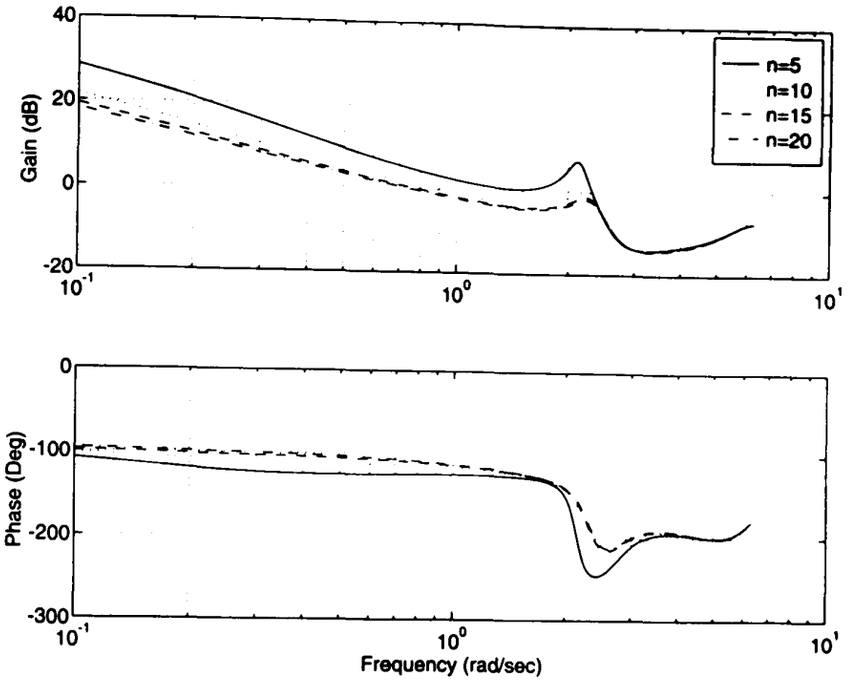

Figure 8.12: Bode plots of below rated system with simple MBPC controllers

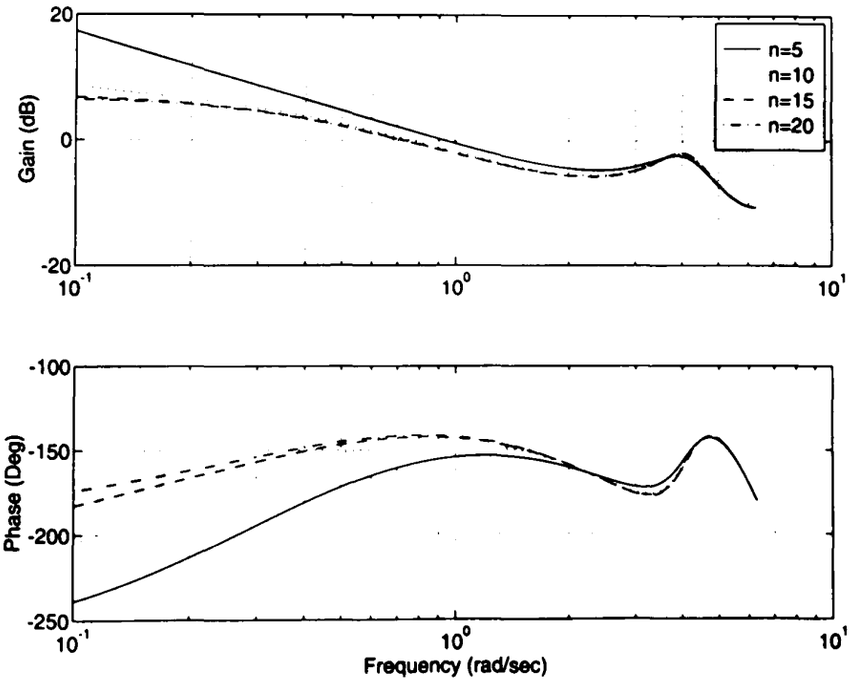

Figure 8.13: Bode plots of above rated system with simple MBPC controllers

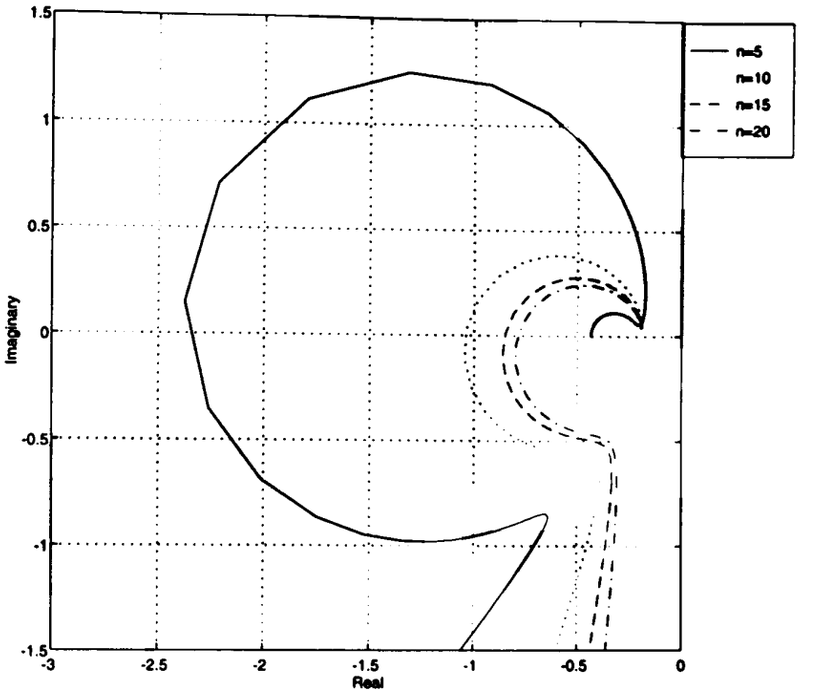

Figure 8.14: Nyquist plots of below rated system with simple MBPC controllers

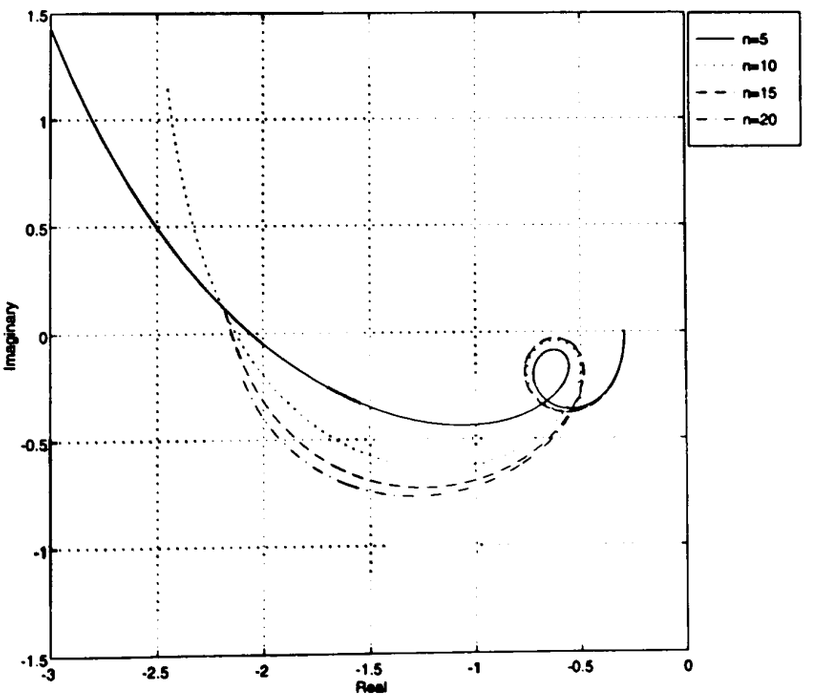

Figure 8.15: Nyquist plots of above rated system with simple MBPC controllers

> "A feedback control system is stable if and only if, for the [Nyquist] contour, the number of counterclockwise encirclements of the (-1,0) point is equal to the number of poles of [the system] with positive real parts." [36]

When counting encirclements the mirror image about the real axis of the contour shown in the nyquist plot is taken into consideration.

For the below rated system P_{3d} (equation 8.14) there are no poles with positive real parts. In the Nyquist diagram for the controlled below rated system, Figure 8.14, the curves for both n=5 and n=10 encircle the (-1,0) point once and the other curves do not encircle the (-1,0) point although they are very close to doing so. This means that the system would be unstable for $n \leq 10$. For values of $n > 10$ the system is theoretically stable but only by a small margin and any changes in the system are likely to make the system unstable. Thus the controlled system lacks robustness.

For the above rated system P_{2d} (equation 8.18) there is one pole with a positive real part. For the Nyquist diagram of the controlled above rated system, Figure 8.15, all values of n give one encirclement of the (-1,0) point implying stability. However, as with the below rated case, the systems lack robustness as they come very close to the (-1,0) point and changes in system dynamics could easily cause the system to become unstable.

8.5.2 Experimental determination of MBPC parameters

The analysis described above showed that the simple form of MBPC control parameters did not give a robust system that, nor one which is likely to be stable. Therefore more complex combinations of control parameters (N_1, N_2, N_U and Λ) must be considered. Due to the complexity of analysing the system when using any but the simple form of control parameters the determination of the optimal control parameters for the MBPC controller must now be carried out by experimentation.

For this the simple controller of the form (n, n, 1, 0) is used initially, to check the theoretical analysis described above for various values of n. After this various prediction horizons and damping factors combinations can be implemented to determine the optimum choice of parameters. In particular the effect of three different horizons is investigated, namely, looking at only a few points not far in the future, looking at only a few points quite far in the future and also looking at lots of points from close to far in the future.

8.5.3 Performance assessment

In order to assess the different controllers and the effects of the various tuning parameters some performance indicators are necessary.

For below rated tracking of the C_{Pmax} curve the obvious performance indicator is the mean value of C_p achieved. Taking the mean value of C_p compared to the maximum possible value of C_p, a percentage efficiency for the controller in tracking the curve can be calculated. The efficiency, C_{Peff}, is defined as

$$C_{Peff} = \frac{mean(C_p)}{max(C_p)} \times 100\% \tag{8.22}$$

For above rated wind speeds such a performance indicator is not so simple. One quantity that can be calculated is the mean power. This should be rated power, however, just the mean on its own is not a full indication of the controller's performance. The controller should seek to minimize the torques and overshoot of power. High values of both of these can damage the turbine structure and components and will cause increased maintenance and a shorter working life. Therefore the maximum torques and power will also be used to assess the above rated controller. The maximum torques in the system are also used to a lesser extent in assessing the below rated controller as it should seek to minimize these too.

In the tests of the controllers wind with a turbulence intensity of 20% is used to give a realistically tough wind regime for the wind turbine. Below rated winds have a mean of 8m/s and above rated a mean of 20m/s.

8.5.4 *MatrixX* simulation

As mentioned in Chapter 6 the simulation program *MatrixX* is used to simulate the wind, the variable speed wind turbine and the appropriate controller. The form of the controller is very similar to that used in Chapter 3 for the solar power plant. The *MatrixX* block which is used to calculate the control move is shown in Figure 8.16. This is a discrete block which runs only every 0.5 seconds to correspond to the chosen time step for the controller. Fed into the main controller block is the filtered error signal which is generated as shown in Figure 8.17. Here the error is calculated for the above rated error from the rated power curve. Also the old values of the error and controller output, which are used in the next time step for the calculation of the new control move, are fed back into the controller as shown in Figure 8.18.

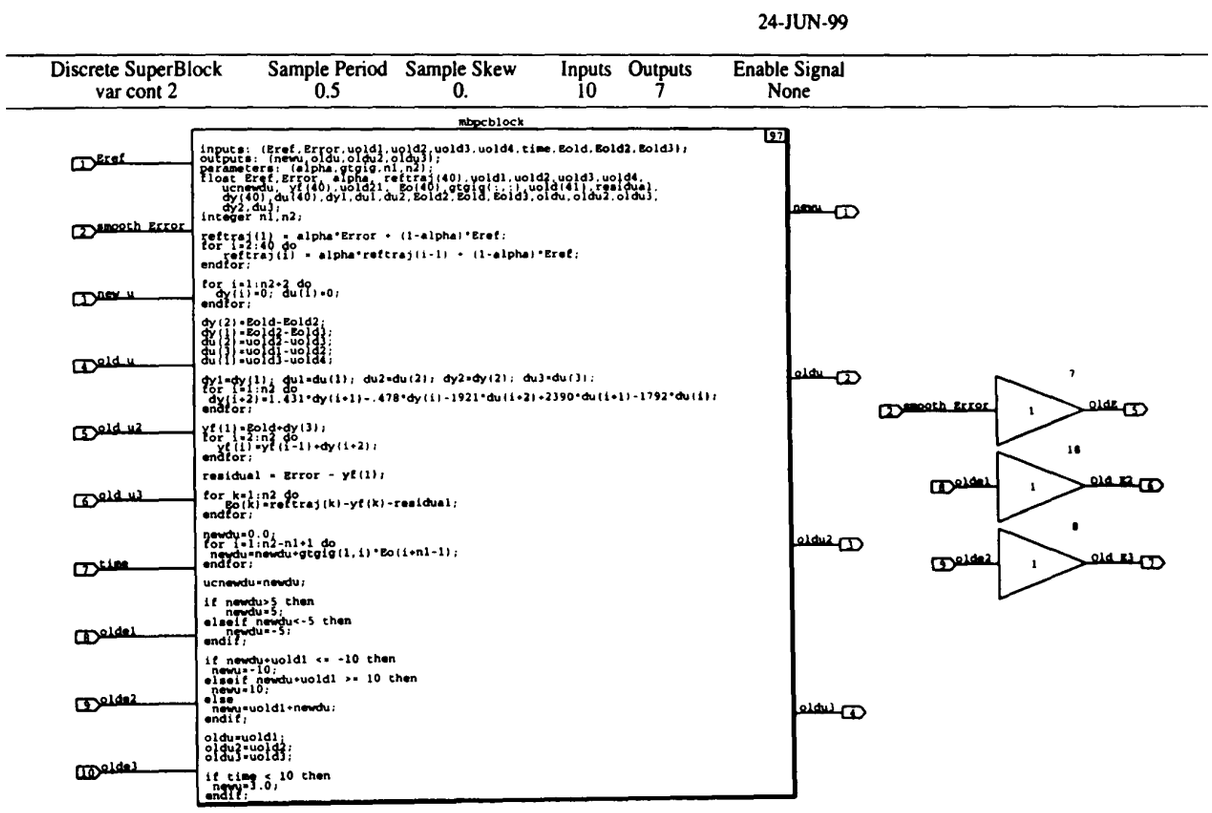

Figure 8.16: MatrixX MBPC controller block

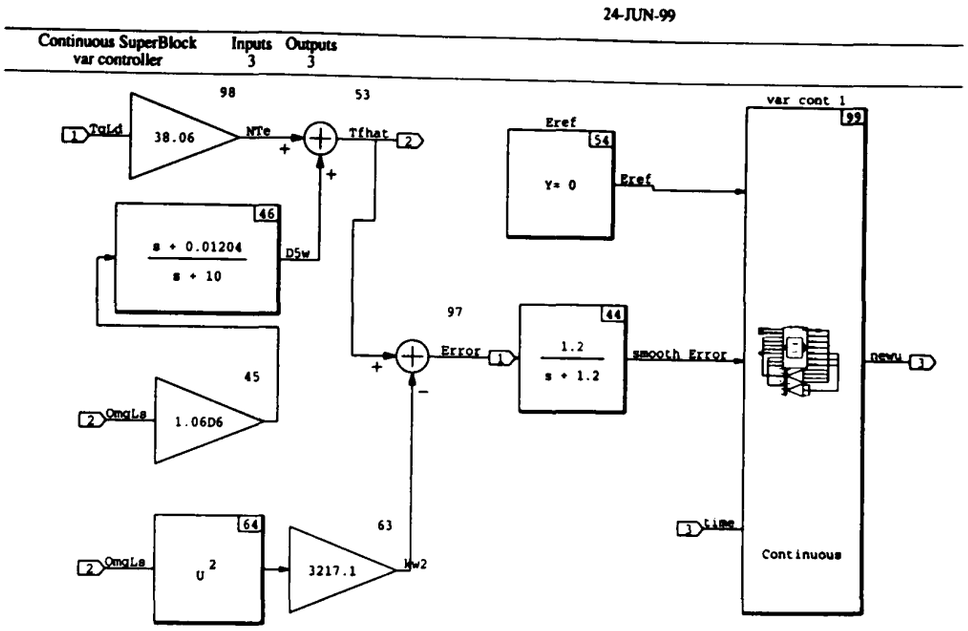

Figure 8.17: MatrixX MBPC error generation

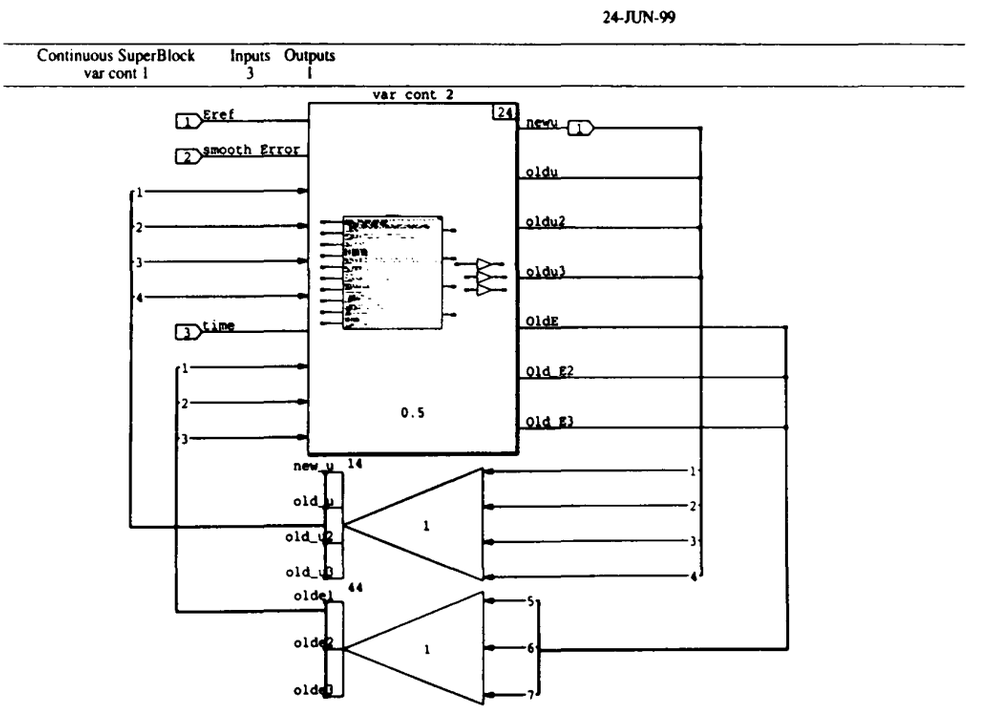

Figure 8.18: MatrixX MBPC signal feedback

8.5.5 Below rated controller parameters

Tracking using estimated aerodynamic torque, $\hat{T}_f$

Initially the below rated controller, tracking with estimated aerodynamic torque is tested. For the basic configuration (n, n, 1, 0), no value of n would stabilize the system thus confirming the conclusions from the analysis in section 8.5.1. For the more complex controllers a prediction horizons of 30 time steps, equivalent to 15 seconds, is estimated to be about as far as it is worth trying to estimate. Therefore 3 classes of controller are attempted: $(2, 30, N_U, \Lambda)$, $(2, 5, N_U, \Lambda)$ and $(10, 20, N_U, \Lambda)$. Initially N_U is set to three, i.e. calculating three control moves, and Λ adjusted to obtain an optimum controller. As would be expected, high values of Λ provide much damping to the control moves and a slow, or even sluggish, response to changes in wind speeds. As Λ is reduced the controller becomes more aggressive, until a certain point where it actually destabilizes the system. Next N_U is set to 2 and 4 controller moves to see if this makes any change to the performance.

Many different combinations of these ranges with choices of Λ are attempted and assessed over a short wind sample of 60 seconds. In each of the controller configurations a very large value of Λ is required to not destabilize the system. These large values of Λ contrast sharply with those used in the solar power plant but reflect the much larger scale of the step response of the system under consideration (compare Figure 3.4 showing the solar power plant step response and Figures 8.5, 8.8 and 8.11 for the VSWT step responses). For the controller of the form (2, 30, 3, Λ), setting Λ less than 8e7 results in the system becoming unstable. With $\Lambda = 9e7$ the system is stable and results in an efficiency of 98.3%. For values of Λ higher than this the efficiency drops away as shown in Table 8.1. Table 8.1 also shows the results for the controller parameters (2,5,3,Λ) and for parameters (10,20,3,Λ).

All these results show little difference in the performance for the best choice of Λ. Changing N_U to 2 and 4 and optimizing Λ also gave no discernible improvement to the performance. If Λ is held constant, changing N_U to 2 from 3 results in a more aggressive controller which actually destabalises the system. To prevent this more damping is added and the efficiency drops below 98%. Changing N_U to 4 from 3 makes very little difference to the response of the system and again the efficiency of 98.4% could not exceeded. Therefore, after analysing the different options, the controller (2, 5, 3, 5e7) is chosen to be be the best and is tested below on the full length simulation.

N_1	N_2	N_U	Λ	C_{Peff}
2	30	3	$< 8e7$	unstable
2	30	3	$9e7$	98.3%
2	30	3	$2e8$	97.5%
2	30	3	$5e8$	96.1%
2	5	3	$< 4e7$	unstable
2	5	3	$5e7$	98.4%
2	5	3	$5e8$	95.1%
10	20	3	$< 9e6$	unstable
10	20	3	$1e7$	98.0%
10	20	3	$1e8$	95.3%

Table 8.1: Efficiencies of below rated controllers, tracking with $\hat{T}_f$

Tracking with T_D

A very similar procedure is repeated for the below rated controller, using drive train torque, T_D, to track the C_{Pmax} curve. No value of n could be found to stabilize the system for the basic control parameters of (n, n, 1, 0). For the controller (2,30,3,Λ) the optimal efficiency is only 83.6% with $\Lambda = 7e7$, but this is only slightly improved by the optimal choice of (2,5,3,7e7) which gave an efficiency of 84.2% over the short wind series, and this controller is chosen for the full test with the results described below.

The large variation in efficiency between tracking with $\hat{T}_f$ and with T_D for below rated wind speeds is discussed below with the full results.

8.5.6 Above rated controller parameters

As indicated above, when defining the performance criteria for above rated operation, the choice of optimal above rated controller is not as simple as below rated. Looking simply at the mean generated power will give an indication of the controller performance, but in the same way that a sine wave of any maximum amplitude has a mean amplitude of zero, other factors have to be examined. Maximum power and maximum drive train torque, both give a good indication of how well the controller is working and a well tuned controller should seek to minimize these. Reducing the maximum drive-train torque and power, while still attempting to give a mean of rated power, should

result in a good effective controller that will not cause fatigue which would reduce the working life of the wind turbine.

Again when selecting MBPC control parameters, the simple basic controller could not stabilize the above rated system for any value of n and a more complex controller is needed. For each of the same ranges of controller prediction horizon, as is used for the below rated controller, a suitable value of Λ can be found to stabilize the system. In general decreasing Λ gives a more aggressive controller which results in a better mean power but larger overshoots in torque and power. A selection of the best results are shown in Table 8.2 detailing the average power obtained and also the maximum generator torque. Again no discernible difference could be found with the different

Parameters	Max Torque (Nm)	Average Power (kW)
2,5,3,3e8	2225.34	300.199
2,5,3,5e8	2176.67	300.260
2,5,3,8e8	2195.66	300.301
2,5,2,5e8	2185.81	300.238
2,5,4,5e8	2176.26	300.260
2,30,3,1e10	2197.13	299.016
2,30,3,4e10	2082.92	293.687

Table 8.2: Results for above rated controller parameters

ranges nor choice of controller moves. An optimum controller which gave good average power with low overshoots is (2,5,3,5e8) and this is chosen as a good first choice for the full simulation.

8.5.7 Below and above rated controller results

Each of the chosen controllers described above are tested on the full non-linear *MATRIXx* simulation for a 300 second run with a turbulence intensity of 20%. This length of simulation ensures that a full range of wind effects and turbulence etc is applied to the wind turbine and gives a thorough test for the controllers. For below rated controllers the mean wind speed is set to 8m/s and for the above rated controller it is set to 20m/s. The above rated mean wind speed of 20m/s causes the controller to experience the hardest wind turbine dynamics to control and thus will give a very tough test for

the controller. Therefore the results obtained for this mean wind speed can be assumed, and has been shown by other simulations at different wind speeds, to be worse case for the controller.

The results are presented as both simple time series showing the relevant parameters of interest to assess the performance, but also as a plot on the torque/rotor speed plane to show the tracking of the C_{Pmax} and rated power curves.

Below rated tracking with $\hat{T}_f$

The results of the below rated controller using estimated aerodynamic torque with controller parameters (2, 5, 3, 5e7), are shown in Figure 8.19 and Figure 8.20. Figure 8.19 shows the time series of wind, aerodynamic torque (T_f), power coefficient (C_p), rotor speed, power, generator torque and firing angle (Alpha). Figure 8.20 shows clearly the tracking of the C_{Pmax} curve on the aerodynamic torque/rotor speed plane.

The results show very good tracking of the C_{Pmax} curve with an efficiency, as defined in 8.5.3, of 99.04%. Figure 8.21 shows the tracking of the C_{Pmax} curve, but this time showing the drive train torque with the rotor speed. This shows a much more fluctuating response and results in a maximum generator torque of 1709.35Nm during this simulation.

Below rated tracking with T_D

In the same way as above, the results from the below rated controller tracking with drive train torque with controller parameters (2, 5, 3, 7e7), are shown as time series in Figure 8.22 and on the aerodynamic torque/rotor speed plane in Figure 8.23. This plot shows a very loose tracking of the C_{Pmax} curve with the efficiency over this period being only 92.65%. This is significantly lower than when tracking with estimated aerodynamic torque and shows the benefit of using the estimate of aerodynamic torque. However tracking using drive train torque actually results in very good control of the drive train torque, as is shown in Figure 8.24, and this results in a much reduced maximum generator torque (1058.72Nm) for this controller.

Above rated controller

The result for the above rated wind speeds with controller parameters (2, 5, 3, 5e8), tracking the rated power curve are shown in Figures 8.25 and 8.26. Figure 8.25 shows the time series of wind speed, aerodynamic torque, rotor speed, generator torque, power generator torque and firing angle. Figure 8.26 shows the tracking of the rated power

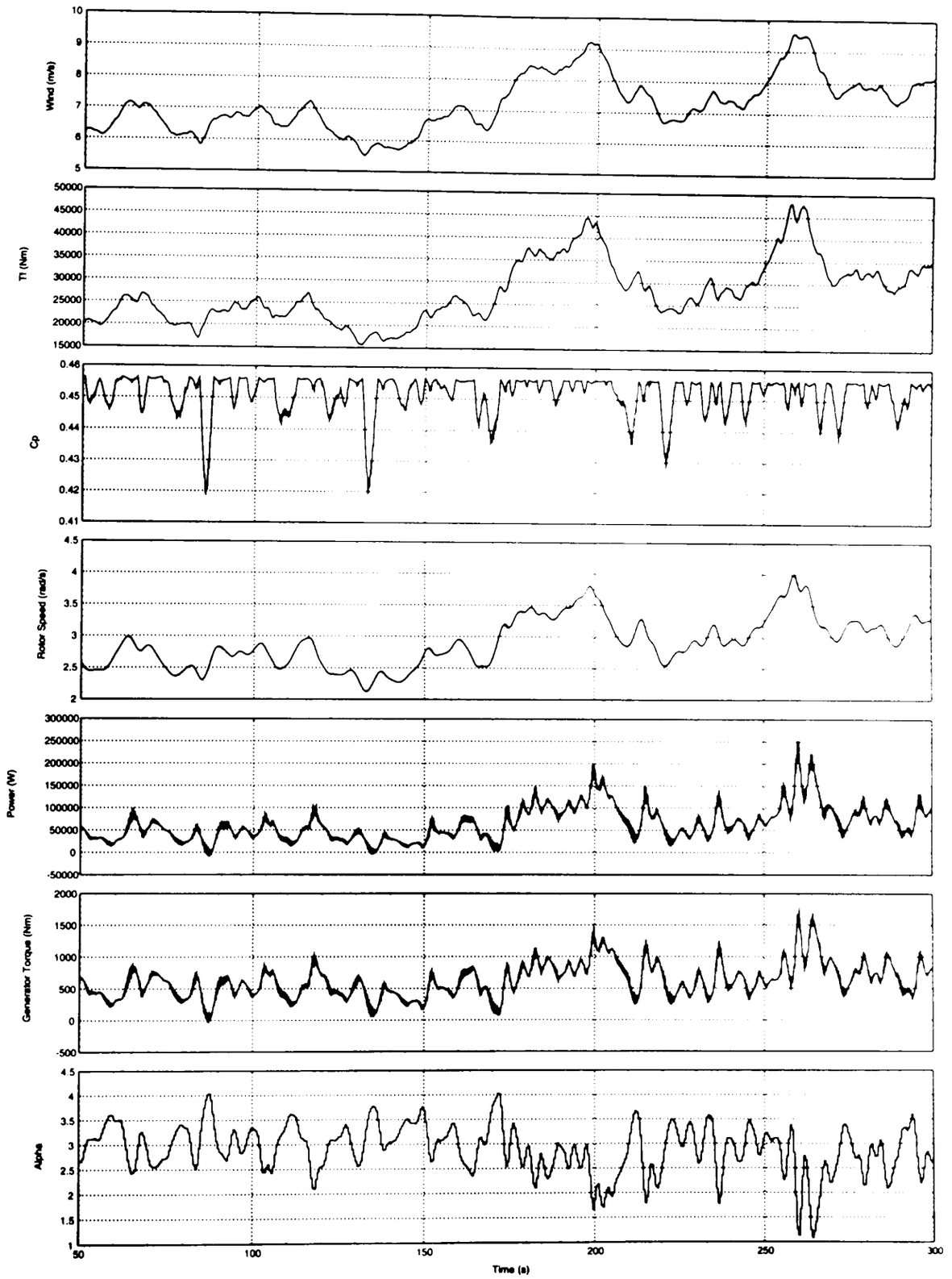

Figure 8.19: Time series for below rated tracking with $\hat{T}_f$

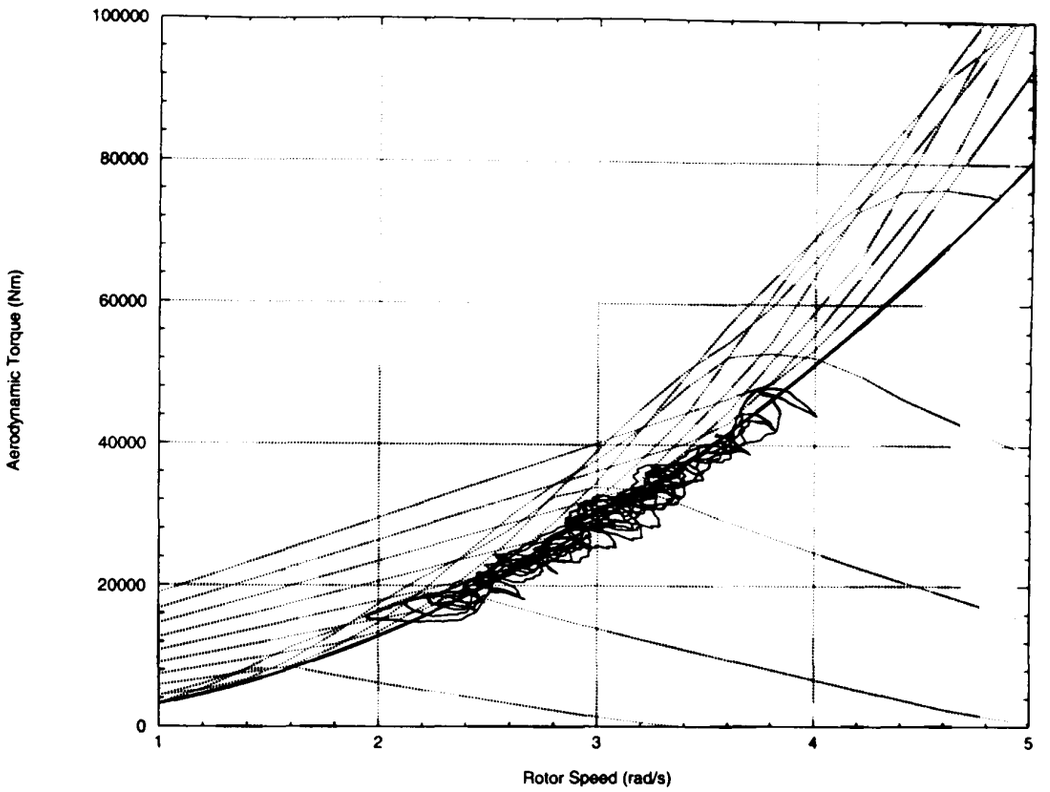

Figure 8.20: Tracking C_{Pmax} with $\hat{T}_f$. Aerodynamic torque vs. rotor speed

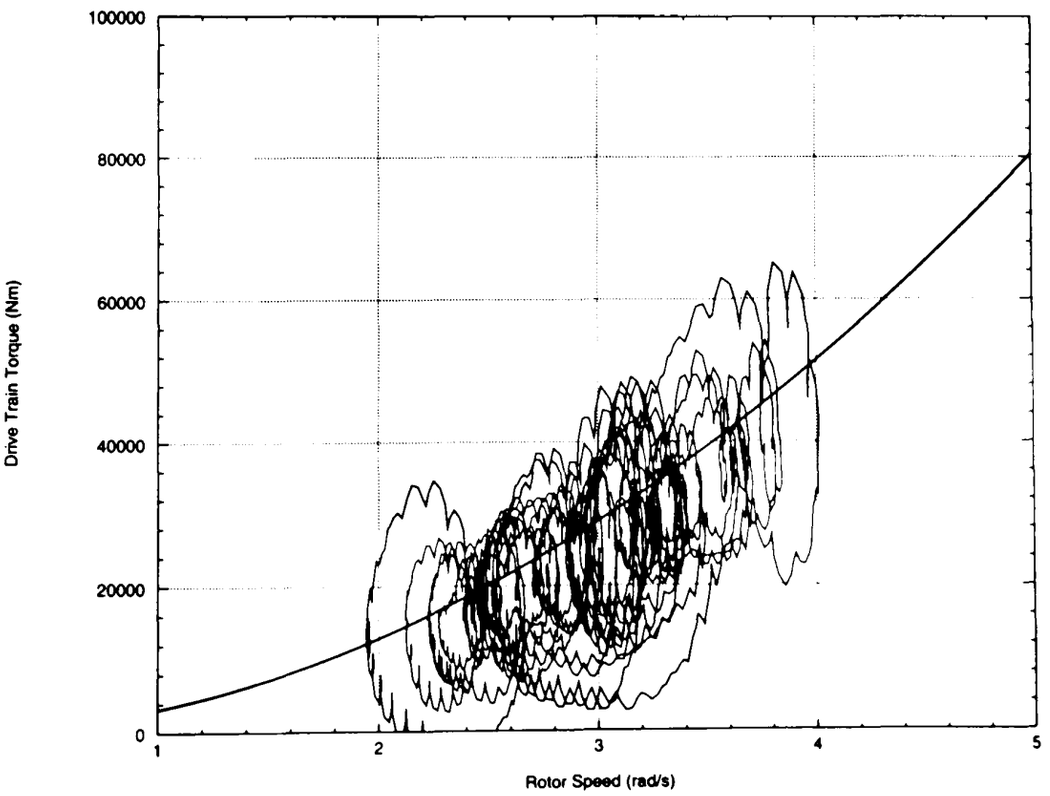

Figure 8.21: Tracking C_{Pmax} with $\hat{T}_f$. Drive train torque vs. rotor speed

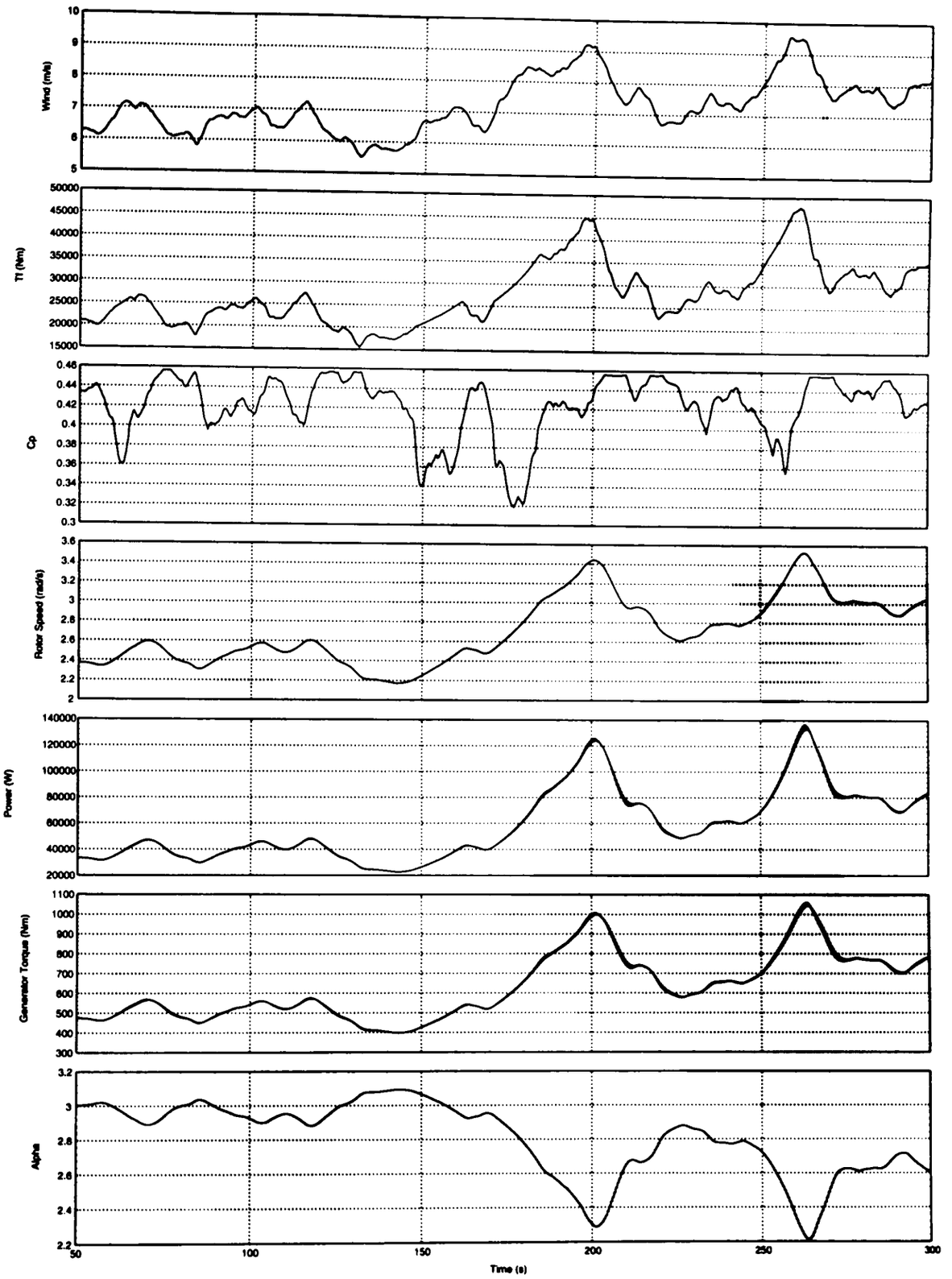

Figure 8.22: Time series for below rated tracking with T_D

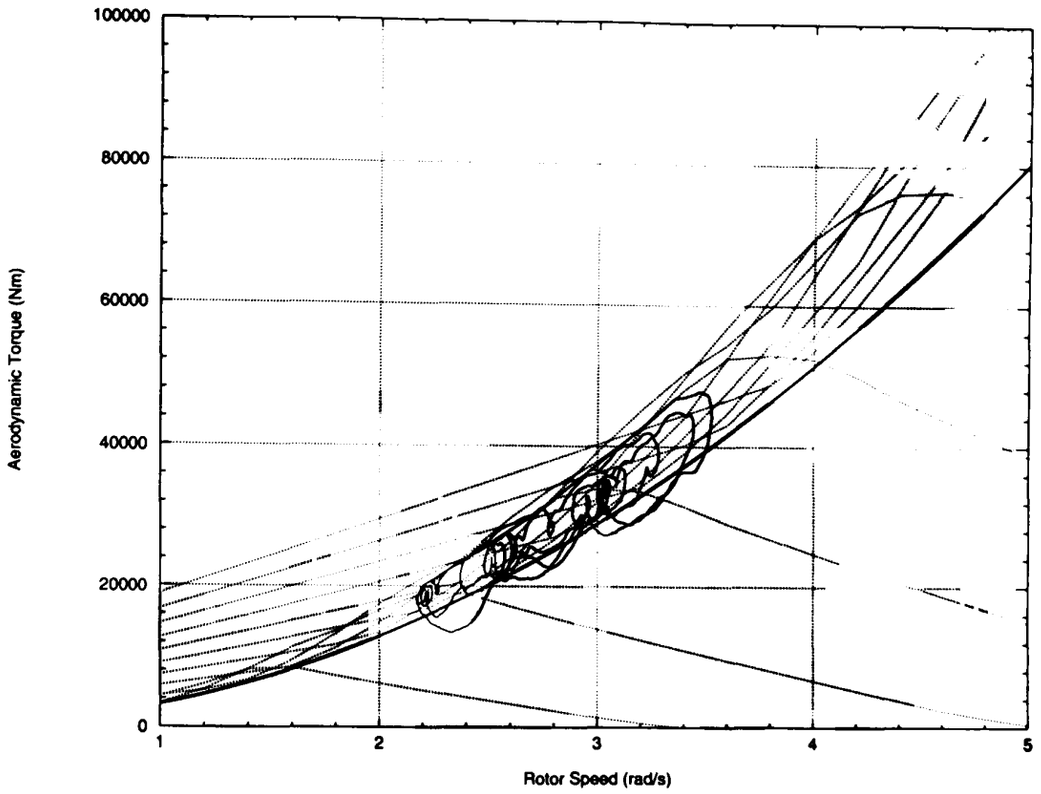

Figure 8.23: Tracking C_{Pmax} with T_D. Aerodynamic torque vs. rotor speed

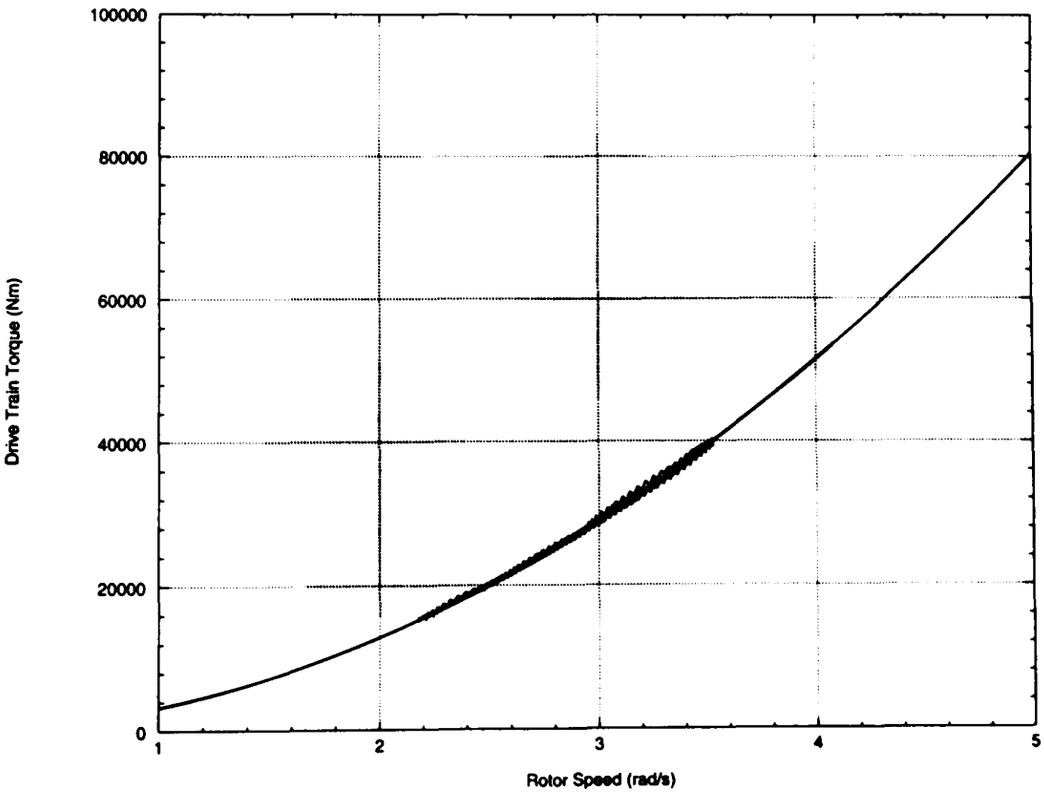

Figure 8.24: Tracking C_{Pmax} with T_D. Drive train torque vs. rotor speed

line on the aerodynamic torque/rotor speed plane and on the drive train torque/rotor speed plane in Figure 8.27.

As is explained above using the mean wind speed of 20m/s provides the hardest test for the controller and although the mean power is very good at 300.281kW, the maximum power is 416.156kW. The maximum generator torque, 2413.86Nm, is also quite high.

8.6 Comparison with classical controllers

To provide a baseline for comparison the MBPC algorithm is replaced in the nonlinear simulation by a very well designed and complex classical controller, designed by Connor [29]. The transfer functions for the below rated controller, tracking by $\hat{T}_f$ is

$$k_4 r_B = -0.0228671 \frac{(s+.12146)(s+.20709)(s+.4037)(s^2+.7662s+163.0741)}{s(s+.2229)(s+1.2)^2(s+4.8288)(s^2+24.229s+163.0729)} \tag{8.23}$$

and the above rated controller for tracking rated power is

$$k_5 r_B = 0.021942 \frac{(s+0.032258)(s+10)(s^2+.7662s+163.0728)}{s(s+2.4)(s+7.7)(s^2+24.229+163.0729)(s^2+10s+169)} \tag{8.24}$$

The performance of the controller is reassessed for both below and above rated operation with the same windspeed traces as used for the MBPC controllers. The results for the classical controller tracking the C_{Pmax} curve and the rated power curve, are both shown in Figure 8.28.

For the below rated wind speed test the efficiency is 99.27%, just slightly better than the equivalent MBPC controller, tracking with $\hat{T}_f$. However the maximum generator torque, 1887.3Nm, is higher than the equivalent MBPC controller.

For the above rated controller the classical controller performs much better for although the mean power, 298.195kW, is marginally less than the equivalent MBPC controller, the maximum torque, 2134.71, and the maximum power, 353.432kW, are both much lower.

8.7 Switching

No matter the performance of the above and below rated controllers when used individually, the real control test of the wind turbine controller comes when the two controllers are combined and tested together for a large range of wind speeds as would

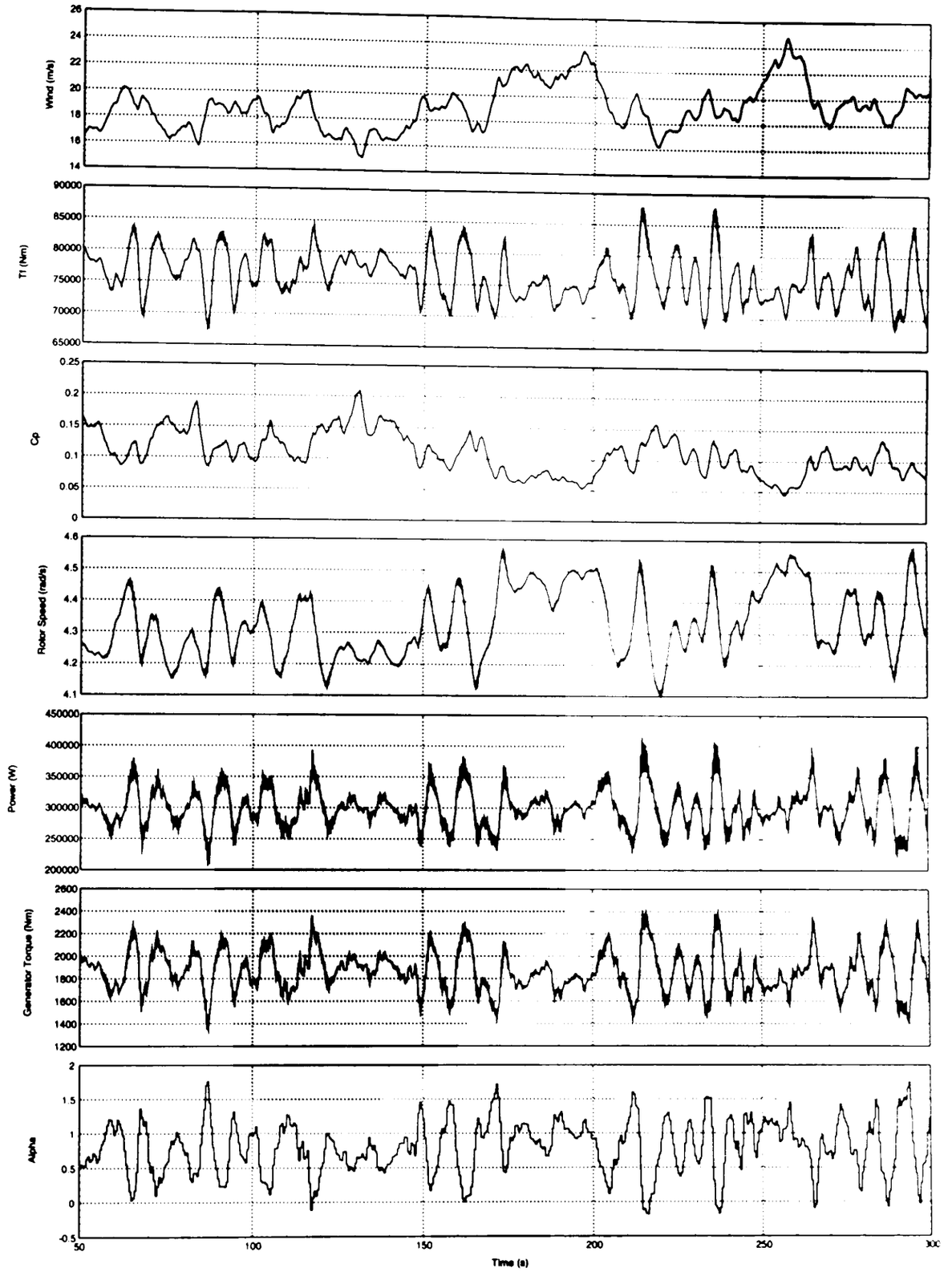

Figure 8.25: Time series for above rated controller

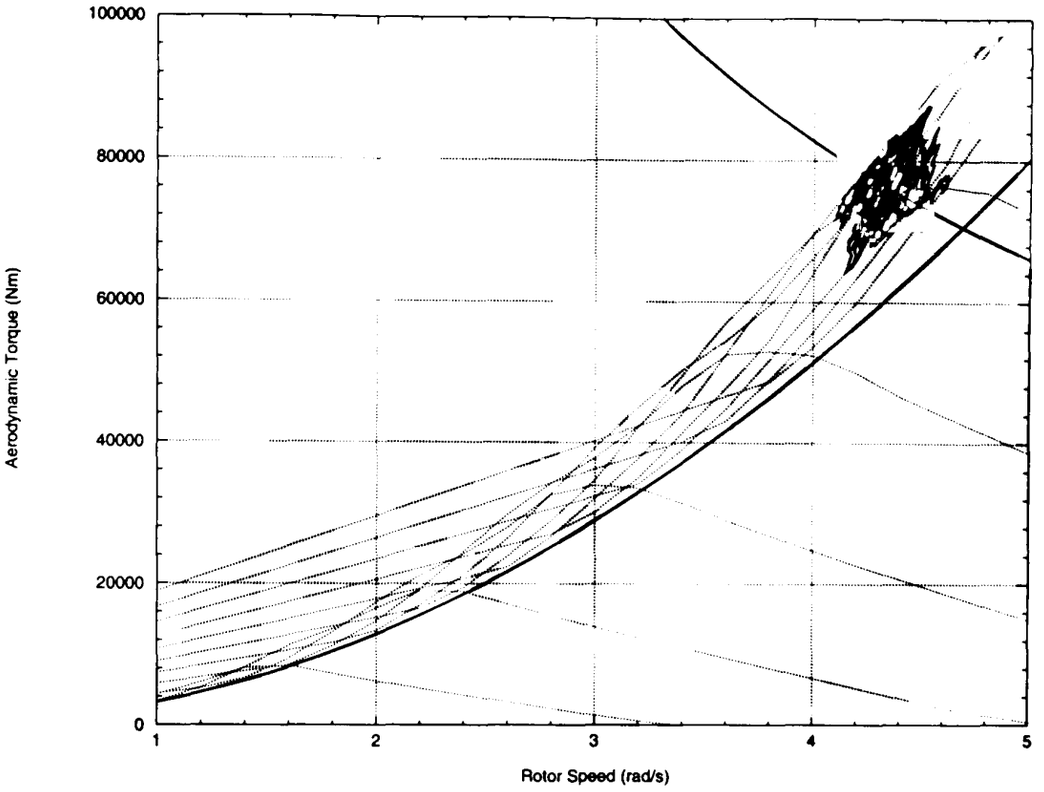

Figure 8.26: Tracking rated power curve. Aerodynamic torque vs. rotor speed

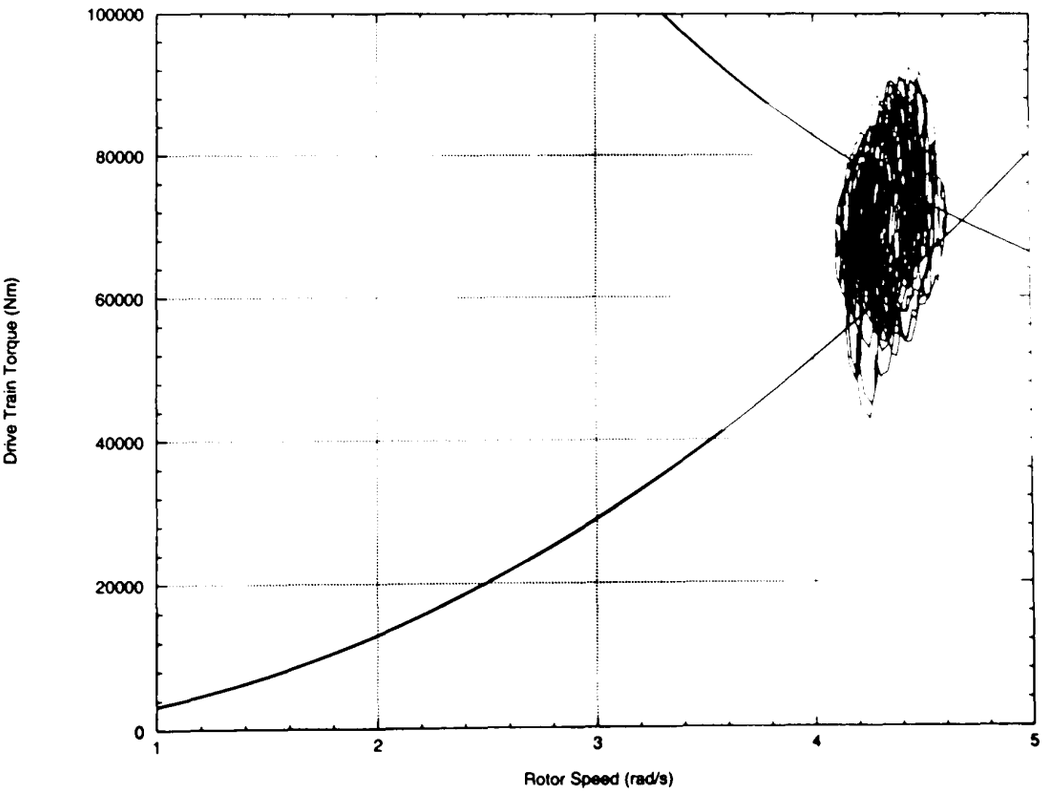

Figure 8.27: Tracking rated power curve. Drive train torque vs. rotor speed

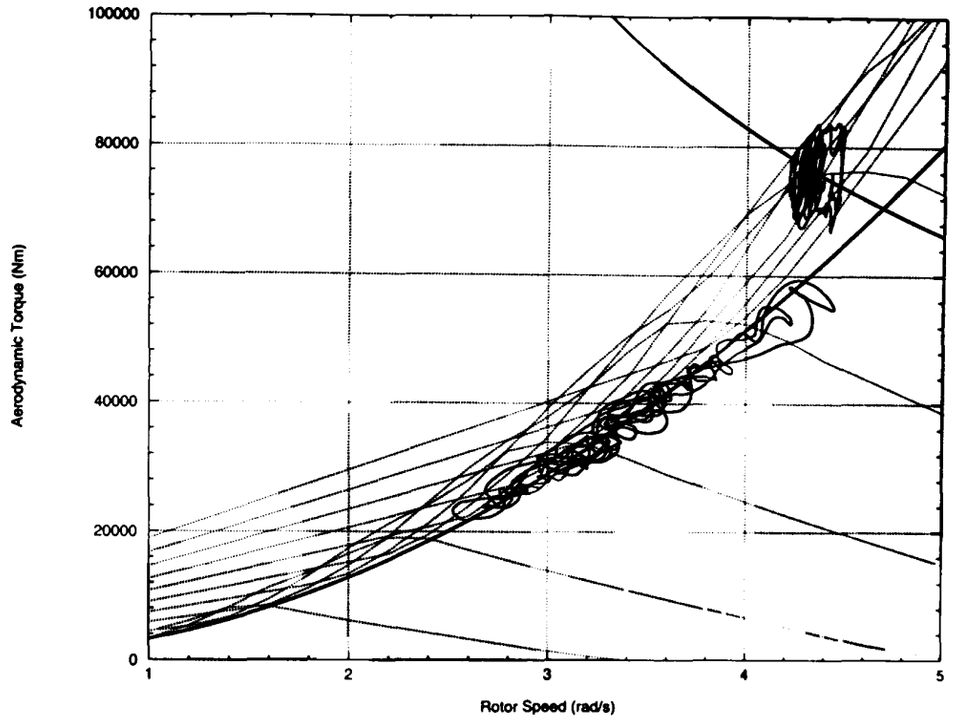

Figure 8.28: Combined below and above rated wind speed plots of classical control tracking. Aerodynamic torque vs. rotor speed

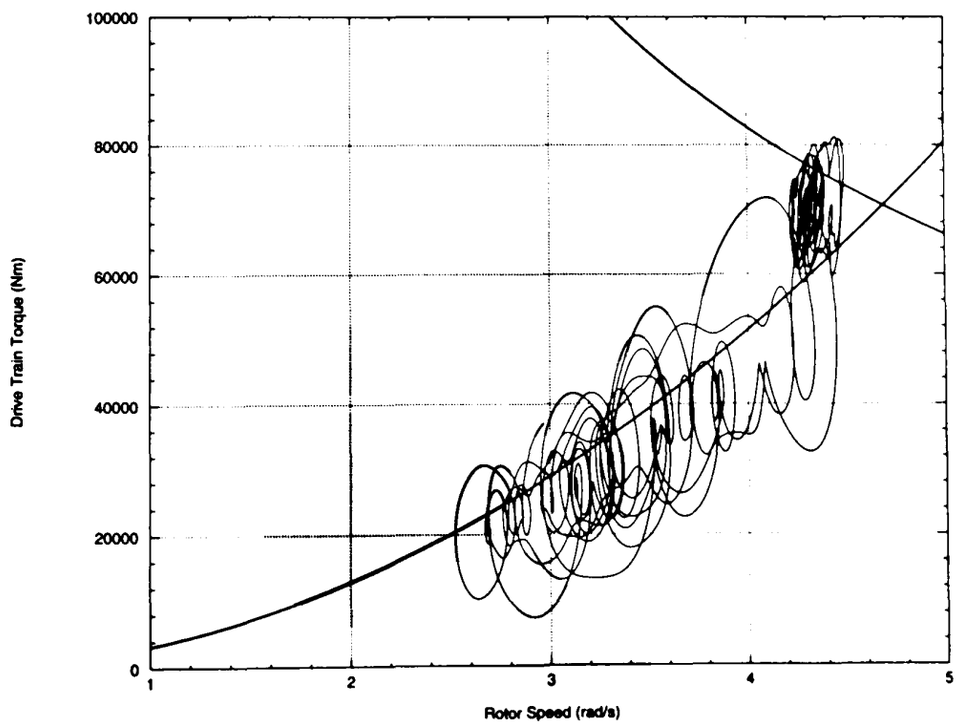

Figure 8.29: Combined below and above rated wind speed plots of classical control tracking. Drive train torque vs. rotor speed

be encountered in the field. The basic switching method is described in Section 5.3.4. For continuous controllers, like the classical controllers used above, methods are devised to help switch between one controller and the other with minimum disruption to the system. However since the MBPC control technique works in the time domain the move between the two controllers is transparent and no complicated additional logic is necessary. This suggests that working in the time domain enables the MBPC technique to handle the switching method well, would be easy to implement and gives the MBPC controller an advantage. However although the implementation is much simpler than that used in continuous controllers the performance of the MBPC controller is poorer. Figure 8.30 shows the tracking for the combined above and below rated controllers described above (tracking with $\hat{T}_f$ for below rated). At each sampling instant the errors from both lines are calculated. The minimum error dictates which controller to use. As can be seen from the figure, reasonable performance is obtained when the controller is tracking the C_{Pmax} curve at low rotor speeds. However when the point on the torque/rotor speed plane comes near the intersection of the two strategies the results are poorer with significant deviations from the curves resulting in high overshoots in terms of generator torque and power.

In order to try and improve the performance over the complete wind range a weighting, as is mentioned in Section 5.3.4, is introduced. The weighting is designed to scale the error from the below rated curve for deciding whether to track the above rated or below rated strategy. Thus if the weighting is 5 the distance from the below rated line is scaled by 5, therefore penalising the chance of tracking the below rated line. Shown in Figure 8.31 a. through e. are results for 5 different weightings (0.1, 0.5, 1, 5 and 8). For clarity only the results between 10 and 100 seconds are shown in each plot and the same wind input is used in each case. These results show the low weights (< 1) giving a better performance than higher weights. Low weights indicate that the controller will tend to track the below rated curve more than the above rated curve. As the below rated system is easier to control and performed well in the individual tests this improvement for low weights should probably be expected.

Figure 8.32 shows the comparison with a combined classical controller. The controllers for above and below rated wind speeds are the same as described above and the switching method is the same as described in Section 5.3.4 with a weight of 1. The combined classical controllers exhibit better performance than the MBPC combined controller, reducing the torque and rotor speed overshoots greatly and providing much tighter control.

Overall even using weights the results for the MBPC combined controller results, as

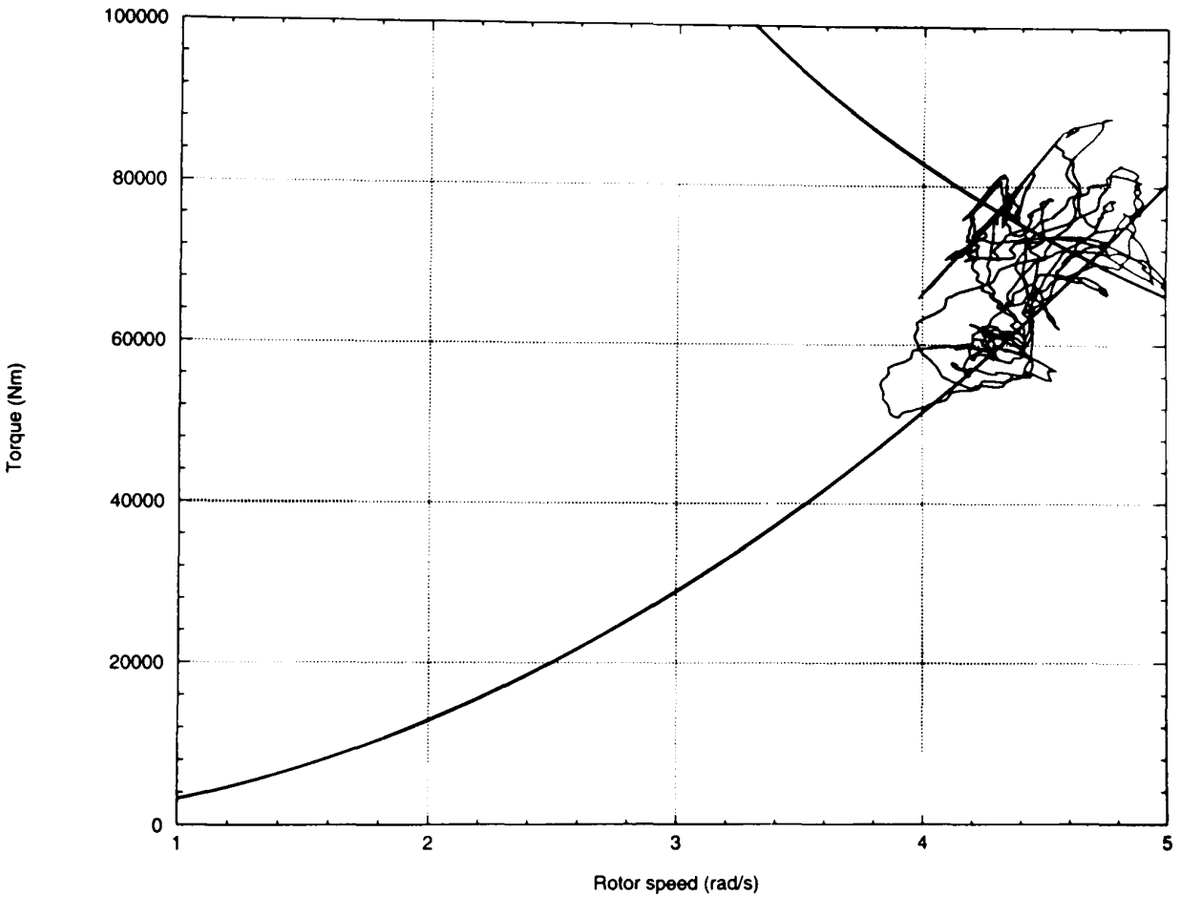

Figure 8.30: Switching results for full wind speed range, MBPC controller. Aerodynamic torque vs. rotor speed

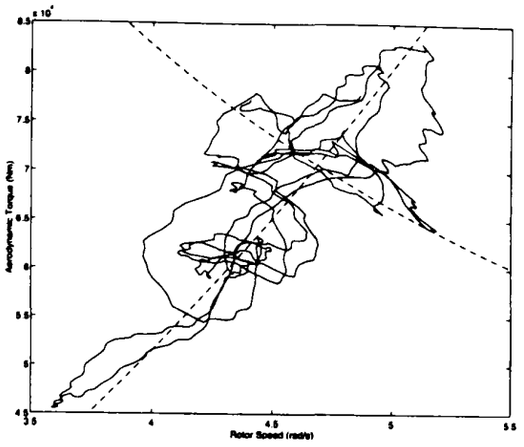

a. Weight = 0.1

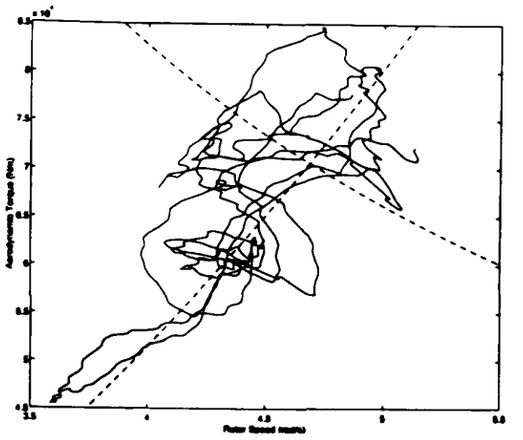

b. Weight = 0.5

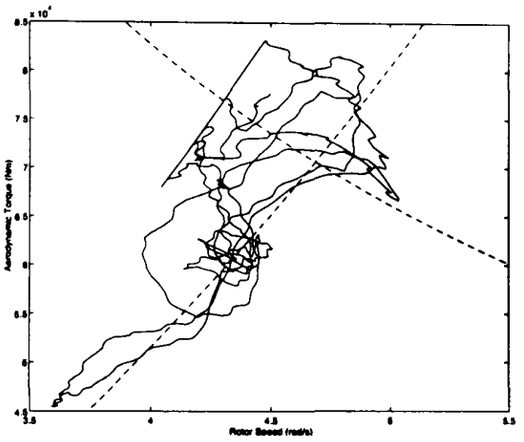

c. Weight = 1

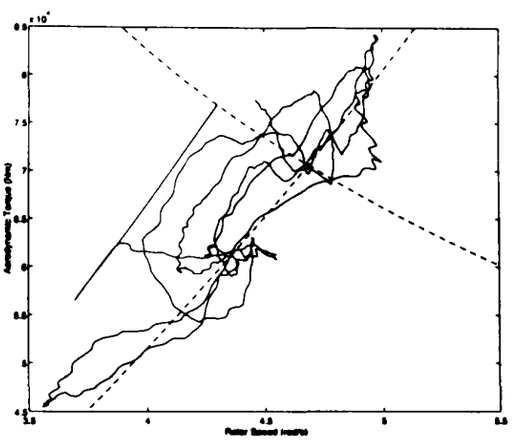

d. Weight = 5

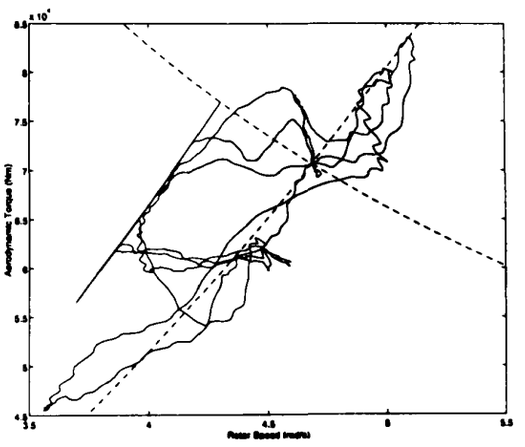

e. Weight = 8

Figure 8.31: Switching results for various weights. All graphs show C_{Pmax} and Rated Power as dashed curves. X-axis "Rotor Speed (rad/s)", min 3.5, max 5.5. Y-axis "Aerodynamic Torque (Nm)", min $4.5 * 10^4$, max $8.5 * 10^4$.

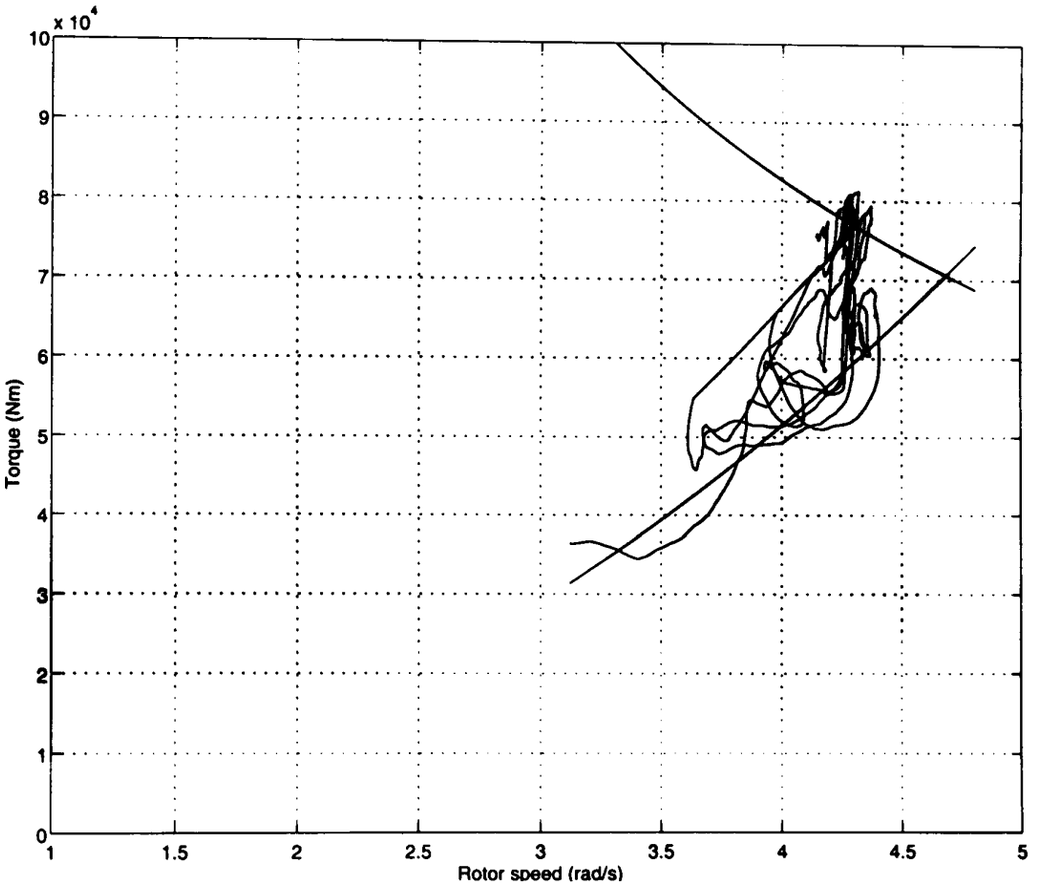

Figure 8.32: Switching results for the full speed range, classical control. Aerodynamic torque vs. rotor speed

compared to those for the classical controllers, could at best be described as reasonable.

8.8 Summary and discussion

The MBPC methodology is applied to a stall regulated variable speed wind turbine with MBPC controllers being designed, developed and then tested through simulations. Throughout, the simulation results are compared to a previously designed classical controller. These time domain results combined with a detailed analysis of the simple form of MBPC controllers in the frequency domain, provide a good analysis of the application of the MBPC technique to a challenging control problem.

The analysis of the simple form of MBPC controller raises questions about the ability of the technique to provide good control on a demanding system. Although only the simplest parameters are used the MBPC controller can destabilise the stable below rated system and for both the above and below rated systems the robustness of the controller is very poor.

When looking at the time domain results in comparison to the well designed classical controller the results, although worse than the classical controller, could be considered at best reasonable. However the best results rely on picking a value of damping (Λ) just high enough as to appear stable. How robust these controllers are must be questioned and a much higher value may be needed in practice which would further degrade the performance of the MBPC controllers. The ability to analyse fully the classical controller in the frequency domain allows the designer to check if the final system will have theoretical robustness. However for the MBPC technique obtaining such a guarantee is much more difficult and therefore the reliability of the final system is not assured. One solution to this is to further develop the method described in Appendix G to cover all types of MBPC controllers. This would allow the analysis of the technique in the frequency domain and could guarantee numerical stability and robustness. One drawback to this approach is that relying on control system designer being able to analyse the system performance in the frequency domain removes the transparency of the MBPC technique which made it attractive originally.

On the whole the results for the individual below and above rated controllers and for the combined controller are slightly disappointing and the reliability of the technique to be able to produce stable and robust controllers must be questioned. The expected advantages through ease of implementation did not appear.

Chapter 9

Final Conclusions and Future Work

In the promotion and development of renewable energy systems, control engineering is identified as one area which can directly affect the overall system performance and economics and thus help to make renewable energies more attractive and popular. Ideally these systems require a control design technique which is very effective yet simple with methods that are transparent enough to allow implementation by non-control engineers. Model Based Predictive Control (MBPC) is chosen as a possible control technique suitable for use in the renewable energy industry. MBPC, which is discussed in Chapter 2, uses simple and fairly transparent methods yet claims to be powerful and to deal with issues, such as non linearities and controller constraints, which are important in renewable energy systems.

The work presented above investigates the application of MBPC to two contrasting renewable energy systems. MBPC is applied to a solar power system and a wind turbine to enable the general applicability of MBPC to renewable energy systems to be tested and the possible benefits to the efficiency of these systems to be assessed. Also by applying the MBPC technique to two strongly contrasting systems much experience is gained about the MBPC technique itself, and its strengths and weaknesses and ease of application are assessed.

The application to the solar power plant in Chapter 3, which is a relatively simple and slow system, allows experience of the MBPC techniques to be gained and the final results from testing on the solar plant are encouraging with a fairly basic controller giving good results in comparison to other controllers tested on the same plant. MBPC seems suitable for such systems.

However the application of MBPC to the stall regulated variable speed wind turbine in Chapter 8, provides a much harder control problem for the MBPC technique. Detailed development, analysis and testing of MBPC controllers by simulation appears to uncover some failings and weaknesses in their performance. In particular the robustness of the final plant is very poor even when the controller is designed and tested using known models. If the MBPC controller is applied to a real plant where the models are not exactly known this lack of robustness would be a serious problem and could cause the system to become unstable.

It is concluded that in order to design an effective and reliable MBPC controller for a fast demanding system like a VSWT more complex system analysis techniques are necessary. However this would exclude most non-control engineers from being able to apply the MBPC method effectively or reliably and thus the expected advantages through ease of application do not appear.

In summary, the investigation into the performance of Model Based Predictive Control and in particular its application in the renewable energy systems industry leads to two contrasting conclusions. For simple systems with non-demanding dynamics and having a good model of the system, MBPC provides a very good and effective solution. In these cases MBPC is to be recommended and can be applied by non-control engineers and, with some work, good results can be expected. The benefits are not quantified here but are likely to be worthy of the extra work in implementing an MBPC controller over the industrial standard PI controller with experimental tuning. However for more demanding systems with complex dynamics and strong non-linearities, a basic MBPC controller, applied by a non-control engineer, cannot be recommended. There is potential for a form of MBPC controller to be applied successfully but only if the system and controller are analysed and developed by a specialist in the control field. A good control system however is essential for systems like wind turbines to be effective, economic and safe. Especially with wind turbines becoming increasingly larger and more complex the extra cost in developing a sophisticated controller can be justified and in many cases will be essential.

Therefore, MBPC, through using a more advanced form than is presented above, may still have its part to play in helping renewable energies to replace polluting forms of energy generation and make our world cleaner with a better environment for future generations.

9.1 Future work

Although conclusions have been reached about the usefulness and the performance of MBPC controllers and their application to renewable energy systems, there is still work which could be carried on.

For both the solar power plant and also the wind turbine application more complex MBPC controllers can be tested to see if the MBPC technique has the potential to give better performance than classical controllers. In particular two aspects which could be investigated are the direct handling of constraints and experimenting with different sampling times.

For the wind turbine controllers designed above extra damping is introduced to prevent the generator firing angle moving too rapidly and destabilising the system. This damping could be lessened if there were limits on the rate of change of firing angle. However unless the controller takes into account these limitations the controller performance is degraded. When constraint handling is introduced, the controller makes its choice of control action based on knowledge of the limits on the system and thus system performance could, perhaps, be improved.

Varying sampling times was briefly experimented with on the solar power plant. The results from this were inconclusive but further work could be carried out to see if this has any effect on the performance of the solar power plant system. This could also be tested on the wind turbine system although the sampling time used in Chapter 8 is very likely to be close to optimal.

Another aspect having the potential to improve the system performance is investigating the possibility of using non-linear models or more models corresponding to different operating points of the system involved. However this would lead to much more complexity and a greater need for effective switching.

One final piece of future work which would prove a very good test of the performance of the MBPC technique is the application to a constant speed wind turbine. Such systems are strongly non-linear in terms of aerodynamics and also in performance of the controller which requires very tight control in high wind speeds. These systems are also controlled through pitching the blades. The actuators which pitch the blades place physical constraints on the system as they are limited in terms of position, speed and acceleration. Applying MBPC to such a system would provide further insight into the claims of ease of dealing with non-linearities and constraints.

References

[1] American Wind Energy Association web site, www.awea.org

[2] Anderson P.M., Bose A. *Stability simulation of a wind turbine*, I.E.E.E. Trans. of Power Appr. and Syst., V.PAS-102, pp. 3791-3795, 1983.

[3] Anderson, C.G., *Private communication*

[4] Arkun, Y. and Hollett, J. and Canney, W. M. and Morari, M., *Experimental study of Internal Model Control*, Ind. Eng. Chem. Process Des. Dev., 1986, Vol. 25, pp 102-108

[5] Berenguel, M., E.F. Camacho and F.R. Rubio, *Simulation Software Package of the Acurex Field.* E.S.I. of Seville, Internal Report, 1993

[6] Bongers, P.M.M., Dijkstra, S. and Kock, Z., Optimal control of a wind turbine in full load, Proc., European Wind Energy Conference EWEC'89, Glasgow, 10-13 July, 1989, pp 345-349

[7] Bongers, P.M.M., Van Holten, T., Dijkstra, S., Control of Wind Turbine Systems for Load Reduction, Proc., European Wind Energy Association Conference EWEC'91, Amsterdam, 14-18 October, 1991, pp. 68-72

[8] Bossanyi, E.A., Smith, E.J., Leithead, W.E., Agius, P.R.D. *Design and testing of a classical controller for MS-3 wind turbine*, Dept. Energy Report, WN/6033, 1992.

[9] Bossanyi, E.A., Jenkins, N., *Electrical aspects of variable speed operation of horizontal axis wind turbine generators*, Report prepared for Dept. Energy by the Wind Energy Group Ltd, Agreement No. E/5A/6051/2426, 1992

[10] British Wind Energy Association web site, www.bwea.com.

[11] Burnham, L. (Executive Editor), *Renewable Energy — sources for fuels and electricity.* Earthscan, 1993

[12] *CADDET Renewable Energy Newsletter*, February 1998. Caddet, ETSU, UK

[13] Camacho, E.F., M. Berenguel and F.R. Rubio, *Application of a Gain Scheduling Generalised Predictive Controller to a Solar Power Plant.* Control Engineering Practice, Vol.2, No.2, 1994, pp.227–238.

[14] Cardenas-Dobson, R., Asher, G.M. and Asher, G., *Torque observer for the control of variable speed wind turbine operating below rated windspeed*, Wind Engineering, 20 (4), pp. 259-285, 1996

[15] Cardenas-Dobson, R. and Asher, G.M., *Power limitation on variable speed wind turbine using pitch control and a mechanical torque observer*, Wind Engineering, 20 (6), pp. 363-387, 1996

[16] Caselitz, P., Kleinkauf, W., Krger, T. and Petschenka, J., *Load reduction by multivariable control of wind energy convertors - simulation and experiments*, Processings of the European Union Wind Energy Conference, Göteborg, Sweden, pp. 821-824, 1996

[17] Chang, T. S. and Soborg, D. E., *A linear programming approach for multivariable feedback control with inequality constraints*, Int. J. Control, 1983, Vol. 37, No. 3, pp 583-597

[18] Chesshire, J., Head of Energy Policy Programme, Uniersity Sussex, *Air Quality, Key Environmental Issues, Number 6.* written with support of British Gas, October 1990

[19] Clarke, D. W. and Mohtadi, C. and Tuffs, P. S., *Generalzed Predictive Control - Part I. The basic algorithm*, Automatica, Vol. 23, No. 2, pp 137-148, 1987

[20] Clarke, D. W., *Generalized Predictive Control*

[21] Clarke, D.W., Scattolini, R., *Constrained receding horizon predictive control.* Proc. IEE, Vol. 138, Pt. D, No. 4, 1991, pp. 347–354

[22] Connell, J.R. *The spectrum of wind speed fluctuations encountered by a rotating blade of a WECS*, Solar Energy, v.29(5), 1982, pp. 363-375.

[23] Connell, J.R., George, R.L. *A new look at turbulence as experienced by a rotating wind turbine*, 2^{nd} ASME Wind Energy Symp., Houston, TX, Jan. 1983, pp. 455-479.

[24] Connor, B. and Leithead, W.E., *Design of a control system for a 450 kW wind turbine with a variable speed capability*, Technical report, University of Strathclyde, 1993

[25] Connor, B., and Leithead, W.E., *Investigation of a fundamental trade-off in tracking the C_{Pmax} curve of a variable speed wind turbine*, Proceedings of the 15th British Wind Energy Conference, York, U.K., pp. 313-319, 1993

[26] Connor, B. and Leithead, W.E., *The Effect of Rotor Characteristics on the Control of Pitch Regulated Variable Speed Wind Turbines.* Proc. 16th British Wind Energy Assoc. Conf, Stirling, June 1994, pp. 67–72.

[27] Connor, B. and Leithead, W.E., *Control stategies applied to variable speed stall regulated wind turbines.* Proc. European Wind Energy Association Conf., Greece, October 1994 pp. 420–425.

[28] Connor, B. and Leithead, W.E., *Performance assessment of variable speed wind turbines*, Proceedings of the IEE International conference on 'Opportunites and Advances in International Electric Power Generation', Durham, U.K., 419, pp. 65-68, 1996

[29] Connor, B., Leithead, W.E., *Stategies for the Control of Variable Speed HAWTs.* University of Strathclyde report prepared for AEA Technology, Feburary 1995.

[30] Cutler, C. R. and Haydel, J. J. and Morshedi, A. M., *An Industrial perspective on advanced control*, Shell, 1983

[31] Cutler, C. R. and Ramaker, B. L., *Dynamic Matrix Control - A computer control algorithm*, AIChE National Mtg, Houston, Texas, 1979; also Proc. Automatic Control Conf, 1980, Sanfancisco, California.

[32] Danish Wind Turbine Manufacturers Association web site www.windpower.dk.

[33] Davenport, A.G., *The spectrum of Horizontal gustiness near the ground in high winds.* Quart. J. Roy. Met. Soc., 1961, **87**, pp. 194–221.

[34] De Keyser, R.M.C., *The MBPC Methodology.* Intensive Training Course on Model Based Predictive Control, Frankfurt/Main, Germany, May 11,12 1995

[35] De Keyser, R.M.C., Van Cauwenberghe, A., *Extended prediction self-adaptive control.* IFAC Symposium of Identification and System Parameter Estimation, York, 1985

[36] Dorf, Richard C., *Modern Control Systems.* 5th Edition. Addison-Wesley, 1989

[37] Economou, C. G. and Morari, M. and Palsson, B. O., *Internal Model Control. 5. Extension to Nonlinear Systems*, Ind. Eng. Chem. Process Des. Dev., 1986, Vol. 25, pp 403-411

[38] Economou, C.G. and Morari, M., *Internal Model Control. 6. Multi loop design*, Ind. Eng. Chem. Process Des. Dev., 1986, Vol. 25, pp 411-419

[39] Ekelund, T., *Modelling and linear quadratic optimal control of wind turbines*, PhD. Thesis, Chalmers University of Technology, 1997

[40] Ekelund, T., Scmidtbauer, B., Trade-off between energy capture and dynamic loads in variable speed wind turbines, Proc. of the 12th IFAC World Congress, Sydney, Australia, 18-23 July, 1993, Vol. 7, pp. 521-524

[41] Ekelund, T., *LQG speed control of wind turbines in the stall region*, Proceedings of the 3rd IEEE Conference on Control Applications, Glasgow, Scotland, pp. 227-232, 1994

[42] Ernst, J. and Leonard, W., *Optimisation of the wind energy output of variable speed wind turbines*, Proceddings of Wind Power '85, San Francisco, USA, pp. 184-188, 1985

[43] Ernst, J., *Control of a variable speed wind energy converter with a synchronous generator and a D.C. link*, Proceedings of the European Wind Energy Conference, Hamburg, Germany, 1984, pp.606-611

[44] ETSU, *An assessment of Renewable Energy for the U.K.*. H.M.S.O. London, 1994

[45] European Wind Energy Association web site, www.ewea.org

[46] EWEA, *The Economics of Wind Energy*, European Wind Energy Association, 1997

[47] EWEA, *The Wind Energy Industry - Status and Prospects*, European Wind Energy Association, 1997

[48] EWEA, *Wind Energy and the Environment*, European Wind Energy Association, 1997

[49] EWEA, *Wind Energy Technology*, European Wind Energy Association, 1997

[50] Fisher, D. Grant, *Process Control: An Overview and Personal Perspective.* The Canadian Journal of Chemical Engineering, Vol.69, February 1991.

[51] Freris, L.L., *Wind Energy Conversion Systems.* Prentice Hall, 1990

[52] Freris, L.L., *Harnessing the wind.* IEE Power Engineering Journal, September 1992, pp 251-260.

[53] Ganander, H., Ulén E., Poppen, M., Björck, A., Ellsén. M., Carlson, O., Stall control with variable speed at the Hönö 2 wind turbine, Department of Electrical Machines and Power Electronics, Technical report no. R-92-11, Chalmers University of Technology, January, 1993

[54] Garcia, C. E. and Prett, D. M. and Morari, M., *Model Predictive Control: Theory and Practice - a survey*, Automatica, 1989, Vol. 25, No. 3, pp 335-349

[55] Garcia, C. E. and Morshedi, A. M., *Quadratic Programming Solution of Dynamic Matrix Control*, Chem. Eng. Commum., 1985, Vol. 46, pp 73-87

[56] Garcia, C. E. and Morari, M., *Internal Model Control. 2. Design Procedure for Multivariable Systems*, Ind. Eng. Chem. Process Des. Dev., 1985, Vol. 24, pp 472-484

[57] Garcia, C. E. and Morari, M., *Internal Model Control. 3. Multivariable Control Law Computation and tuning guidelines*, Ind. Eng. Chem. Process Des. Dev., 1985, Vol. 24, pp 484-494

[58] Holley, W.E., Thresher, R.W., Lin, S-R. *Atmospheric turbulence inputs for horizontal axis wind turbines*, Proc. European Wind Energy Conf., October 1984, Hamburg, Germany, pp. 443-452.

[59] Iqbal, M.T., Coonick, A.H. and Freris, L.L., *Some aspects of a small isolated wind turbine*, Proceedings of the 15th British Wind Energy Conference, York, U.K., pp. 321-325, 1993

[60] Iqbal, M.T., Coonick, A.H. and Freris, L.L., *Dynamic control of a stand alone wind turbine*, Proceedings of the 16th British Wind Energy Conference, Stirling, U.K., pp. 135-140, 1994

[61] Johansen, T.B., Kelly, H., Reddy, A.K.N., Williams, R.H., (Editors), "Renewable Energy - Sources for fuels and electricity". Earthscan, p75, 1993.

[62] Krause, D.C., Man, D.T. *Transient behaviour of a class of turbine generators during electrical disturbances*, I.E.E.E. Trans. of Power Appr. and Syst., V.PAS-100, pp. 2202-2210, 1981.

[63] Kuo, B.C., *Analysis and synthesis of sampled data control systems*, Prentice Hall, 1963.

[64] Law, H., Doubt, H.A. and Cooper, B.J., *Power control for the Orkney wind turbine generator*, GEC Engineering, 2, 1984

[65] Lee, J.H. and Morari, M., *State Space Interpretation of Model Predictive Control*, ftp from imc.caltech.edu, 1992, September 25

[66] Leith, D.J. and Leithead, W.E., *Implementation of wind turbine controllers*, International Journal of Control, 66, pp. 349-380, 1997

[67] Leithead, W.E., Rogers, M.C.M., Connor, B., Pierik, J.T.E., Van Engelen, T.G., O'Reilly, J. *Design of a controller for a test-rig for a variable speed wind turbine.* Proc. 3rd IEEE conference on Control Applications. University of Glasgow, 24-26 August, 1994, Vol. 1, pp. 239-244.

[68] Leithead, W.E., de la Salle, S.A., Reardon, D., Grimble, M.J., *Wind turbine control systems modelling and design - Phase I + II.* report prepared for Dept. of Energy, University of Strathclyde, 1991.

[69] Leithead, W.E., de la Salle, S.A., Reardon, D., *Classical control of active pitch regulation of constant speed horizontal axis wind turbines.* Int. J. of Control, Vol. 55, No. 4, pp 845–876, 1992.

[70] Leithead, W.E. *Effective wind speed models for simple wind turbine simulation*, Proc. BWEA, Nottingham, pp 321-326, March 1992.

[71] Leithead, W.E. and Connor, B., *Control of a variable speed wind turbine with induction generator*, Proceedings of the IEE Conference Control '94, Warwick, pp 256-264, 1994.

[72] Leithead, W.E. and Rogers, M.C.M., *Drive-train characteristics of constant speed HAWTs: Part 1 - Representation by simpledynamic models*. Wind Engineering 20 (3), pp. 149-174, 1996

[73] Lipman, N., Pontin, G. and Musgrove, P. (eds.), *Wind Energy for the Eighties*, Peter Peregrinus, 1983.

[74] Lundstrom, P. and Lee, J. H. and Morari M. and Skogestad, S, *Limitation of Dynamic Matrix Control*, ECC 91, European Control Conference, Grenoble, France, July, pp 1839-1844, 1991

[75] Madsen, P.H., Frandsen, S. *Pitch angle control for power limitation.* Proc. of European Wind Energy Conference, Hamburg, 1984, pp. 612-919.

[76] McVeigh, J.C., *Energy Around the World.* Perganon Press, 1984.

[77] Mercer, A.S., *Stall regulation of variable speed HAWTs*, Report prepared for DTI by Garrad Hassan and Partners Ltd., 1995

[78] Morari, M., *Model Predictive Control: Multivariable Control Technique of Choice in the 1990s*, ftp from imc.caltech.edu, 1994

[79] Morshedi, A.M.,Cutler, C.R. and Skrovanek, T.A., *Optimal Solution of Dynamic Matrix Control with Linear Programming Techniques*, Proc. American Control Conf., 1985, June 19-21

[80] Munz, H., Connor, B. and Leithead, W.E., *Sensitivity of performance of stall regulated variable speed HAWTs to rotor inertia*, Proceedings of the 17th British Wind Energy COnference, Warwick, U.K., pp 261-266, 1995

[81] National Renewable Energy Laboratory, *Dollars from Sense, The Economic Benefits of Renewable Energy.* Produced for the U.S. Departement of Energy, DOE/GO-10097-261, September 1997

[82] Nayar, C.V. and Bundell, J.H., *Modelling and simulation of a wind-driven wound rotor induction generator with tip-speed ratio control*, Electric Energy COnference, Adelaide, Australia, pp. 78-85, 1987

[83] Parliamentary Office of Science and Technology, 1994, Select Committee Briefing. *Environmental Aspects of Wind Generation.*

[84] Parry, Prof. M, School of Georgraphy, University of Birmingham, *Global Climate, Key Environmental Issues, Number 3.* written with support of British Gas, October 1990

[85] Richalet, J., Rault, A., Testud, J. and Papon, J., *Model predicitive heuristic control: applications to an industrial process.* Automatica, 14, 1978, pp 413-428

[86] Richalet, J., *Industrial Applications of Model Based Predictive Control.* Automatica, Vol.29, No.5, 1993, pp1251–1274

[87] Richalet, J., *Observations on Model-Based Predictive Control*, Control Engineering, 1992, August

[88] Robb, D., *Control Strategies for variable speed wind turbines*, MSc thesis, Caledonian University, Scotland, September 1994

[89] Rubio, F.R., F. Gordillo and M. Berenguel, *LQG/LTR Control of the Distributed Collector Field of a Solar Power Plant.* Triennial World Congress, IFAC-96, Vol.O, pp133-138, San Francisco, 1996.

[90] Rubio, F.R., M. Berenguel, E.F. Camacho, *Fuzzy Logic Control of a Solar Power Plant.* IEEE Transactions on Fuzzy Systems, Vol.3, No.4, November 1995

[91] Sanchez, M., M. Beker (Editors), *Solar Thermal Test Facilities.* SolarPACES Technical Report III-5/95, Chapter 4 "Parabolic Trough Test Facilities" P. Balsa and E. Zarza.

[92] Scientific American, *Energy for planet earth, special issue*, September 1990, p22 & p48

[93] Simpson, P.B., *Developments in wind turbine technology*, Proc., 16th British Wind Energy Association Conference, Stirling, 15-17 June, 1994, pp. 29-40

[94] Skogestad, S. and Postlethwaite, I., *Multivariable Feedback Control - Analysis and design.* John Wiley and Sons, 1996

[95] Soeterboek, A. R. M. and Verbruggen, H. B. and Koster, A. J., *Predictive control of an industrial process*, ECC 91, European Control Conference, Grenoble, France, July, pp 1765-1770, 1991

[96] Soeterboek, R., *Predictive Control - Book review by David Clarke*, Automatica, 1994, Vol. 30, No. 7, pp 1213-1215

[97] Spera, David A. (Editor), *Wind Turbine Technology — Fundamental Concepts of Wind Turbine Engineering.* ASME Press, New York, 1994

[98] Steinbuch, M., Dynamic modelling and robust control of a wind energy conversion system, PhD Thesis, Delft University, 1989

[99] Thiringer, T., Linders, J., Control by variable rotor speed of a fixed-pitch wind turbine operating in a wide speed range, IEEE Trans. Energy Conversion, Vol. 8, No. 3, September 1993, pp.520-526

[100] Tsiolis, S., Carlson, O., Ulén E., Björck, A., Stall control with variable speed and an induction generator, Proc., European Community Wind Energy Conference, Germany, 8-12 March 1993, pp.816-819

[101] Wellstead, P.E. and Zarrop, M.B., *Self-Tuning Systems: Control and Signal Processing*, John Wiley and Sons, 1991

[102] Wilkie, J., Leithead, W.E., Anderson, C. *Modelling of wind turbines by simple models*, Wind Engineering Vol 14, 1990, pp 247-275.

[103] Wilmshurst, S.M.B., *Control strategies for wind turbines*, Wind Engineering, 12 (4), pp. 236-249, 1988

[104] Ydstie, B.E., *Extended horizon adaptive control.* IFAC World Congress, Budapest, 1984.

[105] *Solar Energy Research and Development in the European Community series G, vol. 1, Wind energy (1983)*, Proceesings of the EC contractors' meeting held in Brussels, November 1982, Reidel.

Appendix A

Acurex Solar Field Simulation Results

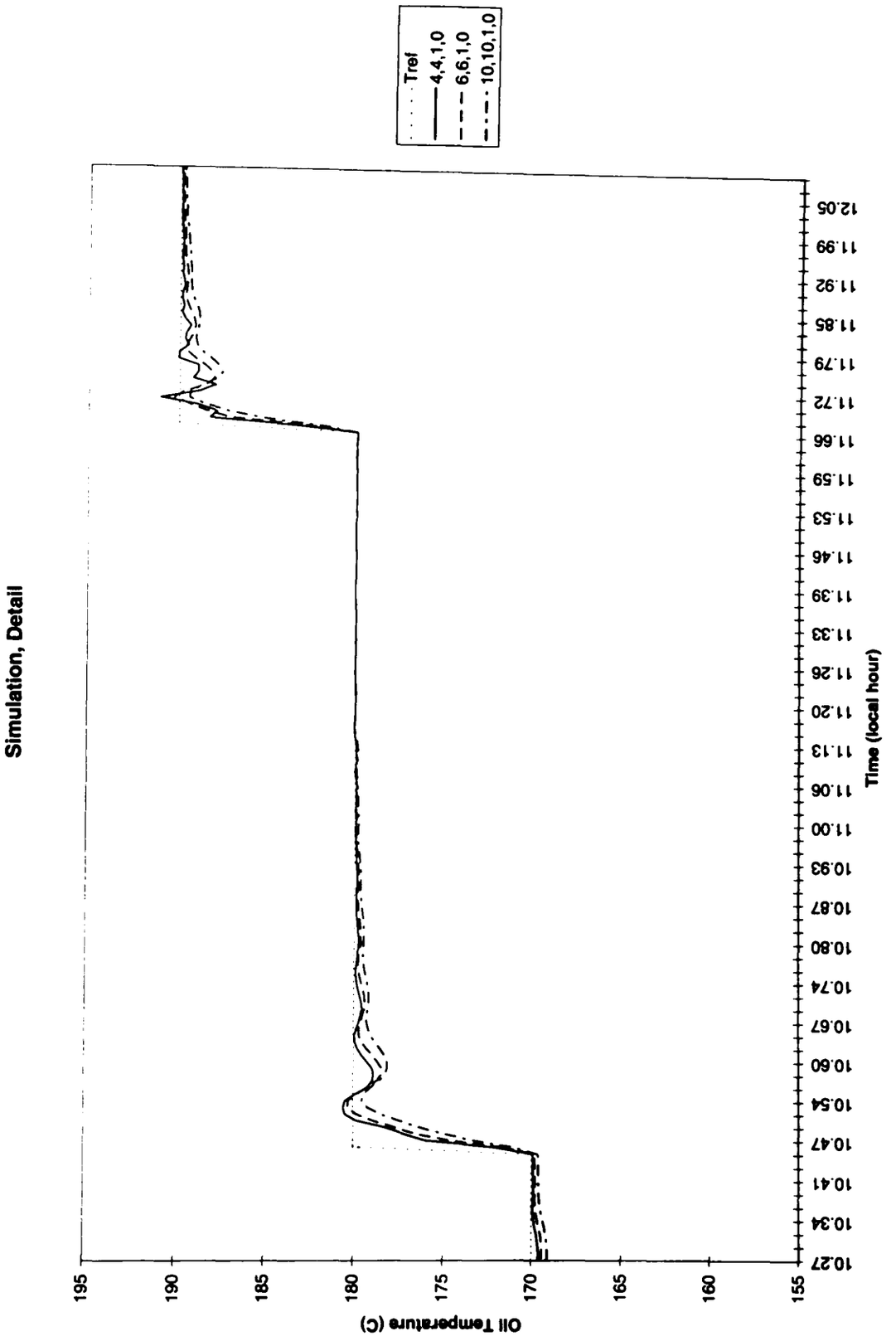

Figure A.1: Simulation comparison. n,n,1,0, n=(4,6,10)

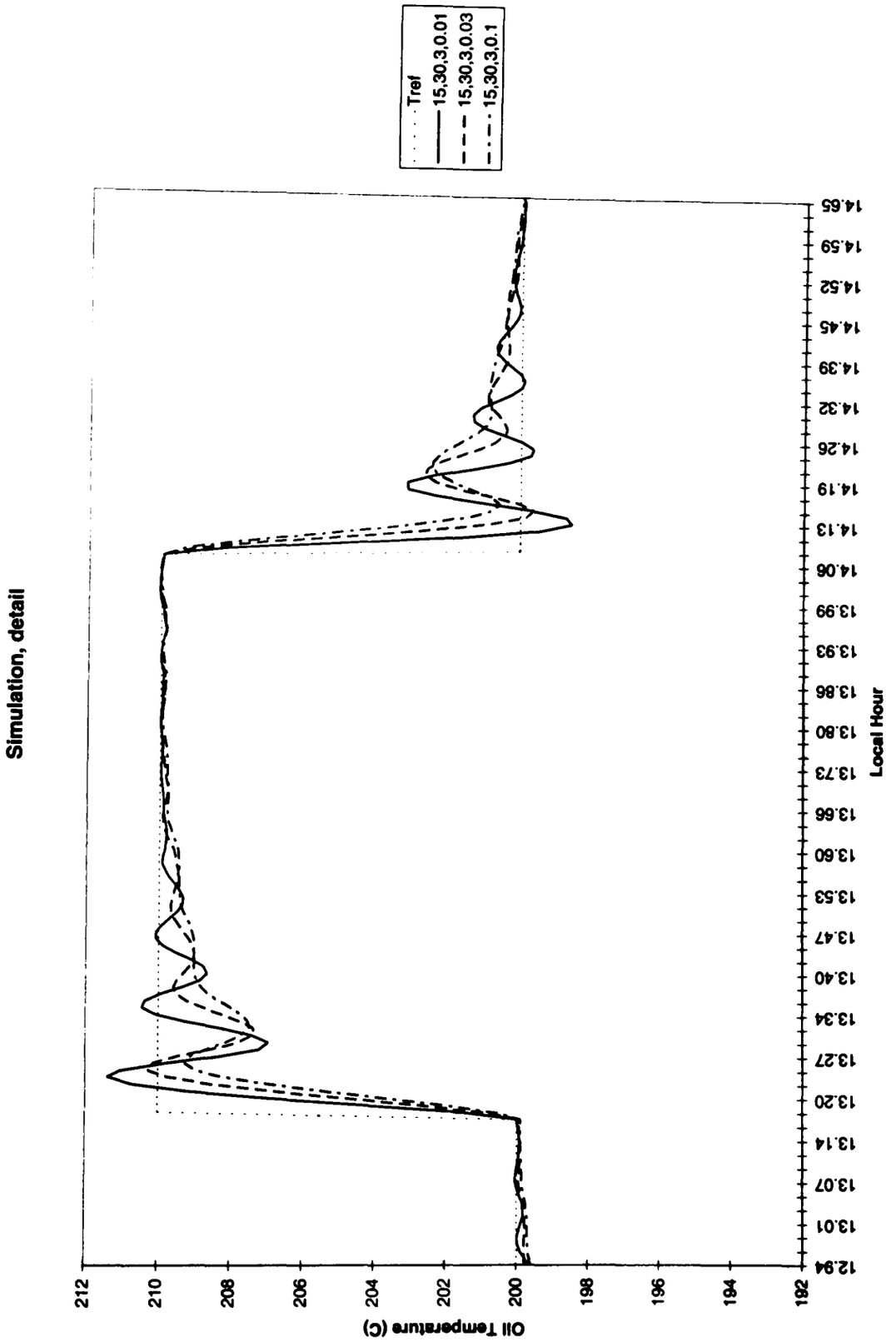

Figure A.2: Simulation comparison. 15,30,3,x

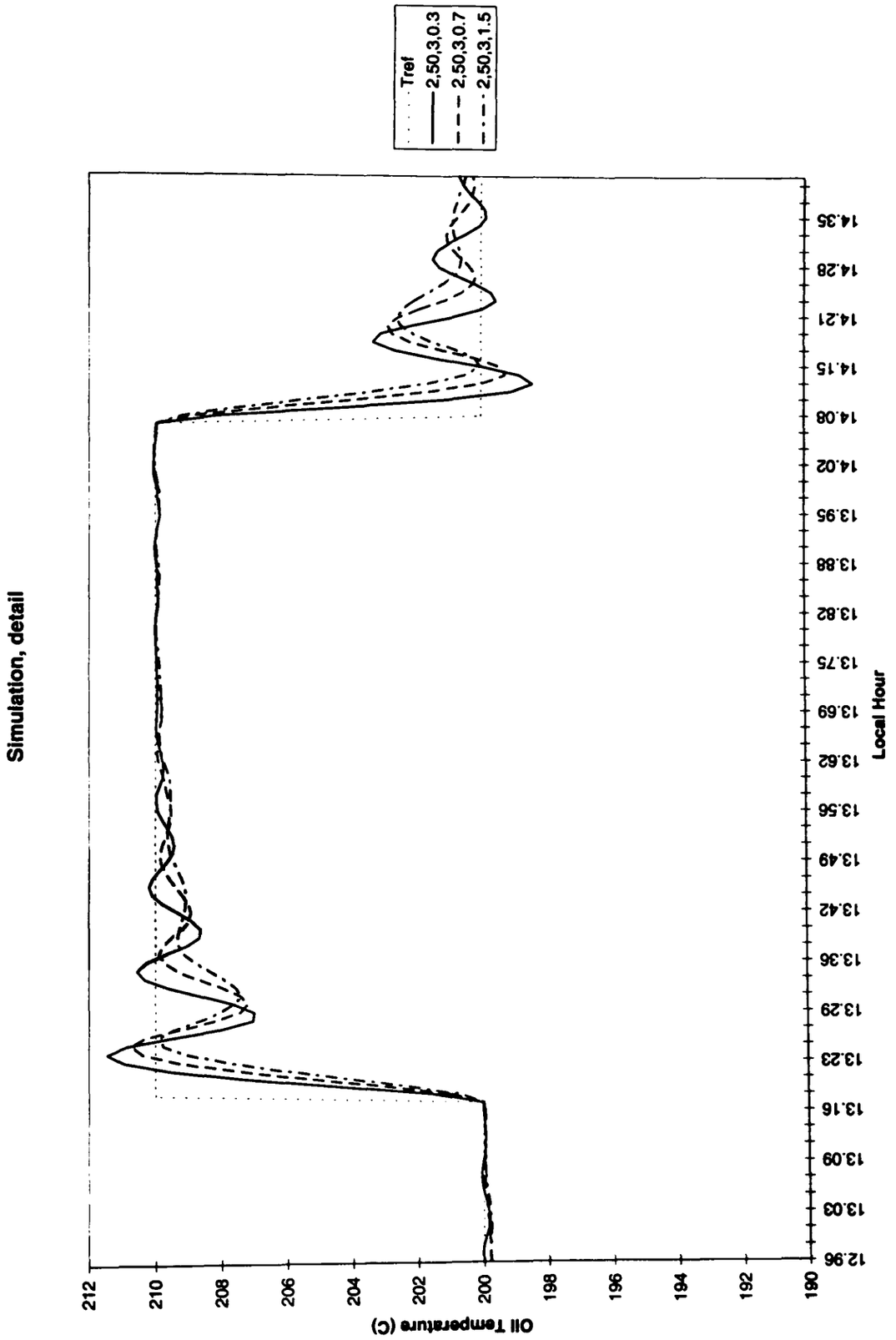

Figure A.3: Simulation comparison. 2,50,3,x

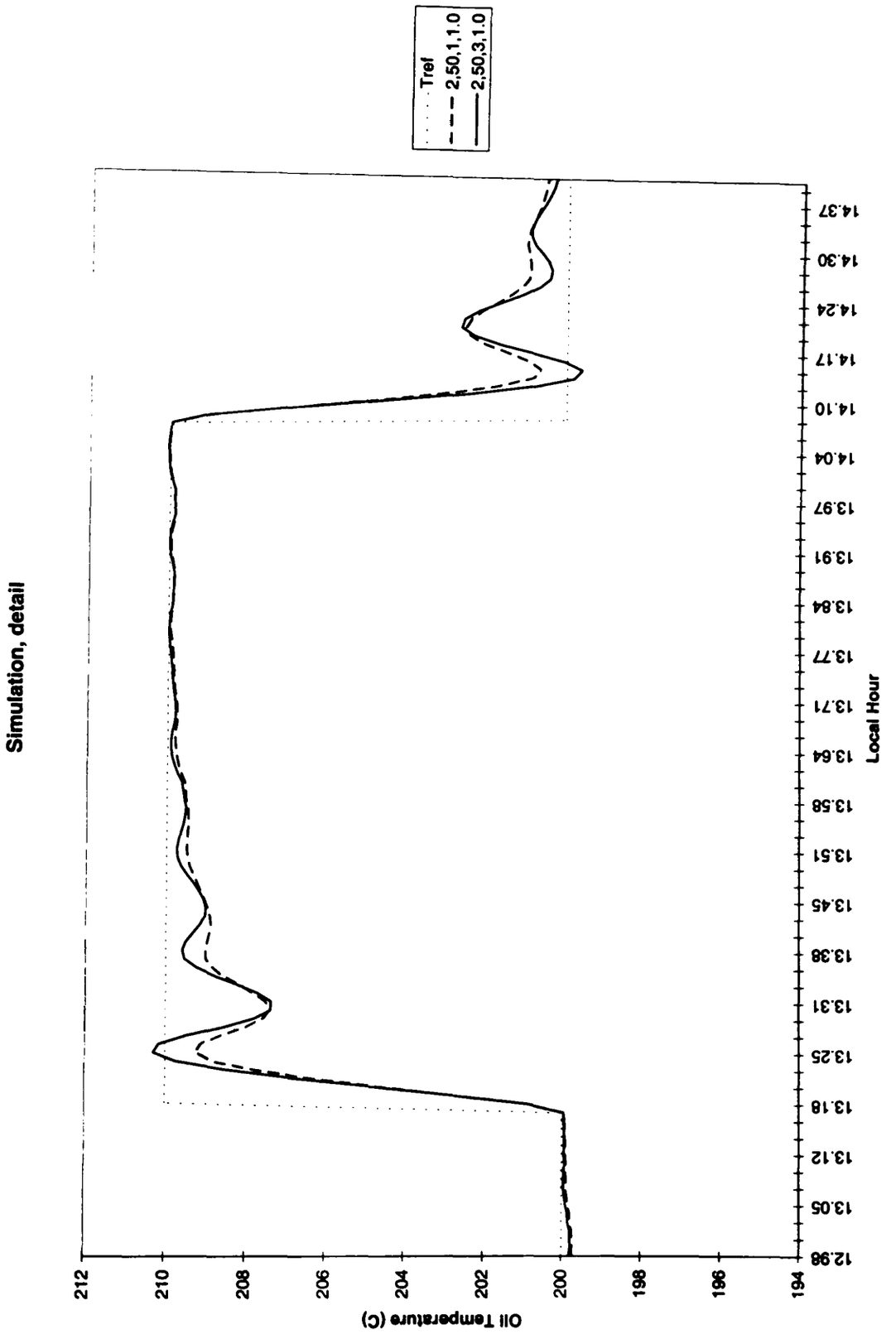

Figure A.4: Simulation comparison. 2,50,x,1

Appendix B

Daily Acurex Solar Field Test Results

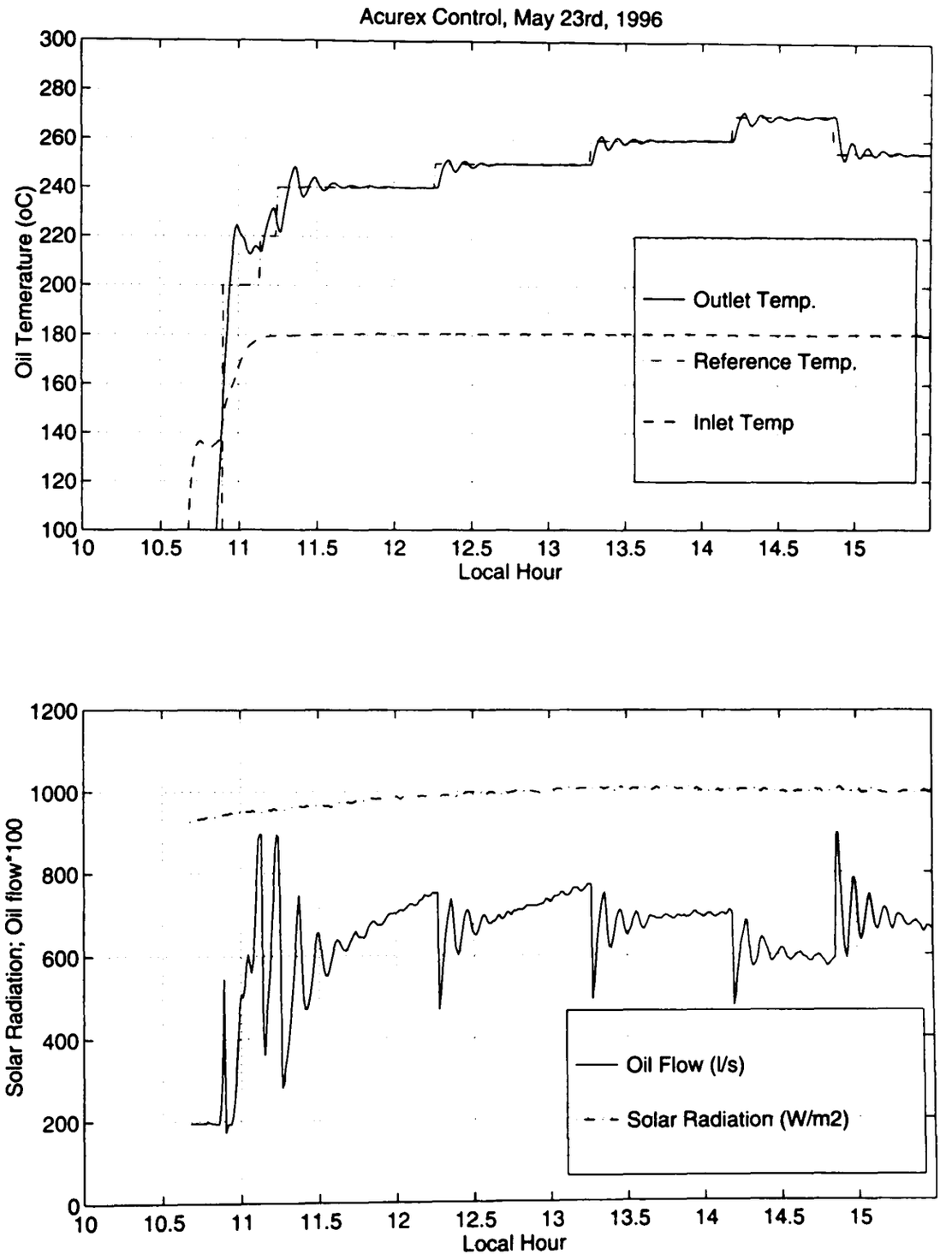

Figure B.1: 23rd May. Controller type 6,6,1,0

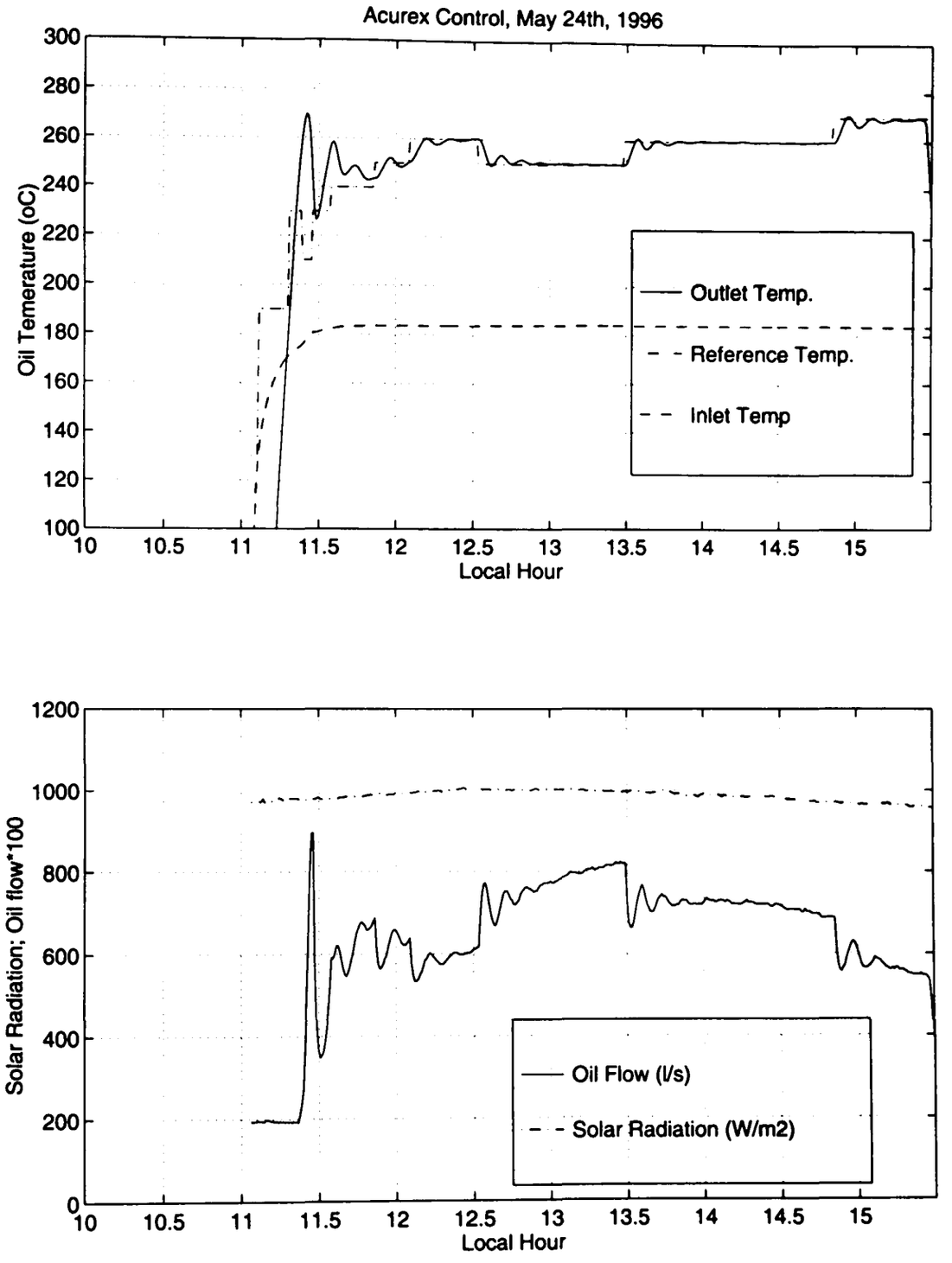

Figure B.2: 24th May. Set point following (2,50,3,1.0)

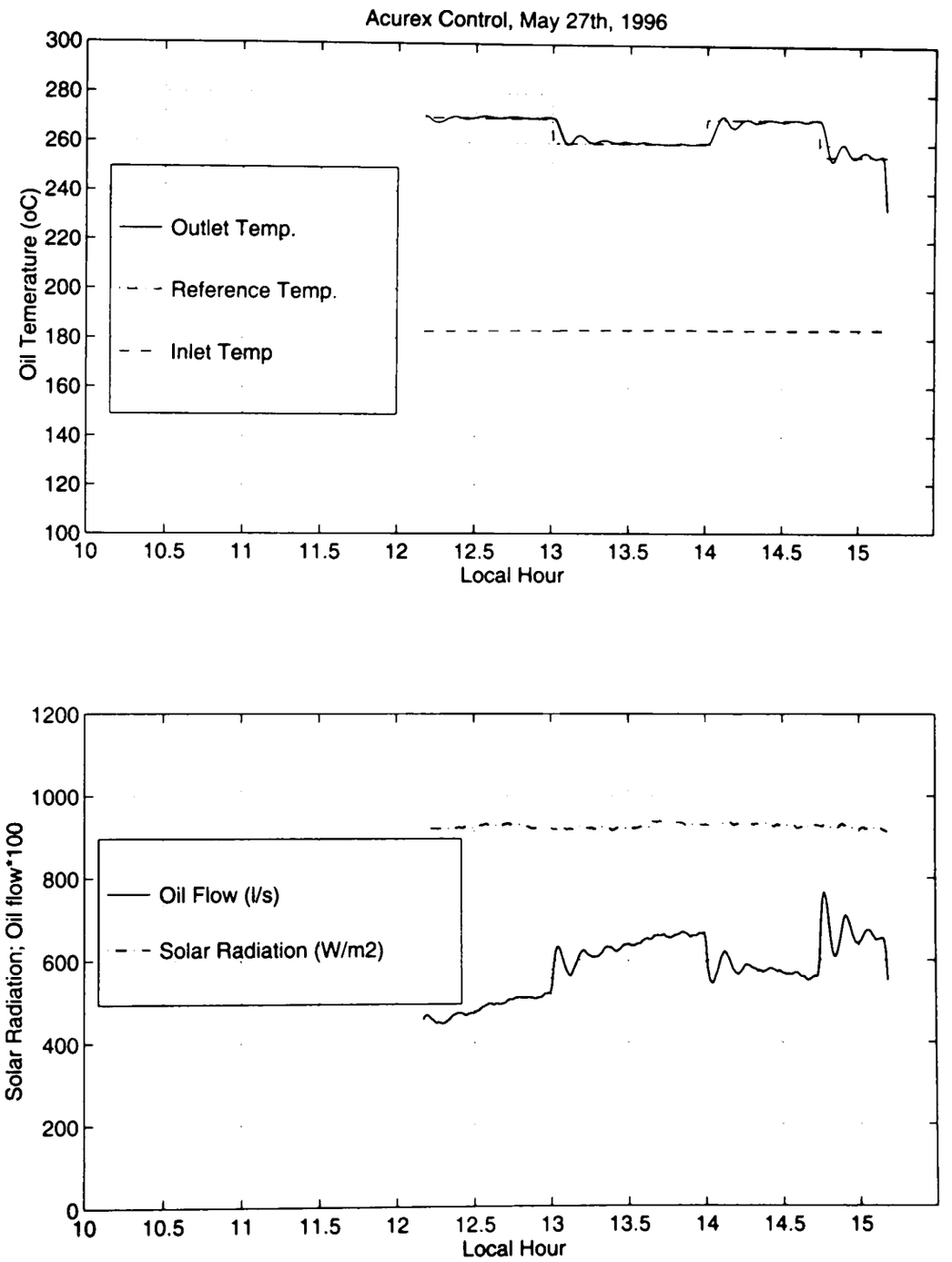

Figure B.3: 27th May. Set point following (2,50,3,1.0)

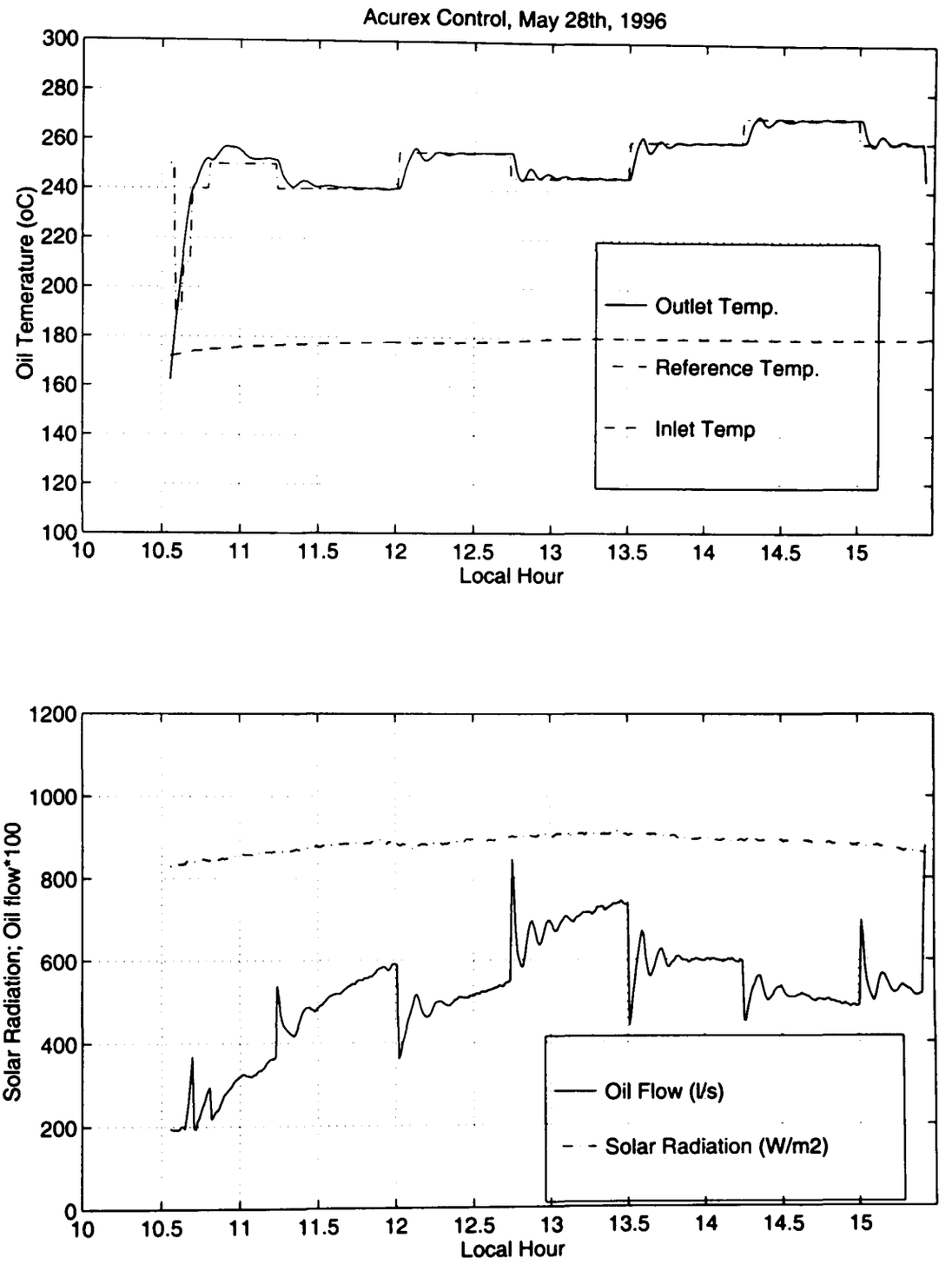

Figure B.4: 28th May. Set point following (8,8,1,0)

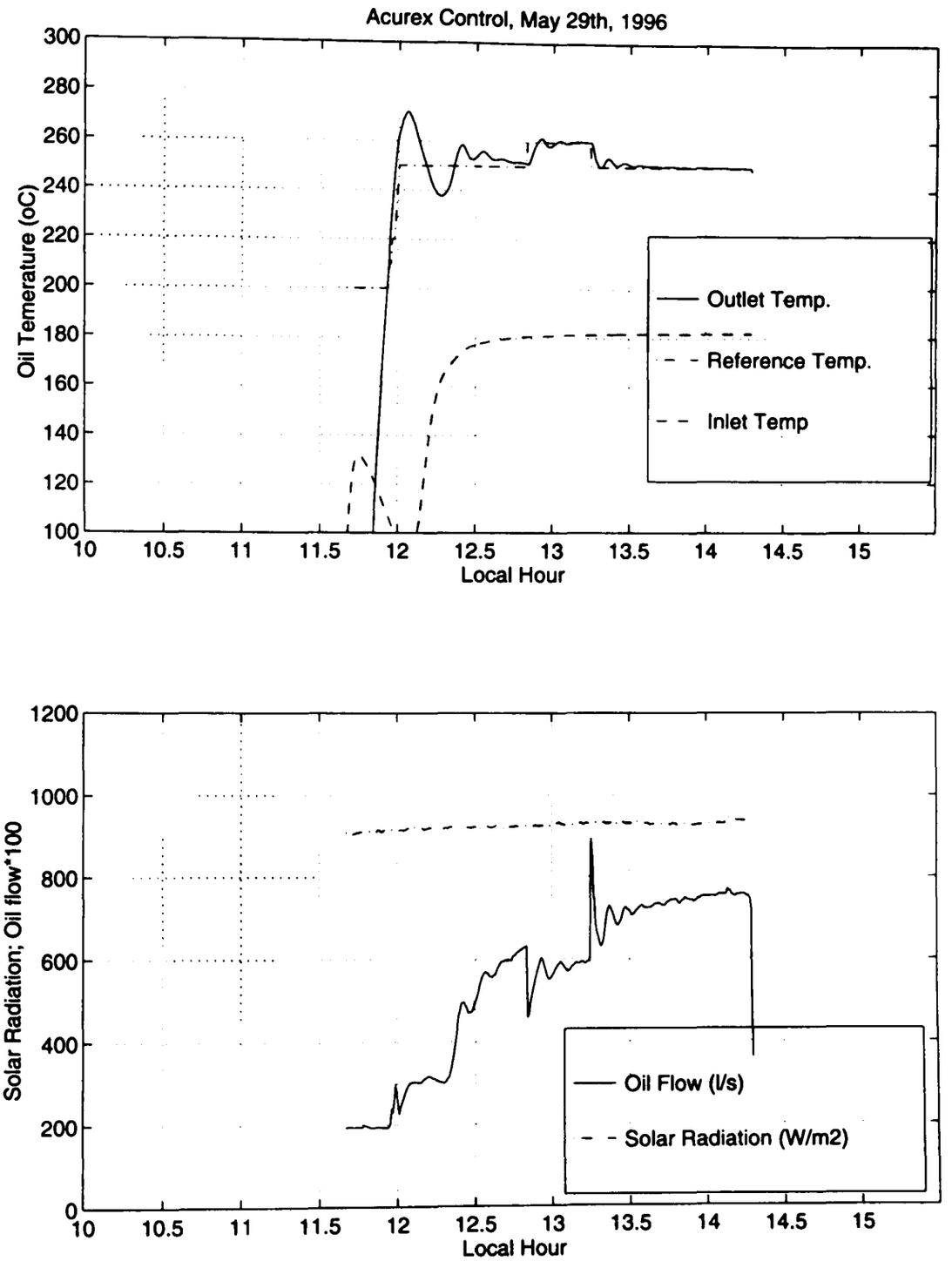

Figure B.5: 29th May. Set point following, Tsamp=13secs (24,24,1,0)

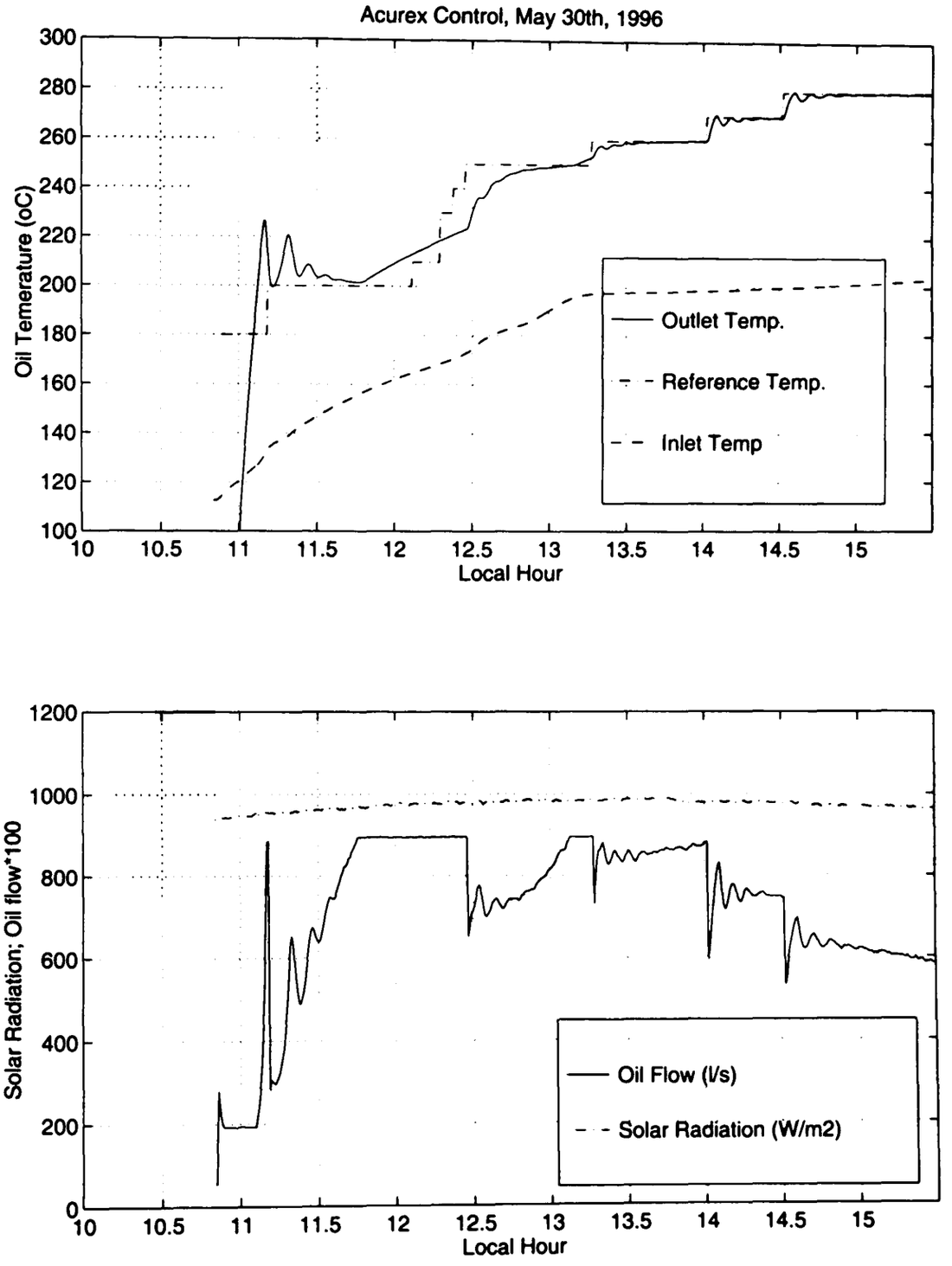

Figure B.6: 30th May. Set point following, Tsamp=13secs (24,24,1,0)

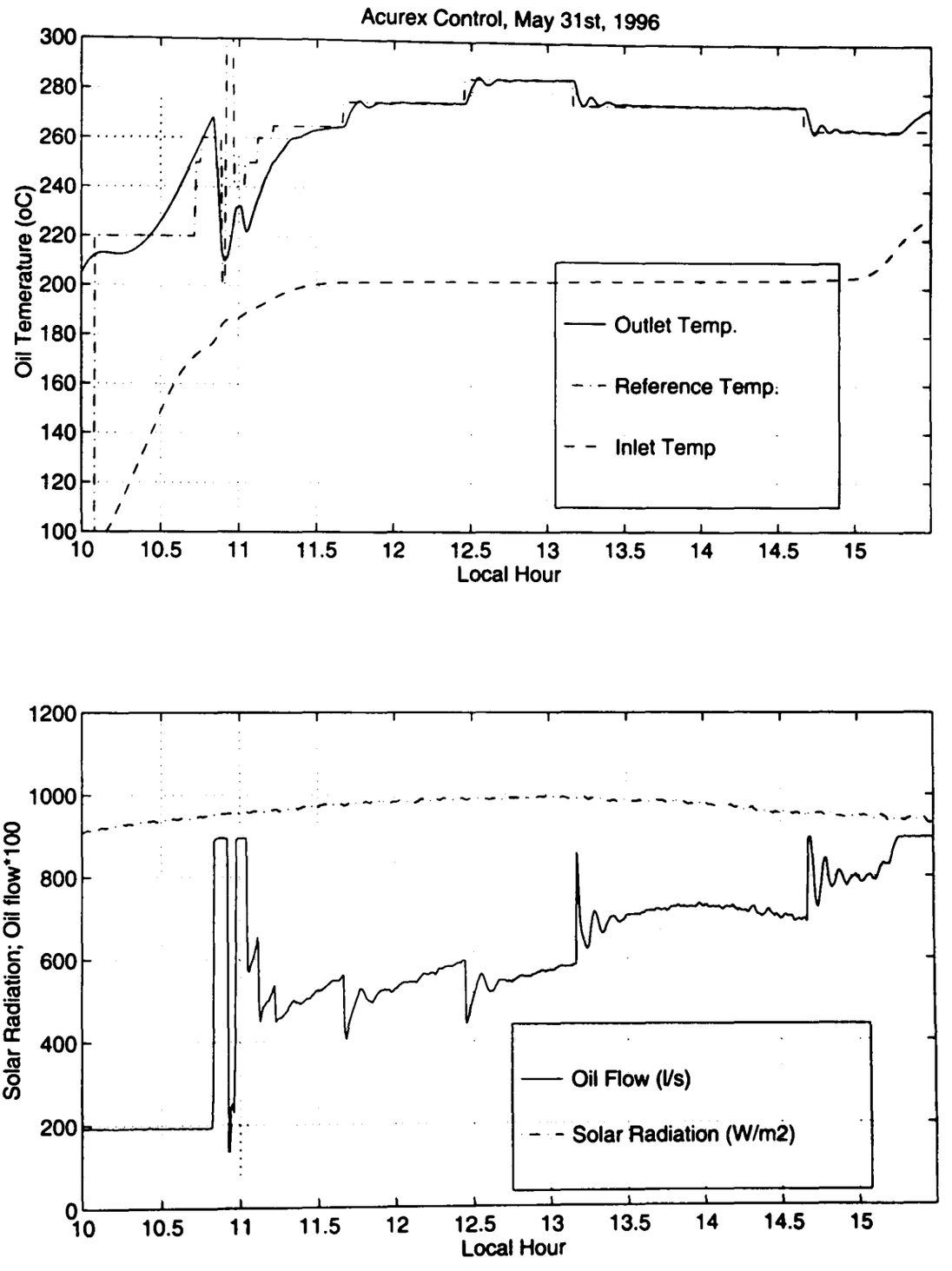

Figure B.7: 31st May. Set point following, Tsamp=13secs (24,24,1,0)

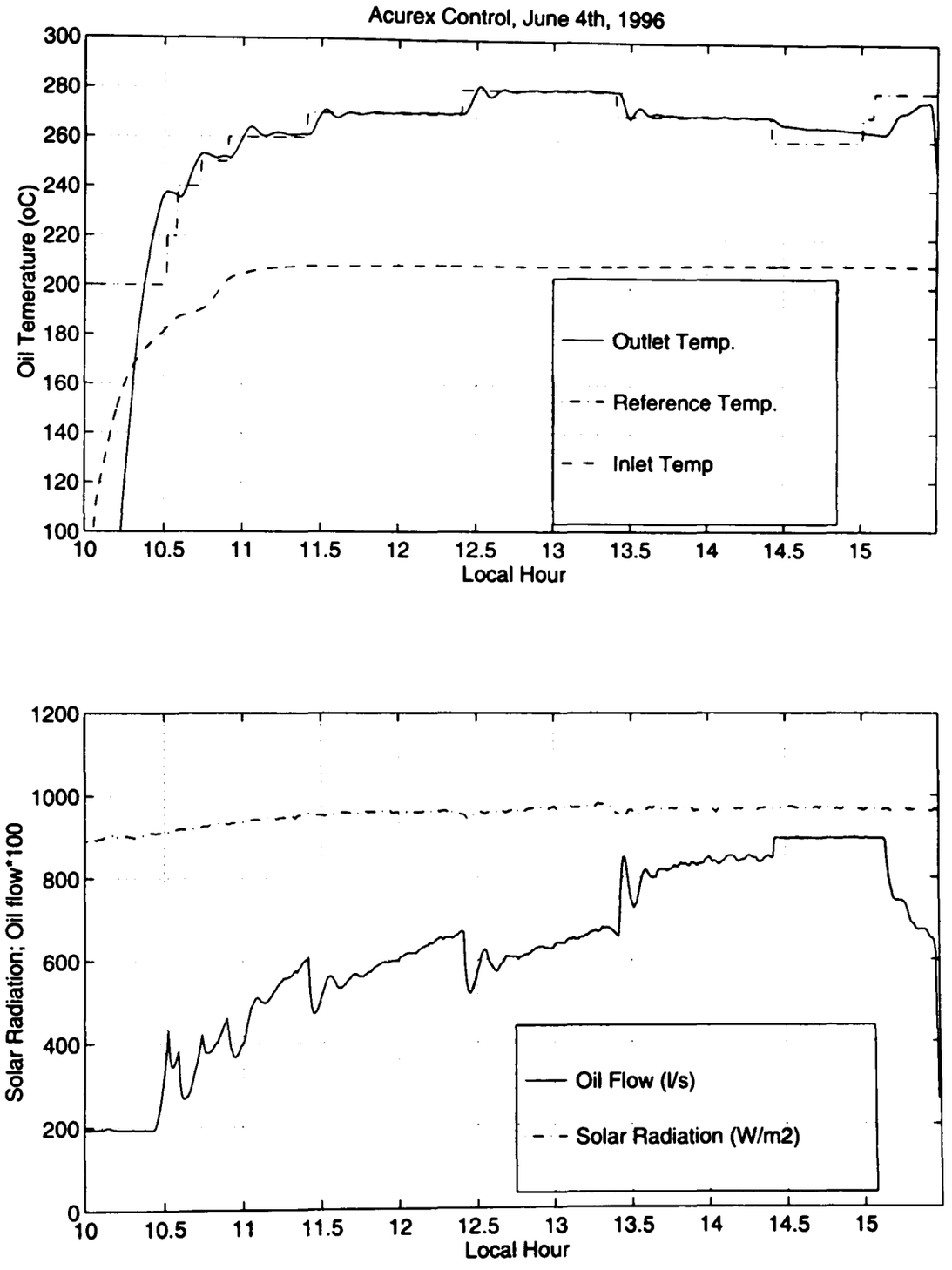

Figure B.8: June 4th. Set point following (2,50,3,.7)

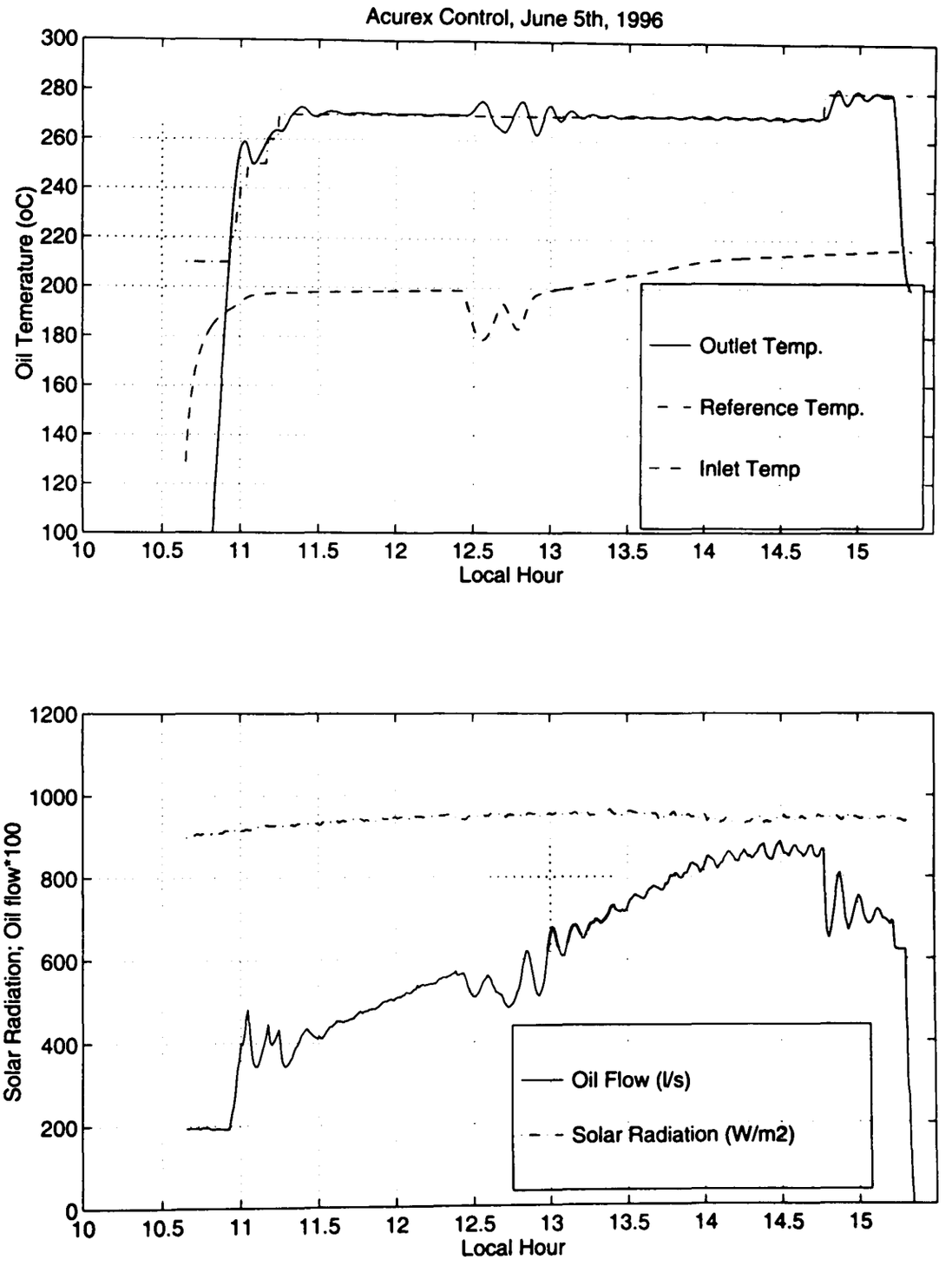

Figure B.9: June 5th. Inlet oil temperature disturbance (2,50,3,.5)

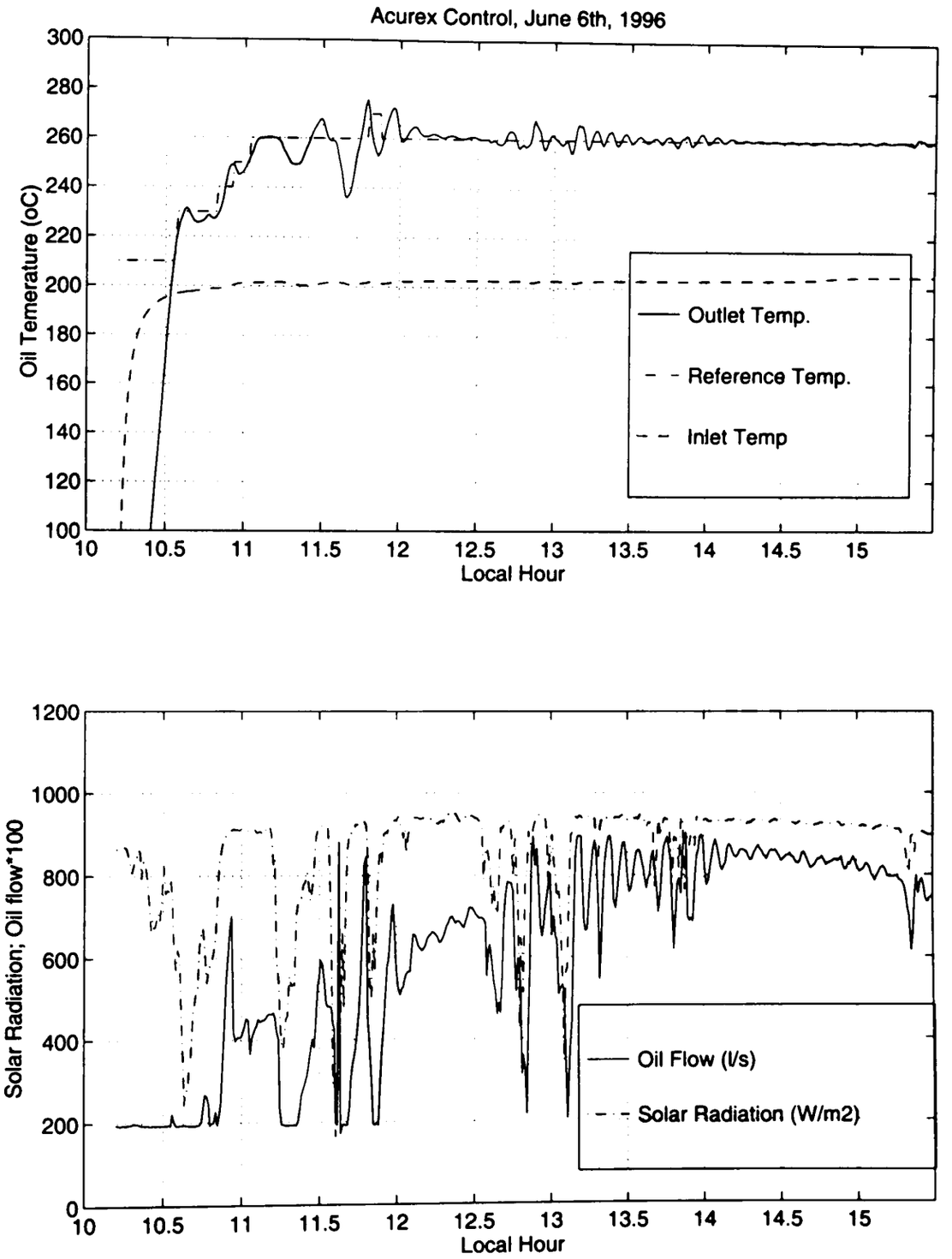

Figure B.10: June 6th. Solar radiation disturbance (7,7,1,0)

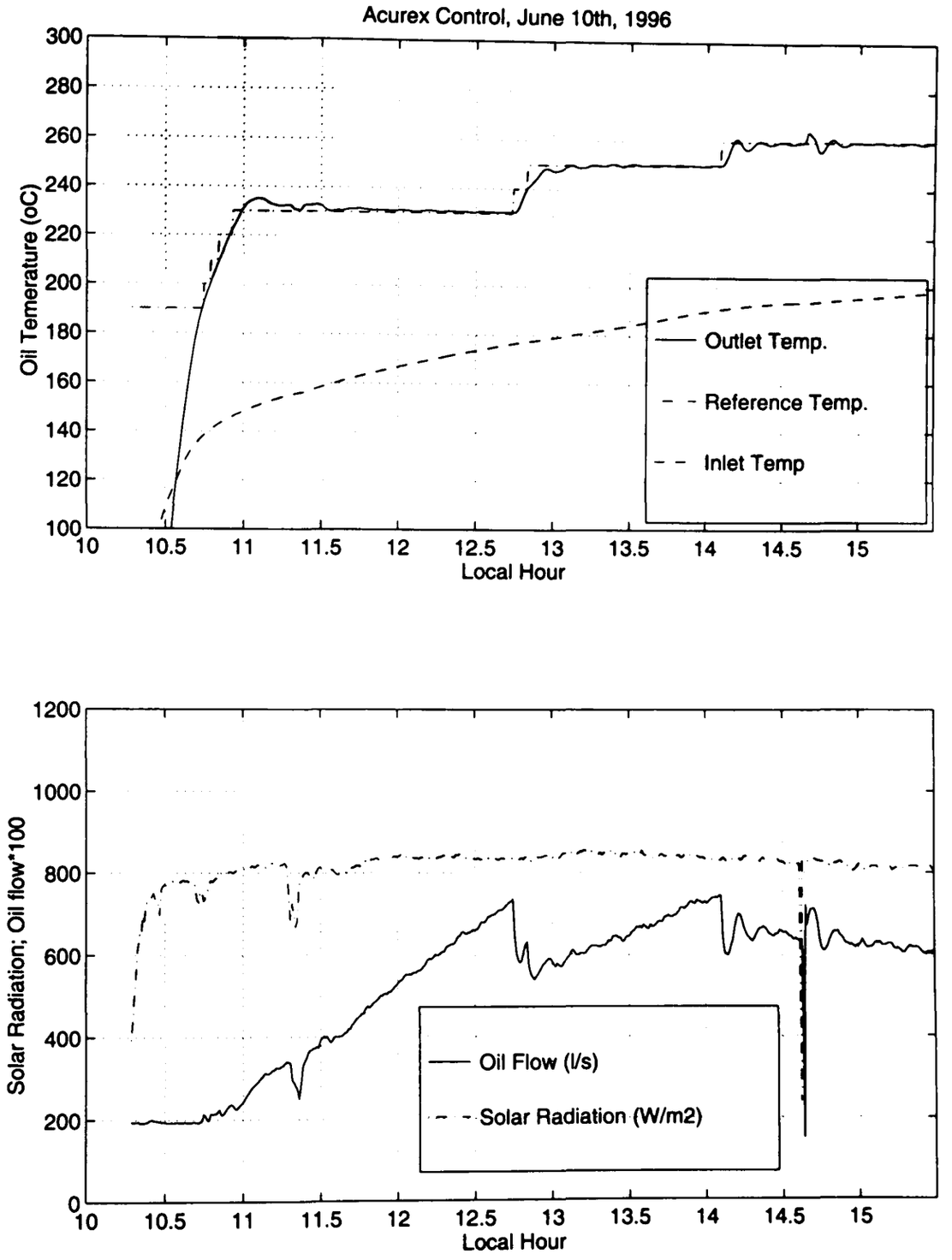

Figure B.11: June 10th. Set point, inlet temp and solar disturbance (15,30,3,.03)

Appendix C

Acurex C program

Below is listed an example of the C code used to implement the MBPC controller on the acurex field.

```
/*
   File        : Regulaci.c
   Author      : David M Robb
   Description: MBPC controller 10/6/96
                N1 = 15, N2 = 30, NU = 3, lambda = 0.03
*/
#include <conio.h>
#include <stdio.h>
#include <math.h>

extern void regula_bomba(float);
extern void crt_write(const char *, char, char [100]);
extern float val_set_point(char);
extern void pitufa();

char v_6[100];
float vari_imp[200], su_flo[101];
char palas[200][35];

/* Point useful values to array vari_imp */
float tin,irr,tout,flow,tref,actflow,irrcor,feed,tamb;

/* Other controller variable */
const int N1=15;        /* These are adjustable in the program by sp3 */
const int N2=30;
const int NU=3;
const float lamb=0.03;
float g[101]=
```

```
{0.0000000e+00 ,0.0000000e+00 ,2.7000000e-02 ,1.0362400e-01 ,
 1.7350509e-01 ,2.3723664e-01 ,2.9535982e-01 ,3.4836815e-01 ,
 3.9671175e-01 ,4.4080112e-01 ,4.8101062e-01 ,5.1768169e-01 ,
 5.5112570e-01 ,5.8162664e-01 ,6.0944349e-01 ,6.3481247e-01 ,
 6.5794897e-01 ,6.7904946e-01 ,6.9829311e-01 ,7.1584331e-01 ,
 7.3184910e-01 ,7.4644638e-01 ,7.5975910e-01 ,7.7190030e-01 ,
 7.8297307e-01 ,7.9307144e-01 ,8.0228116e-01 ,8.1068041e-01 ,
 8.1834054e-01 ,8.2532657e-01 ,8.3169783e-01 ,8.3750842e-01 ,
 8.4280768e-01 ,8.4764061e-01 ,8.5204823e-01 ,8.5606799e-01 ,
 8.5973400e-01 ,8.6307741e-01 ,8.6612660e-01 ,8.6890746e-01 ,
 8.7144360e-01 ,8.7375657e-01 ,8.7586599e-01 ,8.7778978e-01 ,
 8.7954428e-01 ,8.8114438e-01 ,8.8260368e-01 ,8.8393455e-01 ,
 8.8514831e-01 ,8.8625526e-01 ,8.8726480e-01 ,8.8818550e-01 ,
 8.8902517e-01 ,8.8979096e-01 ,8.9048935e-01 ,8.9112629e-01 ,
 8.9170718e-01 ,8.9223695e-01 ,8.9272009e-01 ,8.9316073e-01 ,
 8.9356258e-01 ,8.9392907e-01 ,8.9426332e-01 ,8.9456814e-01 ,
 8.9484615e-01 ,8.9509969e-01 ,8.9533091e-01 ,8.9554179e-01 ,
 8.9573412e-01 ,8.9590951e-01 ,8.9606948e-01 ,8.9621536e-01 ,
 8.9634841e-01 ,8.9646975e-01 ,8.9658041e-01 ,8.9668134e-01 ,
 8.9677338e-01 ,8.9685732e-01 ,8.9693388e-01 ,8.9700370e-01 ,
 8.9706737e-01 ,8.9712544e-01 ,8.9717840e-01 ,8.9722670e-01 ,
 8.9727075e-01 ,8.9731093e-01 ,8.9734757e-01 ,8.9738098e-01 ,
 8.9741145e-01 ,8.9743925e-01 ,8.9746459e-01 ,8.9748771e-01 ,
 8.9750879e-01 ,8.9752802e-01 ,8.9754555e-01 ,8.9756154e-01 ,
 8.9757613e-01 ,8.9758943e-01 ,8.9760156e-01 ,8.9761262e-01 ,
 8.9762271e-01};
float gtgig[]={0.4873,0.4020,0.3241,0.2531,0.1883,0.1293,0.0754,
 0.0263,-0.0185,-0.0594,-0.0966,-0.1306,-0.1616,-0.1899,
 -0.2156,-0.2391};

float du[1000], yf[51], r[51], w[51], uact[1000], Eo[51];
int itter,tfffflag;
float residual, tff, ordflow, acttfford, acttffsev,newdu;

int a = 0;
void initcontr(void);
void control(void);
char comand_control(char *);
void text_control(void);
void grap_control(void);
void can_text_control(void);
void can_grap_control(void);
```

```
void initcontr(void)
{
  float tmax;
  int loop;

  itter=0;
  tff=100;
  tmax=0;
  for (loop=41;loop<=50;loop++)
        tmax=(vari_imp[loop]>tmax)? vari_imp[loop]:tmax;
  uact[0]=tmax/g[100];
};

static void calcff(void)
{
  float time2;
  double NPI;
  double decli,anghor;
  double d3,se1,se2,pn3,a4,aux;
  double e3,so,s9,cang,tang,ang,vvdiv;
  float bdiaju = val_set_point(5);   /* solar day */
  cang=tang=0.0;

  time2=val_set_point(1);
  NPI=3.141592654;

  /* decli=solar declination */

  /* anghor=hour angle       */


  decli=23.45*sin((double)(2*NPI*(284+(bdiaju))/365));
  anghor=(12.0-(time2/3600.0))*15.0;
  decli=decli*NPI/180;
  anghor=anghor*NPI/180;

  d3=sqrt((double)(1.0-cos(decli)*cos(decli)*
            sin(anghor)*sin(anghor)));
  se1=cos(decli)*sin(anghor);
  aux=cos(decli)*cos(anghor);
  se2=sin(decli)*0.7976795-0.6030815364*aux;
  pn3=sin(decli)*0.6030815364-0.7976795*aux;

  if(se2==0.0)
```

```
    {
      if(se1==0.0)
        a4=0.0;
      else
        if(se1>0.0)
          a4= -NPI/2.0;
        else
          a4=NPI/2.0;
    }
   else
    a4=atan2(se1,se2);

   vvdiv=sqrt((double)(se1*se1+se2*se2));

   if(fabs(a4)==NPI/2.0)
   {
    e3=0.0;
    so=0.0;
    s9=0.0;
   }
   else
   {
    vvdiv=sqrt((double)(se2*se2+pn3*pn3));
    if(vvdiv!=0.0) cang= -(se2/vvdiv);
    if((cang!=0.0)&&(fabs((double)cang)<=1.0))
      tang=sqrt((double)(1-cang*cang));

    e3=atan2(tang,cang);
    so=72.84-5.0*fabs((double)(tan(a4)));
   }
   s9=(e3<=(21.47*NPI/180))? (1.83-5.0*(double)sin((double)e3)):0.0;

   /*irrcor es la radiacion efectiva*/
  if(fabs(d3)==0.0)
    irrcor=0.0;
  else
  {
    ang=sqrt((double)(1-d3*d3)/d3);
    irrcor=(float)(irr*d3*(1-(19.0*so*s9+66.9048*tan(ang))/2665.0));
    irrcor=(float)((irrcor)>irr)? 0.0:(irrcor);
  }
  (irrcor)=((irrcor)<0.0)? 0.0:(irrcor);
}
```

```
/*FUNTION TO CALCULATE THE FLOW DEMANDED BY THE FEEDFORWARD CONTROLLER*/

static void feedf(void)
{

  float pl1;
  float reflect=.8;
  float r7,h,pl2;
  float vvdiv;
  float c2,c3;

  c2=val_set_point(22);
  c3=10-c2;

  pl1=0.0;
  reflect=(reflect>0.98)? 0.98:reflect;
  reflect=(reflect<0.5)? 0.5:reflect;

  /*h enthalpy increment between the input
             and output field temperatures*/

  h=1.822*0.001*((tff+273)*(tff+273)-
           (tin+273)*(tin+273))+0.795*(tff-tin);
  r7=(903-0.672*tin)/1000.;
  vvdiv=r7*h;

  /*calculation of the loss functions*/

  if(vvdiv!=0.0)
  {
    pl1=reflect*(irrcor)*2.67/vvdiv;
    pl2=((((tff+tin)/2.0-tamb)*c2)+
                ((tin-tamb)*(10-c2-c3)))/(10*vvdiv);
  }
  (feed)=0.692*pl1*(c2/10.)-1.19*(pl2)+0.05;

  /*saturation of the feedforward term*/

  feed=(feed<0.0)?9.0:feed;
  feed=(feed<2.0)? 2.0:feed;
  feed=(feed>9.0)? 9.0:feed;
}
```

```
/* Function to get a value from an array, but
   protect against negative indexes           */

static float getvalue(anyarray,ndx)
float anyarray[];
int ndx;
{
  float answer;

  if (ndx<0)
    answer=anyarray[0];
  else
    answer=anyarray[ndx];

  return answer;
}

/* Function to implement the MBPC control */
void control(void)
{
   int k,j;
   float alpha=0.5;

   su_flo[50] = val_set_point(21);
   su_flo[51] = val_set_point(22);
   su_flo[52] = val_set_point(23);
   su_flo[53] = val_set_point(24);
   su_flo[54] = val_set_point(25);

   /* Get field inputs */
   tref=val_set_point(21);   /* Reference Temp */
   tin=vari_imp[51];     /* Input oil Temp */
   irr=vari_imp[76];     /* Solar irradiance */
   actflow=vari_imp[61];  /* Oil FLow */
   tamb= vari_imp[60];     /* Ambient temp */

   /* Find highest output temperature loop */
   tout=0;
   for (k=41; k<=50; k++)
   if (vari_imp[k]>tout)
  tout=vari_imp[k];

   /* Increment counter every second and operate control
```

```
every 39th second */
 a++;
 if (a==39)
 {
   itter =itter+1;

   /* Set set Point to equal reference Temperature
   for next 50 itterations */
   for (k=1; k<=50; k++)
     w[k] = tref;

   /* Calculate Reference Trajectory r */
   r[0]=tout;   /*Start at current temperature*/
   for (k=1; k<=50; k++)
     r[k]=alpha*r[k-1]+(1-alpha)*w[k];

   /* Calculate Residual offset */
   residual=tout-yf[1];

   /* Estimate free response for next 50 itterations */
   for (k=1; k<=50; k++)
     {
yf[k]=getvalue(uact,itter+k-101)*g[100];
for (j=1; j<=100; j++)
  yf[k]=yf[k]+g[j]*getvalue(du,itter+k-j);
     }

   /* Calculate Error vector */
   for (k=1; k<=50; k++)
     Eo[k-1]=r[k]-yf[k]-residual;

   /* Calculate New control value */
   newdu=0.0;
   for (k=0; k<=N2-N1; k++)
     newdu=newdu+gtgig[k]*Eo[k+N1-1];

   /* Limit tff between 100 and 350 */
   if (uact[itter-1]+newdu>350)
     du[itter]=350-uact[itter-1];
   else if (uact[itter-1]+newdu < 100)
     du[itter]=100-uact[itter-1];
   else
     du[itter]=newdu;
```

```
      uact[itter]=uact[itter-1]+du[itter];

      tff=uact[itter];

      /* calculate flow */

      feedf();
      calcff();

      if (tff-tin!=0)
        ordflow=(.7869*irrcor-.485*(tff-151.5)-80.7)/(tff-tin);

      /* Limit flow */
      ordflow=(ordflow<0.0)? 9.0:ordflow;
      ordflow=(ordflow<2.0)? 2.0:ordflow;
      ordflow=(ordflow>9.0)? 9.0:ordflow;

      /* Do checks for saturation */
      acttfford=(.7869*irrcor-7.2225+tin*ordflow)/(ordflow+.485);
      acttffsev=(.7869*irrcor-7.2225+tin*feed)/(feed+.485);

      tffflag=0;
      if ((tff!=acttfford)&&(feed==9.0||feed==2.0))
      {
        uact[itter]=acttfford;
        du[itter]=uact[itter]-uact[itter-1];
        tffflag=1;
      }

      regula_bomba(feed);

      a=0;
    }
};

void text_control(void)
{
  printf("\nDavid Robb, Strathclyde University, Glasgow, Scotland\n");
  printf("Model Based Predictive control,
    N1=%2d, N2=%2d, NU=%2d, lambda=%4.3f\n\n",N1,N2,NU,lamb);
  printf("Itteration: %4d Counter: %2d
    No of loops (SP2): %2.0f\n",itter,a, val_set_point(22));
  printf("Tff:          %8.2f Tin:         %8.2f Tamb: %8.2f\n",
                                                    tff,tin,tamb);
```

```
  printf("irr:           %8.2f Irrcor:      %8.2f \n",irr,irrcor);
  printf("Flow Demanded: %8.2f Actual flow: %8.2f\n",feed,actflow);
  printf("Tref:          %8.2f Tout:        %8.2f\n\n\n",tref,tout);
  printf("Residual:      %8.2f\n",residual);
  printf("Time   1     2     3     4     5     10   15   20   30   50\n");
  printf("s.p. %06.2f %06.2f %06.2f %06.2f %06.2f %06.2f %06.2f %06.2f
                              %06.2f %06.2f\n",
   w[1], w[2], w[3], w[4], w[5], w[10],w[15],w[20],w[30],w[50]);
  printf("ref  %06.2f %06.2f %06.2f %06.2f %06.2f %06.2f %06.2f %06.2f
                              %06.2f %06.2f\n",
   r[1], r[2], r[3], r[4], r[5], r[10],r[15],r[20],r[30],r[50]);
  printf("yf   %06.2f %06.2f %06.2f %06.2f %06.2f %06.2f %06.2f %06.2f
                              %06.2f %06.2f\n",
   yf[1], yf[2], yf[3], yf[4], yf[5], yf[10],yf[15],yf[20],yf[30],yf[50]);
  printf("Eo  %7.2f%7.2f%7.2f%7.2f%7.2f%7.2f%7.2f%7.2f%7.2f%7.2f \n",
    Eo[0], Eo[1], Eo[2], Eo[3], Eo[4], Eo[9],Eo[14],Eo[19],Eo[29],Eo[49]);
  printf("newdu= %8.2f, limited to %8.2f.   \n",newdu,du[itter]);
  printf("\n Testing                                    \n");
  printf("tff:%8.2f,    feed:%8.2f, acttffsev:%8.2f       \n",
                                                  tff,feed,acttffsev);
  printf("tff:%8.2f, ordfeed:%8.2f, acttfford:%8.2f, Flag=%2d %\n",
                                        tff,ordflow,acttfford,tfflag);
};
void grap_control(void)
{
};

void can_text_control(void)
{
};

void can_grap_control(void)
{
};

char comand_control(ord)
char *ord;
{
return(0);  /* if command is false */
/* return(1); if command is true */
};
```

Appendix D

MatrixX models of a wind turbine

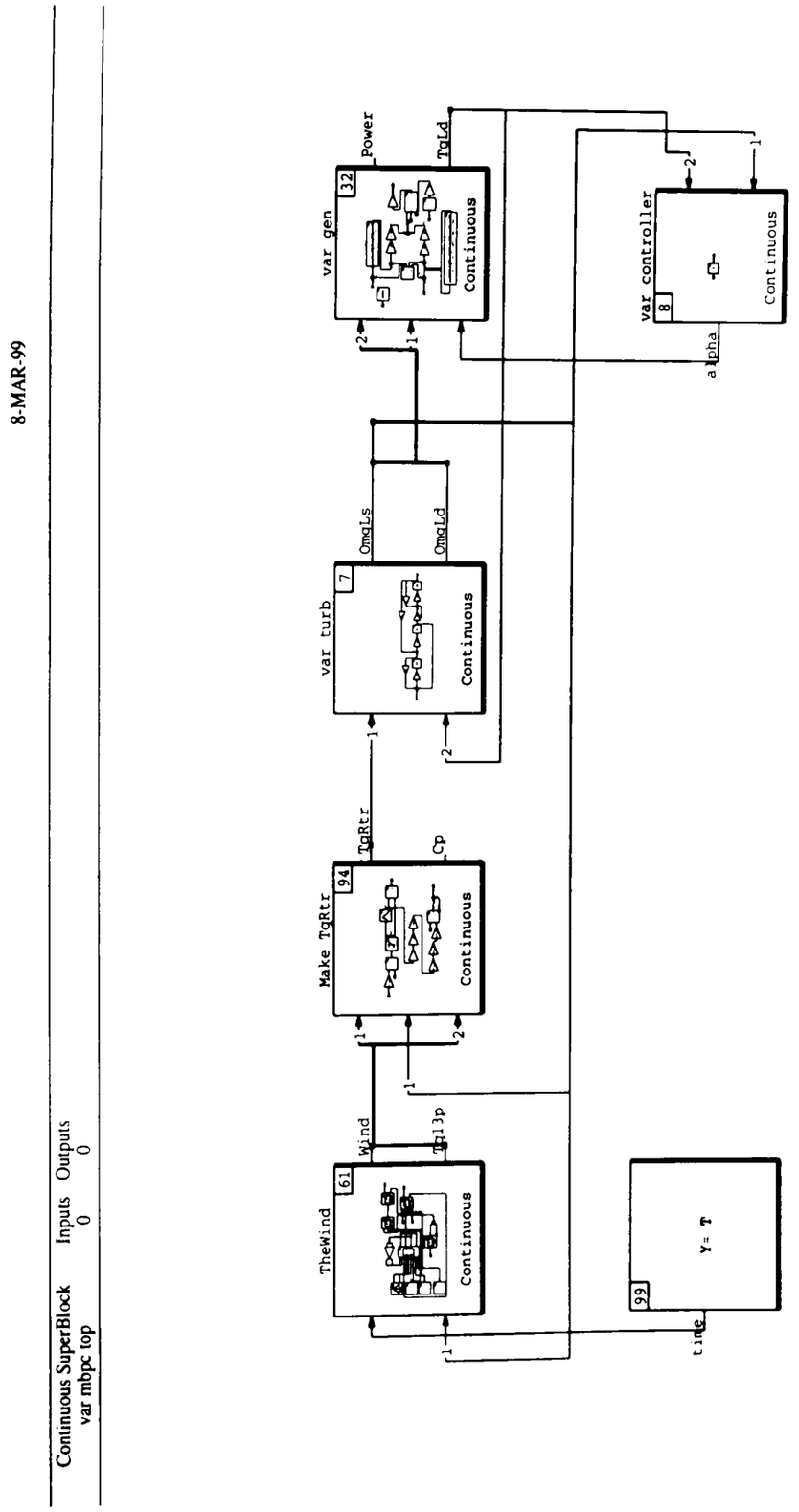

Figure D.1: MatrixX top level model

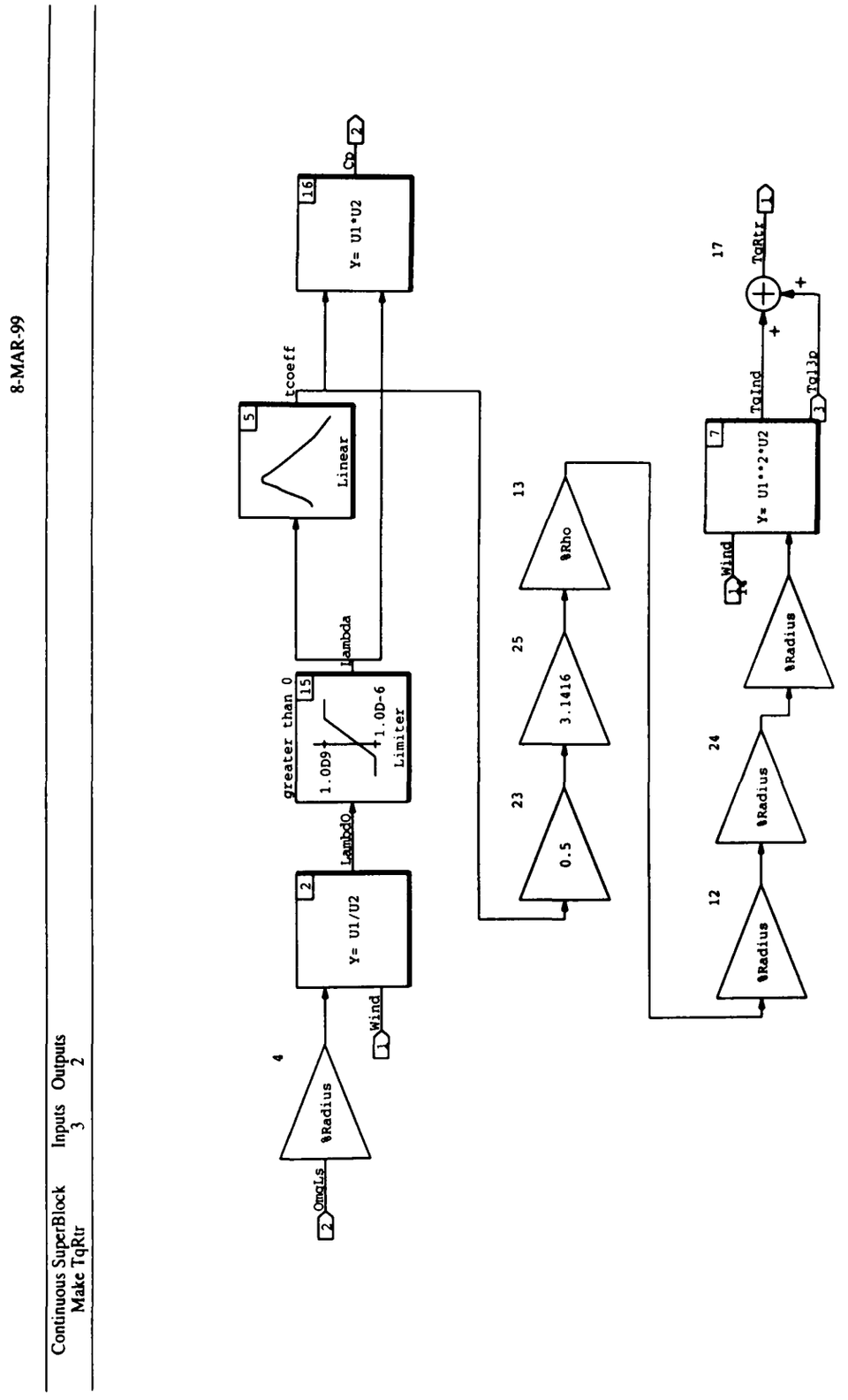

Figure D.2: MatrixX aerodynamic torque model

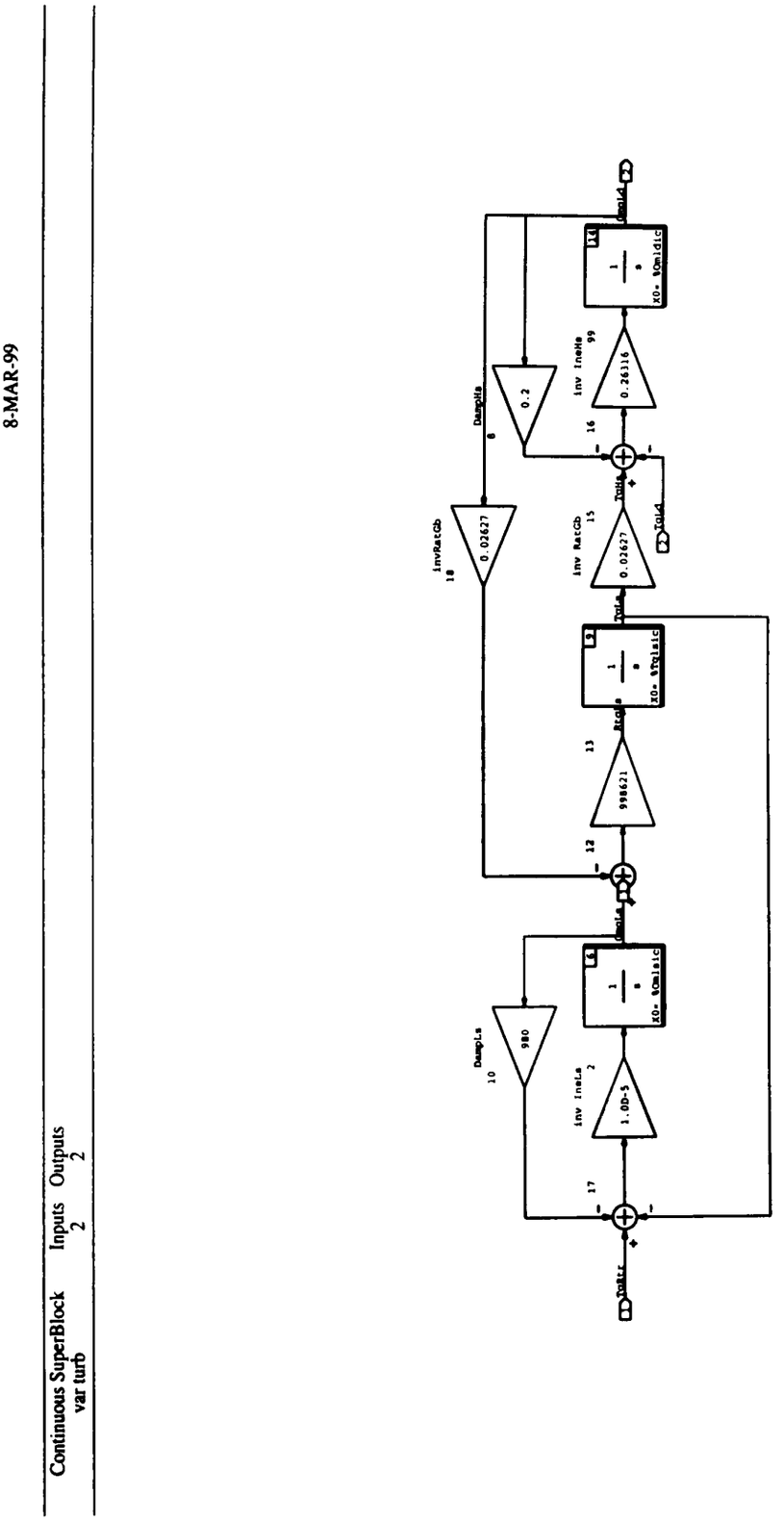

Figure D.3: MatrixX drive train model

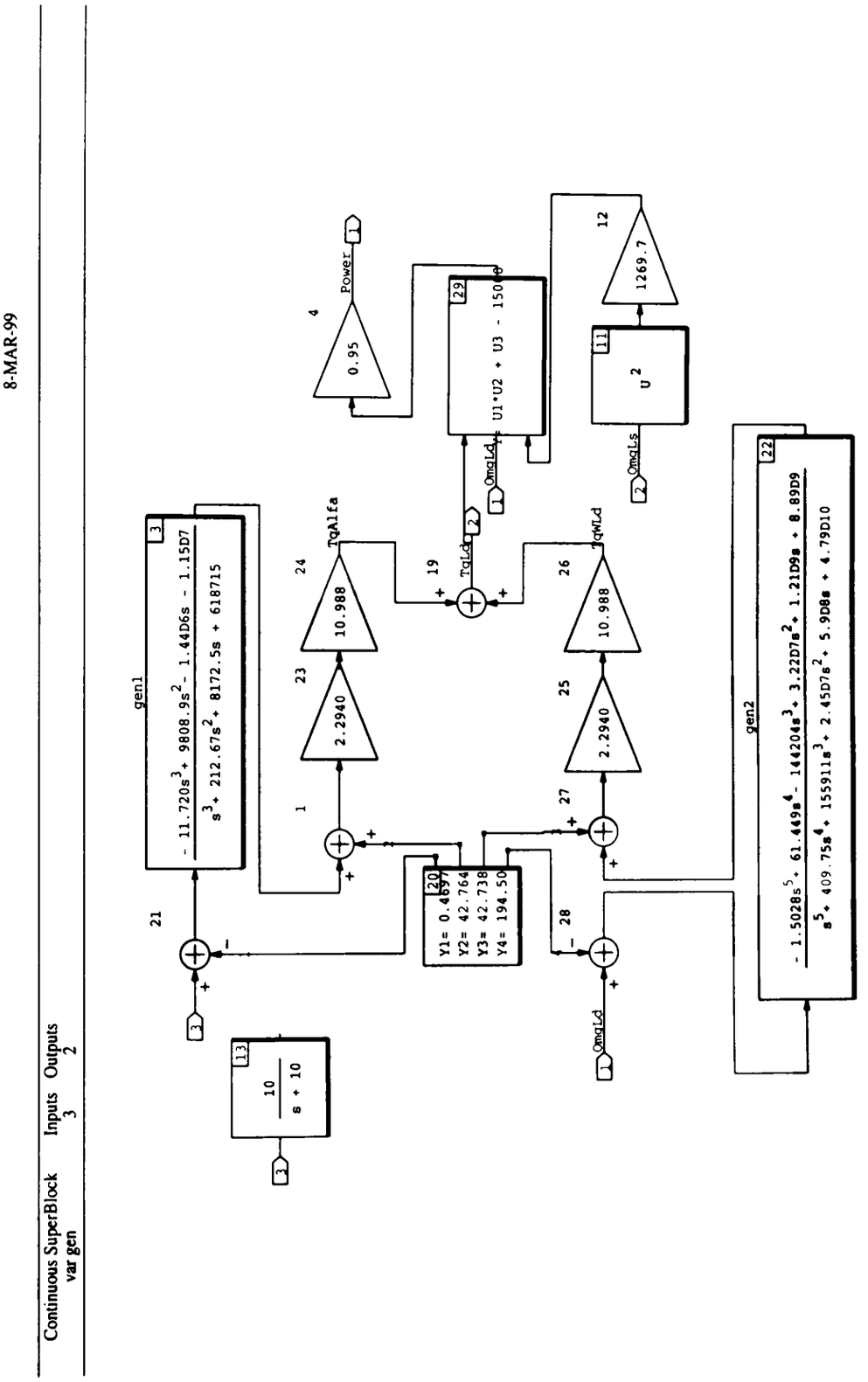

Figure D.4: MatrixX generator model

Appendix E

Filters for correlated wind speeds models

Below are given the calculated values for the filters, $f_1(s)$, $f_2(s)$, $f_{31}(s)$ and $f_{32}(s)$, used in generating the inner and outer effective wind speeds, V_I and V_O, such that

$$\begin{aligned} V_I &= f_1(s).w_1 + f_{31}(s).w_3 \\ V_O &= f_2(s).w_2 + f_{32}(s).w_3 \end{aligned} \tag{E.1}$$

The equations of each of the filters are

$$f_1(s) = \frac{K\sigma s}{(\sigma s + \omega_1)(\sigma s + \omega_2)} \tag{E.2}$$

$$f_2(s) = \frac{K\sigma s(\sigma s + \omega_3)}{(\sigma s + \omega_1)(\sigma s + \omega_2)(\sigma s + \omega_4)} \tag{E.3}$$

$$f_3(s)/f_4(s) = \frac{K(\sigma s^2 + 2\sigma s.\zeta_1.\omega_{n1} + \omega_{n1}^2)}{(\sigma s + 0.263)(\sigma s + 20.5)(\sigma s^2 + 2\sigma s.\zeta_2.\omega_{n2} + \omega_{n2}^2)} \tag{E.4}$$

$$f_3(s).f_4(s) = \frac{K(\sigma s^2 + 2\sigma s.\zeta_1.\omega_{n1} + \omega_{n1}^2)}{(\sigma s + 0.263)(\sigma s + 20.5)(\sigma s^2 + 2\sigma s.\zeta_2.\omega_{n2} + \omega_{n2}^2)} \tag{E.5}$$

The values for each of these filters are shown in Tables E.1 to E.4 below.

R_1 (m)	K	ω_1	ω_2
11.5	1.26	0.379	3.4
12	1.30	0.379	3.6
12.5	1.32	0.39	3.9
13	1.20	0.35	3.7
13.5	1.22	0.36	4.0
14	1.17	0.37	3.8

Table E.1: Values for filter $f_1(s)$

R_1 (m)	K	ω_1	ω_2	ω_3	ω_4
11.5	1.12	0.201	5.18	0.345	0.52
12	1.16	0.184	5.3	0.315	0.54
12.5	1.21	0.184	5.3	0.32	0.59
13	1.20	0.184	5.4	0.32	0.52
13.5	1.26	0.201	5.7	0.415	0.657
14	1.25	0.221	5.5	0.455	0.691

Table E.2: Values for filter $f_2(s)$

R_1 (m)	Gain	ζ_1	ζ_2	ω_{n1}	ω_{n2}
11.5	6.02	3.64	1.56	2.65	2.8
12	7.50	3.55	1.6	2.5	2.95
12.5	6.28	3.8	1.56	2.65	2.86
13	6.39	3.71	1.5	2.71	2.95
13.5	7.40	3.91	1.65	2.73	3.2
14	6.98	3.77	1.5	2.75	3.13

Table E.3: Values for filter $f_{31}(s)$

R_1 (m)	Gain	ζ_1	ζ_2	ω_{n1}	ω_{n2}
11.5	5.39	3.3	1.5	2.8	2.8
12	6.65	3.15	1.5	2.7	3.0
12.5	5.54	3.43	1.5	2.87	2.91
13	5.69	3.5	1.5	2.87	3.18
13.5	6.61	3.59	1.6	2.87	3.18
14	6.28	3.53	1.48	2.87	3.1

Table E.4: Values for filter $f_{32}(s)$

Appendix F

Point Wind Speed Model

Many different spectra have been proposed to represent point wind speed fluctuations. The are generally of the form

$$S_v(\omega) = \frac{K_v|\omega|^\kappa}{[1+(\omega T_v)^\alpha]^\delta} \tag{F.1}$$

The constants K_v and T_v depend on factors such as surface roughness, turbulence intensity and mean wind speed. The parameters α, δ and κ denote powers, the values of which depend on the actual spectrum in question. The most commonly used examples are the Von Karman, Davenport, Dryden and Kaimal spectra.

The Von Karman spectrum, which is perhaps the most appropriate for point wind speed time series of a few minutes duration, is

$$S_{VK}(\omega) = 0.475\sigma_v^2 \frac{(L/\bar{V})}{(1+(\omega L/\bar{V})^2)^{5/6}} \tag{F.2}$$

where σ_v is the standard deviation of the wind speed, $\bar{V}$ is the mean wind speed and L is the turbulence length scale.

The Dryden spectrum is

$$S_D(\omega) = \frac{1}{2\pi}\frac{b_d^2}{(\omega^2+a_d^2)} \tag{F.3}$$

It has the advantage of being a rational polynomial expression and the corresponding wind speed is, thus, readily modelled by

$$\dot{v}_d = -a_d v_d + b_d g$$

where v_d is the wind speed and g is white Gaussian noise. The two parameters, a_d and b_d, are selected so that the wind speed spectrum has the correct characteristics.

A series of Dryden spectra, which are a best fit approximations [68] to the Von Karman spectrum with a turbulent length of 200m, are determined for a range of mean wind speeds. The values for a_d are tabulated in Table F.1 and

$$b_d = \sigma_v \sqrt{2a_d} \tag{F.4}$$

$\bar{V}$	11	12	13	14	15	16	17	18	19	20	21	22	23
a_d	.063	.068	.074	.08	.086	.092	.097	.103	.108	.114	.119	.125	.131

Table F.1: Parameter values for Dryden spectrum

Appendix G

Verifying the MBPC controller

G.1 Introduction

Due to the fact that the MBPC Controller generally takes the form of a series of actions or procedures, it is very difficult to analyse the theoretical effect of the controller on the overall system response, stability, robustness etc. The only way round this problem is to convert all these procedures into a frequency domain relationship and thus allow the application of normal system analysis methods. Presented below is a method derived to convert the MBPC procedures presented in Chapter 2 and applied to the variable speed wind turbine in Chapter 8 into a frequency domain relationship. This relationship can then be used to analyse the effect of the controller on the complete system.

G.2 Summary of the method

The steps involved in deriving the generalised relationship follow the four main steps which constitute the MBPC technique. That is,

1. Evaluate the free response, y_f, which is the output of the system assuming no change in controller output.

2. Calculate the residual, which is the current real output of the system minus the predicted current output. This is used to adjust the free response calculation.

3. Creation of the error vector E_o, which is derived from the the reference trajectory minus the free response.

4. Lastly the control move, Δu, is calculated using the error vector.

The method described below takes each of these stages and builds up a single relationship relating the controller input, y (error from the curve), to controller output, u (generator firing angle). At each stage the equation is simplified into known values of y and u, that is the current or past values.

Below each step is described in relation to the form of the system used in the analysis of the variable speed wind turbine and for the simple MBPC controller parameters of the form (n,n,1,0). Using the method presented below it is possible to determine a method applicable to more complex controller parameter combinations, but this is not considered here.

G.3 Step 1: Free response

In generating a generalised relationship between y and u determining the free response of the system is the most complicated. In order to predict the free response for any time step into the future, the system output prediction must first be converted into a generalised series.

System output series

The general form of the simplified filtered discrete process models used in Chapter 8 (i.e. P_{1dpz} equation (8.13), P_{2dpz} equation (8.20) and P_{3dpz} equation (8.16)) is

$$\Delta y(z) = \frac{a_1 z^{-1} + a_2 z^{-2} + a_3 z^{-3}}{1 - b_1 z^{-1} - b_2 z^{-2}} \Delta u(z) \tag{G.1}$$

Converting equation (G.1) into the time domain gives the general difference equation

$$\Delta y(n) = b_1 \Delta y(n-1) + b_2 \Delta y(n-2) + a_1 \Delta u(n-1) + a_2 \Delta u(n-2) + a_3 \Delta u(n-3) \tag{G.2}$$

Using equation (G.2) and remembering (see Section 2.2.3) that for the free response there are no future control moves, i.e. $\Delta u(i) = 0, \forall i \geq 0$, the estimated system outputs for the current time, $n = 0$, and into the future, $n = 1, 2, 3, \ldots$, are

$$\begin{aligned}
\Delta y(0) &= b_1 \Delta y(-1) + b_2 \Delta y(-2) + a_1 \Delta u(-1) + a_2 \Delta u(-2) + a_3 \Delta u(-3) \\
\Delta y(1) &= b_1 \Delta y(0) + b_2 \Delta y(-1) + a_2 \Delta u(-1) + a_3 \Delta u(-2) \\
\Delta y(2) &= b_1 \Delta y(1) + b_2 \Delta y(0) + a_3 \Delta u(-1) \\
\Delta y(3) &= b_1 \Delta y(2) + b_2 \Delta y(1) \\
\Delta y(4) &= b_1 \Delta y(3) + b_2 \Delta y(2) \\
&\vdots
\end{aligned} \tag{G.3}$$

Generalising this series gives,

$$\Delta y(n) = b_1 \Delta y(n-1) + b_2 \Delta y(n-2), \quad \forall n \geq 3 \tag{G.4}$$

Z-transform of the series

The notation of equation (G.4) is simplified slightly by defining $y_n = \Delta y(n)$,

$$y_n = b_1 y_{n-1} + b_2 y_{n-2} \qquad \text{or rewriting} \tag{G.5}$$

$$y_{n+2} - b_1 y_{n+1} - b_2 y_n = 0 \tag{G.6}$$

Defining the initial conditions $y_0 = \Delta y(1)$ and $y_1 = \Delta y(2)$ allows the z-transformation of equation (G.6) to be made utilising the following two rules for z-transforms, where $\mathcal{Z}$ means the "z-transform of",

$$\mathcal{Z}\{y_{n+2}\} = z^2 \mathcal{Z}\{y_n\} - (z^2 y_0 + z y_1)$$
$$\mathcal{Z}\{y_{n+1}\} = z \mathcal{Z}\{y_n\} - z y_0$$

Therefore the z-transform of equation (G.6), $\mathcal{Z}\{y_{n+2} - b_1 y_{n+1} - b_2 yn = 0\}$, is

$$z^2 \mathcal{Z}\{y_n\} - (z^2 y_0 + z y_1) - b_1 z \mathcal{Z}\{y_n\} + b_1 z y_0 - b_2 \mathcal{Z}\{y_n\} = 0 \tag{G.7}$$

Gathering for $\mathcal{Z}\{y_n\}$ and simplifying gives,

$$\mathcal{Z}\{y_n\} = \frac{z^2 y_0 + z y_1 - b_1 z y_0}{z^2 - b_1 z - b_2} \tag{G.8}$$

$$= \frac{z(y_0 z + (y_1 - b_1 y_0))}{z^2 - b_1 z - b_2} \tag{G.9}$$

Inverse Z-transform of the series

Next the inverse z-transform of equation (G.9) is required. To achieve this equation (G.9) is separated into simpler terms. In order to explain this clearly the method is shown by example.

For the example the above rated system values from Chapter 8 of $b_1 = 1.745$ and $b_2 = -0.649$ are used. First equation (G.9) is expanded by partial factorization,

$$\begin{aligned}
\mathcal{Z}\{y_n\} &= \frac{z(y_0 z + (y_1 - 1.745 y_0))}{z^2 - 1.745 z + 0.649} \\
&= \frac{z(y_0 z + (y_1 - 1.745 y_0))}{(z - 1.208)(z - 0.537)} \\
&= z\left(\frac{1.208 y_0 + y_1 - 1.745 y_0}{(1.208 - 0.537)(z - 1.208)} + \frac{0.537 y_0 + y_1 - 1.745 y_0}{(0.537 - 1.208)(z - 0.537)} \right) \\
&= \frac{\mathcal{C} z}{z - 1.208} + \frac{\mathcal{D} z}{z - 0.537}
\end{aligned}$$

This allows the inverse z-transform to be taken giving,

$$y_n = \mathcal{C}(1.208)^n + \mathcal{D}(0.537)^n, \qquad n \geq 3 \tag{G.10}$$

where

$$\mathcal{C} = \frac{1.208y_0 + y_1 - 1.745y_0}{(1.208 - 0.537)} = -0.8y_0 + 1.49y_1,$$
$$\mathcal{D} = \frac{0.537y_0 + y_1 - 1.745y_0}{(0.537 - 1.208)} = 1.8y_0 - 1.49y_1$$

Finally y_n can be expressed completely in terms of past known values. First $y_0(= \Delta y(1))$ and $y_1(= \Delta y(2))$ are written in terms of past known values, i.e. $\Delta y(-1)$, $\Delta y(-2)$, $\Delta u(-1)$, $\Delta u(-2)$, $\Delta u(-3)$. Using equations from (G.3) with the values $b_1 = 1.745$, $b_2 = -0.649$, $a_1 = 716$, $a_2 = 1.432$, $a_3 = 716$, gives

$$y_0 = 2.396\Delta y(-1) - 1.133\Delta y(-2) - 2680\Delta u(-1) - 1784\Delta u(-2) - 1249\Delta u(-3) \tag{G.11}$$

$$y_1 = 3.049\Delta y(-1) - 1.555\Delta y(-2) - 4930\Delta u(-1) - 4680\Delta u(-2) - 2645\Delta u(-3) \tag{G.12}$$

Therefore

$$\mathcal{C} = 2.627\Delta y(-1) - 1.411\Delta y(-2) - 5202\Delta u(-1) - 5546\Delta u(-2) - 2942\Delta u(-3) \tag{G.13}$$

$$\mathcal{D} = -0.230\Delta y(-1) + 0.278\Delta y(-2) + 2522\Delta u(-1) + 3762\Delta u(-2) + 1639\Delta u(-3) \tag{G.14}$$

Thus, substituting into equation (G.10),

$$\begin{aligned} y_n = &\big[2.627\Delta y(-1) - 1.411\Delta y(-2) \\ &\quad - 5202\Delta u(-1) - 5546\Delta u(-2) - 2942\Delta u(-3)\big](1.208)^n \\ &+ \big[-0.230\Delta y(-1) + 0.278\Delta y(-2) \\ &\quad + 2522\Delta u(-1) + 3762\Delta u(-2) + 1639\Delta u(-3)\big](0.537)^n \end{aligned} \tag{G.15}$$

Note that in the above $\Delta y(k) = y_{k-1}$ since y_0 is defined as $\Delta y(1)$, etc.

Summarizing

Using the example as a guide to performing the inverse z transform the complete method described above can be summarized using only the generalized terms b's and a's as shown below.

Starting from the current time i,

$$\begin{aligned}
\Delta y(i|i) &= b_1\Delta y(i-1) + b_2\Delta y(i-2) \\
&\quad + a_1\Delta u(i-1) + a_2\Delta u(i-2) + a_3\Delta u(i-3) \\
\Delta y(i+1|i) = y_0 &= (b_1^2 + b_2)\Delta y(i-1) + b_1b_2\Delta y(i-2) \\
&\quad + (b_1a_1 + b_2^2)\Delta u(i-1) + (b_1a_2 + a_3)\Delta u(i-2) + b_1a_3\Delta u(i-3) \\
\Delta y(i+2|i) = y_1 &= (b_1^3 + 2b_1b_2)\Delta y(i-1) + (b_1^2b_2 + b_2^2)\Delta y(i-2) \\
&\quad + (b_1^2a_1 + b_1a_2 + b_2a_1 + a_3)\Delta u(i-1) \\
&\quad + (b_1^2a_2 + b_1a_3 + b_2a_2)\Delta u(i-2) \\
&\quad + (b_1^2a_3 + b_2a_3)\Delta u(i-3) \\
\Delta y(i+3|i) &= \mathcal{C}(r_1)^2 + \mathcal{D}(r_2)^2 \\
\Delta y(i+4|i) &= \mathcal{C}(r_1)^3 + \mathcal{D}(r_2)^3 \\
&\vdots \\
\Delta y(i+n|i) &= \mathcal{C}(r_1)^{n-1} + \mathcal{D}(r_2)^{n-1}, \qquad n \geq 3
\end{aligned} \tag{G.16}$$

where

$$\mathcal{C} = \frac{r_1 - b_1}{r_1 - r_2}y_0 + \frac{1}{r_1 - r_2}y_1, \quad \mathcal{D} = \frac{r_2 - b_1}{r_2 - r_1}y_0 + \frac{1}{r_2 - r_1}y_1$$

and

$$r_1 = -\frac{-b_1 + \sqrt{b_1^2 + 4b_2}}{2}, \quad r_2 = -\frac{-b_1 - \sqrt{b_1^2 + 4b_2}}{2}$$

Absolute free response

In the above analysis, it should be noted that, at the beginning, equations (G.1) and (G.2) could have been written in terms of absolute values of y and u instead of change of values (Δy's and Δu's). However using the absolute values of y and u would not have allowed the elimination of Δu's in equations(G.3) and (G.4) which permitted the series to be formed and generalised. However the use of Δ values results in the generalised equation (G.16) only defining the individual changes in future values. To determine the MBPC Error vector the absolute free response y_f is required. Therefore the Δy values must be summed and a new relationship created. The way this is achieved is as follows.

First, $\Delta y(i+n|i)$ from equation (G.16) can be rearranged and written as

$$\Delta y(i+n|i) = E_{n-1}y_0 + F_{n-1}y_1, \quad \forall n \geq 3 \tag{G.17}$$

where,

$$E_n = \frac{r_1 - b_1}{r_1 - r_2}(r_1)^n + \frac{r_2 - b_1}{r_2 - r_1}(r_2)^n \quad \text{and} \quad F_n = \frac{1}{r_1 - r_2}(r_1)^n + \frac{1}{r_2 - r_1}(r_2)^n \tag{G.18}$$

This allows every estimate $\Delta y(i+j|i)$, $\forall j \geq 0$, to be clearly written in terms of the known values of $\Delta y(i-1)$, $\Delta y(i-2)$, $\Delta u(i-1)$, $\Delta u(i-2)$ and $\Delta u(i-3)$.

The absolute free response at any point in the future, p, is found from the summation of the last known output value, $y(i-1)$, plus all the changes in free response, $\sum_{j=0}^{p} \Delta y(i+j|i)$. For example if $p = 2$,

$$y_f(i+2) = y(i-1) + \Delta y(i|i) + \Delta y(i+1|i) + \Delta y(i+2|i) \tag{G.19}$$

Since all the estimates, $\Delta y(i|i)$, $\Delta y(i+1|i)$, $\Delta y(i+2|i)$,... can be written in terms of the known values $\Delta y(i-1)$, $\Delta y(i-2)$, $\Delta u(i-1)$, $\Delta u(i-2)$ and $\Delta u(i-3)$ the summation of these estimates will also be written in terms of these same known values. That is, the answer will be of the form

$$\begin{aligned} y_f(i+p|i) = y(i-1) + c_1\Delta y(i-1) + c_2\Delta y(i-2) + \\ d_1\Delta u(i-1) + d_2\Delta u(i-2) + d_3\Delta u(i-3) \end{aligned} \tag{G.20}$$

c_1 is therefore defined as the summation of all the factors of $\Delta y(-1)$ in the predictions of $\Delta y(i+j|i)$, $j = 0 \ldots N_2$. Thus, using equations (G.16) and (G.17), for the prediction of $\Delta y(i|i)$ the factor of $\Delta y(i-1)$ is b_1, for $\Delta y(i+1|i)$ (which is also y_0) the factor is $(b_1^2+b_2)$, for $\Delta y(i+2|i)$ (which is y_1) the factor is $(b_1^3+2b_1b_2)$ and for $\Delta y(i+k|i)$, $\forall k \geq 3$ the factor is $E_{k-1}(b_1^2 + b_2) + F_{k-1}(b_1^3 + 2b_1b_2)$. The actual value of c_1 can be evaluated using a small function containing a FOR loop. i.e.

```
c1 = b1 + (b1^2 + b2) + (b1^3 + 2*b1*b2);
FOR k=[3:N2] do
  c1=c1+E(k-1)*(b1^2 + b2) + F(k-1)*(b1^3 + 2*b1*b2);
ENDFOR;
```

where `E(k-1)` and `F(k-1)` are functions which evaluate the factors E and F as defined in equation (G.18).

This process can be easily repeated to determine the values of c_2, d_1, d_2 and d_3 which thus allows the general function evaluating the future free response at any time horizon $N2$ in the future to be formed, equation (G.20).

G.4 Steps 2,3 & 4: Residual, error vector and control move

Now that the free response has been derived (equation (G.20)) the residual, the error vector and thus the next control move can be calculated. The residual is defined as the current real output $y(i)$ minus the predicted current output

$$residual = y(i) - (y(i-1) + \Delta y(i|i)) \tag{G.21}$$

The error vector E_o is defined as the reference trajectory minus the free response including the residual,

$$E_o = reftraj - y_f - residual \tag{G.22}$$

The new control value is calculated using the error vector,

$$\Delta u(i|i) = \hat{G}E_o \tag{G.23}$$

where $\hat{G} = 1/g_{N_2}$, g_{N_2} being the step response of the model at time step N_2. Equation (G.20) can be used to evaluate the free response N_2 steps ahead. Therefore the error vector (which is a single value), assuming that the reference trajectory is zero (which is the desired value in the case of curve tracking in wind turbine control), is

$$\begin{aligned} E_o(i+N_2|i) &= reftraj - y_f(i+N_2|i) - residual \\ &= 0 - y_f(i+N_2|i) - [y(i) - (y(i-1) + \Delta y(i|i))] \end{aligned}$$

expanding $yf(i+N_2|i)$ and $\Delta y(i|i)$,

$$\begin{aligned} E_o(i+N_2|i) = &-y(i-1) - c_1\Delta y(i-1) - c_2\Delta y(i-2) \\ &- d_1\Delta u(i-1) - d_2\Delta u(i-2) - d_3\Delta u(i-3) \\ &- y(i) - y(i-1) + b_1\Delta y(i-1) + b_2\Delta y(i-2) \\ &+ a_1\Delta u(i-1) + a_2\Delta u(i-2) + a_3\Delta u(i-3) \\ = &-y(i) + (b_1 - c_1)\Delta y(i-1) + (b_2 - c_2)\Delta y(i-2) \\ &+ (a_1 - d_1)\Delta u(i-1) + (a_2 - d_2)\Delta u(i-2) + (a_3 - d_3)\Delta u(i-3) \end{aligned}$$

Eliminating all Δ values, e.g. $\Delta y(i-1) = y(i-1) - y(i-2)$ etc,

$$\begin{aligned} E_o(i+N_2|i) = &-y(i) + (b_1 - c_1)y(i-1) + (b_2 - c_2 - b_1 + c_1)y(i-2) + (c_2 - b_2)y(i-3) \\ &+ (a_1 - d_1)u(i-1) + (a_2 - d_2 - a_1 + d_1)u(i-2) \\ &+ (a_3 - d_3 - a_2 + d_2)u(i-3) + (d_3 - a_3)u(i-4) \end{aligned}$$

Substituting into equation (G.23) with $\Delta u(i|i) = u(i|i) - u(i-1)$ and solving for the new control move, $u(i|i)$, gives the final generalised equation of the controller,

$$\begin{aligned} u(i|i) &= u(i-1) + \hat{G}E_o(i+N_2) \\ &= \hat{G}[-y(i) + (b_1 - c_1)y(i-1) + (b_2 - c_2 - b_1 + c_1)y(i-2) + (c_2 - b_2)y(i-3) \\ &\quad + (g_{N_2} + a_1 - d_1)u(i-1) + (a_2 - d_2 - a_1 + d_1)u(i-2) \\ &\quad + (a_3 - d_3 - a_2 + d_2)u(i-3) + (d_3 - a_3)u(i-4)] \end{aligned} \tag{G.24}$$

Showing this in a z-transform form,

$$\frac{u(z)}{y(z)} = \frac{-1 + (b_1 - c_1)z^{-1} + (b_2 - c_2 - b_1 + c_1)z^{-2} + (c_2 - b_2)z^{-3}}{g_{N_2} - (g_{N_2} + a_1 - d_1)z^{-1} - (a_2 - d_2 - a_1 + d_1)z^{-2} - (a_3 - d_3 - a_2 + d_2)z^{-3} - (d_3 - a_3)z^{-4}} \tag{G.25}$$

G.5 Validation of the method

In order to check the validity of the method presented equation (G.25) is derived for both the below and above rated MBPC controllers and the control moves checked against that which would be derived using the normal steps of the MBPC controller.

G.5.1 Below rated controller

The below rated MBPC controller (tracking with $\hat{T}_f$) uses the simplified discrete model from equation (8.16),

$$P_{3dpz}(z) = \frac{-1921.2z^{-1} + 2389.6z^{-2} - 1791.9z^{-3}}{1 - 1.431z^{-1} + 0.478z^{-2}}$$

Thus

$$\begin{aligned} a_1 &= -1921.2 & b_1 &= 1.431 \\ a_2 &= 2389.6 & b_2 &= -0.478 \\ a_3 &= -1791.9 \end{aligned}$$

From these values the c and d values are derived for a prediction horizon $N_2 = 5$. Thus

$$\begin{aligned} c_1 &= 7.427 & d_1 &= -7411.8 \\ c_2 &= -3.369 & d_2 &= 6879.4 \\ & & d_3 &= -12624 \end{aligned}$$

Substituting these values into equation (G.25) gives

$$\frac{u(z)}{y(z)} = \frac{-1 - 5.996z^{-1} + 8.887z^{-2} - 2.891z^{-3}}{-7411.8 + 1921z^{-1} + 998.1z^{-2} - 15322z^{-3} + 10833z^{-4}} \quad \text{(G.26)}$$

The new controller output, $u(i|i)$, is calculated for various choices of current and past input and output variables and compared against that which would be obtained by using the code from Chapter 8. Both gave exactly the same values and thus show the validity of the method.

G.5.2 Above rated controller

The above rated MBPC controller uses the simplified discrete model equation (8.20),

$$P_{2dpz}(z) = \frac{-976.7z^{-1} + 5177z^{-2} - 1250z^{-3}}{1 - 1.743z^{-1} + 0.644z^{-2}}$$

Thus

$$a_1 = -976.7 \qquad b_1 = 1.743$$
$$a_2 = 5177 \qquad b_2 = -0.644$$
$$a_3 = -1250$$

From these values the c and d values are derived for a prediction horizon $N_2 = 5$. Thus

$$c_1 = 15.58 \qquad d_1 = 24281$$
$$c_2 = -7.704 \qquad d_2 = 51695$$
$$d_3 = -14953$$

Substituting these values into equation (G.25) gives

$$\frac{u(z)}{y(z)} = \frac{-1 - 13.84z^{-1} + 20.89z^{-2} - 7.06z^{-3}}{24281 + 976.7z^{-1} + 21260z^{-2} - 60221z^{-3} + 13703z^{-4}} \quad \text{(G.27)}$$

As with the below rated controller the new controller output, $u(i|i)$, is calculated for various choices of current and past input and output variables and compared against that which would be obtained by using the code from Chapter 8. Both gave exactly the same values and thus show again the validity of the method.

The method is also verified for any choice of N_2.